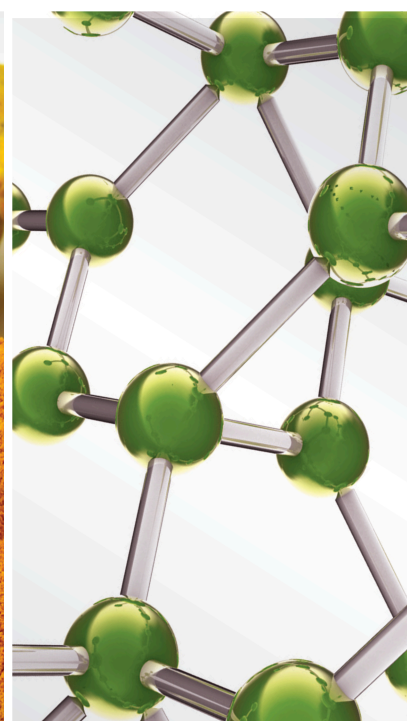


Computer-Aided Drug Design of Natural Candidates for the Treatment of Non-Communicable Diseases

Lead Guest Editor: Hilal Zaid

Guest Editors: Siba Shanak, Akhilesh K. Tamrakar, and Thomas Linn



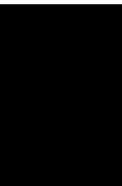


**Computer-Aided Drug Design of Natural
Candidates for the Treatment of Non-
Communicable Diseases**

**Computer-Aided Drug Design of
Natural Candidates for the Treatment of
Non-Communicable Diseases**

Lead Guest Editor: Hilal Zaid

Guest Editors: Siba Shanak, Akhilesh K. Tamrakar,
and Thomas Linn



Copyright © 2022 Hindawi Limited. All rights reserved.

This is a special issue published in "Evidence-Based Complementary and Alternative Medicine." All articles are open access articles distributed under the Creative Commons Attribution License, which permits unrestricted use, distribution, and reproduction in any medium, provided the original work is properly cited.

Chief Editor

Jian-Li Gao, China

Editorial Board

Eman A. Mahmoud, Egypt
Smail Aazza, Morocco
Nahla S. Abdel-Azim, Egypt
Usama Ramadan Abdelmohsen, Germany
Essam A. Abdel-Sattar, Egypt
Mona Abdel-Tawab, Germany
Azian Azamimi Abdullah, Malaysia
Ana Lúcia Abreu-Silva, Brazil
Gustavo J. Acevedo-Hernández, Mexico
Mohd Adnan, Saudi Arabia
Jose C Adsuar, Spain
Duygu AĞAGÜNDÜZ, Turkey
Gabriel A. Agbor, Cameroon
Wan Mohd Aizat, Malaysia
Basiru Ajiboye, Nigeria
Muhammad Furqan Akhtar, Pakistan
Fahmida Alam, Malaysia
Ulysses Paulino Albuquerque, Brazil
Ammar AL-Farga, Saudi Arabia
Ekram Alias, Malaysia
Mohammed S. Ali-Shtayeh, Palestinian Authority
Terje Alraek, Norway
Sergio R. Ambrosio, Brazil
Samson Amos, USA
Won G. An, Republic of Korea
VIJAYA ANAND, India
Adolfo Andrade-Cetto, Mexico
Isabel Andújar, Spain
Letizia Angiolella, Italy
Makoto Arai, Japan
Daniel Arcanjo, Brazil
Hyunsu Bae, Republic of Korea
Neda Baghban, Iran
Winfried Banzer, Germany
Ahmed Bari, Saudi Arabia
Sabina Barrios Fernández, Spain
Samra Bashir, Pakistan
Rusliza Basir, Malaysia
Jairo Kenupp Bastos, Brazil
Arpita Basu, USA
Daniela Beghelli, Italy
Mateus R. Beguelini, Brazil
Olfa Ben Braiek, Tunisia

Juana Benedí, Spain
Roberta Bernardini, Italy
Andresa A. Berretta, Brazil
Monica Borgatti, Italy
Francesca Borrelli, Italy
Samira Boulbaroud, Morocco
Mohammed Bourhia, Morocco
Célia Cabral, Portugal
Nunzio Antonio Cacciola, Italy
Gioacchino Calapai, Italy
Giuseppe Caminiti, Italy
Raffaele Capasso, Italy
Francesco Cardini, Italy
María C. Carpinella, Argentina
Isabella Cavalcanti, Brazil
Shun-Wan Chan, Hong Kong
Harish Chandra, India
Wen-Dien Chang, Taiwan
Jianping Chen, China
Calvin Yu-Chian Chen, China
Kevin Chen, USA
Xiaojia Chen, Macau
Guang Chen, China
Mei-Chih Chen, Taiwan
Evan P. Cherniack, USA
Ching-Chi Chi, Taiwan
Giuseppina Chianese, Italy
Kok-Yong Chin, Malaysia
I. Chinou, Greece
Salvatore Chirumbolo, Italy
Jae Youl Cho, Republic of Korea
Hwi-Young Cho, Republic of Korea
Jun-Yong Choi, Republic of Korea
Seung Hoon Choi, Republic of Korea
Jeong June Choi, Republic of Korea
Kathrine Bisgaard Christensen, Denmark
Shuang-En Chuang, Taiwan
Ying-Chien Chung, Taiwan
Francisco José Cidral-Filho, Florianópolis
88040-900, SC, Brasil., Brazil
Ian Cock, Australia
Guy Cohen, Israel
Daniel Collado-Mateo, Spain
Marisa Colone, Italy

Lisa A. Conboy, USA
Kieran Cooley, Canada
Edwin L. Cooper, USA
José Otávio do Amaral Corrêa, Brazil
Maria T. Cruz, Portugal
Roberto K. N. Cuman, Brazil
Ademar A. Da Silva Filho, Brazil
Chongshan Dai, China
Giuseppe D'Antona, Italy
Nawab Dar, USA
Vincenzo De Feo, Italy
Rocío De la Puerta, Spain
marinella de leo, Italy
Laura De Martino, Italy
Josué De Moraes, Brazil
Arthur De Sá Ferreira, Brazil
Nunziatina De Tommasi, Italy
Gourav Dey, India
Dinesh Dhamecha, USA
Claudia Di Giacomo, Italy
Antonella Di Sotto, Italy
Gabriel O. Dida, Japan
Mario Dioguardi, Italy
Vishal Diwan, Australia
Caigan Du, Canada
Shizheng Du, China
Lin-Rui Duan, China
Jeng-Ren Duann, USA
Nativ Dudai, Israel
Thomas Efferth, Germany
Abir El-Alfy, USA
Mohamed Ahmed El-Esawi, Egypt
Mohd Ramli Elvy Suhana, Malaysia
Talha Bin Emran, Japan
Roger Engel, Australia
Karim Ennouri, Tunisia
Giuseppe Esposito, Italy
Tahereh Eteraf-Oskouei, Iran
Mohammad Faisal, Saudi Arabia
Sharida Fakurazi, Malaysia
Robson Xavier Faria, Brazil
Mohammad Fattahi, Iran
Keturah R. Faurot, USA
Piergiorgio Fedeli, Italy
Nianping Feng, China
Yibin Feng, Hong Kong
Glaura Fernandes, Brazil

Laura Ferraro, Italy
Antonella Fioravanti, Italy
Johannes Fleckenstein, Germany
Carmen Formisano, Italy
Harquin Simplicie Foyet, Cameroon
Huiying Fu, China
Hua-Lin Fu, China
Liz G Müller, Brazil
Dolores García Giménez, Spain
Gabino Garrido, Chile
Safoora Gharibzadeh, Iran
Muhammad N. Ghayur, USA
Roxana Ghiulai, Romania
Angelica Gomes, Brazil
Elena González-Burgos, Spain
Susana Gorzalczany, Argentina
Sebastian Granica, Poland
Jiangyong Gu, China
Maruti Ram Gudavalli, USA
Shanshan Guo, China
Jianming GUO, China
Shuzhen Guo, China
Jian-You Guo, China
Hai-dong Guo, China
Zihu Guo, China
Narcís Gusi, Spain
Svein Haavik, Norway
Fernando Hallwass, Brazil
Gajin Han, Republic of Korea
Ihsan Ul Haq, Pakistan
Md. Areeful Haque, India
Hicham Harhar, Morocco
Kuzhuvelil B. Harikumar, India
Mohammad Hashem Hashempur, Iran
Muhammad Ali Hashmi, Pakistan
Waseem Hassan, Pakistan
Sandrina A. Heleno, Portugal
Pablo Herrero, Spain
Soon S. Hong, Republic of Korea
Md. Akil Hossain, Republic of Korea
Muhammad Jahangir Hossen, Bangladesh
Shih-Min Hsia, Taiwan
Ching-Liang Hsieh, Taiwan
Xiao-Yang (Mio) Hu, United Kingdom
Weicheng Hu, China
Sen Hu, China
Changmin Hu, China

Tao Hu, China
Sheng-Teng Huang, Taiwan
Ciara Hughes, Ireland
Attila Hunyadi, Hungary
Tarique Hussain, Pakistan
Maria-Carmen Iglesias-Osma, Spain
Elisha R. Injeti, USA
H. Stephen Injeyan, Canada
Amjad Iqbal, Pakistan
Chie Ishikawa, Japan
Angelo A. Izzo, Italy
Mohieddin Jafari, Finland
Satveer Jagwani, USA
Rana Jamous, Palestinian Authority
Muhammad Saeed Jan, Pakistan
G. K. Jayaprakasha, USA
Kamani Ayoma Perera Wijewardana
Jayatilaka, Sri Lanka
Kyu Shik Jeong, Republic of Korea
Qing Ji, China
Yanxia Jin, China
Hualiang Jin, China
Leopold Jirovetz, Austria
Won-Kyo Jung, Republic of Korea
Jeeyoun Jung, Republic of Korea
Atul Kabra, India
Sleman Kadan, Israel
Takahide Kagawa, Japan
Nurkhalida Kamal, Saint Vincent and the
Grenadines
Atsushi Kameyama, Japan
Wenyi Kang, China
Kyungsu Kang, Republic of Korea
Shao-Hsuan Kao, Taiwan
Juntra Karbwang, Japan
Nasiara Karim, Pakistan
Morimasa Kato, Japan
Deborah A. Kennedy, Canada
Asaad Khalid Khalid, Saudi Arabia
Haroon Khan, Pakistan
Washim Khan, USA
Bonglee Kim, Republic of Korea
Kyungho Kim, Republic of Korea
Yun Jin Kim, Malaysia
Junghyun Kim, Republic of Korea
Dong Hyun Kim, Republic of Korea
Youn-Chul Kim, Republic of Korea

Cheorl-Ho Kim, Republic of Korea
Jin-Kyung Kim, Republic of Korea
Kibong Kim, Republic of Korea
Woojin Kim, Republic of Korea
Yoshiyuki Kimura, Japan
Nebojša Kladar, Serbia
Mi Mi Ko, Republic of Korea
Toshiaki Kogure, Japan
Jian Kong, USA
Malcolm Koo, Taiwan
Yu-Hsiang Kuan, Taiwan
Robert Kubina, Poland
Omer Kucuk, USA
Victor Kuete, Cameroon
Woon-Man Kung, Taiwan
Chan-Yen Kuo, Taiwan
Joey S. W. Kwong, China
Kuang C. Lai, Taiwan
Fanuel Lampiao, Malawi
Ilaria Lampronti, Italy
Chou-Chin Lan, Taiwan
Mario Ledda, Italy
Sang Yeoup Lee, Republic of Korea
Dong-Sung Lee, Republic of Korea
Kyu Pil Lee, Republic of Korea
Jeong-Sang Lee, Republic of Korea
Byung-Cheol Lee, Republic of Korea
Namhun Lee, Republic of Korea
Yun Jung Lee, Republic of Korea
Gihyun Lee, Republic of Korea
Harry Lee, China
Ju Ah Lee, Republic of Korea
Ankita Leekha, USA
Christian Lehmann, Canada
Marivane Lemos, Brazil
George B. Lenon, Australia
Marco Leonti, Italy
Xing Li, China
Min Li, China
XiuMin Li, Armenia
Chun-Guang Li, Australia
Xuqi Li, China
Hua Li, China
Yi-Rong Li, Taiwan
Yu-cui Li, China
Xi-Wen Liao, China
Vuanghao Lim, Malaysia

Bi-Fong Lin, Taiwan
Shuibin Lin, China
Shih-Chao Lin, Taiwan
Ho Lin, Taiwan
Kuo-Tong Liou, Taiwan
Chian-Jiun Liou, Taiwan
Christopher G. Lis, USA
Gerhard Litscher, Austria
I-Min Liu, Taiwan
Jingping Liu, China
Xiaosong Liu, Australia
Suhuan Liu, China, China
Yujun Liu, China
Emilio Lizarraga, Argentina
Monica Loizzo, Italy
Nguyen Phuoc Long, Republic of Korea
Victor López, Spain
Zaira López, Mexico
Chunhua Lu, China
Ángelo Luís, Portugal
Anderson Luiz-Ferreira, Brazil
Jian-Guang Luo, China
Ivan Luzardo Luzardo-Ocampo, Mexico
Zheng-tao Lv, China
Michel Mansur Machado, Brazil
Filippo Maggi, Italy
Jamal A. Mahajna, Israel
Juraj Majtan, Slovakia
Toshiaki Makino, Japan
Nicola Malafrente, Italy
Giuseppe Malfa, Italy
Francesca Mancianti, Italy
Subashani Maniam, Australia
Carmen Mannucci, Italy
Arroyo-Morales Manuel, Spain
Juan M. Manzanegue, Spain
Fatima Martel, Portugal
Simona Martinotti, Italy
Carlos H. G. Martins, Brazil
Stefania Marzocco, Italy
Maulidiani Maulidiani, Malaysia
Andrea Maxia, Italy
Avijit Mazumder, India
Isac Medeiros, Brazil
Ahmed Mediani, Malaysia
Lewis Mehl-Madrona, USA
Ayikoé Guy Mensah-Nyagan, France

Oliver Micke, Germany
Maria G. Miguel, Portugal
Luigi Milella, Italy
Roberto Miniero, Italy
Letteria Minutoli, Italy
Prashant Modi, India
Daniel Kam-Wah Mok, Hong Kong
Chaowalit Monton, Thailand
Changjong Moon, Republic of Korea
Albert Moraska, USA
Mark Moss, United Kingdom
Yoshiharu Motoo, Japan
Yoshiki Mukudai, Japan
Sakthivel Muniyan, USA
Laura Muñoz-Bermejo, Spain
Saima Muzammil, Pakistan
Massimo Nabissi, Italy
Siddavaram Nagini, India
Takao Namiki, Japan
Srinivas Nammi, Australia
Krishnadas Nandakumar, India
Vitaly Napadow, USA
Edoardo Napoli, Italy
Derek Tantoh Ndinteh, South Africa
Pratibha V. Nerurkar, USA
Jorddy Neves Cruz, Brazil
Benoit Banga N'guessan, Ghana
Marcello Nicoletti, Italy
Eliud Nyaga Mwaniki Njagi, Kenya
Cristina Nogueira, Brazil
Sakineh Kazemi Noureini, Iran
Rômulo Dias Novaes, Brazil
Martin Offenbaecher, Germany
Yoshiji Ohta, Japan
Oluwafemi Adeleke Ojo, Nigeria
Olumayokun A. Olajide, United Kingdom
Olufunmiso Olusola Olajuyigbe, Nigeria
Mozaniel Oliveira, Brazil
Luís Flávio Oliveira, Brazil
Atolani Olubunmi, Nigeria
Abimbola Peter Oluyori, Nigeria
Timothy Omara, Uganda
Vahidreza Ostadmohammadi, Iran
Chiagoziem Anariochi Otuechere, Nigeria
Mustafa Ozyurek, Turkey
Ester Pagano, Italy
Sokcheon Pak, Australia

Antônio Palumbo Jr, Brazil
Zongfu Pan, China
Yunbao Pan, China
Siyaram Pandey, Canada
Niranjan Parajuli, Nepal
Wansu Park, Republic of Korea
Gunhyuk Park, Republic of Korea
Rodolfo Parreira, Brazil
Mohammad Mahdi Parvizi, Iran
Matheus Pasquali, Brazil
Luiz Felipe Passero, Brazil
Visweswara Rao Pasupuleti, Malaysia
Dr. Mitesh Patel, India
Bhushan Patwardhan, India
Claudia Helena Pellizzon, Brazil
Weijun Peng, China
Cheng Peng, Australia
Shagufta Perveen, Saudi Arabia
Raffaele Pezzani, Italy
Sonia Piacente, Italy
Andrea Pieroni, Italy
Richard Pietras, USA
Haifa Qiao, USA
Sheng Qin, China
Cláudia Quintino Rocha, Brazil
Khalid Rahman, United Kingdom
Nor Fadilah Rajab, Malaysia
Elia Ranzato, Italy
Manzoor A. Rather, India
Valentina Razmovski-Naumovski, Australia
Julita Regula, Poland
Kanwal Rehman, Pakistan
Gauhar Rehman, Pakistan
Man Hee Rhee, Republic of Korea
Daniela Rigano, Italy
José L. Rios, Spain
Francisca Rius Diaz, Spain
Eliana Rodrigues, Brazil
Maan Bahadur Rokaya, Czech Republic
Barbara Romano, Italy
Mariangela Rondanelli, Italy
Antonietta Rossi, Italy
DANIELA RUSSO, Italy
Mi Heon Ryu, Republic of Korea
Bashar Saad, Palestinian Authority
Abdul Sadiq, Pakistan
Sabiha Saheed, South Africa

Mohamed Z.M. Salem, Egypt
Avni Sali, Australia
Andreas Sandner-Kiesling, Austria
Manel Santafe, Spain
José Roberto Santin, Brazil
Antonietta Santoro, Italy
Tadaaki Satou, Japan
Roland Schoop, Switzerland
Sven Schröder, Germany
Sindy Seara-Paz, Spain
Veronique Seidel, United Kingdom
Dr. Vijayakumar Sekar, China
Terry Selfe, USA
Senthamil R. Selvan PhD, USA
Arham Shabbir, Pakistan
Suzana Shahr, Malaysia
Hongcai Shang, China
Wen-Bin Shang, China
Xiaofei Shang, China
Ronald Sherman, USA
Karen J. Sherman, USA
She-Po Shi, China
San-Jun Shi, China
Insop Shim, Republic of Korea
Im Hee Shin, Republic of Korea
Yukihiro Shoyama, Japan
Morry Silberstein, Australia
Samuel Martins Silvestre, Portugal
Moganavelli Singh, South Africa
Rajeev K Singla, China
Kuttulebbai N. S. Sirajudeen, Malaysia
slim smaoui, Tunisia
Eun Jung Sohn, Republic of Korea
Francisco Solano, Spain
Maxim A. Solovchuk, Taiwan
Chang G. Son, Republic of Korea
Young-Jin Son, Republic of Korea
Chengwu Song, China
Yanting Song, China
Klaokwan Srisook, Thailand
Vanessa Steenkamp, South Africa
Annarita Stringaro, Italy
Dan Su, China
Shan-Yu Su, Taiwan
Keiichiro Sugimoto, Japan
Valeria Sulsen, Argentina
Zewei Sun, China

Amir Syahir, Malaysia
Sharifah S. Syed Alwi, United Kingdom
Eryvaldo Sócrates Tabosa do Egito, Brazil
Orazio Tagliatela-Scafati, Italy
Shin Takayama, Japan
Takashi Takeda, Japan
Amin Tamadon, Iran
Gianluca Tamagno, Ireland
Jun Jie Tan, Malaysia
Jing-Yu (Benjamin) Tan, Australia
qingfa Tang, China
Nader Tanideh, Iran
Jun-Yan Tao, China
Hamid Tebyaniyan, Iran
Lay Kek Teh, Malaysia
Norman Temple, Canada
Kamani H. Tennekoon, Sri Lanka
Seong Lin Teoh, Malaysia
Mencherini Teresa, Italy
Mayank Thakur, Germany
Menaka Thounaojam, USA
Jinhui Tian, China
Michał Tomczyk, Poland
Loren Toussaint, USA
Md. Sahab Uddin, Bangladesh
Riaz Ullah, Saudi Arabia
Philip F. Uzor, Nigeria
Patricia Valentao, Portugal
Luca Vanella, Italy
Antonio Vassallo, Italy
Cristian Vergallo, Italy
Miguel Vilas-Boas, Portugal
Santos Villafaina, Spain
Aristo Vojdani, USA
Abraham Wall-Medrano, Mexico
Jin-Yi Wan, USA
Chunpeng Wan, China
Almir Gonçalves Wanderley, Brazil
Youhua Wang, China
Huijun Wang, China
Ke-Lun Wang, Denmark
Chong-Zhi Wang, USA
Ting-Yu Wang, China
Jia-bo Wang, China
Jin''An Wang, China
Qi-Rui Wang, China
Shu-Ming Wang, USA



Xiao Wang, China
Yong Wang, China
Guang-Jun Wang, China
Yun WANG, China
Xue-Rui Wang, China
Ru-Feng Wang, China
Kenji Watanabe, Japan
Jintanaporn Wattanathorn, Thailand
Silvia Wein, Germany
Meng-Shih Weng, Taiwan
Jenny M. Wilkinson, Australia
Katarzyna Winska, Poland
Sok Kuan Wong, Malaysia
Christopher Worsnop, Australia
Xian Wu, USA
Jih-Huah Wu, Taiwan
Sijin Wu, China
Xu Wu, China
Zuoqi Xiao, China
Rafael M. Ximenes, Brazil
Guoqiang Xing, USA
JiaTuo Xu, China
Yong-Bo Xue, China
Mei Xue, China
Haruki Yamada, Japan
Nobuo Yamaguchi, Japan
Jing-Wen Yang, China
Longfei Yang, China
Wei-Hsiung Yang, USA
Qin Yang, China
Sheng-Li Yang, China
Junqing Yang, China
Mingxiao Yang, Hong Kong
Swee Keong Yeap, Malaysia
Albert S. Yeung, USA
Ebrahim M. Yimer, Ethiopia
Yoke Keong Yong, Malaysia
Fadia S. Youssef, Egypt
Zhilong Yu, Canada
Yanggang Yuan, China
Hilal Zaid, Israel
Paweł Zalewski, Poland
Armando Zarrelli, Italy
Y Zeng, China
Xiaobin Zeng, Shenzhen People's Hospital,
2nd Clinical Medical College of Jinan












University, Shenzhen 518120, Guangdong
Province, China, China
Bimeng Zhang, China
Zhiqian Zhang, China
Jianliang Zhang, China
Mingbo Zhang, China
Jiu-Liang Zhang, China
Fangbo Zhang, China
RONGJIE ZHAO, China
Jing Zhao, China
Zhangfeng Zhong, Macau
Yan Zhu, USA
Guoqi Zhu, China
Suzanna M. Zick, USA
Stephane Zingue, Cameroon

Contents






Computer-Aided Drug Design of Natural Candidates for the Treatment of Non-Communicable Diseases

Hilal Zaid , Siba Shanak , and Akhilesh K. Tamrakar
Editorial (3 pages), Article ID 9769173, Volume 2022 (2022)








Overexpression of MAL2 Correlates with Immune Infiltration and Poor Prognosis in Breast Cancer

Yue Zhong , Zhenjie Zhuang , PeiJu Mo , Qi Shang , Mandi Lin , JiaQian Gong , JiaRong Huang , HaiYan Mo , and Mei Huang 
Research Article (15 pages), Article ID 5557873, Volume 2021 (2021)

In Vitro and In Silico Evaluation for the Inhibitory Action of *O. basilicum* Methanol Extract on α -Glucosidase and α -Amylase

Siba Shanak , Najlaa Bassalat , Raghad Albzoor , Sleman Kadan , and Hilal Zaid 
Research Article (9 pages), Article ID 5515775, Volume 2021 (2021)

Tyrosinase Inhibitors from the Stems of *Streblus ilicifolius*

Nhan T. Nguyen , Phu H. Dang , Hai X. Nguyen , Truong N. V. Do , Tho H. Le , Tuyen Q. H. Le , and Mai T. T. Nguyen 
Research Article (7 pages), Article ID 5561176, Volume 2021 (2021)

Investigation of the Mechanism of Traditional Chinese Medicines in Angiogenesis through Network Pharmacology and Data Mining

Wingyan Yun , Wenchao Dan , Jinlei Liu , Xinyuan Guo , Min Li , and Qingyong He 
Research Article (13 pages), Article ID 5539970, Volume 2021 (2021)



Computer-Aided Drug Discovery Identifies Alkaloid Inhibitors of Parkinson's Disease Associated Protein, Prolyl Oligopeptidase

Apoorva M. Kulkarni, Shailima Rampogu, and Keun Woo Lee 
Research Article (10 pages), Article ID 6687572, Volume 2021 (2021)









The Use of Traditional Chinese Medicine in Relieving EGFR-TKI-Associated Diarrhea Based on Network Pharmacology and Data Mining

Shuaihang Hu , Wenchao Dan , Jinlei Liu , Peng Ha, Tong Zhou, Xinyuan Guo , and Wei Hou 
Research Article (16 pages), Article ID 5530898, Volume 2021 (2021)




Virtual Screening of Cablin Patchouli Herb as a Treatment for Heat Stress: A Study Based on Network Pharmacology, Molecular Docking, and Experimental Verification

Yan Xu, Lizhong Ding, Zhongtian Wang, Yanbo Wang , and Liping Sun 
Research Article (14 pages), Article ID 8057587, Volume 2021 (2021)

Design and Synthesis of 4-O-Podophyllotoxin Sulfamate Derivatives as Potential Cytotoxic Agents






Ammar Bader , Majdi M. Bkhaitan , Ashraf N. Abdalla , Qasem M. A. Abdallah , Hamed I. Ali , Dima A. Sabbah , Ghadeer Albadawi , and Ghassan M. Abushaikha 
Research Article (7 pages), Article ID 6672807, Volume 2021 (2021)

Use of Network Pharmacology to Investigate the Mechanism by Which Allicin Ameliorates Lipid Metabolism Disorder in HepG2 Cells

Bijun Cheng , Tianjiao Li , and Fenglin Li 


Research Article (11 pages), Article ID 3956504, Volume 2021 (2021)

Diarylalkanoids as Potent Tyrosinase Inhibitors from the Stems of *Semecarpus caudata*

Phu H. Dang , Tho H. Le , Truong N. V. Do , Hai X. Nguyen , Mai T. T. Nguyen , and Nhan T. Nguyen 



Research Article (8 pages), Article ID 8872920, Volume 2021 (2021)

Determining Pharmacological Mechanisms of Chinese Incompatible Herbs Fuzi and Banxia in Chronic Obstructive Pulmonary Disease: A Systems Pharmacology-Based Study

Kaiwen Ni, Xiaolu Cai, Yaling Chen, Linshui Zhou, Ruilin Chen, Suqun Zheng, and Zhen Wang 

Research Article (14 pages), Article ID 8365603, Volume 2020 (2020)

To Explore the Mechanism and Equivalent Molecular Group of Fuxin Mixture in Treating Heart Failure Based on Network Pharmacology

Yi-ding Yu , Yi-ping Xiu, Yang-fan Li, and Yi-tao Xue 

Research Article (10 pages), Article ID 8852877, Volume 2020 (2020)

Study on Medication Rules of Traditional Chinese Medicine against Antineoplastic Drug-Induced Cardiotoxicity Based on Network Pharmacology and Data Mining

Wenchao Dan , Jinlei Liu , Xinyuan Guo , Boran Zhang , Yi Qu , and Qingyong He 

Research Article (15 pages), Article ID 7498525, Volume 2020 (2020)

Editorial

Computer-Aided Drug Design of Natural Candidates for the Treatment of Non-Communicable Diseases

Hilal Zaid ^{1,2}, Siba Shanak ³ and Akhilesh K. Tamrakar⁴

¹Qasemi Research Center-Al-Qasemi Academy, P.O. Box 124, Baqa El-Gharbia 30100, Israel

²Faculty of Medicine, Arab American University, P.O. Box 240, Jenin, State of Palestine

³Faculty of Sciences, Arab American University, P.O. Box 240, Jenin, State of Palestine

⁴CSIR-Central Drug Research Institute, Lucknow 226031, India

Correspondence should be addressed to Hilal Zaid; hilal.zaid@gmail.com

Received 21 November 2021; Accepted 22 April 2022; Published 26 June 2022

Copyright © 2022 Hilal Zaid et al. This is an open access article distributed under the Creative Commons Attribution License, which permits unrestricted use, distribution, and reproduction in any medium, provided the original work is properly cited.

Noncommunicable diseases (NCDs) impose a significant burden on the health care systems in developed and developing countries. Indeed, the incidence of NCDs (e.g., diabetes, cancers, chronic respiratory diseases, and cardiovascular diseases) has increased in epidemic proportions worldwide [1]. According to estimates made by the WHO, about 41 million people die annually worldwide, equivalent to 71% of all deaths, because of NCDs. 37% of those who died with NCDs are between the ages 30 and 69 years old. Lack of access to essential medicines for NCDs is a major challenge, especially in developing countries [2, 3].

Drug discovery for medicinal plant provides important leads against various pharmacological targets. A large number of plants used in the traditional medicine have now become a part of the modern world health care system. Natural novel drugs are now more achievable due to modern techniques for separation, structure elucidation, screening, and bio- and chemo-informatics [4, 5].

Over the last decades, the amount of biological and chemical information has escalated drastically. Thus, the need for new scientific branches that handle big data has arisen. Computational chemistry and bioinformatics are now well-established scientific fields that offer the scientific community the opportunity to study drug-disease relationship. One such way to study this relationship is via understanding the connection of the disease to the target, and the consequent mechanism of interaction between the target and the drug [6, 7].

The heterogeneity and lacking of enough data can be an obstacle that hinders the mechanistic comprehension of drug-disease relationship. In this regard, predictive computational approaches in the field of computational chemistry, e.g., network pharmacology approaches, predictive ADMET (absorption, distribution, metabolism, and elimination-toxicity), and pharmacophore modeling, can be used to build scientific algorithms, which are developed to overcome this barrier [8, 9]. Such approaches are cost-effective in identifying drug candidates, as they limit the extensive use of animal models against all plausible lead compounds, while identifying safe and effective drugs. Within this field of research, we launched a research topic entitled “Computer-Aided Drug Design of Natural Candidates for the Treatment of Non-Communicable Diseases.” For the aforementioned reasons, this research topic attracted the attention of scientists and received a number of submitted manuscripts. Twenty-one papers were submitted for publication in this issue. After an extensive review process, thirteen original research articles have been published within this special research topic. These research articles cover various topics in drug design, reporting advance in *in silico* methods in drug discovery.

Network pharmacology has emerged as an important tool to understand the mechanism of action of a drug/drug candidate. It uses computational power to systematically catalogue the molecular interactions of a drug molecule in a living cell. Hu et al. exploited network pharmacology and data mining to elucidate the role of traditional Chinese

medicine (TCM) in relieving epidermal growth factor receptor-tyrosine kinase inhibitor (EGFR-TKI)-associated diarrhea. Using various approaches, they obtained 23 potential therapeutic TCM targets for the treatment of EGFR-TKI-related diarrhea. Based on the findings, they proposed that TCMs can provide data to support experimental and clinical studies on the relief of EGFR-TKI-associated diarrhea. Concomitantly, Xu et al. presented a pioneer report on the use of TCM to treat summer fever, especially in children.

Yun et al. aimed to provide the basis for understanding the mechanisms of action for active ingredients of TCM against angiogenesis. GeneCards was used to explore angiogenesis-related targets. The TCM system pharmacology platform was used to uncover natural compounds. Target-compound, compound-medicine, and target-compound-medicine networks were constructed using Cytoscape. To predict the target-compound binding, molecular docking was used. Of 79 targets for angiogenesis, 41 targets were matched to 3839 compounds. 110 compounds from the dataset were found to have high correlation with angiogenesis. As a result of molecular docking, fifty-five combinations were constructed. Top combinations were for PTGS2-astragalin (-9.18 kcal/mol), KDR-astragalin (-7.94 kcal/mol), PTGS2-quercetin (-7.41 kcal/mol), and PTGS2-myricetin (-7.21 kcal/mol). Using the network, eighty other combinations were obtained and classified according to their affinities. Top combinations were KDR-beta-carotene (-10.13 kcal/mol), MMP9-beta-sitosterol (-8.04 kcal/mol), MMP9-astragalin (-7.82 kcal/mol), and MMP9-diosgenin (-7.51 kcal/mol).

Cheng et al. described use of network pharmacology to investigate the mechanism of action of allicin to modulate lipid metabolism for the management of NAFLD. Using an *in vitro* cellular model, they predicted two hundred and nineteen potential targets of allicin PharmMapper. Out of those, 44 potential targets related to lipid metabolism were screened out as protein targets of allicin. In the same line, Ni et al. determined pharmacological mechanisms of Chinese incompatible herbs Fuzi and Banxia (FB) in chronic obstructive pulmonary disease (COPD) using network pharmacology. From the identified targets, they proposed that effect of FB against COPD may involve the regulation of immunological function. This study provides an excellent example of the application of network pharmacology in evaluating mechanisms of action and molecular targets of an herb. Another study by Dan et al. explored the material basis and the rule of TCM against antineoplastic drug-induced cardiotoxicity (ADIC) using network pharmacology and data mining. They identified 21 potential targets, 332 candidate compounds, and 400 kinds of herbs for the management of ADIC.

Two new tyrosinase inhibitors from the stems of *Streblus ilicifolius* were reported by Nguyen et al. One molecule possesses strong tyrosinase inhibitory activity with an IC_{50} value of 0.01 μ M. Docking studies showed different binding affinity of the two molecules for *oxy*-tyrosinase. An independent study by Bader et al. presented the design and synthesis of 4-O-podophyllotoxin sulfamate derivatives and

their evaluation in various cancer cell lines as potential cytotoxic agents.

Yu et al. conducted network pharmacology to uncover the possible mechanisms in Fuxin mixture or FXHJ for the treatment of heart failure. Ingredients of FXHJ were analysed, and 39 active ingredients were explored. 47 action targets were found to bind to these compounds. The network was constructed and enrichment analysis undertaken. The treatment of heart failure by FXHJ mixture was predicted to be via regulating several cascades, including the MAPK signaling pathway, PI3K/Akt signaling pathway, cAMP signaling pathway, TNF signaling pathway, toll-like receptor signaling pathway, VEGF signaling pathway, NF-kappa B signaling pathway, and the apoptotic signaling molecule BCL2.

The manuscript by Shanak et al. presented the inhibitory effect of the *Ocimum basilicum* extract and its major constituents on α -amylase and α -glucosidase using *in vitro* and *in silico* techniques and proposed *Ocimum basilicum* as a potential source to identify antidiabetic leads [10]. Similarly, Dang et al. conducted an *in vitro* and *in silico* study, where two new diarylalkanoids, semedienone, and semetrienone were isolated from a $CHCl_3$ -soluble extract of the stems of *Semecarpus caudata* (Anacardiaceae), and their structures were resolved using NMR. These compounds were analysed for their inhibitory activity against tyrosinase inhibitory activity, and the IC_{50} values were 0.033 and 0.11 μ M, respectively. *In silico* docking studies of the two compounds against *oxy*-tyrosinase were carried out to analyze their interactions. Of the two compounds, semedienone showed decent interactions with the amino acid and peroxide group residues of the target enzyme.

Protein alpha synuclein is a protein that shows high accumulation during Parkinson's disease. Prolyl oligopeptidase (POP) is a serine protease that was shown to affect the accumulation of alpha synuclein and is a key target for the treatment of Parkinson's disease. Kulkarni et al. carried out an *in silico* study to evaluate the efficacy of an alkaloid class of phytochemicals against POP. Chemical Entities of Biological Interest (ChEBI), a publicly available database was used to retrieve the chemicals. Discovery Studio was used to predict the ADMET properties of the alkaloids to calculate their drug likeness using the Lipinski's rule of 5 and to filter the parameters based on their feasibility for the central nervous system and to cross the blood-brain barrier (BBB). To scan the strength of compound-target binding, molecular docking was performed followed by molecular dynamic (MD) simulations that enable checking the stability of alkaloid-protein complexes. The following alkaloids were selected as plausible lead compounds against POP: metergolone, pipercollosine, celacinnine, lobeline, cystodytin G, lycoperine A, hookerianamide J and martefragin A. Among these, metergolone, pipercollosine, hookerianamide J, and lobeline showed the most promising results comparable docking scores to three POP inhibitors that had reached clinical trials, i.e., Z-321, S-17092, and JTP-4819. MD simulations showed high stability of the plausible lead compounds in the active site when compared to the binding modes of the known inhibitors.

Myelin and lymphocyte and T cell differentiation protein 2 (MAL2) are expressed in several forms of cancer, including breast cancer. Zhong et al. studied the relationship between the expression of MAL2 and breast cancer using the Oncomine database and the Cancer Genome Atlas database. Quantitative real-time polymerase chain reaction (RT-qPCR) was used to measure MAL2 expression experimentally. Gene set enrichment analysis (GSEA) was used to identify the biological pathways correlated with MAL2 expression in breast cancer, e.g., the relationship between the level of immune infiltration and MAL2 in breast cancer. Experimental and computational techniques showed that MAL2 was expressed at high levels in breast cancer tissues compared with the surrounding tissues. As a result, high MAL2 expression can be used as an independent biomarker for breast cancer. MAL2 expression level was also found to correlate with lower immune infiltrating levels in breast cancer.

Conflicts of Interest

The authors declare that there are no conflicts of interest.

Hilal Zaid

Siba Shanak

Akhilesh K. Tamrakar

Acknowledgments

The authors are thankful to all authors who contributed to this special issue. The authors are grateful to Dr. Thomas Linn and the reviewers for their constructive criticisms and timely response that made this special issue possible. The editorial board hope that readers will enjoy this special issue.

References

- [1] H. Zaid, A. K. Tamrakar, M. S. Razzaque, and T. Efferth, "Diabetes and metabolism disorders medicinal plants: a glance at the past and a look to the future," *Evidence-based Complementary and Alternative Medicine*, vol. 2018, Article ID 5843298, 2018.
- [2] Y. Wang and J. Wang, "Modelling and prediction of global non-communicable diseases," *BMC Public Health*, vol. 20, no. 1, pp. 822–835, 2020.
- [3] A. Cameron, M. Ewen, D. Ross-Degnan, and D. Ball, "Medicine prices, availability, and affordability in 36 developing and middle-income countries: a secondary analysis," *The Lancet*, vol. 373, no. 9659, pp. 240–249, 2009.
- [4] N. E. Thomford, D. A. Senthebane, A. Rowe et al., "Natural Products for drug discovery in the 21st century: innovations for novel drug discovery," *International Journal of Molecular Sciences*, vol. 25, no. 6, p. 1578, 2018.
- [5] J. K. Weng, R. N. Philippe, and J. P. Noel, "The rise of chemodiversity in plants," *Science*, vol. 336, no. 6089, pp. 1667–1670, 2012.
- [6] R. L. Davis, "Mechanism of action and target identification: a matter of timing in drug discovery," *iScience*, vol. 23, no. 9, Article ID 101487, 2020.
- [7] J. P. Hughes, S. Rees, S. B. Kalindjian, and K. L. Philpott, "Principles of early drug discovery," *British Journal of Pharmacology*, vol. 162, no. 6, pp. 1239–1249, 2011.
- [8] A. F. Moubock, J. Li, P. Mishra, M. Gao, and S. Günther, "Current computational methods for predicting protein interactions of natural products," *Computational and Structural Biotechnology Journal*, vol. 17, pp. 1367–1376, 2019.
- [9] F. E. Agamah, G. K. Mazandu, R. Hassan et al., "Computational/in silico methods in drug target and lead prediction," *Briefings in Bioinformatics*, vol. 21, no. 5, pp. 1663–1675, 2020.
- [10] S. Kadan, B. Saad, Y. Sasson, and H. Zaid, "In vitro evaluation of anti-diabetic activity and cytotoxicity of chemically analyzed *Ocimum basilicum* extracts," *Food Chemistry*, vol. 196, pp. 1066–1074, 2016.

Research Article

Overexpression of MAL2 Correlates with Immune Infiltration and Poor Prognosis in Breast Cancer

Yue Zhong ¹, Zhenjie Zhuang ¹, PeiJu Mo ¹, Qi Shang ¹, Mandi Lin ²,
JiaQian Gong ¹, JiaRong Huang ¹, HaiYan Mo ¹, and Mei Huang ²

¹Guangzhou University of Chinese Medicine, Guangzhou, Guangdong, China

²Department of Breast Diseases, The First Affiliated Hospital of Guangzhou University of Chinese Medicine, Guangzhou, Guangdong, China

Correspondence should be addressed to Mei Huang; huangmeigztc@163.com

Received 26 January 2021; Revised 7 July 2021; Accepted 9 August 2021; Published 15 September 2021

Academic Editor: Siba Shanak

Copyright © 2021 Yue Zhong et al. This is an open access article distributed under the Creative Commons Attribution License, which permits unrestricted use, distribution, and reproduction in any medium, provided the original work is properly cited.

Background. Myelin and lymphocyte, T cell differentiation protein 2 (MAL2) is highly expressed in various cancers and associated with the development and prognosis of cancer. However, the relationship between MAL2 and breast cancer requires further investigation. This study aimed to explore the prognostic significance of MAL2 in breast cancer. **Methods.** MAL2 expression was initially assessed using the Oncomine database and The Cancer Genome Atlas (TCGA) database and verified by quantitative real-time polymerase chain reaction (RT-qPCR). The chi-square test or Fisher's exact test was used to explore the association between clinical characteristics and MAL2 expression. The prognostic value of MAL2 in breast cancer was assessed by the Kaplan–Meier method and Cox regression analysis. Gene set enrichment analysis (GSEA) was performed to identify the biological pathways correlated with MAL2 expression in breast cancer. Besides, a single-sample GSEA (ssGSEA) was used to assess the relationship between the level of immune infiltration and MAL2 in breast cancer. **Results.** Both bioinformatics and RT-qPCR results showed that MAL2 was expressed at high levels in breast cancer tissues compared with the adjacent tissues. The chi-square test or Fisher's exact test indicated that MAL2 expression was related to stage, *M* classification, and vital status. Kaplan–Meier curves implicated that high MAL2 expression was significantly associated with the poor prognosis. Cox regression models showed that high MAL2 expression could be an independent risk factor for breast cancer. GSEA showed that 14 signaling pathways were enriched in the high-MAL2-expression group. Besides, the MAL2 expression level negatively correlated with infiltrating levels of eosinophils and plasmacytoid dendritic cells in breast cancer. **Conclusion.** Overexpression of MAL2 correlates with poor prognosis and lower immune infiltrating levels of eosinophils and plasmacytoid dendritic cells in breast cancer and may become a biomarker for breast cancer prognosis.

1. Introduction

Among women, breast cancer is the most commonly diagnosed cancer and the main cause of cancer death [1]. The incidence of breast cancer has increased every year [2]. Nearly 3.8 million women in the United States have been diagnosed with breast cancer, including 268,600 new cases in 2019 [3].

Despite the advances in surgery, chemotherapy, radiotherapy, and endocrine therapy for breast cancer, more than 20% of patients still develop metastatic disease with a poor prognosis [4]. Since the molecular mechanisms of breast

cancer remain unclear, the identification of novel prognostic biomarkers for breast cancer is necessary, which could contribute to the early detection and treatment of breast cancer [5]. MAL2, as an essential member of the MAL proteolipid family, is a four-pass membrane protein consisting of 176 amino acid residues. By encoding a multi-transmembrane protein, MAL2 mainly participates in endocytosis under physiological conditions and mediates the transport of substances between cells [6]. MAL2 is located in chromosome 8q23, an area where the copy number often increases in various types of cancer [7]. Previous studies have confirmed the increased expression of MAL2 in ovarian

cancer [6], pancreatic cancer [8], thyroid cancer [9], and colorectal cancer [10]. Moreover, MAL2 expression was associated with pancreatic cancer and colorectal cancer overall survival [8], which suggested that MAL2 might be an important molecule involved in the progression and prognosis of tumors. Besides, MAL2 was recently identified as a breast cancer immunology target. Reduction of MAL2 in breast tumor cells can enhance CD8+ T cell-mediated cytotoxicity and inhibit the growth of breast tumors [11]. Although some previous studies suggested that MAL2 was overexpressed in breast cancer [7, 12, 13], the prognostic value of the MAL2 expression and its correlation with clinical features and immunotherapy in breast cancer requires further investigation, and whether MAL2 could be a specific marker for breast cancer still needs to be elucidated. In the present study, we applied a comprehensive strategy to uncover the importance of MAL2 in breast cancer.

2. Materials and Methods

2.1. Oncomine Database. The Oncomine database [14] (<http://www.oncomine.org>), a gene chip-based database and data mining platform, served to analyze the expression of MAL2 in various types of cancers. The filter conditions set were as follows: gene, MAL2; cancer type, breast cancer; differential analysis, cancer vs normal analysis; and data type, mRNA. Besides, we selected P value = $1E-4$, twofold change, and top 10% gene rank as the threshold [15]. All statistical methods and results were obtained from Oncomine.

2.2. The Cancer Genome Atlas. The Cancer Genome Atlas (TCGA) is a landmark cancer genomics program that comprised over 20,000 primary cancer data and matched normal samples spanning 33 cancer types. Raw counts of RNA-sequencing data and corresponding clinical information were obtained from The Cancer Genome Atlas (TCGA) data set (<https://www.cancer.gov/tcga>).

2.3. The Verification of MAL2 by qRT-PCR. Tumor tissues and paired adjacent tissues were collected from patients diagnosed with breast cancer at the First Affiliated Hospital of Guangzhou University of Chinese Medicine between 2019 and 2020. None of these patients received therapy before surgery. Specimens from surgery were stored at -80°C . Study approval was obtained from the Research Ethics Committee of the First Affiliated Hospital of Guangzhou University of Chinese Medicine, and patients signed informed consent forms before operation.

Total RNA was extracted from 32 pairs of breast cancer tissues and adjacent nontumor tissues frozen in liquid nitrogen using TRIzol reagent (Invitrogen, United States). The isolated RNA was measured at 260/280 nm using a NanoDrop 2000 spectrophotometer (Thermo Fisher Scientific, USA). Evo M-MLV RT Premix for qPCR (AG11706, China) was used to reverse-transcribe RNA into cDNA. According to the manufacturer's instructions, cDNAs were amplified using the SYBR Green Premix Pro Taq HS qPCR Kit (AG11701, China). β -actin was used as an internal control

for mRNA expression. The primer sequences were as follows: MAL2 Forward: 5'-ACGTAGCAGCCTCAATTTT-TGC-3' and Reverse: 5'-CATCTTCGTAAAGCCAGACCC-3'; β -actin, forward: 5'-TGGCACCCAGCACAATGAA-3' and reverse: 5'-CTAAGTCATAGTCCGCCTAGAAGCA-3'. Each sample was carried out three times, and data were calculated using the $2^{-\Delta\Delta\text{Ct}}$ (2 to the power of minus Delta Delta CT) method.

2.4. Statistical Analyses. Data analysis was performed using SPSS software 26.0 (IBM Corporation, Armonk, NY, USA) and R version 3.6.3 [16]. The ggplot2 package [17] was used to draw boxplots of clinical features according to MAL2 expression variation. The chi-square test or Fisher's exact test was used to explore the association between clinical characteristics and MAL2 expression. The Wilcoxon signed rank sum test and Kruskal-Wallis test were utilized to measure the differential expression of MAL2 in the subgroup, including age; tumor (T), node (N), and metastasis (M) classification; estrogen receptor (ER) status; progesterone receptor (PR) status; human epidermal growth factor receptor-2 (HER2) status; and vital status. The impact of MAL2 expression levels on the overall survival (OS) of patients with breast cancer was analyzed by Kaplan-Meier curves using an R package named survminer [16].

Since we aimed to analyze the relationship of MAL2 with clinical features and its significance on the survival of patients with breast cancer, the median expression value of MAL2 was applied as a cut-off value for further analysis according to the previous studies [18–21]. Therefore, the median value of MAL2 expression was utilized as a cut-off value to divide patients with complete clinical data from the TCGA database into the high-MAL2-expression group and low-MAL2-expression group.

Then, the univariate and multivariate Cox analyses were performed to determine the related variables.

2.5. Gene Set Enrichment Analysis. Gene set enrichment analysis (GSEA) [22] was conducted to determine the biological processes activated in the low-MAL2-expression and high-MAL2-expression groups. GSEA software (version 4.0) was downloaded from their official website. Tumor tissue samples were divided into high-expression groups and low-expression groups according to the median value of MAL2 expression level. The gene set of `h.all.v7.4.symbols.gmt` and `c2.cp.kegg.v7.4.symbols.gmt`, containing a large number of tumors signaling pathway gene sets, were obtained from the MSigDB database. Depending on the default parameters of GSEA software, 1,000 times a random combination was used for enrichment analysis. Sorted by false discovery rates (FDRs), the gene set with $\text{FDR} < 0.25$ and normal P value < 0.05 was the significantly enriched gene set [22].

2.6. Immune Infiltration Analysis of MAL2. The transcripts per million (TPM) normalized RNA-seq data of breast cancer were downloaded from UCSC Xena (<https://xena.ucsc.edu/>) [23]. Twenty-eight immune gene sets, including

different classic immune cell types, were obtained from the study by Charoentong et al. [24]. Next, the ssGSEA was performed by R package GSVA [25] to assess the immune infiltration level of each sample of breast cancer and calculate the responding immune infiltration score based on the TPM data and gene sets [25]. Subsequently, Spearman's correlation analysis between the MAL2 expression data and the immune infiltration score of 28 immune gene sets was performed. The threshold was set as P value < 0.05 and $|r| \geq 0.3$ to filter the immune cell types that have significantly infiltrating level correlation with the MAL2 expression.

3. Results

3.1. Overexpression of MAL2 in Breast Cancer Based on Oncomine. We used Oncomine to analyze the difference between MAL2 tumor and normal tissues in different cancer types. Altogether, 214 different types of research results were collected in the Oncomine database. Among them, 25 results showed statistically different expressions of MAL2, including 13 with increased expression and 12 with decreased expression. Results revealed that the MAL2 expression level increased in breast, ovarian, prostate, and pancreatic cancers. On the contrary, MAL2 expression decreased in some cancer types, such as sarcoma, brain and CNS, esophageal, kidney, and lymphoma cancer (Figure 1(a)) [14]. To assess further the MAL2 expression in breast cancer, we analyzed MAL2 across six public expressions, containing 10 analyses from the Oncomine database. As a result, MAL2 was found to significantly upregulate in breast carcinoma tissues. Details are shown in Table 1. Based on the results of the meta-analysis of six data sets, including 10 analyses using the Oncomine database, the results indicated MAL2 overexpression in tumor tissues (median rank = 476.5, $P = 6.77E - 13$) (Figure 1(b)).

3.2. MAL2 Was Upregulated in Breast Cancer Tissues Compared with Adjacent Tissues Based on TCGA. The MAL2 expression data of 1098 breast cancer samples and 113 adjacent controls were retrieved from the TCGA database. We measured the differences in MAL2 expression in tumor and adjacent tissues using the independent-sample Wilcoxon rank sum test and the paired Wilcoxon rank sum test. Results showed that MAL2 expression was significantly higher in different tissues (tumor tissues vs. adjacent tissues, $P = 1.24e - 37$, Figure 2(a); paired tumor vs. adjacent tissues, $P = 1.139e - 37$, Figure 2(b)).

3.3. Verification of MAL2 Upregulation in Breast Cancer by RT-qPCR. To certify the difference in MAL2 expression in the TCGA data set, we performed RT-qPCR to detect the expression of MAL2 in 32 pairs of breast cancer tissues (including 32 tumor tissues and 32 adjacent tissues). The result showed that MAL2 mRNA was significantly increased in breast cancer tumors compared with adjacent tissues ($P = 0.0205$, Figure 2(c)), which was consistent with the Oncomine data sets analyses.

3.4. Association of MAL2 Expression with Clinical Features in Breast Cancer. We downloaded mRNA-seq data and clinical information of breast cancer patients from TCGA. There were 1211 cases of mRNA-seq data (1098 tumor samples; 113 adjacent tissues) derived from 1091 breast cancer patients in the TCGA database of 1090 equipped with complete clinical data. 1090 patients were finally enrolled in the study. The detailed clinical characteristics—age, gender, T , N , M classification, stage, ER, PR, HER2 status, vital status, and MAL2 expression—are presented in Table 2. In Figure 3, boxplots presented the MAL2 was expressed with the significant difference in the subgroup by M classification ($P = 0.0028$), ER status ($P = 0.016$), HER2 status ($P = 0.012$), and vital status ($P = 0.00014$).

3.5. Relationship between MAL2 Expression and Clinical Features in Breast Cancer. To determine correlations of MAL2 expression with clinical factors, we conducted a chi-square test. The median value of MAL2 expression was used to divide patients into a MAL2 high-expression group and a low-expression group. We observed that MAL2 expression was significantly associated with stage ($P = 0.044$), M classification ($P = 0.002$), and vital status ($P = 0.003$) (Table 3).

3.6. MAL2 Overexpression Independently Predicted Poor Overall Survival. Kaplan–Meier curves with the log-rank test were applied to explore the prognostic value of MAL2 expression and the overall breast cancer survival rate. As shown in Figure 4, breast cancer patients with high MAL2 expression were associated with worse overall survival ($P = 0.00093$). In addition, high MAL2 expression was associated with poor overall survival in old patients ($P = 0.0015$); clinical stage I/II and III/IV ($P = 0.028$ and $P = 0.033$); subgroup analysis of T classification ($T1/T2$ and $T3/T4$) ($P = 0.037$ and $P = 0.033$); patients with lymphatic invasion ($P = 0.0002$); patients with nondistant metastasis ($P = 0.00038$); and patients with positive ER, PR, and HER2 status ($P = 0.00026$, $P = 0.00028$, and $P = 0.0061$, respectively).

The univariate Cox proportional hazards model showed that MAL2 expression, stage, T classification, N classification, and M classification of breast cancer patients were significantly correlated with the prognosis of patients. Moreover, the multivariate Cox proportional hazards model indicated that high MAL2 expression (hazard ratio = 1.792, $P = 0.021$), stage (hazard ratio = 1.473, $P = 0.033$), and M classification (hazard ratio = 3.093, $P = 0.0018$) were independent risk factors for overall survival. The median overall survival of the high-expression group was 9.5 years, while that of the low-expression group was 18 years. Both the log-rank test and Cox proportional hazards model showed that the expression of MAL2 was significantly correlated with the prognosis of breast cancer. These results are described in Table 4 and Figure 5.

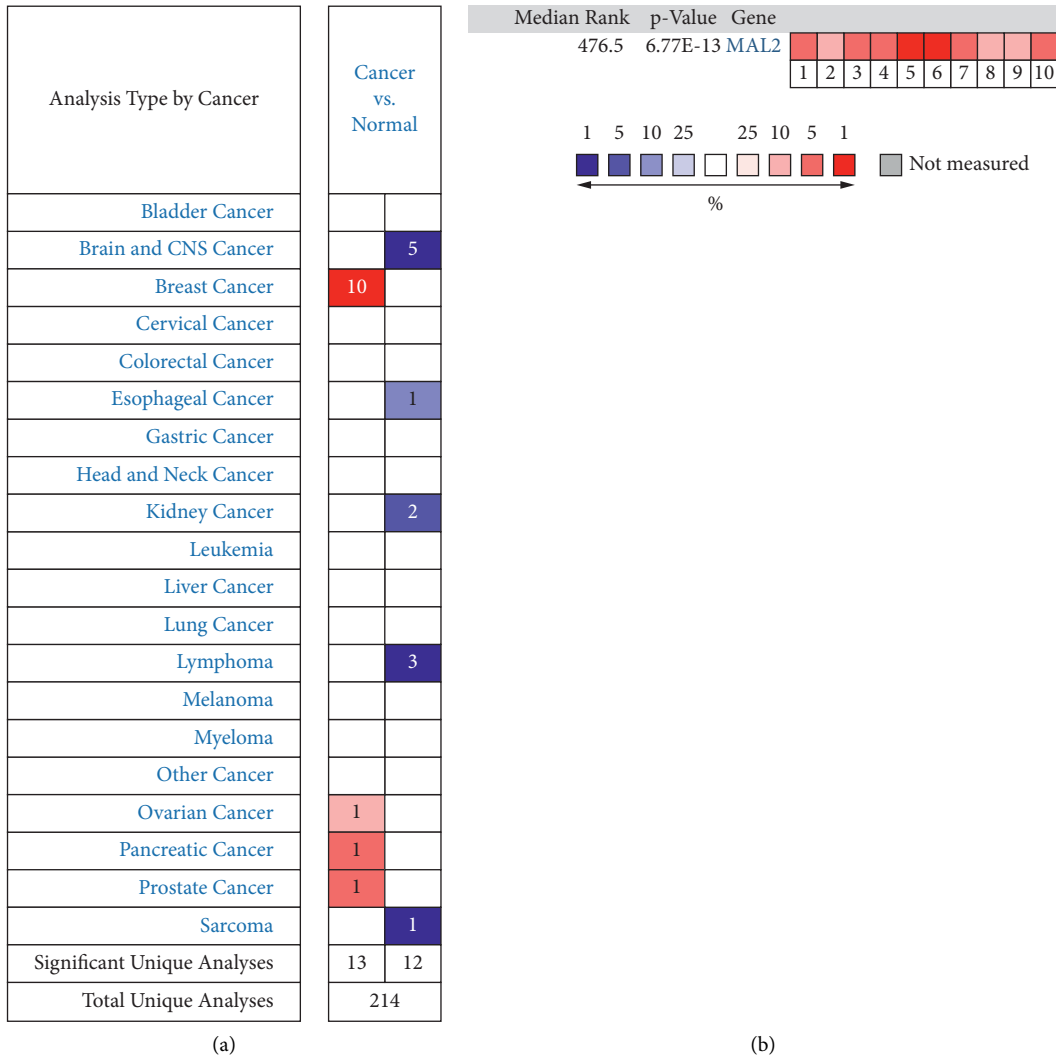


FIGURE 1: MAL2 expression in different types of cancers. (a) Expression of MAL2 gene in various cancers compared with matched normal tissues by the Oncomine database. Red and blue represent the number of data sets of increasing and decreasing MAL2 gene levels, respectively. (b) A meta-analysis of MAL2 expression across 10 analyses from the Oncomine database. Curtis breast (1–3), Ma breast (4), Perou breast (5), Sorlie breast (6–7), and TCGA breast (8–10). The colored squares represent the median rank of these genes (tumor tissues vs. normal tissues) across the 10 data sets. The significance level for the median rank analysis was set at $P < 0.05$.

TABLE 1: Details of MAL2 across six public expression data sets in the Oncomine database.

Data sets (sample size)	Comparison groups	Fold change	P value	Overexpression gene rank
Perou breast (65)	Ductal breast carcinoma vs. normal	3.586	1.59E-11	8 (in top 1%)
Sorlie breast (85)	Ductal breast carcinoma vs. normal	3.480	9.61E-9	31 (in top 1%)
Sorlie breast 2 (167)	Ductal breast carcinoma vs. normal	3.326	5.89E-5	148 (in top 3%)
Ma breast 4 (66)	Ductal breast carcinoma in situ epithelia vs. normal	2.417	5.26E-5	266 (in top 2%)
	Invasive ductal and invasive lobular breast carcinoma vs. normal	2.286	1.51E-27	432 (in top 3%)
Curtis breast (2136)	Tubular breast carcinoma vs. normal	2.093	1.80E-20	852 (in top 5%)
	Invasive ductal breast carcinoma vs. normal	2.168	5.89E-45	1803 (in top 10%)
	Invasive lobular breast carcinoma vs. normal	2.437	1.35E-12	521 (in top 3%)
TCGA breast (593)	Invasive breast carcinoma vs. normal	2.317	2.15E-12	1744 (in top 9%)
	Invasive ductal breast carcinoma vs. normal	2.403	1.29E-18	1851 (in top 10%)

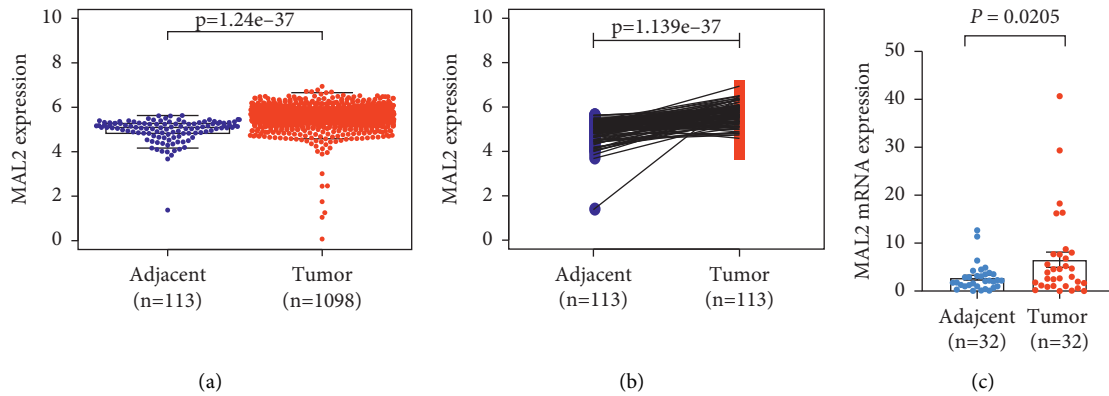


FIGURE 2: Different MAL2 mRNA expression in tumor tissues compared with adjacent tissues isolated from breast cancer patients. (a) MAL2 mRNA expression was significantly higher in tumor tissues than in adjacent tissues. (b) Paired breast cancer patient samples revealed that MAL2 expression was also higher in tumor tissues than in paired adjacent tissues. (c) RT-qPCR analysis of MAL2 mRNA expression in 32 pairs of breast cancer tissues and adjacent tissues.

TABLE 2: Clinical characteristics of TCGA breast cancer cohort.

Characteristics	Number of sample size (%)
Age	
<40	75 (6.88)
≥40	1015 (93.12)
Gender	
Female	1079 (98.90)
Male	12 (1.10)
Stage	
I	182 (16.70)
II	620 (56.88)
III	249 (22.84)
IV	21 (1.93)
X	18 (1.65)
T classification	
T1	280 (25.69)
T2	630 (57.80)
T3	138 (12.66)
T4	39 (3.58)
TX	3 (0.28)
M classification	
M0	900 (82.57)
M1	22 (2.02)
MX	168 (15.41)
N classification	
N0	484 (44.40)
N1	390 (35.78)
N2	180 (16.51)
N3	27 (2.48)
NX	9 (0.83)
ER status	
Negative	236 (21.65)
Positive	805 (73.85)
Unknown	49 (4.50)
PR status	
Negative	695 (63.76)
Positive	52 (4.77)
Unknown	559 (51.28)
HER2 status	
Negative	163 (14.95)
Positive	368 (33.76)
Unknown	236 (21.65)
	805 (73.85)

TABLE 2: Continued.

Characteristics	Number of sample size (%)
Vital status	
Living	941 (86.33)
Deceased	149 (13.67)
MAL2 expression	
High	545 (50.00)
Low	545 (50.00)

NA, not available.

In conclusion, both in the Kaplan–Meier model and the Cox proportional hazard regression model, the results indicated that MAL2 expression in breast cancer was significantly correlated with the prognosis of patients.

3.7. Identification of MAL2-Related Signaling Pathways by GSEA. Data sets from GSEA showed significant differences ($|NES| > 1$, $FDR < 0.25$, $NOM P < 0.05$) in MSigDB Collection. The details are described in Figure 6 and Table 5.

The significant pathways by GSEA included MYC targets V1, mTORC1 signaling pathway, insulin signaling pathway, E2F targets, UA response, G2M checkpoint, oocyte meiosis, mitotic spindle, peroxisome, spliceosome, cell cycle, and ubiquitin-mediated proteolysis enriched differentially in MAL2 high-expression phenotype.

3.8. High-Expressed MAL2 Correlates with Reduced Immune Infiltration in Breast Cancer. By Spearman's correlation test, the MAL2 expression level was found to be negatively correlated with infiltrating levels of eosinophils ($r = -0.38$, $P < 0.01$) and plasmacytoid dendritic cells ($r = -0.33$, $P < 0.01$) (Figures 7(a)–7(c)). Additionally, the abundance of infiltration of both eosinophils and plasmacytoid dendritic cells was significantly lower in tumor tissues than in adjacent tissues (Figure 7(d)).

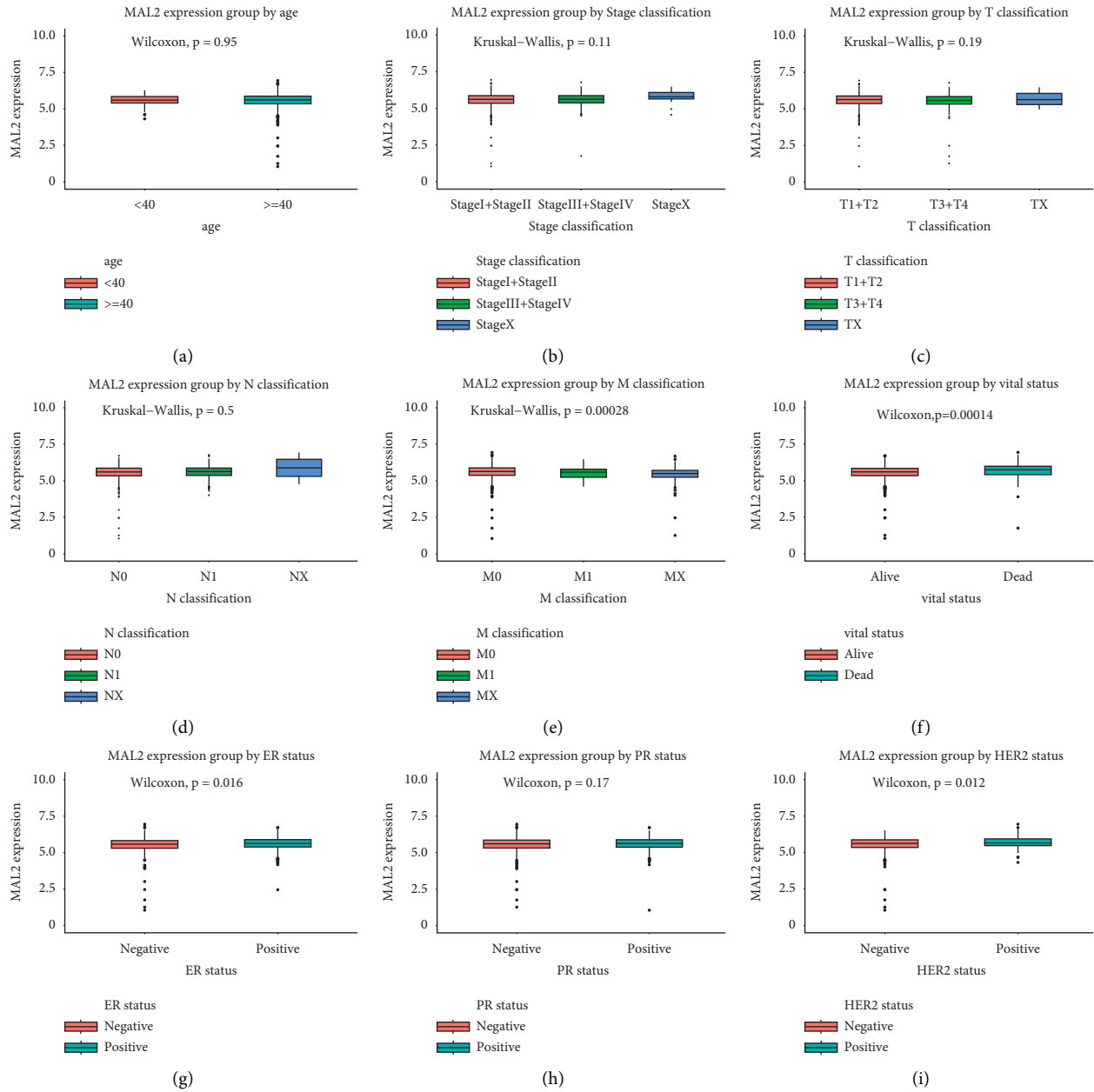


FIGURE 3: Differential MAL2 expressions in the boxplot. The expression of MAL2 is grouped by age (a), stage (b), T classification (c), N classification (d), M classification (e), vital status (f), ER status (g), PR status (h), and HER2 status (i).

TABLE 3: Correlation between MAL2 mRNA expression and clinicopathologic parameters of breast cancer.

Parameters	Variables	N	MAL2 mRNA expression				χ^2	P value
			High	(%)	Low	(%)		
Age	<40	75	37	6.79	38	6.97	0	1
	≥ 40	1015	508	93.21	507	93.03		
Stage*	I + II	802	392	73.82	410	75.79	—	0.044
	III + IV	270	139	26.18	131	24.21		
	X	18	14	2.57	4	0.73		
T classification*	T1 + T2	910	466	85.82	444	81.62	—	0.115
	T3 + T4	177	77	14.18	100	18.38		
	TX	3	2	0.37	1	0.18		

TABLE 3: Continued.

Parameters	Variables	N	MAL2 mRNA expression				χ^2	P value
			High	(%)	Low	(%)		
M classification	M0	900	472	86.61	428	78.53	12.83	0.002
	M1	22	10	1.83	12	2.20		
	MX	168	63	11.56	105	19.27		
N classification*	N0	484	233	43.15	251	46.4	—	0.399
	N1 + N2 + N3	597	307	56.85	290	53.6		
	NX	9	5	0.92	4	0.73		
ER status	Negative	236	103	19.92	133	25.38	5.47	0.065
	Positive	805	414	80.08	391	74.62		
	Unknown	49	28	5.14	21	3.85		
PR status	Negative	343	166	32.11	177	33.97	0.73	0.694
	Positive	695	351	67.89	344	66.03		
	Unknown	52	28	5.14	24	4.4		
HER2 status	Negative	559	282	76.01	277	78.92	2.51	0.285
	Positive	163	89	23.99	74	21.08		
	Unknown	368	174	31.93	194	35.6		
Vital status	Living	941	453	83.12	488	89.54	8.99	0.003
	Deceased	149	92	16.88	57	10.46		

ER, estrogen receptor; HER2, human epidermal growth factor receptor-2; PR, progesterone receptor. Note. Bold values indicate statistically significant $P < 0.05$. *means Fisher's test.

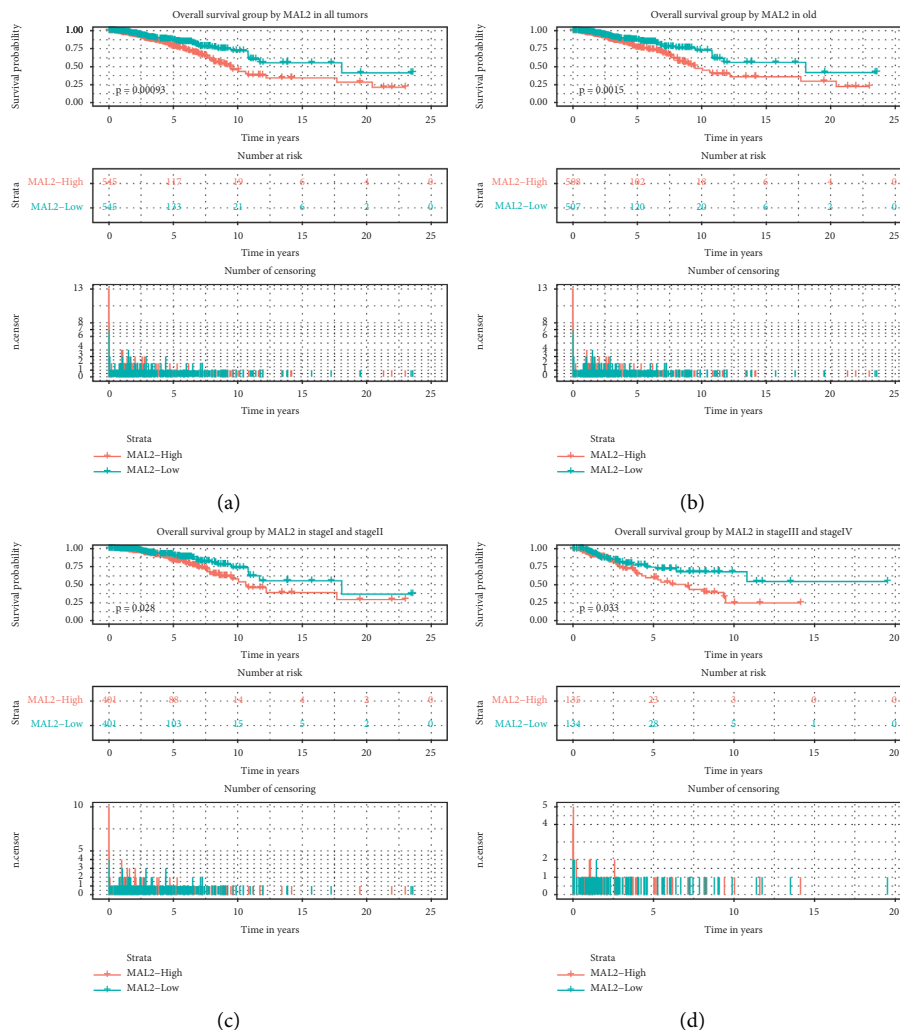


FIGURE 4: Continued.

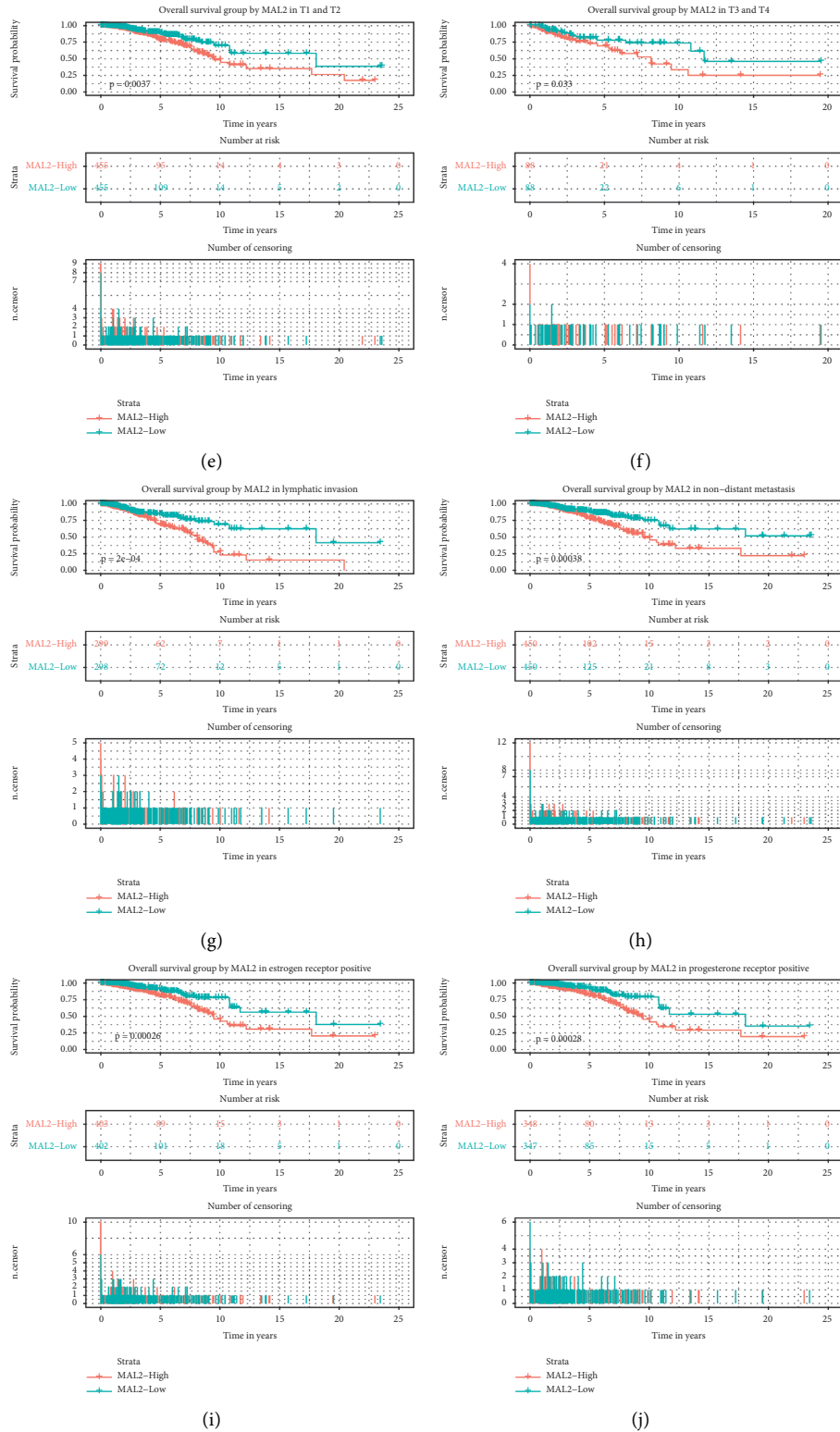


FIGURE 4: Continued.

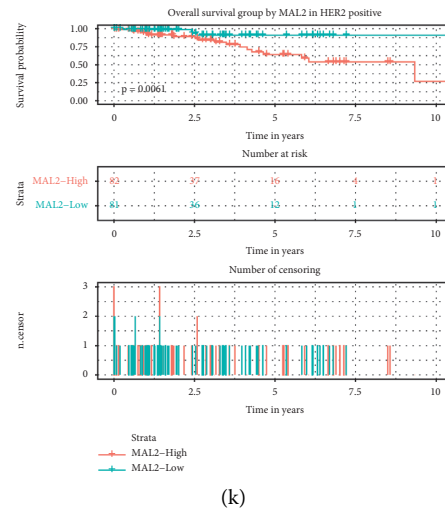


FIGURE 4: Survival analysis of MAL2 expression in terms of overall survival. Kaplan—Meier survival curve analysis of all tumors (a), subgroup analysis of old patients (b), clinical stage I/II and III/IV (c and d), subgroup analysis of *T* classification (*T*₁/*T*₂ and *T*₃/*T*₄) (e and f), patients with lymphatic invasion (g), patients with nondistant metastasis (h), and patients with ER-, PR-, and HER2-positive status (i–k, respectively).

TABLE 4: Univariate and multivariate analyses of overall survival in breast cancer.

Parameter	Univariate analysis			Multivariate analysis		
	Hazard ratio	95% CI	<i>P</i> value	Hazard ratio	95% CI	<i>P</i> value
Age (≥ 40 / <40)	1.564	0.568 –4.306	0.387	1.871	0.672 –5.205	0.230
Stage (III + IV/I + II)	1.745	1.376–2.212	<0.001	1.473	1.032 – 2.102	0.033
<i>T</i> classification (<i>T</i> ₃ + <i>T</i> ₄ / <i>T</i> ₁ + <i>T</i> ₂)	1.595	1.220–2.084	0.001	1.394	0.993–1.956	0.055
<i>N</i> classification (<i>N</i> ₁ + <i>N</i> ₂ + <i>N</i> ₃ / <i>N</i> ₀)	1.675	1.023–2.742	0.040	0.992	0.542–1.816	0.979
<i>M</i> classification (<i>M</i> ₁ / <i>M</i> ₀)	7.873	3.378–18.351	<0.001	3.093	1.215–7.878	0.018
Estrogen receptor (positive/negative)	0.612	0.369–1.015	0.057	0.506	0.220–1.160	0.107
Progesterone receptor (positive/negative)	0.748	0.465–1.205	0.233	0.932	0.425–2.047	0.862
HER2 (positive/negative)	1.553	0.914–2.638	0.104	1.256	0.723–2.180	0.419
MAL2 (high/low)	1.626	1.012–2.612	0.045	1.792	1.093–2.937	0.021

4. Discussion

Breast cancer is the dominating cause of cancer-related mortality among females worldwide. With the rapid development of genomics and molecular biology, identifying the crucial biomarkers for the diagnosis and treatment of breast cancer has become an important research tendency. Recently, numerous research studies showed that MAL2 could be a promising biomarker in various solid tumors. Jennifer et al. showed that MAL2 was increased in ovarian carcinoma, and the overexpression of D52, the binding partner of MAL2, was linked to low overall survival in breast cancer [13]. Chen et al. found that MAL2 was utilized to distinguish pancreatic ductal adenocarcinoma from chronic pancreatitis [26]. Also, the high expression of MAL2 contributed to the short survival time and high distant metastasis rate of postoperative pancreatic cancer patients [8]. Besides, it was reported that MAL2 expression increased in colon cancer tissues and lymph nodes with metastasis with high accuracy and specificity in the diagnosis of colon cancer [10].

As for breast cancer, previous studies showed that MAL2 could induce proliferation and invasion of breast cancer cell lines by adjusting the epithelial-mesenchymal transition [12]. MAL2 was also proved to promote immune evasion by suppressing tumor antigen presentation in breast cancer [11]. However, a further study about the correlation between MAL2 and breast cancer was needed. Here, we conducted this study to consider further the significance of MAL2 expression in the prognosis of breast cancer.

Our study proved the value of MAL2 in breast cancer. MAL2 was upregulated significantly in breast cancer based on the results of the Oncomine and TCGA database analyses. Furthermore, the RT-qPCR outcome verified the high expression of MAL2 in breast cancer, which coincides with the results of the bioinformatics assay and previous studies in other tumors. Moreover, MAL2 expression was correlated with the prognosis of breast cancer. MAL2 could be a potential biomarker for breast cancer.

In clinical factors' analysis, MAL2 expression was found to be associated with vital status, ER, PR status, and M

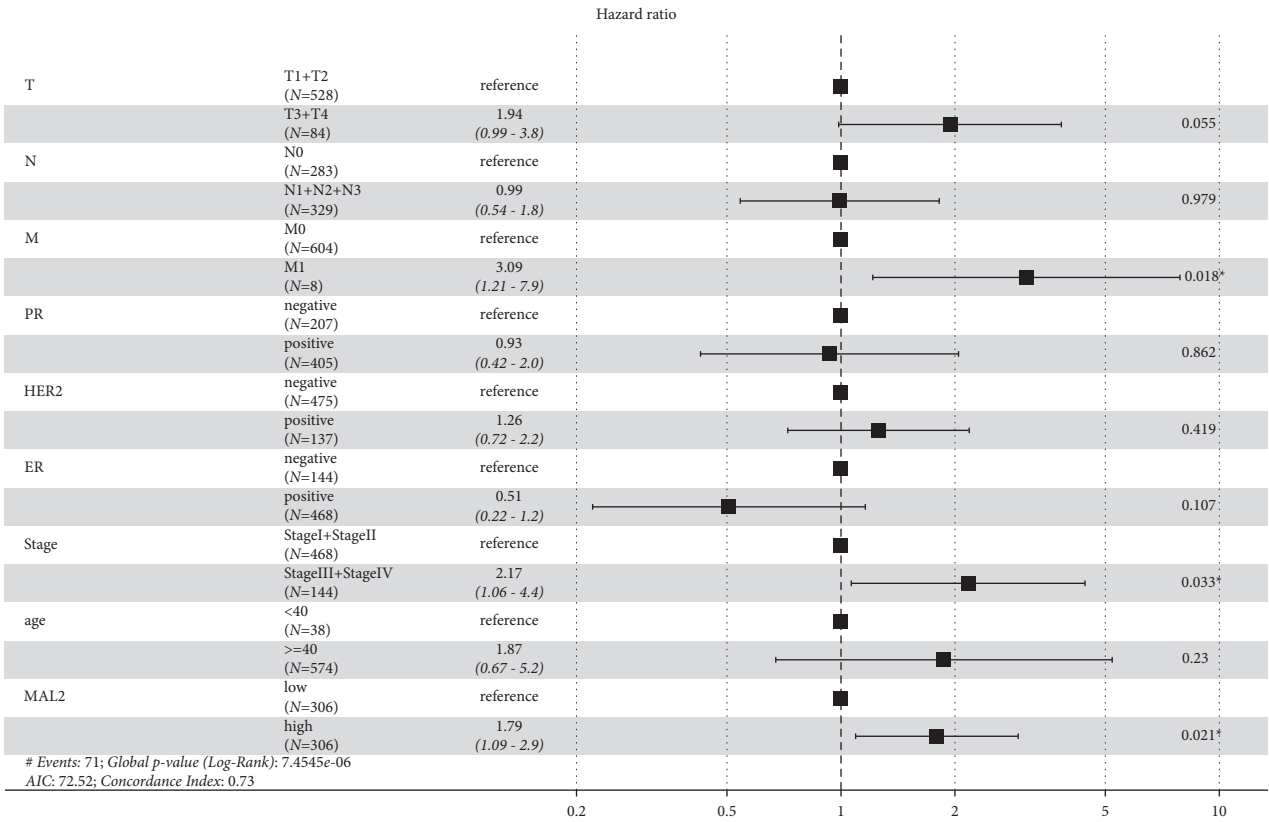


FIGURE 5: Forest plot for Cox proportional hazards model of overall survival in breast cancer.

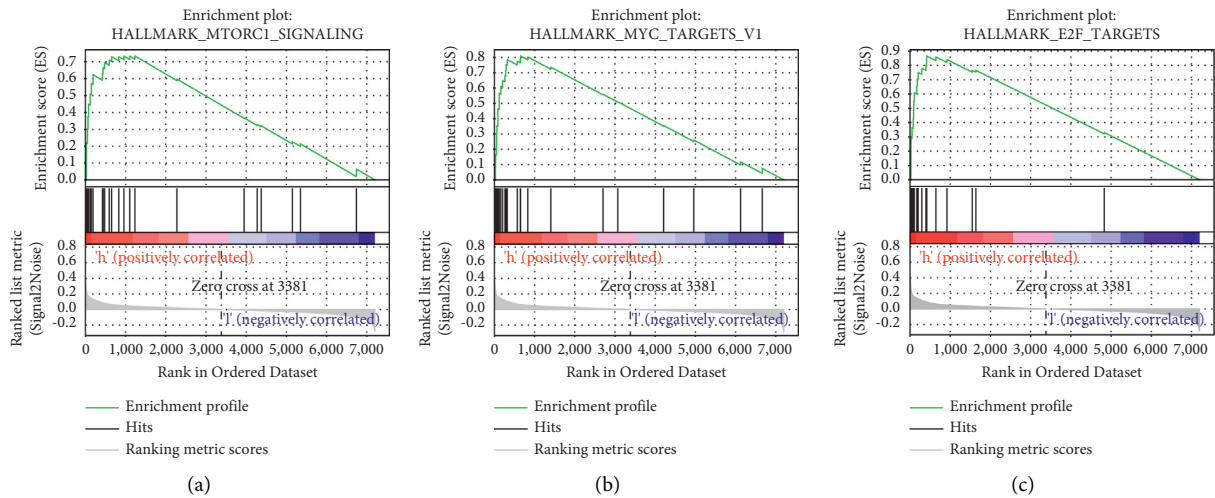


FIGURE 6: Continued.

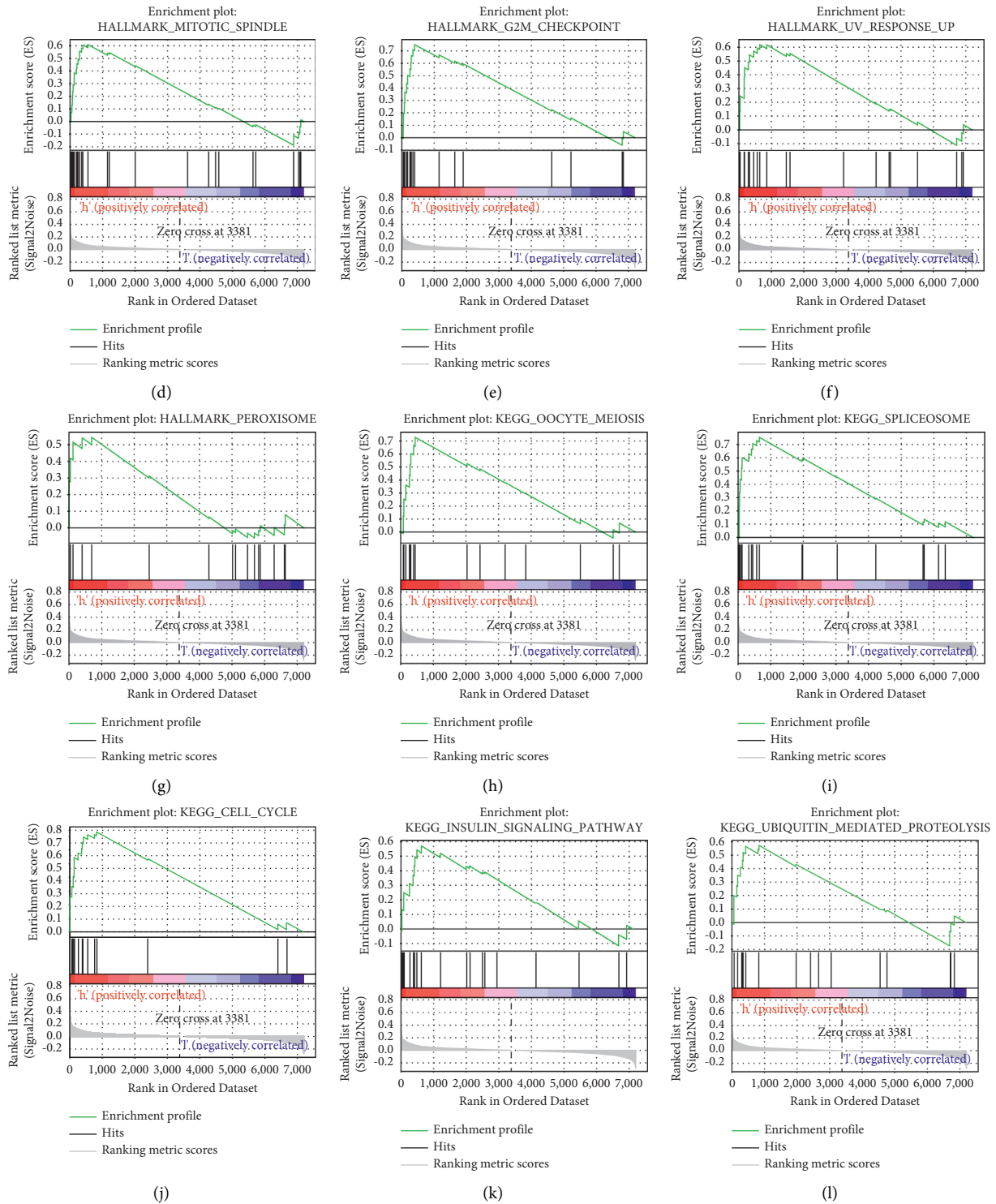


FIGURE 6: Enrichment plots of GSEA in breast cancer with a high-MAL2-expression phenotype. GSEA results showed that MYC targets V1 (a), mTORC1 signaling pathway (b), E2F targets (c), mitotic spindle (d), G2M checkpoint (e), UA response (f), peroxisome (g), oocyte meiosis (h), spliceosome (i), cell cycle (j), insulin signaling pathway (k), and ubiquitin-mediated proteolysis (l) were enriched in high MAL2 expression in breast cancer.

classification. The MAL2 level of dead patients was higher than that of alive patients, implying that patients with high MAL2 expression were more aggressive. Additionally, patients without metastasis had a higher MAL2 expression level

than patients with metastasis, and high MAL2 expression was associated with ER- and HER2-positive patients.

Both the chi-square test and multivariate analysis showed that MAL2 expression is associated with stage and M

TABLE 5: Gene sets enriched in high-MAL2-expression phenotype.

MSigDB collection	Name	ES	NES	NOM <i>P</i> value	FDR <i>q</i> -value
h.all.v7.4.symbols.gmt	HALLMARK_MYC_TARGETS_V1	0.809	2.089	<0.001	0.002
	HALLMARK_MTORC1_SIGNALING	0.734	2.012	0.002	0.007
	HALLMARK_E2F_TARGETS	0.866	1.964	0.000	0.011
	HALLMARK_MITOTIC_SPINDLE	0.751	1.948	0.004	0.010
	HALLMARK_G2M_CHECKPOINT	0.609	1.941	0.010	0.010
	HALLMARK_UV_RESPONSE_UP	0.618	1.724	0.018	0.049
	HALLMARK_PEROXISOME	0.545	1.581	0.035	0.113
c2.cp.kegg.v7.4.symbols.gmt	KEGG_OOCYTE_MEIOSIS	0.728	2.039	<0.001	0.011
	KEGG_SPLICEOSOME	0.755	1.974	0.004	0.011
	KEGG_CELL_CYCLE	0.785	1.940	0.002	0.010
	KEGG_INSULIN_SIGNALING_PATHWAY	0.574	1.725	0.015	0.051
	KEGG_UBIQUITIN_MEDIATED_PROTEOLYSIS	0.575	1.681	0.047	0.055

FDR, false discovery rate; ES, enrichment score; NES, normalized enrichment score; NOM, nominal. Notes: $|\text{NES}| > 1$, FDR *q*-value < 0.25 , and NOM-*P* value < 0.05 were considered significantly different.

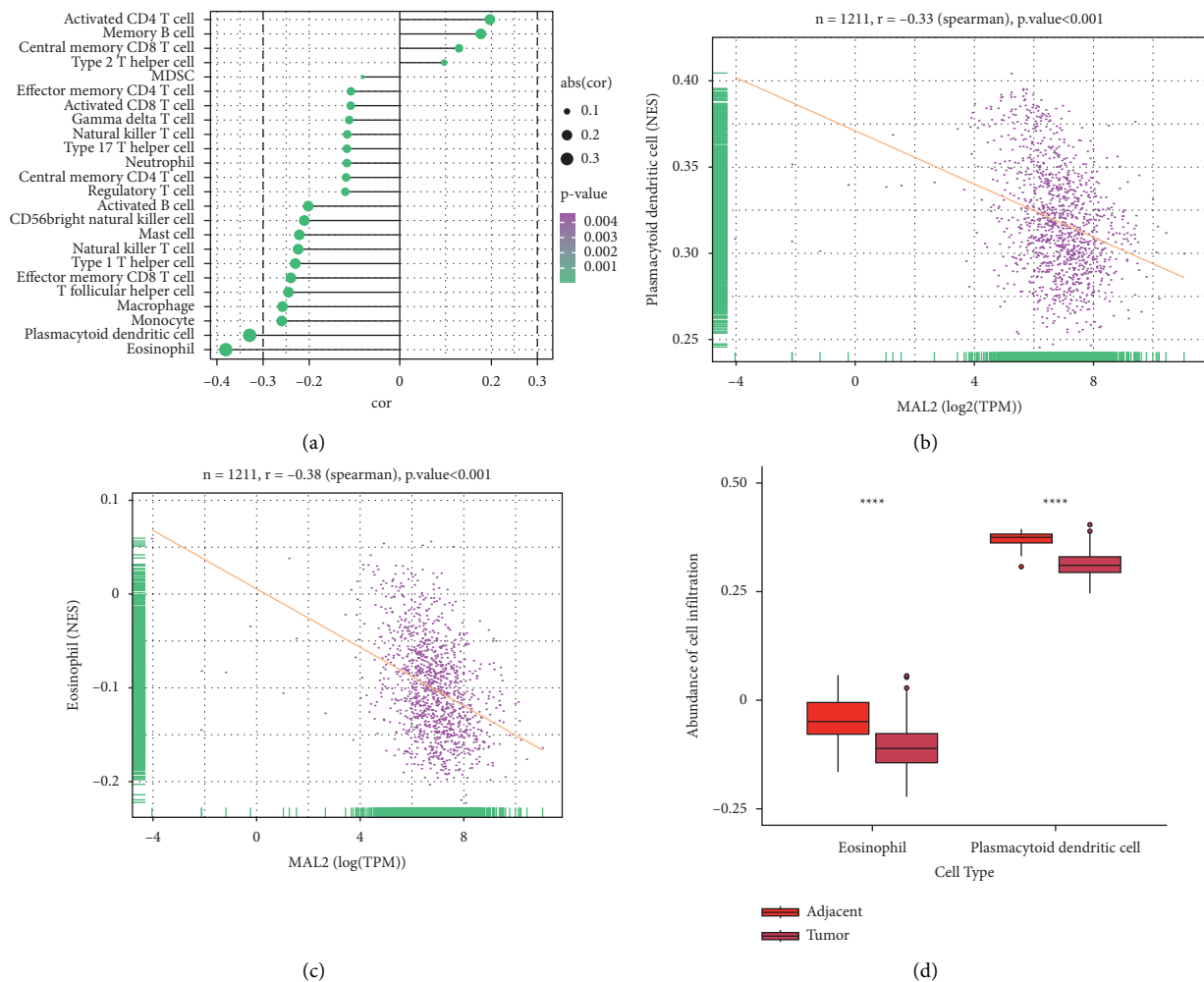


FIGURE 7: Association analysis of MAL2 gene expression and immune infiltration: (a) association analysis between MAL2 expression and immune cells; (b) association analysis of MAL2 expression with immune infiltration levels of eosinophils; (c) association analysis of MAL2 expression with immune infiltration levels of plasmacytoid dendritic cells; and (d) abundance of cell infiltration of eosinophils and plasmacytoid dendritic cells in breast cancer.

classification. In our study, breast cancer patients with high expression had shorter overall survival. In the multivariate model, stage, *M* classification, and MAL2 expression were

significantly related to OS (all $P < 0.05$), especially high MAL2 expression, advanced breast cancer patients, and those with distant metastasis. This finding may serve as a

basis for the proper selection of specific and personalized treatment for breast cancer. Moreover, we found that MAL2 was an independent prognostic factor and might become a biomarker for breast cancer.

To identify the biological function of MAL2 in breast cancer, we used GSEA analysis to predict the pathway associated with MAL2. MYC target V1, mTORC1 signaling pathway, and E2F targets were closely related to the progression of breast cancer.

The high-MAL2-expression phenotype was associated with the activated MYC targets v1 and E2F targets v1 gene sets based on the enrichment score. MYC, a prominent gene in MYC targets v1 gene set, is common in aggressive tumors and contributes to cancer development [27, 28]. Also, MYC gene is overexpressed in triple-negative breast cancer and targeting the gene provides a new treatment [29]. Schulze's study showed that high MYC Targets v1 enrichment scores were associated with high mutation load, increased infiltration of pro- and anticancerous immune cells, tumor aggressiveness, and poor prognosis of ER-positive cancer [30].

Besides, the E2F transcription factors are downstream effectors of the retinoblastoma protein (pRB) pathway, which is essential to regulate numerous genes essential for DNA replication and cell cycle progression [31]. A previous study showed that E2F transcription factors played key roles in mediating tumor development and metastasis for knockout E2F, leading to the decreased tumor angiogenesis and metastatic capacity of breast cancer. E2Fs could control the expression of genes critical to angiogenesis, remodeling the extracellular matrix, tumor cell survival, and tumor cell interactions with vascular endothelial cells that boost breast cancer metastasis to the lungs [32]. Furthermore, the E2F enrichment score is a marker of breast cancer aggressiveness and predicts the responsiveness of ER-positive/HER2-negative patients to neoadjuvant chemotherapy [33]. Similar research also found that ER-dependent E2F transcription enhanced endocrine resistance in breast cancer [34]. Taken together, speculated high MAL2 expression might be associated with proliferation, metastasis, and prognosis of breast cancer by regulating the genes in these two gene sets.

We finally identified the relationship between the infiltrating level of immune cells and MAL2 using ssGSEA. Interestingly, MAL2 expression was found to be significantly associated with the negatively infiltrating level of eosinophils and plasmacytoid dendritic cells.

A prior study showed eosinophil infiltration was considered a favorable prognosis in breast cancer [35]. In addition, a previous study indicated that low baseline eosinophil count was related to a higher recurrence rate in 419 patients diagnosed with breast cancer [36]. Similar results could be found in recent studies. Low blood eosinophilic relative count was associated with a worse prognosis in 930 breast cancer patients [37]. Moreover, there was a positive correlation between eosinophilic relative counts and both pathological complete remission and survival rate in triple-negative and hormone receptor-negative/HER2-positive breast cancer patients [38].

As for plasmacytoid dendritic cells, it was reported that the proportion of plasmacytoid dendritic cells in triple-negative breast cancer was higher than other

subtypes of breast cancer [39]. Besides, high plasmacytoid dendritic cells in triple-negative breast cancer were bound up with a favorable immune response and predicted better survival in 2968 breast cancer patients [39]. Interestingly, in the present study, we found the overexpression of MAL2 was significantly associated with the low infiltrating level of eosinophilic relative counts and plasmacytoid dendritic cells. Interestingly, in the present study, we found that the high MAL2 expression level had a significantly negative correlation with the infiltrating level of eosinophils and plasmacytoid dendritic cells. Moreover, high MAL2 expression was associated with poor OS in patients with breast cancer. Since high eosinophils and plasmacytoid dendritic cells predicted better breast cancer survival in previous research, we speculate that high-expressed MAL2 might impact the eosinophils and plasmacytoid dendritic cells, which triggered a disadvantageous immune response, leading to poor prognosis in breast cancer.

To the best of our knowledge, this is the first research further analyzing the relationship between MAL2 expression and clinical features and immune infiltration. MAL2 expression may be an independent predictor of a poor disease survival prognosis in breast cancer patients. However, there are a few shortcomings in this study. The sample size included in the experimental validation part was small. And the collected breast cancer tissues were fresh samples, which could not be followed up according to the prognosis of the patients. Besides, further studies are needed to explore the mechanism of MAL2 in breast cancer.

5. Conclusion

In conclusion, our study showed MAL2 expression increased markedly in breast cancer patients and was related to overall survival. MAL2 might be a novel prognostic biomarker of breast cancer. Moreover, high MAL2 expression correlates with reduced immune infiltration of eosinophils and plasmacytoid dendritic cells in breast cancer. However, further studies are warranted to verify the value of MAL2 in breast cancer prognosis evaluation.

Data Availability

Publicly available datasets were analyzed in this study. The data can be found at TCGA repository, <https://www.cancer.gov/tcga>, and Oncomine repository, <http://www.oncomine.org>. The data used to support the findings are available from the corresponding author upon request.

Conflicts of Interest

Yue Zhong and Zhenjie Zhuang are co-first authors.

Authors' Contributions

Yue Zhong and Zhenjie Zhuang contributed equally to this work and are co-first authors.

Acknowledgments

The authors also thank the Lingnan Medical Research Center of Guangzhou University of Chinese Medicine for providing associated facilities.






References

- [1] F. Bray, J. Ferlay, I. Soerjomataram, R. L. Siegel, L. A. Torre, and A. Jemal, "Global cancer statistics 2018: GLOBOCAN estimates of incidence and mortality worldwide for 36 cancers in 185 countries," *CA: A Cancer Journal for Clinicians*, vol. 68, no. 6, pp. 394–424, 2018.
- [2] R. Kasiappan and D. Rajarajan, "Role of MicroRNA regulation in obesity-associated breast cancer: nutritional perspectives," *Advances in Nutrition: An International Review Journal*, vol. 8, no. 6, pp. 868–888, 2017.
- [3] K. D. Miller, L. Nogueira, A. B. Mariotto et al., "Cancer treatment and survivorship statistics, 2019," *CA: A Cancer Journal for Clinicians*, vol. 69, no. 5, pp. 363–385, 2019.
- [4] R. Huang, Z. Chen, L. He et al., "Mass spectrometry-assisted gel-based proteomics in cancer biomarker discovery: approaches and application," *Theranostics*, vol. 7, no. 14, pp. 3559–3572, 2017.
- [5] M. J. Duffy, S. Walsh, E. W. McDermott, and J. Crown, "Biomarkers in breast cancer," *Advances in Clinical Chemistry*, vol. 71, pp. 1–23, 2015.
- [6] J. A. Byrne, S. Maleki, J. R. Hardy et al., "MAL2 and tumor protein D52 (TPD52) are frequently overexpressed in ovarian carcinoma, but differentially associated with histological subtype and patient outcome," *BMC Cancer*, vol. 10, no. 1, p. 497, 2010.
- [7] S. H. Wilson, A. M. Bailey, C. R. Nourse, M. G. Mattei, and J. A. Byrne, "Identification of MAL2, a novel member of the mal proteolipid family, though interactions with TPD52-like proteins in the yeast two-hybrid system," *Genomics*, vol. 76, no. 1, pp. 81–88, 2001.
- [8] D. Eguchi, K. Ohuchida, S. Kozono et al., "MAL2 expression predicts distant metastasis and short survival in pancreatic cancer," *Surgery*, vol. 154, no. 3, pp. 573–582, 2013.
- [9] X. Gao, Z. Chen, A. Li, X. Zhang, and X. Cai, "MiR-129 regulates growth and invasion by targeting MAL2 in papillary thyroid carcinoma," *Biomedicine & Pharmacotherapy*, vol. 105, pp. 1072–1078, 2018.
- [10] J. ShROUT, M. Yousefzadeh, A. Dodd et al., " β 2-microglobulin mRNA expression levels are prognostic for lymph node metastasis in colorectal cancer patients," *British Journal of Cancer*, vol. 98, no. 12, pp. 1999–2005, 2008.
- [11] Y. Fang, L. Wang, C. Wan et al., "MAL2 drives immune evasion in breast cancer by suppressing tumor antigen presentation," *Journal of Clinical Investigation*, vol. 131, p. 1, 2021.
- [12] A. Bhandari, Y. Shen, N. Sindan et al., "MAL2 promotes proliferation, migration, and invasion through regulating epithelial-mesenchymal transition in breast cancer cell lines," *Biochemical and Biophysical Research Communications*, vol. 504, no. 2, pp. 434–439, 2018.
- [13] M. Shehata, I. Bièche, R. Boutros et al., "Nonredundant functions for tumor protein D52-like proteins support specific targeting of TPD52," *Clinical Cancer Research*, vol. 14, no. 16, pp. 5050–5060, 2008.
- [14] D. R. Rhodes, S. Kalyana-Sundaram, V. Mahavisno et al., "Oncomine 3.0: genes, pathways, and networks in a collection of 18,000 cancer gene expression profiles," *Neoplasia*, vol. 9, no. 2, pp. 166–180, 2007.
- [15] D. R. Rhodes, J. Yu, K. Shanker et al., "ONCOMINE: a cancer microarray database and integrated data-mining platform," *Neoplasia*, vol. 6, no. 1, pp. 1–6, 2004.
- [16] R. C. T., R: A Language and Environment for Statistical Computing, Vienna, Austria, 2020, R Foundation for Statistical Computing, <https://www.R-project.org/>.
- [17] C. Ginestet, "ggplot2: elegant graphics for data analysis," *Journal of the Royal Statistical Society: Series A*, vol. 174, p. 1, 2011.
- [18] Y. Jiao, Y. Li, Z. Lu, and Y. Liu, "High trophinin-associated protein expression is an independent predictor of poor survival in liver cancer," *Digestive Diseases and Sciences*, vol. 64, no. 1, pp. 137–143, 2018.
- [19] Q. Li, W. Ma, S. Chen et al., "High integrin α 3 expression is associated with poor prognosis in patients with non-small cell lung cancer," *Translational Lung Cancer Research*, vol. 9, no. 4, pp. 1361–1378, 2020.
- [20] E. Zhao, C. Zhou, and S. Chen, "Flap endonuclease 1 (FEN1) as a novel diagnostic and prognostic biomarker for gastric cancer," *Clinics and Research in Hepatology and Gastroenterology*, vol. 45, no. 1, p. 101455, 2021.
- [21] Z. Sun, L. Sun, M. He, Y. Pang, Z. Yang, and J. Wang, "Low BCL7A expression predicts poor prognosis in ovarian cancer," *Journal of Ovarian Research*, vol. 12, no. 1, p. 41, 2019.
- [22] A. Subramanian, P. Tamayo, V. K. Mootha et al., "Gene set enrichment analysis: a knowledge-based approach for interpreting genome-wide expression profiles," *Proceedings of the National Academy of Sciences*, vol. 102, no. 43, pp. 15545–15550, 2005.
- [23] M. J. Goldman, B. Craft, M. Hastie et al., "Visualizing and interpreting cancer genomics data via the Xena platform," *Nature Biotechnology*, vol. 38, no. 6, pp. 675–678, 2020.
- [24] P. Charoentong, F. Finotello, M. Angelova et al., "Pan-cancer immunogenomic analyses reveal genotype-immunophenotype relationships and predictors of response to checkpoint blockade," *Cell Reports*, vol. 18, no. 1, pp. 248–262, 2017.
- [25] S. Hänzelmann, R. Castelo, and J. Guinney, "GSVA: gene set variation analysis for microarray and RNA-seq data," *BMC Bioinformatics*, vol. 14, no. 1, p. 7, 2013.
- [26] Y. Chen, B. Zheng, D. H. Robbins et al., "Accurate discrimination of pancreatic ductal adenocarcinoma and chronic pancreatitis using multimarker expression data and samples obtained by minimally invasive fine needle aspiration," *International Journal of Cancer*, vol. 120, no. 7, pp. 1511–1517, 2007.
- [27] N. M. Sodir, R. M. Kortlever, V. J. A. Barthet et al., "MYC instructs and maintains pancreatic adenocarcinoma phenotype," *Cancer Discovery*, vol. 10, no. 4, pp. 588–607, 2020.
- [28] D. A. Lawson, N. R. Bhakta, K. Kessenbrock et al., "Single-cell analysis reveals a stem-cell program in human metastatic breast cancer cells," *Nature*, vol. 526, no. 7571, pp. 131–135, 2015.
- [29] R. Camarda, A. Y. Zhou, R. A. Kohnz et al., "Inhibition of fatty acid oxidation as a therapy for MYC-overexpressing triple-negative breast cancer," *Nature Medicine*, vol. 22, no. 4, pp. 427–432, 2016.
- [30] A. Schulze, M. Oshi, I. Endo, and K. Takabe, "MYC targets scores are associated with cancer aggressiveness and poor survival in ER-positive primary and metastatic breast cancer," *International Journal of Molecular Sciences*, vol. 21, p. 21, 2020.
- [31] D. P. Hollern, J. Honeysett, R. D. Cardiff, and E. R. Andrechek, "The E2F transcription factors regulate tumor development and metastasis in a mouse model of

- metastatic breast cancer,” *Molecular and Cellular Biology*, vol. 34, no. 17, pp. 3229–3243, 2014.
- [32] A. P. Bracken, M. Ciro, A. Cocito, and K. Helin, “E2F target genes: unraveling the biology,” *Trends in Biochemical Sciences*, vol. 29, no. 8, pp. 409–417, 2004.
- [33] M. Oshi, H. Takahashi, Y. Tokumaru et al., “The E2F pathway score as a predictive biomarker of response to neoadjuvant therapy in ER+/HER2- breast cancer,” *Cells*, vol. 9, p. 7, 2020.
- [34] T. W. Miller, J. M. Balko, E. M. Fox et al., “Era-dependent E2F transcription can mediate resistance to estrogen deprivation in human breast cancer,” *Cancer Discovery*, vol. 1, no. 4, pp. 338–351, 2011.
- [35] S. Sakkal, S. Miller, V. Apostolopoulos, and K. Nurgali, “Eosinophils in cancer: favourable or unfavourable?” *Current Medicinal Chemistry*, vol. 23, no. 7, pp. 650–666, 2016.
- [36] H. E. Ownby, L. D. Roi, R. R. Isenberg, and M. J. Brennan, “Peripheral lymphocyte and eosinophil counts as indicators of prognosis in primary breast cancer,” *Cancer*, vol. 52, no. 1, pp. 126–130, 1983.
- [37] C. E. Onesti, C. Josse, D. Boulet et al., “Blood eosinophilic relative count is prognostic for breast cancer and associated with the presence of tumor at diagnosis and at time of relapse,” *OncoImmunology*, vol. 9, no. 1, Article ID 1761176, 2020.
- [38] C. E. Onesti, C. Josse, A. Poncin et al., “Predictive and prognostic role of peripheral blood eosinophil count in triple-negative and hormone receptor-negative/HER2-positive breast cancer patients undergoing neoadjuvant treatment,” *Oncotarget*, vol. 9, no. 72, pp. 33719–33733, 2018.
- [39] M. Oshi, S. Newman, Y. Tokumaru et al., “Plasmacytoid dendritic cell (pDC) infiltration correlate with tumor infiltrating lymphocytes, cancer immunity, and better survival in triple negative breast cancer (TNBC) more strongly than conventional dendritic cell (cDC),” *Cancers*, vol. 12, p. 11, 2020.

Research Article

In Vitro and *In Silico* Evaluation for the Inhibitory Action of *O. basilicum* Methanol Extract on α -Glucosidase and α -Amylase

Siba Shanak ¹, Najlaa Bassalat ^{1,2}, Raghad Albzoor ¹, Sleman Kadan ³,
and Hilal Zaid ^{2,3}

¹Faculty of Sciences, Arab American University, P.O Box 240, Jenin, State of Palestine

²Faculty of Medicine, Arab American University, P.O Box 240, Jenin, State of Palestine

³Qasemi Research Center, Al-Qasemi Academic College, P.O Box 124, Baqa-El-Gharbia 30100, Israel

Correspondence should be addressed to Hilal Zaid; hilalz@qsm.ac.il

Received 17 January 2021; Accepted 29 June 2021; Published 7 July 2021

Academic Editor: Akhilesh K. Tamrakar

Copyright © 2021 Siba Shanak et al. This is an open access article distributed under the Creative Commons Attribution License, which permits unrestricted use, distribution, and reproduction in any medium, provided the original work is properly cited.

Diabetes mellitus is a metabolic disease that predominates, nowadays. It causes hyperglycemia and consequently major health complications. Type II diabetes is the most common form and is a result of insulin resistance in the target tissues. To treat this disease, several mechanisms have been proposed. The most direct route is via inhibiting the intestinal enzymes, e.g., α -glucosidase and α -amylase, responsible for intestinal polysaccharide digestion that therefore would reduce the absorption of monosugars through the intestinal walls. In this study, we shed the light on this route by testing the inhibitory effect of *Ocimum basilicum* extract on the enzymes α -glucosidase and α -amylase *in vitro* and *in silico*. Experimental procedures were performed to test the effect of the *O. basilicum* methanol extract from aerial parts followed by the *in silico* docking. 500 μ g/mL of the extract led to $70.2\% \pm 8.6$ and $25.4\% \pm 3.3$ inhibition on α -glucosidase and α -amylase activity, respectively. Similarly, the effect of caffeic acid, a major extract ingredient, was also tested, and it caused $42.7\% \pm 3.0$ and $47.1\% \pm 4.0$ inhibition for α -amylase and α -glucosidase, respectively. Docking experiments were performed to predict the phytochemicals responsible for this robust inhibitory activity in the *O. basilicum* extracts. Several compounds have shown variable levels of inhibition, e.g., caffeic acid, pyroglutamic acid, and uvasol. The results indicated that *O. basilicum* can be a potent antidiabetic drug.

1. Introduction

Diabetes mellitus (DM) is a metabolic disorder. It results from the resistance to insulin or the reduced secretion of insulin. A major consequence of this disorder is the distorted carbohydrate, fat, and protein metabolism and the increased levels of serum glucose. This would result in hyperglycemia and elevated plasma LDL [1], which would cause damage in blood vessels and consequently microvascular and macrovascular disorders, including atherosclerosis, retinopathy, and nephropathy. Weight loss, polyphagia, blurred vision, polyuria, and polydipsia are additional complications [2]. These complications are the major causes of mortality in patients with diabetes [3]. Two major forms of diabetes predominate. In type I diabetes, which has a low prevalence, the pancreatic β -cells are labeled for destruction by the immune system, and insulin

levels are distorted [4, 5]. The more common form, type II diabetes mellitus (T2DM), mainly results from insulin resistance in the target tissues [6]. A major consequence of this insulin disorder is an imbalance in carbohydrate, fat, and protein metabolism. Fasting plasma glucose levels, the postprandial levels of plasma glucose, and hemoglobin A1C levels are elevated to ≥ 7 mM, ≥ 11 mM, and 6.5%, respectively [7]. Prolonged hyperglycemia leads to the destruction of blood vessels and destruction in the heart, eyes, kidneys, and nervous system [3].

To treat type I DM, several routes can be followed. These include insulin replacement therapy and the transplantation of pancreatic islets [8]. Type II DM can be treated with drugs that act via different modes of actions. Some drugs target hepatic enzymes involved in gluconeogenesis and glycogenolysis for inhibition. Other drugs induce an increased production and

secretion of insulin in the β -pancreatic cells. Even more, some drugs act on enzymes of skeletal muscles and adipose tissues and stimulate the two organs to increase blood glucose uptake [9, 10]. Another route of action is via drugs that target the inhibition of lipolysis, where imbalanced lipolysis is known to induce the reduced secretion of insulin and consequently hyperglycemia. Furthermore, abnormal lipolysis can result in lipotoxicity, with the accumulation of toxic lipid metabolites (ceramide, diacylglycerol, and fatty acyl CoA) in the liver, muscle, adipose tissues, and pancreas [11]. Drugs that target this side effect can relieve the injury and reduce the inflammation [12]. Anti-inflammatory drugs can treat the complications of diabetes, including the inflammatory responses [13]. The route for glycemic control under a microscope in this work introduces the inhibition of intestinal enzymes responsible for intestinal polysaccharide digestion and consequently the absorption of absorbable sugar monomers through the intestinal walls [14]. Examples include the mammalian α -glucosidase and α -amylase competitive inhibitors [15]. Digestive enzymes in the small intestine hydrolyze complex polysaccharides and disaccharides into smaller fragments of monosaccharides. The inhibition of these enzymes directly prevents the escape of the resulting monosaccharides to the bloodstream and the consequent utilization by the liver, muscle, and fat tissues.

Several antidiabetic drugs are confined by their limited action and pharmacokinetic influence and have side effects, e.g., biguanides and sulfonylurea. Traditional medicine utilizes herbal-based remedies by about 80% of the world's population. Herbal-derived active compounds or chemically modified herbal phytochemicals are used to produce safer pharmaceutically active drugs [16, 17]. Indeed, many plant extracts have shown antidiabetic effects in *in vitro* experiments, in animal test models, and in clinical trials. [17].

Ocimum basilicum is among one of the antidiabetic herbs [18]. The genus *Ocimum* belongs to the family Lamiaceae [19]. A number of species of *Ocimum* are used to treat different types of diseases, mainly the species *Ocimum basilicum*, also known as sweet basil—an herbaceous, perennial plant used in traditional medicine and also an ornamental plant [20, 21]. A number of virulent metabolites exist in this species that have strong action against diseases [22, 23]. It has a wide range of pharmacological activities, much as the antimicrobial effect. This was seen against *Aspergillus ochraceus* [24] for extracts from the hairy root of *O. basilicum* against species such as *P. aeruginosa* strains, *A. rhizogenes*, *P. fluorescens*, *X. campestris*, and *E. carotovora* [25] and for the leaf extract against *E. coli* and *Staphylococcus aureus* [26]. The essential oil extract from *O. basilicum* leaves showed an insecticidal activity against larval stages of *Culex tritaeniorhynchus*, *Aedes albopictus*, and *Anopheles subpictus* [27, 28]. *O. basilicum* contains several active antioxidant compounds, e.g., polyphenoid rosmarinic acid, a derivative of cinnamic acid [29]. Extracts from *Ocimum basilicum* aerial parts have robust anti-inflammatory activity against macrophages and human primary chondrocytes [30]. Extracts of *Ocimum basilicum* aerial parts have also shown antiplatelet activity through inhibiting ADP-induced platelet aggregation [31], anticonvulsant activity [32], and antithrombotic activity [33]. *O. basilicum* extract significantly

showed antihyperlipidemic effects and could lower both plasma triglycerides (TG) and cholesterol in rats [31]. *Ocimum basilicum* aerial extracts (methanol, hexane, and dichloromethane) reported recently to augment glucose transporter-4 (GLUT4) translocation to the muscle plasma membrane *in vitro* and thus enhance glucose uptake [18].

α -Glucosidase (α -glucosidase, EC 3.2.1.20) is a carbohydrate hydrolase that breaks down terminal nonreducing (α -1 \rightarrow 4)-linkage to release α -glucose residues. Two families of α -glucosidase are examined so far according to the primary structure [34]. The gene coding for human lysosomal α -glucosidase is about 20 kb long, and the structure for the protein it codes for has been resolved [35]. The Trp-516 and Asp-518 residues are crucial for the enzyme's catalytic functionality [36]. It was found that the conformation of the enzyme's active site is less stable than the whole enzyme conformation [37]. Deficiency in α -glucosidase may result in several disorders, e.g., Pompe disease or glycogen storage disease type II [38].

α -Amylase (α -amylase, EC 3.2.1.1) is an enzyme that hydrolyses alpha bonds of polysaccharides, such as starch and glycogen, to produce glucose and maltose. At least, two major forms of amylase are found in humans. Salivary α -amylase breaks starch into maltose and dextrin. The pancreatic α -amylase digests sugars in the diet to small saccharides such as maltose for the uptake in the small intestine on reaching the duodenum. Pancreatic α -amylase was discovered to bind with N-linked oligosaccharides of glycoproteins, which regulates the activities of glycoproteins related to the blood glucose level [39, 40]. Three α -amylase genes, AMY1 (the salivary α -amylase gene), AMY2A, and AMY2B (pancreatic α -amylase genes), form a cluster on chromosome 1 P21, with a pairwise sequence homology of 93%–94% [41, 42].

A number of distinct protein domains make up α -amylases: The catalytic domain has an eight-stranded alpha/beta barrel containing the active site, an \sim 70-amino acid calcium-binding domain protrudes in the catalytic domain between alpha helix 3 and beta strand 3, and a Greek key beta-barrel domain is the carboxyl terminal. [43–46]. Acarbose is a complex oligosaccharide that serves as an oral inhibitor of α -glucosidase and α -amylase in the treatment of T2DM [47].

The progress in drug discovery has bloomed hugely nowadays. Chemoinformatics is used to scan hundreds of plausible protein ligands. One method for screening is the ligand-based approach. With the escalating number of resolved crystal structures, modeling for the binding of ligands to the target proteins can be configured. Docking is a structure-based method that acts at the atomic resolution for the screening of robust ligand-protein interactions, including the calculation for ligand position, orientation, inhibition constants, and binding affinities. In this study, we examined the inhibitory effect of methanol *O. basilicum* extract on α -glucosidase and α -amylase *in vitro* and *in silico*.

2. Materials and Methods

2.1. Preparation of Plant Material. The selected plants were extracted according to Kadan et al. [18] with methanol. 10 g

of grounded OB was packed in the thimble of the Soxhlet apparatus and were extracted with 150 mL of methanol (MeOH) and then refluxed for 24 h to give a dark green extract. The yield of the extract was 1.05 g (10.5%). Supernatants obtained from the extract were passed through a 0.2 μm filter and stored in aliquots at -80°C for further experimental work.

2.2. α -Amylase Inhibitory Method. The pancreatic α -amylase inhibition assay was performed according to Adisakwattana et al. [48] using acarbose as a positive control. Porcine pancreatic α -amylase (4 units/mL) was dissolved in 0.1 M sodium phosphate buffer, pH 6.9.

The plant extract, caffeic acid, or acarbose as a positive control of different dilutions was preincubated with 250 μL of the enzyme solution at 37°C for 10 min. The reaction was initiated by adding 500 μL of the substrate solution (1% starch in 0.1 M sodium phosphate buffer, pH 6.9). After 5 min of incubation, the reaction was stopped by adding 1 mL of 96 mM 3,5-dinitrosalicylic acid solution to the reaction mixture. The mixtures were heated at 100°C for 10 min in order to stop the reaction and then cooled to room temperature in a cold water bath. Subsequently, the reaction mixtures were diluted 10 times with distilled water. The absorbance was recorded at 540 nm using a spectrophotometer. The α -amylase inhibitory potential was calculated utilizing the following equation:

$$I(\%) = \frac{[\text{ABS}_{\text{blank}} - \text{ABS}_{\text{test}}]}{[\text{ABS}_{\text{blank}}]} * 100\%, \quad (1)$$

where $I(\%)$ is the α -amylase inhibitory percentage.

2.3. Intestinal α -Glucosidase Inhibitory Method. The assessment of intestinal α -glucosidase inhibitory activity was performed according to Kim et al. [49], with a slight modification. The reaction mixture consisting of plant extract, caffeic acid, or acarbose as a positive control at varying concentrations was premixed with 100 μL of 0.1 M sodium phosphate buffer, pH 6.9. 15 μL of α -glucosidase (0.1 unit/ μL) was added and preincubated at 37°C for 10 min. The reaction mixture was set to 750 μL with distilled water. The reaction was initiated by adding 250 μL of 20 mM p-nitrophenyl α -D-glucopyranoside and further incubated for 10 min. The reaction was terminated by the addition of 100 μL of 0.1 M Na_2CO_3 . The amount of released product (p-nitrophenol) was measured at 405 nm using a spectrometer.

The intestinal α -glucosidase enzyme inhibitory potential was measured utilizing the following equation:

$$I(\%) = \frac{[\text{ABS}_{\text{blank}} - \text{ABS}_{\text{test}}]}{[\text{ABS}_{\text{blank}}]} * 100\%, \quad (2)$$

where $I(\%)$ is the α -glucosidase inhibitory percentage.

2.4. Docking Experiments. Input PDB files were prepared for the natural compounds that were extracted from *O. basilicum*, including caffeic acid. The SMILES structures of the

compounds were retrieved from the systemic IUPAC structures [50] and then converted to the PDB form using the Open Babel server [51]. These compounds were docked against the *apo* forms for the structures of the α -glucosidase enzyme (PDB: 5KZW) and the α -amylase enzyme (PDB: 1C8Q) with the AutoDock program, version 4.2 [52]. In each docking experiment, the receptor protein was kept rigid. Protein polar hydrogen atoms were added, and the input files were prepared using AutoDock tools [52]. Docking was performed within parallel rectangular boxes of $126 \times 126 \times 126 \text{ \AA}$ dimensions. The center of the grid was placed at the center of the mass of the original protein receptor in its *apo* form in crystal structures. A total of 20 independent docking runs were carried out for each compound against each of the enzymes starting from random positions. The PDB files were extracted and evaluated for the best-ranked fit of the enzyme-ligand interaction for each of the ligands.

3. Results

We have recently reported the phytochemical analysis of *O. basilicum* [18] with the objective to identify more potential antidiabetic active compounds (and test their potency in inhibiting carbohydrates digestive enzymes); the methanol *O. basilicum* extract from dried aerial parts was tested herein *in vitro* and *in situ*. The potential inhibitory effect of the extract on α -amylase and α -glucosidase was examined as described in the Materials and Methods section. Similarly, caffeic acid (as a major compound in the extract and one that displayed *in situ* inhibition) inhibitory effect was also tested.

The *in vitro* antidiabetic activities of *O. basilicum* methanol extract and for caffeic acid were investigated by the assessment of their pancreatic α -amylase and intestinal α -glucosidase inhibitory effects. Acarbose was used as a standard inhibitory drug. The results revealed that *O. basilicum* extract inhibited α -glucosidase in a dose-dependent manner and the IC_{50} value was $160 \pm 10 \mu\text{g/mL}$ (Figure 1(a) and Table 1). Caffeic acid also inhibited α -glucosidase in a dose-dependent manner, and the IC_{50} value was $1.05 \pm 0.25 \text{ mM}$ (Figure 1(b) and Table 1).

O. basilicum inhibited also α -amylase yet at less potency compared with its inhibition to α -glucosidase. 500 $\mu\text{g/mL}$ of *O. basilicum* extract inhibited α -amylase by only $25.4\% \pm 3.3$ (Figure 2(a)). Caffeic acid inhibited α -amylase in a dose-dependent manner and led to $42.7\% \pm 3.0$ inhibition at 1 mM (Figure 2(b)).

Results for the docking experiments met well with the *in vitro* evaluation. Phytochemicals screened in the extract from OB were tested for their binding affinities, inhibition constants, and the root mean square deviation (RMSD) values for the ligand structure upon docking from the reference one. Three compounds showed potent inhibition to both α -glucosidase and α -amylase: beta-sitosterol followed by 4,7-dimethoxyindan-1-one and then caffeic acid (Tables 2 and 3). Weak nonpolar contacts accounted for most of the interactions at the binding interface, with few polar contacts seen as hydrogen bonding between the ligand and the indicated amino acid residues (Figure 3).

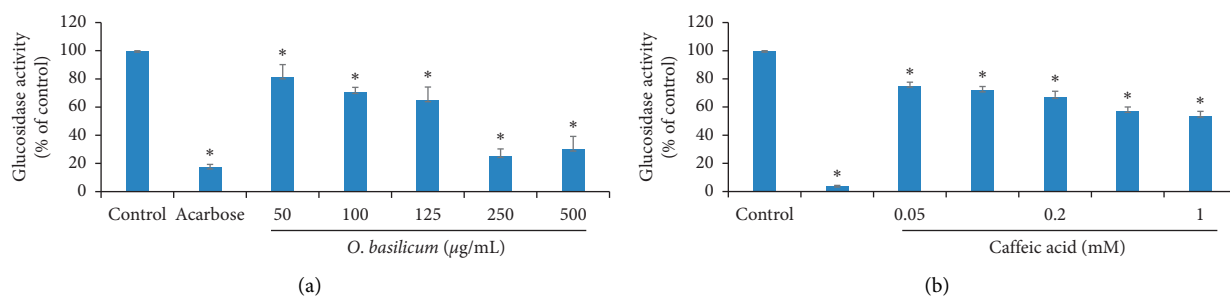


FIGURE 1: Effects of *O. basilicum* (a) and caffeic acid (b) on intestinal α -glucosidase. Values represent the mean \pm SEM of three experiments. The *t*-test of statistical calculations was conducted using SPSS, version 23.0. * $p < 0.05$, which is considered significant as compared with controls.

TABLE 1: The IC₅₀ values of *O. basilicum* and caffeic acid for intestinal α -glucosidase and α -amylase.

	<i>O. basilicum</i>	Caffeic acid
α -Glucosidase	160 \pm 10 μ g/mL	1.05 \pm 0.25 mM
α -Amylase	>500 μ g/mL	>1 mM

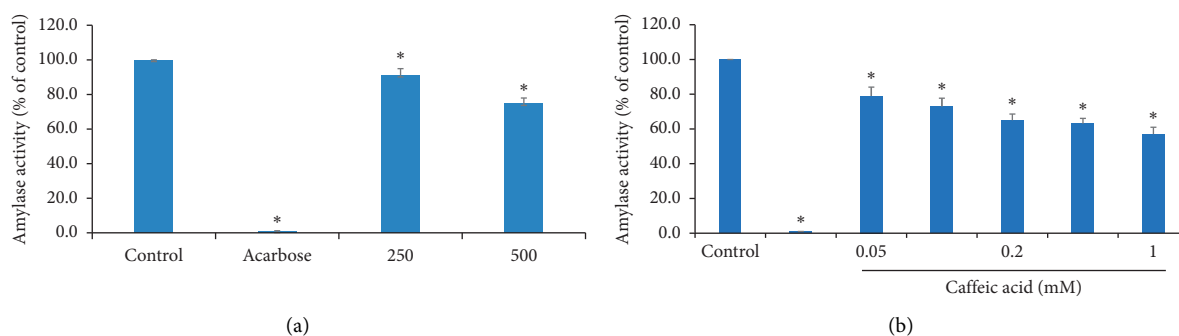


FIGURE 2: Effects of *Ocimum basilicum* (a) and caffeic acid (b) on pancreatic α -amylase. Values represent the mean \pm SEM of three experiments. The *t*-test of statistical calculations was conducted using SPSS, version 23.0. * $p < 0.05$, which is considered significant as compared with controls.

Other potent inhibitors also existed that showed only an inhibitory effect against α -glucosidase but not α -amylase: E-isoeugenol ($K_i = 22.33 \mu\text{M}$) followed by linalool ($K_i = 78.91 \mu\text{M}$), beta-D-glucopyranoside, 5-methyl-2-1-methylethyl-phenyl ($K_i = 86.74 \mu\text{M}$), and finally uvasol ($K_i = 118.93 \mu\text{M}$) in a descending order with respect to their inhibition constants (Figure 4). This might explain why the extract had more potent effect on the enzyme α -glucosidase than the α -amylase enzyme in the *in vitro* experiments. Indeed, the inhibition constants for the common inhibitory phytochemicals had very similar effects.

Pyroglutamic acid existed in both inhibitor lists for α -glucosidase and α -amylase, but the inhibition was predicted to be weak when compared with other phytochemicals ($K_i = 298.88 \mu\text{M}$, 276.50 μM for α -glucosidase and α -amylase, respectively, see Figure 3).

4. Discussion

O. basilicum has been reported as a potential antidiabetic herb, yet the action mechanisms and the potential antidiabetic compounds in *O. basilicum* that inhibit intestinal

digestive enzymes were not discussed and some were not identified. Here, *O. basilicum* methanol extract and one of the major compounds, i.e., caffeic acid inhibited α -amylase and α -glucosidase in a dose-dependent manner. Docking experiments were undertaken to understand the mechanism by which the *O. basilicum* extracts would inhibit the two enzymes. Phytochemicals in the *O. basilicum* extract were screened for their inhibitory potency, binding interface, and structural fluctuations. The number of inhibitors that were predicted to work against α -glucosidase was twofold more than those inhibiting α -amylase (8 active phytochemicals for α -glucosidase vs 4 active phytochemicals for α -amylase). Still, the inhibition level of the four common phytochemicals was comparable for the two enzymes. This would justify the higher inhibition levels for α -glucosidase when compared with α -amylase *in vitro*. The deviations from the reference structure (the RMSD values) were highly reasonable for all plausible inhibitors. Of the four common inhibitors, the binding interface for caffeic acid and pyroglutamic acid showed more polar contacts than beta-sitosterol and 4,7-dimethoxyindan-1-one. Thus, more polarity did not contribute to a more stable binding interface and the binding

TABLE 2: Binding free energies, inhibition constants, and the RMSD values calculated by AutoDock for ligand binding to α -glucosidase.

OB phytochemical	AutoDock binding free energy (kcal/mol)	AutoDock inhibition constant (K_i)	RMSD for the ligand from the reference structure (Å)
2-Hydroxymethyl-6-3,4,5-trihydroxy-2-hydroxymethyl	-3.37	3.36 mM	11.463
3,3-Dihydroxyacrylic acid	-3.33	3.61 mM	15.571
4,7-Dimethoxyindan-1-one	-5.79	56.88 μ M	8.094
Alpha-hydroxyhydrocaffeic acid	-4.29	721.41 μ M	7.700
Alpha-linolenic acid	-4.74	337.32 μ M	9.710
Arabinitol	-1.35	102.52 mM	49.393
Beta-D-galactofuranose	-4.19	853.24 μ M	6.313
Beta-D-glucopyranoside,5-methyl-2-1-methylethyl-phenyl	-5.54	86.74 μ M	12.272
Beta-D-ribofuranose	-3.64	2.16 mM	26.731
Beta-sitosterol	-7.93	1.53 μ M	30.109
Caffeic acid	-5.45	100.99 μ M	10.935
Cyanuric acid	-4.66	382.74 μ M	14.773
D-Xylopyranose	-3.88	1.42 mM	28.285
D-Xylose	-2.26	22.04 mM	23.337
E-but-2-ene-1-4-diol	-3.79	1.67 mM	9.428
E-Isoeugenol	-6.35	22.33 μ M	10.075
Glucopyranose	-2.97	6.70 mM	6.426
Hydroquinone	-4.55	461.18 μ M	8.566
Inositol	-4.48	520.07 μ M	38.863
Linalool	-5.60	78.91 μ M	48.561
Linoleic acid	-3.46	2.91 mM	17.302
Mannitol	-3.26	4.05 mM	9.698
Palmitic acid	-3.91	1.35 mM	59.142
Pentane-1,2,5-triol	-3.23	4.26 mM	49.447
Pyroglutamic acid	-4.81	298.88 μ M	16.630
Talose	-2.91	7.34 mM	6.730
Uvasol	-5.35	118.93 μ M	45.174
Glycerol	-1.11	152.58 mM	—
L-Valine	-2.93	7.10 mM	—
Succinate	-3.77	1.71 mM	—
Threitol	-1.58	69.02 mM	—
Urea	-2.96	6.82 mM	—

TABLE 3: Binding free energies, inhibition constants, and the RMSD values calculated by AutoDock for ligand binding to α -amylase.

OB phytochemical	AutoDock binding free energy (kcal/mol)	AutoDock inhibition constant (K_i)	RMSD for the ligand from the reference structure (Å)
2-Hydroxymethyl-6-3,4,5-trihydroxy-2-hydroxymethyl	-3.26	4.09 mM	45.065
3,3-Dihydroxyacrylic acid	-3.99	1.20 mM	56.124
4,7-Dimethoxyindan-1-one	-5.77	59.10 μ M	44.384
Alpha-hydroxyhydrocaffeic acid	-4.67	379.57 μ M	64.753
Alpha-linolenic acid	-4.03	1.11 mM	50.314
Arabinitol	-2.05	31.56 mM	41.922
Beta-D-galactofuranose	-3.52	2.61 mM	48.439
Beta-D-glucopyranoside,5-methyl-2-1-methylethyl-phenyl	-4.02	1.14 mM	44.414
Beta-D-ribofuranose	-3.35	3.48 mM	44.547
Beta-sitosterol	-8.38	719.79 nm	48.783
Caffeic acid	-5.25	140.92 μ M	68.360
Cyanuric acid	-4.79	310.58 μ M	81.408
D-Xylopyranose	-3.48	2.83 mM	45.736
D-Xylose	-2.48	15.29 mM	70.312
E-but-2-ene-1-4-diol	-4.30	708.76 μ M	39.448
E-Isoeugenol	-4.64	397.34 μ M	48.923
Glucopyranose	-3.80	1.65 mM	46.170

TABLE 3: Continued.

OB phytochemical	AutoDock binding free energy (kcal/mol)	AutoDock inhibition constant (K_i)	RMSD for the ligand from the reference structure (Å)
Hydroquinone	-4.13	933.22 μ M	44.919
Inositol	-3.78	1.68 mM	90.688
Linalool	-4.13	933.83 μ M	53.531
Linoleic acid	-3.75	1.77 mM	79.184
Mannitol	-2.41	17.08 mM	44.479
Palmitic acid	-4.02	1.13 mM	57.625
Pentane-1,2,5-triol	-2.99	6.45 mM	36.675
Pyroglutamic acid	-4.85	276.50 μ M	58.241
Talose	-2.43	16.69 mM	64.498
Uvasol	-4.39	603.30 μ M	45.065
Glycerol	-1.35	102.76 mM	—
L-Valine	-2.47	15.48 mM	—
Succinate	-4.00	1.16 mM	—
Threitol	-0.80	259.66 mM	—
Urea	-2.68	10.78 mM	—

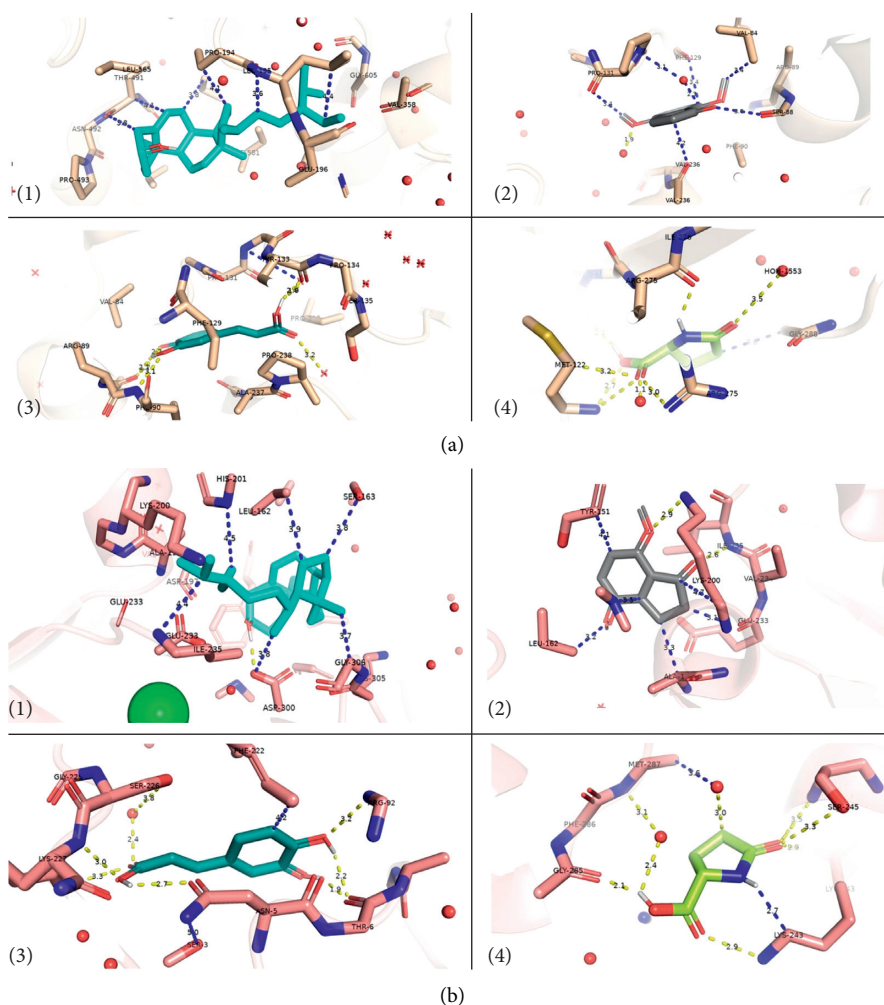


FIGURE 3: Binding interface between plausible inhibitors and (a) the α -glucosidase enzymes: (1) beta-sitosterol, (2) 4,7-dimethoxyindan-1-one, (3) caffeic acid, and (4) pyroglutamic acid; and (b) the α -amylase enzymes: (1) beta-sitosterol, (2) 4,7-dimethoxyindan-1-one, (3) caffeic acid, and (4) pyroglutamic acid. All amino acids that are within 5 Å from the ligand are shown as sticks. The rest of the protein is shown in an 80% transparent cartoon model. Polar contacts are shown in yellow, whereas other possible contacts are in blue. The green ball in label (1) of subset 3(b) refers to a chloride ion near the active site.

- [10] H. Zaid, B. Saad, A. A. Mahdi, A. K. Tamrakar, P. S. Haddad, and F. U. Afifi, "Medicinal plants and natural active compounds for diabetes and/or obesity treatment," *Evidence-Based Complementary and Alternative Medicine*, vol. 2015, Article ID 469762, 2 pages, 2015.
- [11] R. A. DeFronzo, "Insulin resistance, lipotoxicity, type 2 diabetes and atherosclerosis: the missing links. the Claude Bernard lecture 2009," *Diabetologia*, vol. 53, no. 7, pp. 1270–1287, 2010.
- [12] M. Kitada, Z. Y. Zhang, A. Mima, and G. L. King, "Molecular mechanisms of diabetic vascular complications," *Journal of Diabetes Investigation*, vol. 1, no. 3, pp. 77–89, 2010.
- [13] K. A. Deans and N. Sattar, "Anti-inflammatory drugs and their effects on type 2 diabetes," *Diabetes Technology & Therapeutics*, vol. 8, no. 1, pp. 18–27, 2006.
- [14] K. Hanhineva, R. Torronen, I. Bondia-Pons et al., "Impact of dietary polyphenols on carbohydrate metabolism," *International Journal of Molecular Sciences*, vol. 11, no. 4, pp. 1365–1402, 2010.
- [15] F. A. van de Laar, P. L. Lucassen, R. P. Akkermans, F. H. van de Lisdonk, G. E. Rutten, and C. van Weel, "Alpha-glucosidase inhibitors for patients with type 2 diabetes—results from a cochrane systematic review and meta-analysis," *Diabetes Care*, vol. 28, no. 1, pp. 154–163, 2005.
- [16] O. Said, S. Fulder, K. Khalil, H. Azaizeh, E. Kassis, and B. Saad, "Maintaining a physiological blood glucose level with glucolevel, a combination of four anti-diabetes plants used in the traditional Arab herbal medicine," *Evidence-Based Complementary and Alternative Medicine*, vol. 5, no. 4, pp. 421–428, 2008.
- [17] B. Saad, H. Zaid, S. Shanak, and S. Kadan, *Anti-Diabetes and Anti-Obesity Medicinal Plants and Phytochemicals*, Springer, Berlin, Germany, 2017.
- [18] S. Kadan, B. Saad, Y. Sasson, and H. Zaid, "In vitro evaluation of anti-diabetic activity and cytotoxicity of chemically analysed *Ocimum basilicum* extracts," *Food Chemistry*, vol. 196, pp. 1066–1074, 2016.
- [19] J. Simon, M. Morales, W. Phippen, R. Vieira, and Z. Hao, *Basil: A Source of Aroma Compounds and a Popular Culinary and Ornamental Herb. Perspectives on New Crops and New Uses Alexandria*, ASHS Press, Richmond, VA, USA, 1999.
- [20] B. S. Siddiqui, H. A. Bhatti, S. Begum, and S. Perwaiz, "Evaluation of the antimycobacterium activity of the constituents from *Ocimum basilicum* against mycobacterium tuberculosis," *Journal of Ethnopharmacology*, vol. 144, no. 1, pp. 220–222, 2012.
- [21] F. Bantis, T. Ouzounis, and K. Radoglou, "Artificial LED lighting enhances growth characteristics and total phenolic content of *Ocimum basilicum*, but variably affects transplant success," *Scientia Horticulturae*, vol. 198, pp. 277–283, 2016.
- [22] K. S. Bora, S. Arora, and R. Shri, "Role of *Ocimum basilicum* L. in prevention of ischemia and reperfusion-induced cerebral damage, and motor dysfunctions in mice brain," *Journal of Ethnopharmacology*, vol. 137, no. 3, pp. 1360–1365, 2011.
- [23] J. H. Loughrin and M. J. Kasperbauer, "Light reflected from colored mulches affects aroma and phenol content of sweet basil (*Ocimum basilicum* L.) leaves," *Journal of Agricultural and Food Chemistry*, vol. 49, no. 3, pp. 1331–1335, 2001.
- [24] M. Z. Basilio and J. C. Basilio, "Inhibitory effects of some spice essential oils on *Aspergillus ochraceus* NRRL 3174 growth and ochratoxin A production," *Letters in Applied Microbiology*, vol. 29, no. 4, pp. 238–241, 1999.
- [25] H. P. Bais, T. S. Walker, H. P. Schweizer, and J. A. Vivanco, "Root specific elicitation and antimicrobial activity of rosmarinic acid in hairy root cultures of *Ocimum basilicum*," *Plant Physiology and Biochemistry*, vol. 40, pp. 983–995, 2002.
- [26] A. Khalil, "Antimicrobial activity of ethanolic extracts of *Ocimum basilicum* leaf from Saudi Arabia," *Biotechnology*, vol. 12, pp. 61–64, 2013.
- [27] P. Kathirvel and S. Ravi, "Chemical composition of the essential oil from basil (*Ocimum basilicum* Linn.) and its in vitro cytotoxicity against HeLa and HEP-2 human cancer cell lines and NIH 3T3 mouse embryonic fibroblasts," *Natural Product Research*, vol. 26, no. 12, pp. 1112–1118, 2012.
- [28] M. A. Hossain, M. J. Kabir, S. M. Salehuddin et al., "Antibacterial properties of essential oils and methanol extracts of sweet basil *Ocimum basilicum* occurring in Bangladesh," *Pharmaceutical Biology*, vol. 48, no. 5, pp. 504–511, 2010.
- [29] W. B. Phippen and J. E. Simon, "Anthocyanins in basil (*Ocimum basilicum* L.)," *Journal of Agricultural and Food Chemistry*, vol. 46, no. 5, pp. 1734–1738, 1998.
- [30] P. Raina, M. Deepak, C. V. Chandrasekaran, A. Agarwal, N. Wagh, and R. Kaul-Ghanekar, "Comparative analysis of anti-inflammatory activity of aqueous and methanolic extracts of *Ocimum basilicum* (basil) in RAW264.7, SW1353 and human primary chondrocytes in respect of the management of osteoarthritis," *Journal of Herbal Medicine*, vol. 6, no. 1, pp. 28–36, 2016.
- [31] S. Amrani, H. Harnafi, D. Gadi et al., "Vasorelaxant and anti-platelet aggregation effects of aqueous *Ocimum basilicum* extract," *Journal of Ethnopharmacology*, vol. 125, no. 1, pp. 157–162, 2020.
- [32] C. M. M. Freire, M. O. M. Marques, and M. Costa, "Effects of seasonal variation on the central nervous system activity of *Ocimum gratissimum* L. essential oil," *Journal of Ethnopharmacology*, vol. 105, no. 1–2, pp. 161–166, 2006.
- [33] I. Tohti, M. Tursun, A. Umar, S. Turdi, H. Imin, and N. Moore, "Aqueous extracts of *Ocimum basilicum* L. (sweet basil) decrease platelet aggregation induced by ADP and thrombin in vitro and rats arterio-venous shunt thrombosis in vivo," *Thrombosis Research*, vol. 118, no. 6, pp. 733–739, 2006.
- [34] S. Chiba, "Molecular mechanism in alpha-glucosidase and glucoamylase," *Bioscience Biotechnology and Biochemistry*, vol. 61, no. 8, pp. 1233–1239, 1997.
- [35] L. H. Hoefsloot, M. Hoogveenwesterveld, A. J. J. Reuser, and B. A. Oostra, "Characterization of the human lysosomal alpha-glucosidase gene," *Biochemical Journal*, vol. 272, no. 2, pp. 493–497, 1990.
- [36] M. M. P. Hermans, M. A. Kroos, J. Vanbeeumen, B. A. Oostra, and A. J. J. Reuser, "Human lysosomal alpha-glucosidase—characterization of the catalytic site," *Journal of Biological Chemistry*, vol. 266, no. 21, pp. 13507–13512, 1991.
- [37] X.-Q. Wu, H. Xu, H. Yue, K.-Q. Liu, and X.-Y. Wang, "Inhibition kinetics and the aggregation of alpha-glucosidase by different denaturants," *Protein Journal*, vol. 28, no. 9–10, pp. 448–456, 2009.
- [38] J. A. Lim, L. S. Li, and N. Raben, "Pompe disease: from pathophysiology to therapy and back again," *Frontiers in Aging Neuroscience*, vol. 6, p. 177, 2014.
- [39] H. Matsushita, M. Takenaka, and H. Ogawa, "Porcine pancreatic alpha-amylase shows binding activity toward N-linked oligosaccharides of glycoproteins," *Journal of Biological Chemistry*, vol. 277, no. 7, pp. 4680–4686, 2002.
- [40] K. Asanuma-Date, Y. Hirano, N. Le et al., "Functional regulation of sugar assimilation by N-Glycan-specific interaction of pancreatic alpha-amylase with glycoproteins of duodenal brush border membrane," *Journal of Biological Chemistry*, vol. 287, no. 27, pp. 23104–23118, 2012.

- [41] J. V. Tricoli and T. B. Shows, "Regional assignment of human amylase (AMY) to $p22-p21$ of chromosome-1," *Somatic Cell and Molecular Genetics*, vol. 10, no. 2, pp. 205–210, 1984.
- [42] D. Carpenter, S. Dhar, L. M. Mitchell et al., "Obesity, starch digestion and amylase: association between copy number variants at human salivary (AMY1) and pancreatic (AMY2) amylase genes," *Human Molecular Genetics*, vol. 24, no. 12, pp. 3472–3480, 2015.
- [43] A. Abe, H. Yoshida, T. Tonozuka, Y. Sakano, and S. Kamitori, "Complexes of *Thermoactinomyces vulgaris* R-47 alpha-amylase 1 and pullulan model oligosaccharides provide new insight into the mechanism for recognizing substrates with alpha-(1,6) glycosidic linkages," *FEBS Journal*, vol. 272, no. 23, pp. 6145–6153, 2005.
- [44] A. Kadziola, M. Sogaard, B. Svensson, and R. Haser, "Molecular structure of a barley alpha-amylase-inhibitor complex: implications for starch binding and catalysis," *Journal of Molecular Biology*, vol. 278, no. 1, pp. 205–217, 1998.
- [45] A. Kadziola, J. Abe, B. Svensson, and R. Haser, "Crystal and molecular-structure of barley alpha-amylase," *Journal of Molecular Biology*, vol. 239, no. 1, pp. 104–121, 1994.
- [46] M. Machius, G. Wiegand, and R. Huber, "Crystal-structure of calcium-depleted bacillus-licheniformis alpha-amylase at 2.2- \AA resolution," *Journal of Molecular Biology*, vol. 246, no. 4, pp. 545–559, 1995.
- [47] A. O. Ademiluyi and G. Oboh, "Aqueous extracts of roselle (*Hibiscus sabdariffa* linn.) varieties inhibit alpha-amylase and alpha-glucosidase activities in vitro," *Journal of Medicinal Food*, vol. 16, no. 1, pp. 88–93, 2013.
- [48] S. Adisakwattana, T. Ruengsamran, P. Kampa, and W. Sompong, "In vitro inhibitory effects of plant-based foods and their combinations on intestinal α -glucosidase and pancreatic α -amylase," *BMC Complementary Medicine and Therapies*, vol. 12, no. 1, p. 110, 2010.
- [49] Y. M. Kim, M. H. Wang, and H. I. Rhee, "A novel alpha-glucosidase inhibitor from pine bark," *Carbohydrate Research*, vol. 339, no. 3, pp. 715–717, 2004.
- [50] D. M. Lowe, P. T. Corbett, P. Murray-Rust, and R. C. Glen, "Chemical name to structure: OPSIN, an open source solution," *Journal of Chemical Information and Modeling*, vol. 51, no. 3, pp. 739–753, 2011.
- [51] N. M. O'Boyle, M. Banck, C. A. James, C. Morley, T. Vandermeersch, and G. R. Hutchison, "Open babel: an open chemical toolbox," *Journal of Cheminformatics*, vol. 3, p. 33, 2011.
- [52] G. M. Morris, R. Huey, W. Lindstrom et al., "AutoDock4 and AutoDockTools4: automated docking with selective receptor flexibility," *Journal of Computational Chemistry*, vol. 30, no. 16, pp. 2785–2791, 2009.
- [53] S. Ghosh, M. Ahire, S. Patil et al., "Antidiabetic activity of *gnidia glauca* and *dioscorea bulbifera*: potent amylase and glucosidase inhibitors," *Evidence-Based Complementary and Alternative Medicine*, vol. 2012, Article ID 929051, 10 pages, 2012.
- [54] M. Malekaneh and A. Zarban, "Antidiabetic activity of water extract of B-100 (a herbal formulation) in streptozotocin-induced diabetic rats," *Clinical Biochemistry*, vol. 44, no. 13, p. S348, 2014.
- [55] L. Moradabadi, S. M. Kouhsari, and M. F. Sani, "Hypoglycemic effects of three medicinal plants in experimental diabetes: inhibition of rat intestinal alpha-glucosidase and enhanced pancreatic insulin and cardiac glut-4 mRNAs expression," *Iranian Journal of Pharmaceutical Research*, vol. 12, no. 3, pp. 387–397, 2013.

Research Article

Tyrosinase Inhibitors from the Stems of *Streblus ilicifolius*

Nhan T. Nguyen ^{1,2,3}, Phu H. Dang ^{1,2}, Hai X. Nguyen ^{1,2}, Truong N. V. Do ^{1,2},
Tho H. Le ^{1,2}, Tuyen Q. H. Le ^{1,2} and Mai T. T. Nguyen ^{1,2,3}

¹Faculty of Chemistry, University of Science, 227 Nguyen Van Cu Street, Ward 4, District 5, Ho Chi Minh City, Vietnam

²Vietnam National University, Quarter 6, Linh Trung Ward, Thu Duc District, Ho Chi Minh City, Vietnam

³Cancer Research Laboratory, University of Science, 227 Nguyen Van Cu Street, District 5, Ho Chi Minh City, Vietnam

Correspondence should be addressed to Mai T. T. Nguyen; nttmai@hcmus.edu.vn

Received 18 March 2021; Accepted 25 June 2021; Published 1 July 2021

Academic Editor: Hilal Zaid

Copyright © 2021 Nhan T. Nguyen et al. This is an open access article distributed under the Creative Commons Attribution License, which permits unrestricted use, distribution, and reproduction in any medium, provided the original work is properly cited.

Two new stilbene derivatives, named strebluses C and D, were isolated from the EtOAc-soluble fraction of the stems of *Streblus ilicifolius* (Moraceae). Its absolute configuration was elucidated based on NMR spectroscopic data interpretation and optical rotation calculation. Streblus C possesses strong tyrosinase inhibitory activity with an IC₅₀ value of 0.01 μM. Docking studies of **1** and **2** with *oxy*-tyrosinase were carried out to analyze their interactions. The analysis of the docked poses confirmed that **1** showed better binding affinity for *oxy*-tyrosinase than that of **2**.

1. Introduction

Tyrosinase (EC 1.14.18.1), which is a binuclear copper-containing monooxygenase, is a key enzyme in the oxidation of phenol to the corresponding *o*-quinone [1, 2]. It plays a main factor causing freckles, brown age spots, and melasma. Some commercial compounds, such as hydroquinone, arbutin, kojic acid, azelaic acid, L-ascorbic acid, ellagic acid, and tranexamic acid, were reported as the well-known tyrosinase inhibitors. These compounds have been used as skin whitening agents in cosmetic products, but they have certain drawbacks [3]. Thus, the finding of the new efficient and safe tyrosinase inhibitors is necessary for antihyperpigmentation product development.

Streblus ilicifolius (Vidal) Corner, which belongs to Moraceae family, was found and cultivated in Vietnam. Its barks have been traditionally used as an antipimple medicine. In a few published studies, some phenolic compounds have been reported in this plant [4–7]. In our continued studies on the screening of medicinal plants for tyrosinase inhibitory activity [8–12], it was found that a MeOH-soluble extract of the stems of *Streblus ilicifolius* showed a strong inhibitory effect, with an IC₅₀ value of 0.63 μg·mL⁻¹. Thus,

our study on chemical constituents of the stems of *S. ilicifolius* was carried out, leading to the isolation of two undescribed stilbene derivatives, strebluses C (**1**) and D (**2**). Compound **1** showed a strong tyrosinase inhibitory activity with an IC₅₀ value of 0.01 μM, which makes it 4400 times more potent than that of kojic acid (IC₅₀, 44.6 μM). In addition, molecular docking studies of **1** and **2** with the *oxy*-form of the copper-bound *Streptomyces castaneoglobisporus* tyrosinase were performed.

2. Materials and Methods

2.1. General Experimental Procedures. Optical values were measured on a Shimadzu UV-1800 spectrophotometer (Shimadzu Pte., Ltd., Singapore). IR spectra were measured with a Shimadzu IR-408 infrared spectrometer (Shimadzu Pte., Ltd., Singapore). NMR spectra were acquired on a Bruker Avance III 500 spectrometer (Bruker BioSpin AG, Bangkok, Thailand). Chemical shifts are expressed as δ values. HRESIMS data were acquired on Bruker micrOTOF-QII mass spectrometer (Bruker Singapore Pte., Ltd., Singapore). Column chromatography was carried out using silica gel 60, 0.06–0.2 mm (Scharlau, Barcelona, Spain), and

LiChroprep RP-18, 40–63 μm (Merck KGaA, Darmstadt, Germany). Kieselgel 60 F₂₅₄ or RP-18 F₂₅₄ plates for TLC were purchased from Merck (Merck KGaA, Darmstadt, Germany). Tyrosinase (EC 1.14.18.1) from mushroom (3933 U·mL⁻¹) and L-dihydroxyphenylalanine (L-DOPA) were obtained from Sigma-Aldrich (Sigma-Aldrich Pte Ltd, Singapore). Other chemicals were of the highest grade available.

2.2. Plant Material. The stems of *Streblus ilicifolius* were collected at Hoai Nhon District, Binh Dinh Province, Vietnam, in October 2017. The plant was identified by Dr. rer. nat. Anh Tuan Dang-Le, Faculty of Biology and Biotechnology, University of Science, Ho Chi Minh City, Vietnam. A voucher sample (MCE0052) has been deposited at the Department of Medicinal Chemistry, Faculty of Chemistry, University of Science, Ho Chi Minh City, Vietnam.

2.2.1. Extraction and Isolation. The dried powdered stems of *S. ilicifolius* (7.0 kg) were exhaustively extracted in a Soxhlet extractor with *n*-hexane, EtOAc, and MeOH to yield *n*-hexane-(64.8 g), EtOAc-(117.2 g), and MeOH-(378.0 g) soluble fractions, respectively. The EtOAc-soluble fraction was chromatographed by silica gel column chromatography (15 × 150 cm) and eluted with MeOH–CHCl₃ (v/v, 0:100 → 100:0) mixtures to afford 18 fractions (Fr.1–Fr.18). Fraction Fr.8 (0.8 g) was separated by silica gel column chromatography with MeOH–CHCl₃ (v/v, 0:100 → 30:70) mixtures to obtain six subfractions (Fr.8.1–Fr.8.6). Subfraction Fr.8.1 (34.8 mg) was loaded onto a silica gel column and eluted with EtOAc–CHCl₃ mixtures (v/v, 0:100 → 100:0) and then purified by preparative TLC with an EtOAc–CHCl₃ mixture (v/v, 15:85) to afford compound **2** (2.0 mg). Fraction Fr.14 (19.6 g) was subjected to further silica gel column chromatography and was eluted with CHCl₃–*n*-hexane (v/v, 0:100 → 100:0) mixtures to yield 11 subfractions (Fr.14.1–Fr.14.11). Subfraction Fr.14.2 (69.0 mg) was chromatographed over a silica gel column with CHCl₃–*n*-hexane (v/v, 0:100 → 100:0) mixtures to obtain two subfractions (Fr.14.2.1 and Fr.14.2.2). Subfraction Fr.14.2.2 (28.1 mg) was again chromatographed with CHCl₃–*n*-hexane (v/v, 0:100 → 100:0) mixtures to give four subfractions (Fr.14.2.2.1–Fr.14.2.2.4). Subfraction Fr.14.2.2.3 (8.5 mg) was purified by preparative TLC with EtOAc–*n*-hexane (v/v, 20:80) mixture to afford **1** (3.9 mg).

2.2.2. Streblus C (1). Yellow, amorphous powder; ¹H and ¹³C NMR (500 MHz, acetone-*d*₆, see Table 1 and Figures S2–S7); HRESIMS *m/z* 393.1704 [M + Na]⁺ (Figure S8) (calcd for C₂₂H₂₆O₅Na, 393.1678).

2.2.3. Streblus D (2) (Figures S9–S15). Yellow, amorphous powder; ¹H and ¹³C NMR (500 MHz, acetone-*d*₆, see Table 1 and Figures S8–S14); HRESIMS *m/z* 351.1224 [M + Na]⁺ (Figure S15) (calcd for C₁₉H₂₀O₅Na, 351.1208).

2.3. Tyrosinase Inhibitory Assay. All pure compounds were dissolved in DMSO and tested at concentrations ranging from 0.01 to 100 μM . Assay mixtures in 0.1 M phosphate buffer pH 6.8 were prepared immediately before use, consisting of 100 μL of tyrosinase solution (15 U/mL) and 1900 μL of test solution. These mixtures were preincubated at 32°C for 30 min, followed by addition of 1000 μL of L-DOPA 1.5 mM in pH 6.8 phosphate buffer, and incubated at 32°C for 7 min. The absorbance (*A*) at 475 nm was acquired on Shimadzu UV-1800 spectrophotometer. The inhibitory percentage (%) was calculated according to the formula: $I\% = [(A_{\text{control}} - A_{\text{sample}}) / A_{\text{control}}] \times 100\%$. Data were represented as means ± standard error (*n* = 3). The IC₅₀ values were determined by using GraphPad Prism software with multivariate nonlinear regression and $R^2 > 0.9$. Kojic acid was used as positive control.

2.4. HPLC Data of the EtOAc-Soluble Fraction from S. ilicifolius. The concentrations of the EtOAc-soluble fraction and streblus C (**1**) were approximately 12,000 ppm and 200 ppm, respectively. The detection wavelength was set at 385 nm. An Agilent Zorbax SB-C18 column (150 × 4.6 × 5 mm) was used with a flow rate of 1 mL/min. The injection volume was 10 mL, and the column temperature was maintained at 30°C. The mixtures of water and ACN were used as the mobile phase with gradient elution (20 → 40% ACN for 30 min).

2.5. Optical Rotation Calculation. The conformational searches were performed on Spartan'18 (Wave function, Inc., Irvine, USA) by using Merck molecular force field (MMFF). All conformers with Boltzmann weight >10% were optimized using DFT method at the B3LYP/6-31G* level in the gas phase, to give the preferred conformers with the Boltzmann weight >90%. The optical rotation calculations at sodium D line frequency were carried out using the B3LYP functional and the 6-311++G(2d, 2p) basis set in IEFPCM solvation model for methanol. These calculations were performed on Gaussian 09 (Gaussian, Inc., Wallingford, USA). The calculated optical rotation values were expressed as Boltzmann-weighted average of all output data.

2.6. Molecular Docking. Docking studies of **1** and **2**, positive reference (kojic acid), and decoy (hypoxanthine) were performed with Molecular Operating Environment 2019 (MOE 2019.0102) suite (Chemical Computing Group ULC, Montreal, Canada). The structures of these compounds were constructed by using the Builder module. Subsequently, all compounds were minimized up to 0.0001 gradients using the Amber12: EHT force field. The crystal structure of the oxy-tyrosinase was taken from the Protein Data Bank (PDB ID: 1WX2). The caddie protein (ORF378) and water molecules were removed. The enzyme structure was prepared using the QuickPrep module. The binding site was determined based on the Propensity for Ligand Binding (PLB) score in the Site Finder module. The molecular docking was performed by Dock Module, using Triangle Matcher

TABLE 1: ^1H (500 MHz) and ^{13}C (125 MHz) NMR data (acetone- d_6) for compounds **1** and **2**.

Position	1		2	
	δ_{C} , type C	δ_{H} (J, Hz)	δ_{C} , type C	δ_{H} (J, Hz)
1	116.3, C		122.0, C	
2	158.3, C		158.0, C	
3	103.6, CH	6.46, d (2.4)	98.3, CH	7.00, d (2.1)
4	160.8, C		158.9, C	
5	108.9, CH	6.42, dd (8.5, 2.4)	114.3, CH	6.87, dd (8.5, 2.1)
6	129.6, CH	7.48, d (8.5)	123.4, CH	7.52, d (8.5)
1'	153.9, C		143.6, C	
2'	125.0, CH	5.97, d (2.0)	118.7, CH	6.48, d (2.1)
3'	199.2, C=O		200.6, C=O	
4'	82.8, C		79.6, C	
5'	77.3, CH	4.48, dd (4.3, 1.6)	73.0, CH	4.27, dd (5.9, 2.7)
6'	27.4, CH ₂	3.19, dd (18.8, 1.6) 2.82, ddd (18.8, 4.3, 2.0)	32.0, CH ₂	3.15, ddd (18.5, 5.9, 2.1) 3.08, dd (18.5, 2.7)
α	132.3, CH	7.40, d (16.4)	110.7, CH	7.31, s
β	126.4, CH	7.01, d (16.4)	153.2, C	
1''	33.0, CH ₂	2.54, dd (14.4, 8.0) 2.39, dd (14.4, 7.2)	35.3, CH ₂	2.47, dd (14.9, 7.7) 2.40, dd (14.9, 7.0)
2''	118.1, CH	5.18, brs	118.8, CH	5.22, brt (7.3)
3''	136.0, C		135.0, C	
4''	26.0, CH ₃	1.68, s	26.1, CH ₃	1.67, s
5''	18.1, CH ₃	1.63, s	18.1, CH ₃	1.58, s
1'''	108.0, C			
2'''	27.8, CH ₃	1.32, s		
3'''	26.8, CH ₃	1.18, s		
4-OH				8.88, s
4'-OH				4.18, s
5'-OH				3.83, s

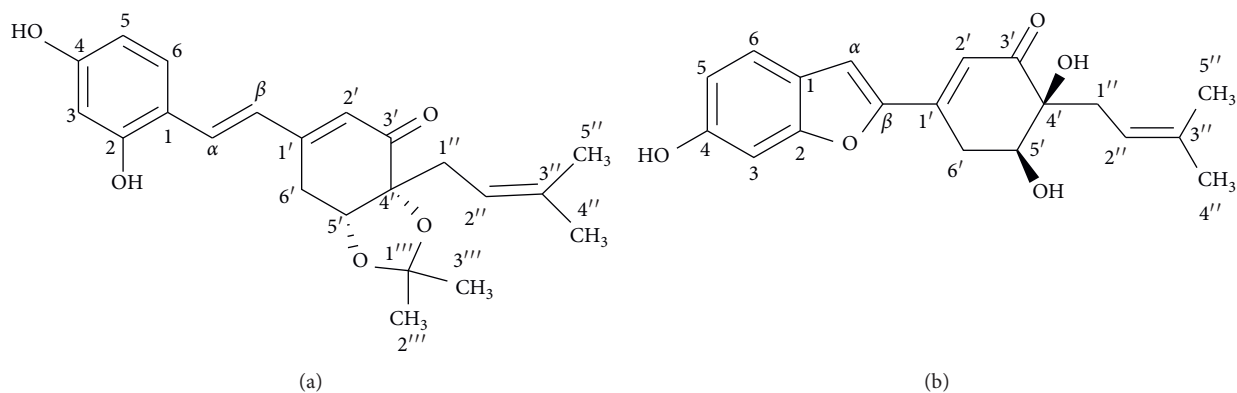
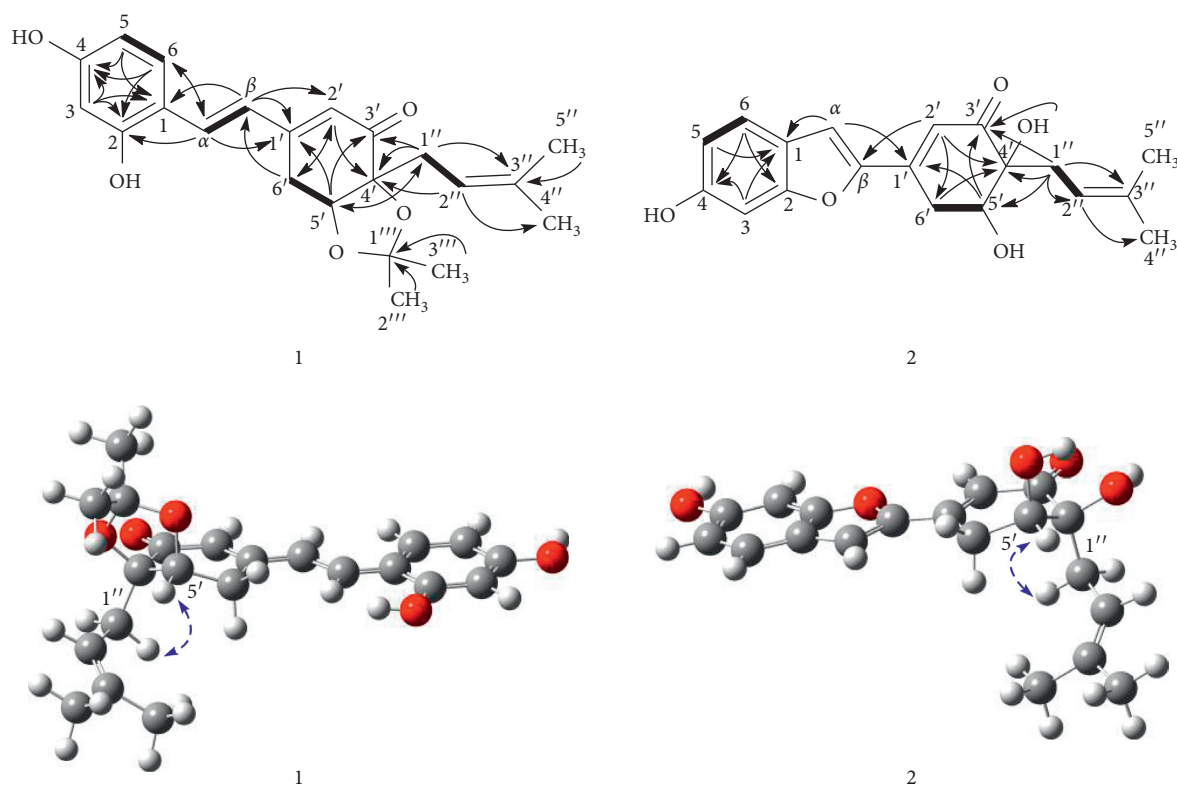
Placement, Induced Fit Refinement, London Dg, and GBVI/WSA dG scoring methods. Five top poses showed up based on the negative binding free energy value (S value). The best pose was selected to analyze the receptor–ligand interactions by using BIOVIA Discovery Studio Visualizer 2016 (Dassault Systèmes Americas Corp., Waltham, USA).

3. Results and Discussion

3.1. Extraction and Isolation. The dried powdered stems of *S. ilicifolius* were exhaustively extracted in a Soxhlet extractor with *n*-hexane, EtOAc, and MeOH to yield the corresponding fractions. The EtOAc-soluble fraction was repeatedly chromatographed using silica gel CC and preparative TLC to obtain two undescribed stilbene derivatives, strebluses **C** (**1**) and **D** (**2**) (Figure 1).

3.2. Structural Elucidation of Two New Isolated Compounds from *S. ilicifolius*. Compound **1**, streblus **C**, showed a molecular formula to be $\text{C}_{22}\text{H}_{26}\text{O}_5$ based on the HRESIMS sodium adduct ion at m/z 393.1704 $[\text{M} + \text{Na}]^+$ (calcd for $\text{C}_{22}\text{H}_{26}\text{O}_5\text{Na}$, 393.1678). The ^1H NMR spectrum showed signals for a 1,2,4-trisubstituted aromatic ring [δ_{H} 7.48 (d, $J = 8.5$ Hz, H-6), 6.46 (d, $J = 2.4$ Hz, H-3), 6.42 (dd, $J = 8.5$, 2.4 Hz, H-5), two *trans*-coupling olefinic protons [δ_{H} 7.40 (d, $J = 16.4$ Hz, H- α), 7.01 (d, $J = 16.4$ Hz, H- β)], an α -olefinic proton of α , β -unsaturated carbonyl group [δ_{H} 5.97 (d, $J = 2.0$ Hz, H-2')], an oxymethine proton [δ_{H} 4.48 (dd,

$J = 4.3$, 1.6 Hz, H-5')], a prenyl group [δ_{H} 2.54 (dd, $J = 14.4$, 8.0 Hz, H-1''a), 2.39 (dd, $J = 14.4$, 7.2 Hz, H-1''b), 5.18 (brs, H-2''), 1.68 (s, H₃-4'''), 1.63 (s, H₃-5''')], two methyl groups [δ_{H} 1.32 (s, H₃-2'''), 1.18 (s, H₃-3''')], and a methylene group [δ_{H} 3.19 (dd, $J = 18.8$, 1.6 Hz, H₂-6'a), 2.82 (ddd, $J = 18.8$, 4.3, 2.0 Hz, H₂-6'b)]. The ^{13}C NMR data (Table 1) exhibited resonances for a keto-carbonyl (δ_{C} 199.2), six aromatic carbons and six olefinic carbons [δ_{C} 103.6–160.8], an acetone group [δ_{C} 108.0, 27.8, 26.8], two oxygenated carbons [δ_{C} 82.8, 77.3], two methylene carbons [δ_{C} 33.0, 27.4], and two methyl carbons [δ_{C} 26.0, 18.1]. The HMBC correlations (Figure 2) from H-3 to C-1, C-2, and C-4, from H-5 to C-1 and C-4, from H-6 to C-2 and C-4, from H- α to C-2 and C-6, and from H- β to C-1, indicated that two hydroxy groups and $\text{C}\alpha$ - $\text{C}\beta$ double bond located at C-2, C-4, and C-1, respectively, of the 1,2,4-trisubstituted aromatic ring. The presence of the cyclohex-2-en-1-one 5,6-acetonide moiety in **1** was established based on the observed HMBC correlations. The HMBC correlations from H- α to C-1' and from H- β to C-1' and C-2' were supportive of the $\text{C}\beta$ - $\text{C}1'$ linkage. In addition, the prenyl group was determined to be located at C-4' by the HMBC correlations from H-1'' to C=O, C-4', and C-5' and from H-5' to C-1''. Therefore, **1** was suggested to be a prenylated stilbene-like compound. The difference in chemical shifts of the methyl groups of the dimethylacetone moiety in **1** is 0.14 ppm, which established the presence of the *cis*-acetone [13]. Moreover, it was unambiguously confirmed based on the NOESY correlation between H-5' and H₂-1'' (Figure 2). The preferred

FIGURE 1: Structure of compounds **1** and **2**.FIGURE 2: Significant HMBC (solid arrows) and NOESY (blue, dashed arrows) correlations observed for **1** and **2**.

conformations of the *cis*-(*R,R*)-acetonide **1** were generated by the MM2 calculation using MMFF94 force field [14]. These conformers were reoptimized by DFT-B3LYP method using basis set 6-31G*, to obtain the most preferred conformer with 92.8% Boltzmann distribution (Table S1). The optical rotation value at sodium D line frequency was computed using B3LYP/6-311++G(2d, 2p) level with IEFPCM solvent model for methanol. The large basis set with diffuse functions such as 6-311++G(2d, 2p) was applied to give very consistent results [15, 16]. The calculated $[\alpha]_D$ value of (*R,R*)-acetonide **1** was -102.36 , compared with its experimental value $[\alpha]_D$: -101.7 (c 0.023, MeOH). Thus, a (*R,R*) absolute configuration was concluded for streblus C (**1**).

A careful HPLC analysis of the EtOAc-soluble fraction was accomplished, which revealed a peak at t_R 20.766 min in the chromatogram in accord with that of **1** (t_R 20.800 min) (Figure S1). Thus, the presence of **1** in the EtOAc-soluble fraction from *S. ilicifolius* was confirmed, and the possibility of **1** being artifact could be ignored.

Compound **2**, streblus D, showed a molecular formula to be $C_{19}H_{20}O_5$ based on the HRESIMS sodium adduct ion at m/z 351.1224 $[M+Na]^+$ (calcd for $C_{19}H_{20}O_5Na$, 351.1208). The 1H and ^{13}C NMR data of **2** (Table 1) resembled those of **1**, except for the presence of the singlet olefinic proton at δ_H 7.31 instead of two *trans*-coupling olefinic protons in **1** and disappearance of the acetonide group. Based on the ^{13}C NMR data and observed HMBC

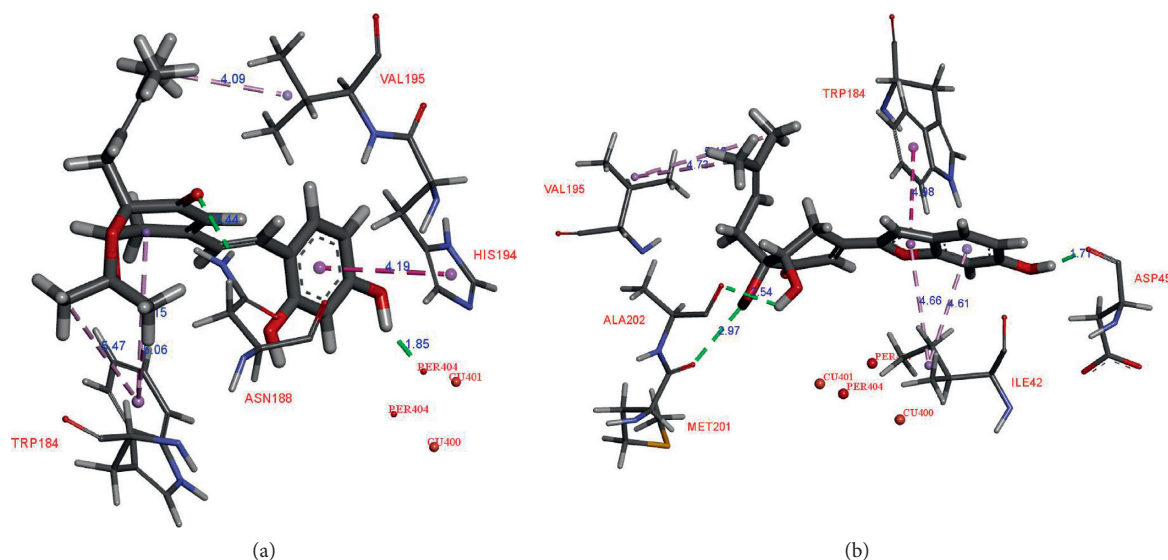


FIGURE 3: Docked pose of best ranked docking score of compounds 1 (a) and 2 (b).

correlations for **2** (Figure 2), the structure of **2** was assigned as a benzofuran-type stilbene. The NOESY correlations between H-5' and H₂-1'' indicated the presence of the *cis*-diol configuration. The ³J_{H-5'/H-6'} coupling constants were 5.9 and 2.7 Hz, to suggest the equatorial configuration of H-5', which was supportive of the (*R,R*) or (*S,S*) absolute configurations for **2**. The conformational search for (*R,R*)-**2** was generated and optimized to obtain six conformers with total Boltzmann weight >90% (Table S1). The Boltzmann-weighted calculated [α]_D value of (*R,R*)-**2** was +301.74, compared with its experimental value [α]_D: -228.9 (*c* 0.002, MeOH). Thus, a (*S,S*) absolute configuration was concluded for streblus D (**2**).

3.3. Tyrosinase Inhibitory Activity of Isolated Compounds from *S. ilicifolius*. Compounds **1** and **2** were tested for their tyrosinase inhibitory activities [18]. Kojic acid, a purported skin lightening agent, was used as a positive control. Streblus C (**1**) exhibited remarkable inhibitory effect with an IC₅₀ value of 0.01 μM, which was 4400 times more potent than that of kojic acid (IC₅₀, 44.6 μM). Meanwhile, streblus D (**2**) was inactive with an IC₅₀ value > 100 μM. These results were consistent with a previous report on the structure–activity relationships of stilbene derivatives. Compound **1** having 2,4-resorcinol subunit contributed the most to inhibitory activity [19]. In addition, the 2-arylbenzofuran derivatives showed lower tyrosinase inhibitory activities than the corresponding stilbene derivatives, suggesting that the formation of the five-membered ring led to the loss of inhibitory activity [20].

3.4. Docking Studies of Compounds 1 and 2. Tyrosinase is an oxidase, which is represented as one of four possible forms (*deoxy*-, *oxy*-, *met*-, and *deact*- forms) [21]. *Oxy*-tyrosinase form oxidizes both phenols and catechols to

o-quinones. Herein, mushroom tyrosinase (EC 1.14.18.1) plays the same role with respect to *oxy*-tyrosinase form. Two bound Cu²⁺ ions bind to six histidine residues, and the peroxide group is in the binding site of *oxy*-tyrosinase, which has a role in the catalytic oxidation [22]. To explore the strong inhibitory activity of **1** against tyrosinase, the molecular docking studies of **1** and **2**, respectively, with *oxy*-tyrosinase (PDB ID:1WX2) were carried out [23].

The docking studies were performed with MOE. The top-ranked pose with the highest negative binding free energy value (*S* value) was selected for further interaction analysis with Discovery Studio Visualizer. Following our previous *in silico* study on tyrosinase inhibition, this docking procedure was already validated based on the docking results of the positive control (kojic acid) and the decoy (hypoxanthine) [12].

In the binding site, compound **1** showed the H-donor interaction between the C-4 hydroxy group and peroxide bridge PER404, presenting the distances of 1.85 Å. The C-3' carbonyl group formed the H-acceptor interaction with ASN188 residue (Figure 3). The aromatic ring exhibited the π-π stacking interaction with HIS194 residue localized in the active pocket. In addition, two methyls of the acetonide group showed the π-σ interactions with TRP184 residue. Compound **2** did not show any interaction with the catalytic site (i.e., Cu²⁺ ions and peroxide bridge), whereas kojic acid showed the interactions with a Cu²⁺ ion, HIS194, and THR203 residues in the binding site. Three hydroxy groups of **2** interacted with ASP45, ALA202, and MET201 residues via the H-donor bonding. The furan ring formed the π-π and π-σ interactions with TRP184 and ILE42 residues, respectively. The *S* values and these interactions suggested that **1** showed high binding affinity for *oxy*-tyrosinase than that of **2** (Table 2). This result confirmed that the formation of furan ring in **2** led to the loss of inhibitory activity.

TABLE 2: Docking results of **1** and **2** with *oxy*-tyrosinase.

Compound	S values	<i>oxy</i> -tyrosinase (1 WX2)		
		Interactions	Targeting residues	Distance (Å)
1	-6.56	H-donor	PER404	1.85
		H-acceptor	ASN188	2.44
		π - π	HIS194	4.19
		π - σ	TRP184	5.15
				5.06
				5.47
2	-6.17	σ - σ	VAL195	4.09
		H-donor	ASP45	1.71
			ALA202	2.54
			MET201	2.97
		π - π	TRP184	4.98
		π - σ	ILE42	4.66
Kojic acid ^a	-4.50		4.61	4.61
		σ - σ	VAL195	4.73
		H-donor	THR203	2.04
		Metal-acceptor	CU401	2.92
		π - π	HIS194	4.30

^aPositive control.

4. Conclusions

Two new stilbene derivatives were isolated from the stems of *S. ilicifolius*. Their structures were elucidated based on the NMR spectroscopic interpretation and optical rotation calculation. Compound **1** was found to possess strong tyrosinase inhibitory activity with an IC₅₀ value of 0.01 μ M. Binding interaction analyses between the isolated compounds (**1** and **2**) and *oxy*-tyrosinase active site have been performed.

Data Availability

The NMR data used to support the findings of this study are included within the supplementary information file.

Conflicts of Interest

The authors declare that there are no conflicts of interest regarding the publication of this paper.

Acknowledgments

This research was funded by Vietnam National University Ho Chi Minh City (VNU-HCM) under grant number NCM2020-18-01.

Supplementary Materials

Figure S1: HPLC chromatogram of **1** from the stems of *S. ilicifolius*. Table S1: conformational data. Figures S2–S15: copies of spectroscopic data for **1** and **2**. (*Supplementary Materials*)

References

- [1] J. N. Rodríguez-López, J. Tudela, R. Varón, F. García-Carmona, and F. García-Cánovas, "Analysis of a kinetic model for melanin biosynthesis pathway," *Journal of Biological Chemistry*, vol. 267, no. 6, pp. 3801–3810, 1992.
- [2] H. Decker and F. Tuzcek, "Tyrosinase/catecholoxidase activity of hemocyanins: structural basis and molecular mechanism," *Trends in Biochemical Sciences*, vol. 25, no. 8, pp. 392–397, 2000.
- [3] T. Pillaiyar, M. Manickam, and V. Namasivayam, "Skin whitening agents: medicinal chemistry perspective of tyrosinase inhibitors," *Journal of Enzyme Inhibition and Medicinal Chemistry*, vol. 32, no. 1, pp. 403–425, 2017.
- [4] S. Dej-adisai, K. Parndaeng, and C. Wattanapiromsakul, "Determination of phytochemical compounds, and tyrosinase inhibitory and antimicrobial activities of bioactive compounds from *Streblus ilicifolius* (S Vidal) Corner," *Tropical Journal of Pharmaceutical Research*, vol. 15, no. 3, pp. 497–506, 2016.
- [5] G. Zhang, L. Hao, D. Zhou et al., "A new phenylpropanoid glycoside from the bark of *Streblus ilicifolius* (Vidal) Corner," *Biochemical Systematics and Ecology*, vol. 87, Article ID 103962, 2019.
- [6] Y. Huang, X. Huang, G. Tian et al., "Two new amide glycosides with anti-inflammatory activity from the leaves of *Streblus ilicifolius* (Vidal) corner," *Natural Product Research*, pp. 1–9, 2021.
- [7] N. T. Nguyen, H. X. Nguyen, T. H. Le et al., "Two new derivatives of 8-prenyl-5,7-dihydroxycoumarin from the stems of *Streblus ilicifolius* (S.Vidal) Corn," *Natural Product Research*, pp. 1–6, 2021.
- [8] N. T. Nguyen, M. H. K. Nguyen, H. X. Nguyen, N. K. N. Bui, and M. T. T. Nguyen, "Tyrosinase inhibitors from the wood of *Artocarpus heterophyllus*," *Journal of Natural Products*, vol. 75, no. 11, pp. 1951–1955, 2012.
- [9] H. X. Nguyen, N. T. Nguyen, M. H. K. Nguyen et al., "Tyrosinase inhibitory activity of flavonoids from *Artocarpus heterophyllous*," *Chemistry Central Journal*, vol. 10, no. 1, p. 2, 2016.
- [10] P. H. Dang, T. T. Nguyen, T. H. Le, H. X. Nguyen, M. T. T. Nguyen, and N. T. Nguyen, "A new bischromanone from the stems of *Semecarpus caudata*," *Natural Product Research*, vol. 32, no. 15, pp. 1745–1750, 2018.
- [11] P. H. Dang, L. T. T. Nguyen, H. T. T. Nguyen et al., "A new dimeric alkylresorcinol from the stem barks of *Swintonia floribunda* (Anacardiaceae)," *Natural Product Research*, vol. 33, no. 20, pp. 2883–2889, 2019.
- [12] P. H. Dang, T. H. Le, T. N. V. Do, H. X. Nguyen, M. T. T. Nguyen, and N. T. Nguyen, "Diarylalkanoids as potent tyrosinase inhibitors from the stems of *Semecarpus caudata*," *Evidence-Based Complementary and Alternative Medicine*, vol. 2021, Article ID 8872920, 8 pages, 2021.
- [13] L. C. Dias, T. Augusto, C. C. Perez, and L. J. Steil, "Addition of chiral and achiral allyltrichlorostannanes to chiral \pm -alkoxy aldehydes," *Journal of the Brazilian Chemical Society*, vol. 20, no. 4, pp. 802–812, 2009.
- [14] T. Lewis-Atwell, P. A. Townsend, and M. N. Grayson, "Comparisons of different force fields in conformational analysis and searching of organic molecules: a review," *Tetrahedron*, vol. 79, Article ID 131865, 2021.
- [15] P. J. Stephens, F. J. Devlin, J. R. Cheeseman, and M. J. Frisch, "Calculation of optical rotation using density functional

- theory," *The Journal of Physical Chemistry A*, vol. 105, no. 22, pp. 5356–5371, 2001.
- [16] T. Aharon and M. Caricato, "Compact basis sets for optical rotation calculations," *Journal of Chemical Theory and Computation*, vol. 16, no. 7, pp. 4408–4415, 2020.
- [17] Z. Lin, T. Zhu, Y. Fang, Q. Gu, and W. Zhu, "Polyketides from *Penicillium* sp. JP-1, an endophytic fungus associated with the mangrove plant *Aegiceras corniculatum*," *Phytochemistry*, vol. 69, no. 5, pp. 1273–1278, 2008.
- [18] E. T. Arung, I. W. Kusuma, Y. M. Iskandar, S. Yasutake, K. Shimizu, and R. Kondo, "Screening of Indonesian plants for tyrosinase inhibitory activity," *Journal of Wood Science*, vol. 51, no. 5, pp. 520–525, 2005.
- [19] S. Khatib, O. Nerya, R. Musa, M. Shmuel, S. Tamir, and J. Vaya, "Chalcones as potent tyrosinase inhibitors: the importance of a 2,4-substituted resorcinol moiety," *Bioorganic & Medicinal Chemistry*, vol. 13, no. 2, pp. 433–441, 2005.
- [20] Z.-P. Zheng, K.-W. Cheng, Q. Zhu, X.-C. Wang, Z.-X. Lin, and M. Wang, "Tyrosinase inhibitory constituents from the roots of *Morus nigra*: a structure–activity relationship study," *Journal of Agricultural and Food Chemistry*, vol. 58, no. 9, pp. 5368–5373, 2010.
- [21] C. A. Ramsden and P. A. Riley, "Tyrosinase: the four oxidation states of the active site and their relevance to enzymatic activation, oxidation and inactivation," *Bioorganic & Medicinal Chemistry*, vol. 22, no. 8, pp. 2388–2395, 2014.
- [22] M. Kanteev, M. Goldfeder, and A. Fishman, "Structure–function correlations in tyrosinases," *Protein Science*, vol. 24, no. 9, pp. 1360–1369, 2015.
- [23] Y. Matoba, T. Kumagai, A. Yamamoto, H. Yoshitsu, and M. Sugiyama, "Crystallographic evidence that the dinuclear copper center of tyrosinase is flexible during catalysis," *Journal of Biological Chemistry*, vol. 281, no. 13, pp. 8981–8990, 2006.

Research Article

Investigation of the Mechanism of Traditional Chinese Medicines in Angiogenesis through Network Pharmacology and Data Mining

Wingyan Yun ^{1,2}, Wenchao Dan ^{1,2}, Jinlei Liu ¹, Xinyuan Guo ³, Min Li ¹,
and Qingyong He ¹

¹Guang'anmen Hospital, China Academy of Chinese Medical Sciences, Beijing 100053, China

²Graduate School of Beijing University of Chinese Medicine, Beijing 100029, China

³Cancer Hospital Chinese Academy of Medical Sciences, Beijing 100021, China

Correspondence should be addressed to Qingyong He; heqingyong@163.com

Received 12 February 2021; Revised 20 March 2021; Accepted 15 April 2021; Published 29 April 2021

Academic Editor: Siba shanak

Copyright © 2021 Wingyan Yun et al. This is an open access article distributed under the Creative Commons Attribution License, which permits unrestricted use, distribution, and reproduction in any medium, provided the original work is properly cited.

Although traditional Chinese medicine is effective and safe for the treatment of angiogenesis, the *in vivo* intervention mechanism is diverse, complex, and largely unknown. Therefore, we aimed to explore the active ingredients of traditional Chinese medicine and their mechanisms of action against angiogenesis. Data on angiogenesis-related targets were collected from GeneCards, Therapeutic Target Database, Online Mendelian Inheritance in Man, DrugBank, and DisGeNET. These were matched to related molecular compounds and ingredients in the traditional Chinese medicine system pharmacology platform. The data were integrated and based on the condition of degree > 1, and relevant literature, target-compound, compound-medicine, and target-compound-medicine networks were constructed using Cytoscape. Molecular docking was used to predict the predominant binding combination of core targets and components. We obtained 79 targets for angiogenesis; 41 targets were matched to 3839 compounds, of which 110 compounds were selected owing to their high correlation with angiogenesis. Fifty-five combinations in the network were obtained by molecular docking, among which PTGS2-astragalol (−9.18 kcal/mol), KDR-astragalol (−7.94 kcal/mol), PTGS2-quercetin (−7.41 kcal/mol), and PTGS2-myricetin (−7.21 kcal/mol) were top. These results indicated that the selected potential core compounds have good binding activity with the core targets. Eighty new combinations were obtained from the network, and the top combinations based on affinity were KDR-beta-carotene (−10.13 kcal/mol), MMP9-beta-sitosterol (−8.04 kcal/mol), MMP9-astragalol (−7.82 kcal/mol), and MMP9-diosgenin (−7.51 kcal/mol). The core targets included PTGS2, KDR, VEGFA, and MMP9. The essential components identified were astragalol, kaempferol, myricetin, quercetin, and beta-sitosterol. The crucial Chinese medicines identified included *Polygoni Cuspidati Rhizoma et Radix*, *Morus alba* Root Bark, and *Forsythiae Fructus*. By systematically analysing the ingredients of traditional Chinese medicine and their targets, it is possible to determine their potential mechanisms of action against pathological angiogenesis. Our study provides a basis for further research and the development of new therapeutics for angiogenesis.

1. Introduction

John Hunter provided the first recorded scientific insights into angiogenesis and coined the term angiogenesis in 1787 [1]. Folkman [2–6] proposed the role of angiogenesis in tumour growth in 1971. He hypothesised that tumour growth depends on angiogenesis to increase blood supply and proposed stopping the blood supply from inhibiting

tumour growth, which subsequently initiated the field of research on the relationship between angiogenesis and diseases. Angiogenesis is the process of capillary sprouting from preexisting vasculature, and it is highly induced by hypoxia and other biological processes [5, 7]. The mechanisms underlying angiogenesis can be divided into two types. The first is sprouting angiogenesis, wherein vascular endothelial cell growth factor (VEGF) stimulates tip cells in

the original blood vessel network to induce vascular sprouting [8, 9]. The second is intussusceptive angiogenesis, which proceeds through transluminal tissue pillar formation and subsequent vascular splitting to the expansion and remodelling of microvascular networks [9–11].

Under normal circumstances, angiogenesis is a balance between inhibiting and growth factors. If the functions of either the inhibiting or growth factors are abnormal, it presents as overgrowth, defect, or malformation. Angiogenesis is essential for the growth and development of tumour cells. Under hypoxic conditions, tumours stimulate neovascularisation via the expression of growth factors such as VEGF [12]. Thus, exploring the inhibition of angiogenesis for the treatment of tumours has gained increased attention. However, some studies have shown that using anti-angiogenic agents can induce potential resistance mechanisms such as autophagy, VEGF-dependent alterations, non-VEGF pathways, and stromal cell interactions [13–17]. Tumour cells may become accustomed to hypoxia or nutrient deprivation or induce angiogenesis via other growth factors [18, 19]. Such events can lead to higher survival levels of the tumour cells. Moreover, some antiangiogenic agents can cause side effects such as acne-like rash, hypertension, and diarrhoea [20, 21].

Traditional Chinese medicine is valuable for the treatment of various diseases, especially refractory diseases. More importantly, some studies proved that traditional Chinese medicine inhibits endothelial progenitor cells migration and tube formation without any cytotoxic activity [22]. Co-administration of traditional Chinese medicine and chemotherapy drugs could regulate angiogenesis, favour the delivery of chemotherapy drugs to the tumour lesion, promote apoptosis of tumour cells, enhance the effective treatment performance of chemotherapy drugs, and minimize the toxic side effects caused by chemotherapy drugs [23, 24]. Therefore, traditional Chinese medicine is more effective and safer in treating diseases. Previously, we found that many herbal extracts such as *Epimedium brevicornu* Maxim, *Dalbergia odorifera* T. Chen, and *Trichosanthes kirilowii* Maxim can regulate angiogenesis [25]. Cucurbitacin E, a compound in herbal extracts, can inhibit tumour angiogenesis by inhibiting vascular endothelial growth factor receptor 2- (KDR/VEGFR2-) mediated Jak-STAT3 and mitogen-activated protein kinase (MAPK) signalling pathways [26]. Astragaloside IV and curcumin can suppress the expression of fibroblast growth factor-2, matrix metalloproteinase 2, VEGF, hepatocyte growth factor, thrombosis-related factor tissue factor, and coagulation factor VII, thereby reducing the microvessel count [27]. The above herbal studies focused on single or several compounds related to angiogenesis. Nevertheless, during treatment, multiple herbal compounds interact or cross-react to regulate different targets and pathways. Thus, even though traditional Chinese medicine is safe for clinical treatment, the *in vivo* intervention mechanism is diverse, complex, and largely unknown.

Network pharmacology is a combination of pharmacology, biomedicine, systems biology, and network biology. Through various methods such as data mining, statistics, and modelling information visualization to recognize

multicomponent synergy and assess each specific agent combinations' synergistic relationship [28–30], the mechanism of drugs in the biological network was analysed as well as determining which pathophysiological mechanisms are involved in the disease [28]. In this study, the angiogenesis targets were explored through network pharmacology, and the corresponding compounds and herbs were matched. Furthermore, the effect of herbal compounds on angiogenesis and the intervention mechanism was demonstrated. The findings of this study are expected to provide insights into the development of novel therapeutics for angiogenesis. The detailed workflow of the investigation is shown in Figure 1.

2. Materials and Methods

2.1. Collection of Data regarding Angiogenesis-Related Targets.

Data were collected from GeneCards (<https://www.genecards.org/>) [31], Therapeutic Target Database (TTD; <http://db.idrblab.net/ttd/>) [32], Online Mendelian Inheritance in Man (OMIM, <https://omim.org>) [33], DrugBank (<http://www.drugbank.ca>) [34], and DisGeNET (<http://www.disgenet.org>) [35]. The keyword used to search these databases was “angiogenesis.” After sorting and removing repeated targets, matching targets' full name was established using the UniProt database (<https://www.uniprot.org/>) [36].

2.2. Screening of Related Herbal Compounds.

The targets were used to match the compounds related to angiogenesis in the Traditional Chinese Medicine Systems Pharmacology Database and Analysis Platform (TCMSP; <http://tcmssp.com/>) [37] and Encyclopedia of Traditional Chinese Medicine (ETCM; <http://www.tcmip.cn/ETCM/index.php/Home/Index/>) [38]. The compounds and targets were imported to Cytoscape version 3.8.1 (Institute for Systems Biology, Seattle, WA, USA) [39] to construct a “target-compound” network. After preliminary screening, the related compounds were verified through a literature review, and the compounds closely related to diseases were screened as related compounds.

2.3. Collection of Related Traditional Chinese Medicines and Construction of a Target-Compound-Traditional Chinese Medicine Network.

By collecting the traditional Chinese medicines related to compounds and constructing the “compound-traditional Chinese medicine” network combined with the “compound-target” network, the “target-compound-traditional Chinese medicine” network was constructed using Cytoscape 3.8.1 to explore and mine the relationships within the network. Key nodes were found by calculating the topological parameters of each node in the network using NetworkAnalyzer to preliminarily evaluate the effectiveness of traditional Chinese medicine and the compounds on angiogenesis.

2.4. Statistics and Frequency Analysis of Traditional Chinese Medicine Information.

Information related to traditional

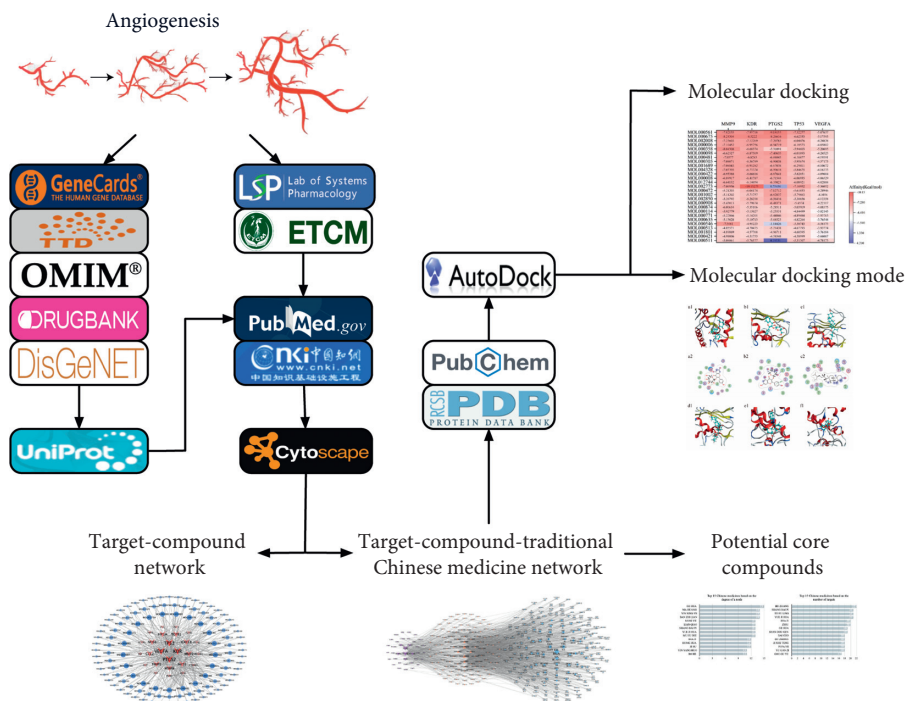


FIGURE 1: The workflow of the investigation.

Chinese medicine, including the four natures, five flavours, and meridians, was collected from the Chinese Pharmacopoeia (2020 edition) [40], the 13th five-year plan textbook of Traditional Chinese Medicine Pharmacy [41], and the Chinese Dictionary of Clinical Drugs [42]. If the information did not exist in these three documents, that medicine was excluded. IBM SPSS Statistics 26.0 was used to perform statistical tests and frequency analysis.

2.5. Molecular Docking for Targets and Compounds. To define the reliability of the interaction relationship between the core targets and core components in the “target-compound-traditional Chinese medicine network” and explore the new drug–target combinations, the top five targets with a moderate value for target-compound-traditional Chinese medicine were selected as receptors. The crystal structures of these proteins were selected and preserved in PDB format from Biological Macromolecular Structures Enabling Breakthroughs in Research and Education (RCSB; <http://www.rcsb.org/pdb/>). The 3D structures of the candidate compounds were downloaded and saved in SDF format from PubChem (<https://pubchem.ncbi.nlm.nih.gov/>). These SDF files were converted to the PDB format using Open Babel. The water molecules in the ligands were removed using AutoDock Tools 1.5.6 (Molecular Graphics Lab, La Jolla, CA, USA). After dispersing the ligands and receptors, nonpolar hydrogen bonds were added, and Gasteiger charges were calibrated and stored as pdbqt files. The selected potential core ligands were treated with energy minimisation, and the ligand atom type and calculated charge were saved in the pdbqt format. AutoDock Vina 1.1.2 [43] was used to calculate the docking score between the

target and ligand to evaluate its matching degree and docking activity. A docking score of less than -4.25 indicated binding between the ligand and target. A score of less than -5.0 indicated better binding activity, and a score of less than -7.0 indicated vigorous docking activity. The ideal combinations were selected according to the affinity value, and the molecular docking pattern was displayed by MOE2019.

3. Results

3.1. Target Acquisition. We obtained 4609 targets related to angiogenesis from the GeneCards database. We identified the targets with strong correlation by calculating the median of their correlation coefficients because of the large number of targets. After six calculations, the medians were 0.65, 1.39, 3.25, 4.96, 7.47, and 10.52, and 74 targets with higher correlation coefficients were obtained. Furthermore, 5, 1, 0, and 0 related targets were separately obtained from the TTD, OMIM, DrugBank, and DisGeNET databases, respectively. After removing duplicate values and standardising them using the UniProt database, 79 angiogenesis targets were finally acquired. Containing the target information from TCMSP and ETCM databases were 49 and 4 target information, respectively. However, four were duplicate targets, and eight targets did not match any compound because the databases did not have information on related ingredients. Thus, only 41 targets were matched with small-molecule compounds and became potential targets. Table 1 shows the targets with over ten corresponding compounds.

A total of 3839 small-molecule compounds were matched with 41 potential targets to construct a target-compound network consisting of 3440 nodes and 3839

TABLE 1: Target's information.

Number	Gene	UniProt number	Protein
1	PTGS2	P35354	Prostaglandin G/H synthase 2
2	KDR	P35968	Vascular endothelial growth factor receptor 2
3	VEGFA	P15692	Vascular endothelial growth factor A
4	FGF1	P05230	Acidic fibroblast growth factor
5	TP53	P04637	Cellular tumour antigen p53
6	MMP9	P14780	Matrix metalloproteinase-9
7	AKT1	P31749	RAC-alpha serine/threonine-protein kinase
8	MMP2	P08253	72 kDa type IV collagenase
9	CXCL8	P10145	Interleukin-8
10	FGF2	P09038	Basic fibroblast growth factor
11	HIF1A	Q16665	Hypoxia-inducible factor 1-alpha
12	TGFB1	P01137	Transforming growth factor beta-1
13	CCL2	P13500	C-C motif chemokine 2
14	NOS3	P29474	Nitric oxide synthase, endothelial

Identification of candidate compounds and target-compound network construction.

edges. Although many small-molecule compounds showed a match, some were less related to the target or were associated with fewer studies. Hence, under the “Degree >1” condition, the targets and compounds with a greater degree of interaction were screened out, resulting in 28 targets and 264 candidate compounds. These were then screened through a literature review for *in vivo* and *in vitro* activities. Finally, 110 compounds with research significance and 26 related targets were determined; these were used to construct the “target-compound” network (Figure 2), which contained 136 nodes and 370 edges.

3.2. Identification of Traditional Chinese Medicines and Target-Compound-Chinese Medicine Network Construction.

A total of 447 Chinese medicines were obtained from 110 candidate compounds through database and literature matching. A compound-Chinese medicine network was first constructed according to the relationship between the compounds and Chinese medicines, and it contained 594 nodes and 2240 edges. Based on the connections of the node, the top nine Chinese medicines were Puerariae Flos (Ge Hua), Ephedra Herba (Ma Huang), Ginkgo Folium (Yin Xing Ye), Scutellariae Barbatae Herba (Ban Zhi Lian), Mori Folium (Sang Ye), Forsythiae Fructus (Lian Qiao), *Morus alba* Root Bark (Sang Bai Pi), Rosae Chinensis Flos (Yue Ji Hua), and Oroxyli Semen (Mu Hu Die), which contain the candidate compounds 15, 14, 14, 14, 13, 13, 13, 13, and 13, respectively. Through the bridging effect of candidate compounds, the targets of various Chinese medicines were obtained. The top six Chinese medicines were Polygoni Cuspidati Rhizoma et Radix (Hu Zhang), *Morus alba* Root Bark (Sang Bai Pi), Smilacis Glabrae Rhizoma (Tu Fu Ling), Rosae Chinensis Flos (Yue Ji Hua), *Hippophae fructus* (Sha Ji), and *Perilla frutescens* (Zi Su), which contain compounds 22, 21, 21, 21, 20, and 20, respectively. Therefore, it can be inferred that these six Chinese medicines have a strong regulatory effect on the development of angiogenesis. Figure 3 shows the top 15 candidate compounds of traditional Chinese medicines based on the number of related targets and the degree of a node in the compound-Chinese medicine

network. According to a previous study, the median compound degree value of the network was seven [44]. According to the three conditions of closeness centrality, betweenness centrality, and compound degree value greater than 20, there were 27 potential core compounds. The top five ingredients were quercetin, $\beta\beta$ -sitosterol, kaempferol, luteolin, and ursolic acid. The remaining potential core compounds are shown in Table 2.

The target-compound-traditional Chinese medicine network was reconstructed by selecting traditional Chinese medicines with a degree > 4. Their associated compounds and targets were organised to display the relationships among angiogenesis-related targets, compounds, and traditional Chinese medicines more intuitively (Figure 4).

3.3. Statistics and Frequency Analysis of Chinese Medicine Information.

Information regarding flavour, natures, and meridian was collected and analysed for 413 traditional Chinese medicines. The highest frequencies of the four natures were warm and cold, accounting for 25.5% and 24.5%, respectively. Flavour analysis revealed that the most predominant flavours were acrid and bitter, accounting for 28.9% and 27.6%, respectively. The highest-ranked meridians related to angiogenesis were the liver, lungs, and stomach, accounting for 20.8%, 16.7%, and 14.2%, respectively. The results of the statistical analyses are shown in Table 3 and Figure 5.

3.4. Molecular Docking.

The 27 core potential compounds were molecularly docked with five core targets, namely, matrix metalloproteinase 9 (MMP9), VEGFR2, prostaglandin-endoperoxide synthase 2 (PTGS2), TP53, and vascular endothelial growth factor A (VEGFA), and 135 sets of receptor-ligand docking results were obtained. Among the 135 receptor-ligand groups, 94 groups (69.63%) showed affinity < -5, and 22 groups (16.30%) showed affinity < -7.

Among the 135 combinations, 55 combinations were present in the target-compound network. Among these 55 combinations, the highest score for docking was observed for PTGS2-astragalii (-9.18 kcal/mol), and the lowest

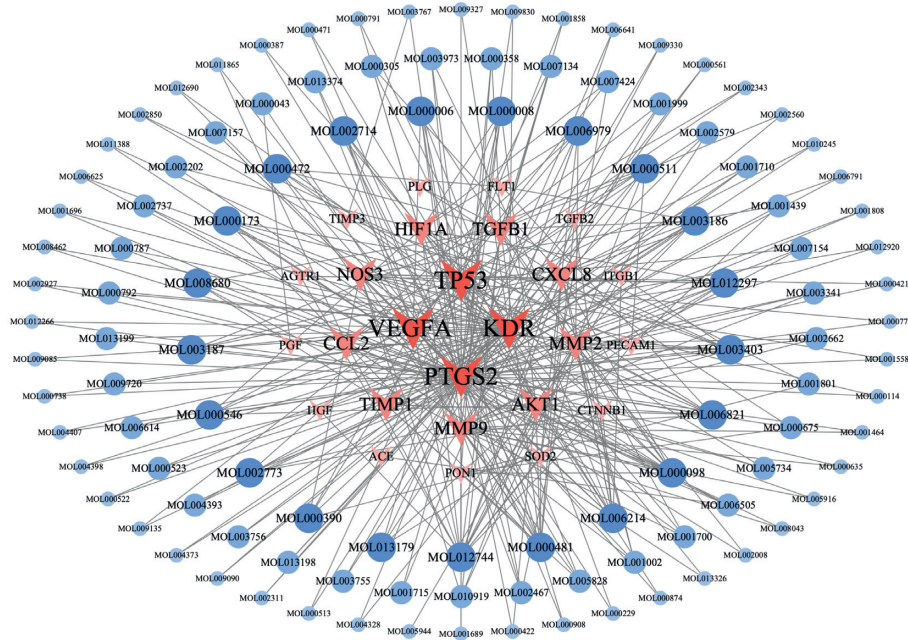


FIGURE 2: Target-compound network.

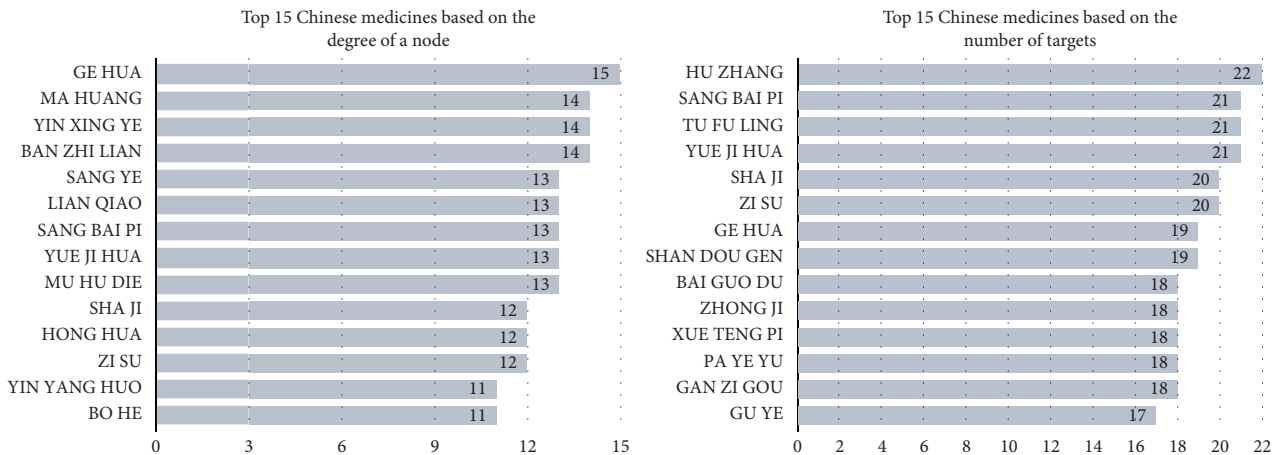


FIGURE 3: Number of candidate compounds and targets related to traditional Chinese medicines.

docking score was observed for PTGS2-ursolic acid (4.20 kcal/mol). The average of the above combinations was -5.56 kcal/mol. This result indicates that the screened potential core compounds may have better binding activity with the core target and supports the reliability of drug-target interactions in the target-compound network to a certain extent.

Molecular docking results revealed 80 new combinations outside the target-compound network. The more ideal combinations outside the target-compound network were KDR-beta-carotene (-10.13 kcal/mol), MMP9-beta-sitosterol (-8.04 kcal/mol), MMP9-astragaloside (-7.82 kcal/mol), and MMP9-diosgenin (-7.51 kcal/mol). There were 52 new combinations with affinity < -5 kcal/mol, suggesting that they all have good docking activity. The docking activity of these

four combinations exceeded that of most combinations in the target-compound network; therefore, these are more likely to have a strong drug-target relationship. These docking results can provide data for the experimental screening and design of related Chinese medicines and ingredients in the future. The results are shown in Figure 6.

Considering the ideal combination of the affinity value of molecular docking and degree value of the target-compound-drug network, nine more ideal combinations were selected. Their docking conditions are displayed in three-dimensional and two-dimensional molecular docking patterns. Each ligand was embedded in the active pocket of the target and interacted with multiple residues of the target through hydrophobic interaction and hydrogen bond formation (Figure 7).

TABLE 2: Candidate compounds and targets information (degree > 20).

MolID	CAS	MolName	Degree	OB	DL
MOL000098	117-39-5	Quercetin	201	46.43	0.28
MOL000358	83-46-5	Beta-sitosterol	192	36.91	0.75
MOL000422	520-18-3	Kaempferol	136	41.88	0.24
MOL000675	112-80-1	Oleic acid	120	33.13	0.14
MOL000006	491-70-3	Luteolin	99	36.16	0.25
MOL000511	77-52-1	Ursolic acid	88	16.77	0.75
MOL000008	520-36-5	Apigenin	87	23.06	0.21
MOL000114	121-34-6	Vanillic acid	86	35.47	0.04
MOL000305	143-07-7	Lauric acid	69	23.59	0.04
MOL000513	149-91-7	3,4,5-Trihydroxybenzoic acid (Gallic acid)	57	31.69	0.04
MOL000908	515-13-9	Beta-elemene	51	25.63	0.06
MOL000771	501-98-4	p-Coumaric acid	48	43.29	0.04
MOL000635	121-33-5	Vanillin	48	52.00	0.03
MOL000561	480-10-4	Astragalin	39	14.03	0.74
MOL000472	518-82-1	Emodin	37	24.40	0.24
MOL002850	128-37-0	Butylated hydroxytoluene	35	40.0	0.07
MOL002773	7235-40-7	Beta-carotene	34	37.18	0.58
MOL001801	69-72-7	Salicylic acid	30	32.13	0.03
MOL000874	552-41-0	Paeonol	30	28.79	0.04
MOL000481	446-72-0	Genistein	26	17.93	0.21
MOL000421	59-67-6	Nicotinic acid	25	47.65	0.02
MOL002008	529-44-2	Myricetin	25	13.75	0.31
MOL004328	67604-48-2	Naringenin	24	59.29	0.21
MOL001689	480-44-4	Acacetin	23	34.97	0.24
MOL012744	501-36-0	Resveratrol	23	19.07	0.11
MOL001002	476-66-4	Ellagic acid	21	43.06	0.43
MOL000546	512-04-9	Diosgenin	20	80.88	0.81

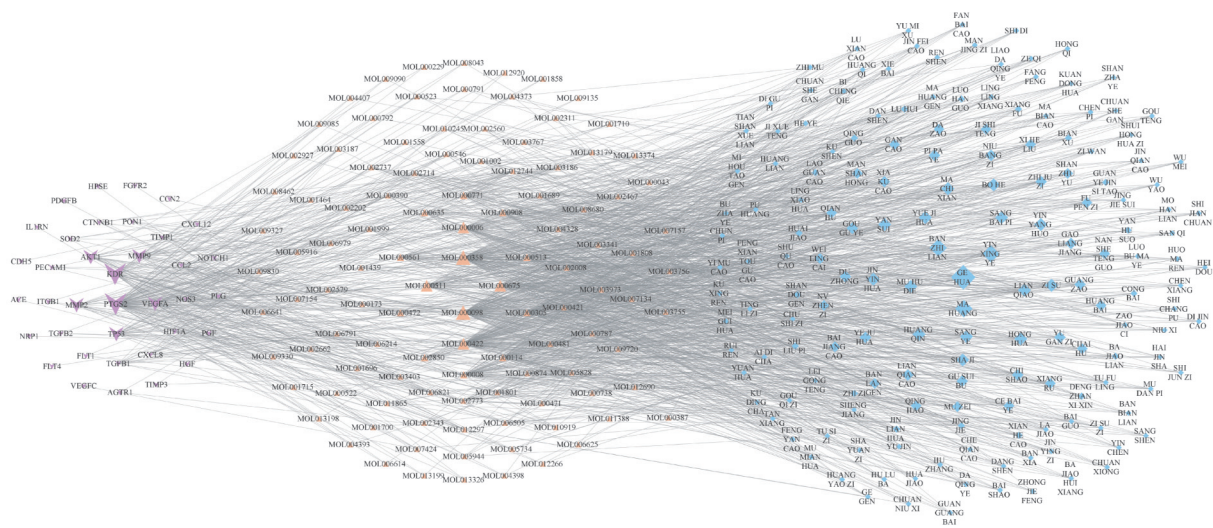


FIGURE 4: Target-compound-traditional Chinese medicine network. The diamond-shaped nodes represent Chinese medicine, the triangular nodes represent the ingredients, and the V-shaped nodes represent the target. The icon size of each node is positively correlated with its degree value.

4. Discussion

Angiogenesis is a complex process that requires the coordinated regulation of several activating and inhibitory pathways. It participates in developing many diseases, such as cancers, atherosclerosis, rheumatoid arthritis, hepatitis, and inflammation. There are many factors involved in the

regulation of angiogenesis. As traditional Chinese medicines, which have a curative effect in clinical treatment, are applied in combination, they contain multiple components and targets. Therefore, elucidating the mechanism and exploring the potential components of traditional Chinese medicines are of great significance in developing novel drugs.

TABLE 3: Natures and flavours of traditional Chinese medicine regulating angiogenesis.

Four natures	Frequency	Percentage	Five flavours	Frequency	Percentage
Warm	103	25.5	Acrid	160	28.9
Cold	99	24.5	Bitter	153	27.6
Neutral	84	20.8	Sweet	139	25.1
Slightly cold	49	12.1	Sour	27	4.9
Cool	34	8.4	Astringent	25	4.5
Slightly warm	23	5.7	Slightly bitter	22	4
Hot	10	2.5	Salty	12	2.2
Great cold	1	0.2	Bland	9	1.6
Great hot	1	0.2	Slightly acrid	3	0.5
			Slightly sweet	3	0.5
			Slightly sour	1	0.2

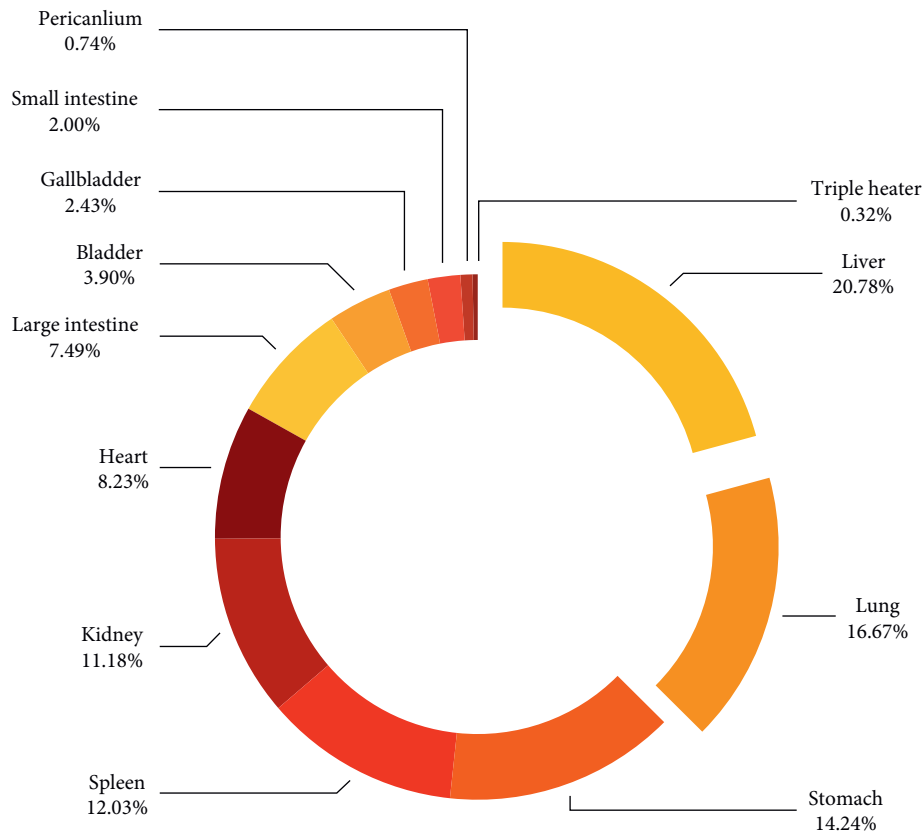


FIGURE 5: Channel entry of traditional Chinese medicine regulating angiogenesis.

4.1. Target. According to the target-compound network screening results, the top scores were obtained for PTGS2, KDR, VEGFA, and MMP9. The primary role of PTGS2 in angiogenesis is to induce the synthesis of individual prostanooids such as PGD2, PGE2, PGF2a, PGI2, and TXA2. Prostaglandin (PG) can boost VEGF production in a paracrine, intracrine, or autocrine manner. Moreover, VEGF stimulates PTGS2 expression, thereby triggering PG production. This, in turn, increases the levels of PGs and stimulates the expression of angiogenic factors such as VEGF and bFGF [45]. VEGF expression is regulated by many factors such as epidermal growth factor, hypoxia-inducible factor (HIF), and platelet-derived growth factor

(PDGF). During angiogenesis, VEGF signalling regulates the activities of several kinases through VEGFR2 and guides the proliferation, migration, and survival of cells.

An increased number of endothelial cells, both tip and stalk cells, is a significant feature of vascular proliferation. Endothelial tip cells are induced by VEGF gradients and promote the formation of filopodia. The molecular regulation of these events occurs via the activation of Notch signalling and increased expression of Notch ligands on endothelial cells. A high level of Notch signalling can decrease VEGFR2 expression. Physiological homeostasis requires this negative feedback loop [46]. One crucial event implicated in the migration and proliferation of vascular

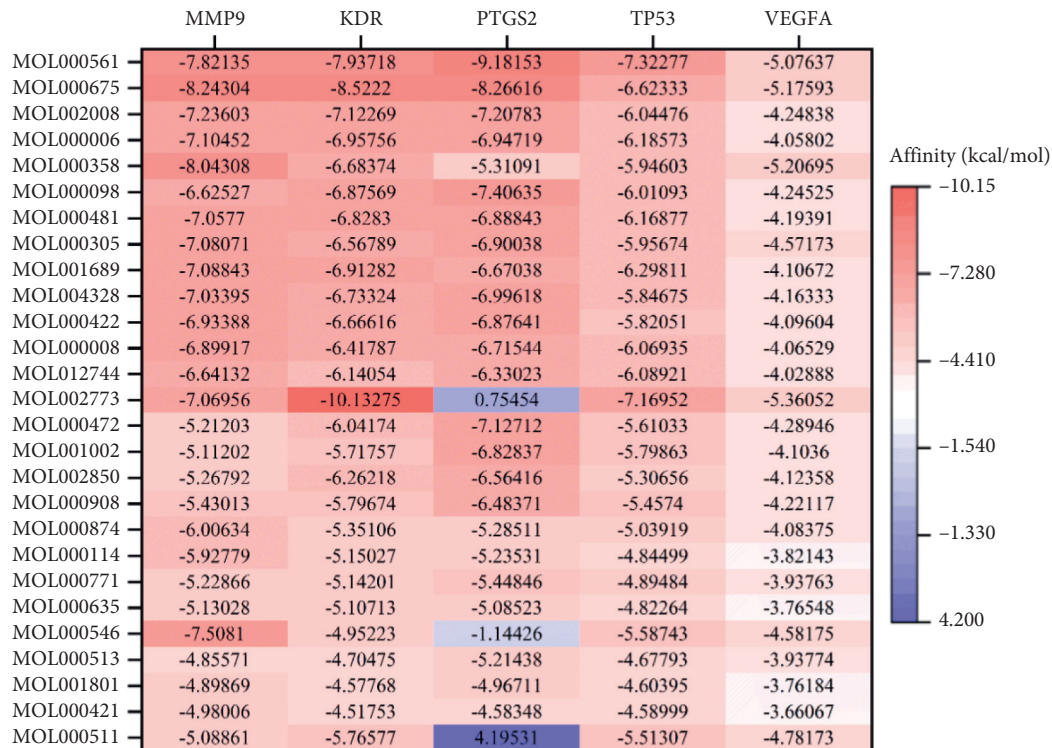


FIGURE 6: Molecular docking results.

endothelial cells is the proteolytic degradation of basement membranes and extracellular matrix (ECM) components by matrix metalloproteinases (MMPs) [47]. The secretion of MMPs allows endothelial cells to penetrate their underlying basement membrane and eliminate the contact inhibition that blocks endothelial cell proliferation [48]. The gene expression of MMPs may stimulate the production and secretion of major proangiogenic factors such as VEGF and fibroblast growth factor-2, which promote angiogenesis [48–50]. MMP9 cleaves ECM proteins and activates cytokines and chemokines to regulate tissue remodelling [51]. In the intracardiac injection experiment, the injected ECM-derived substance promoted cell attachment, migration, and proliferation, induced extracellular signal-regulated kinase (ERK) 1/2 activation, and promoted arteriogenesis [50]. In summary, the above targets play an essential role in regulating angiogenesis, and they are the preferred targets for traditional Chinese medicine intervention in angiogenesis.

4.2. Ingredients. Molecular docking showed that the components that bind well to the targets are astragaloside, kaempferol, myricetin, quercetin, and β -sitosterol. Astragaloside suppresses interleukin-1 β (IL-1 β) induced inflammatory mediators by activating peroxisome proliferator-activated receptor- γ , which subsequently inhibits IL-1 β -induced nuclear factor- (NF-) κ B and MAPK activation [52]. NF- κ B subunit p65 activates the transcription of HIF-1 α and its target gene VEGF-A. Regulating HIF-1 α via NF- κ B activation can contribute to angiogenesis [53]. Kaempferol is an antioxidant that reduces reactive oxygen species (ROS) metabolism by inhibiting the NF- κ B pathway and

upregulation of the associated transcriptional pathway [54]. ROS regulate angiogenesis via two different mechanisms: the HIF-VEGF/VEGFR2 signalling pathway and the VEGF-independent mechanism involving the generation of lipid oxidation products [55]. Endothelial nitric oxide synthase (eNOS) plays an essential role in regulating cell migration activities and vascular permeability [56]. Myricetin and quercetin inhibit thioredoxin reductase (TrxR) in an NADPH- and concentration-dependent manner [57]. TrxR is a part of the thioredoxin (Trx) system, including Trx and NADPH [58]. This system plays essential roles in regulating cellular redox signalling and contributes to the regulation of VEGF-mediated signalling [59–61]. For example, Trx1, in endothelial cells, prevents von Hippel-Lindau-mediated degradation of the transcription factor HIF1, leading to the induction of VEGF expression [62]. The action mechanism of myricetin and quercetin in angiogenesis is not yet well understood, but it may be related to the Trx system. β -sitosterol administration was reported to reduce the expression of chemokines and the activity of MMP2 and MMP9 [63]. In summary, the above components of traditional Chinese medicine can be investigated for intervention in angiogenesis.

4.3. Chinese Medicine. An experiment using umbilical vein endothelial cells demonstrated that angiogenesis could be regulated by the extract of *Polygoni Cuspidati Rhizoma et Radix* via the inhibition of the phosphorylation of downstream signalling molecules such as ERK, Akt, and eNOS by VEGF/VEGFR2 [64]. These molecules can regulate endothelial cell survival, proliferation, and migration [65, 66]. The

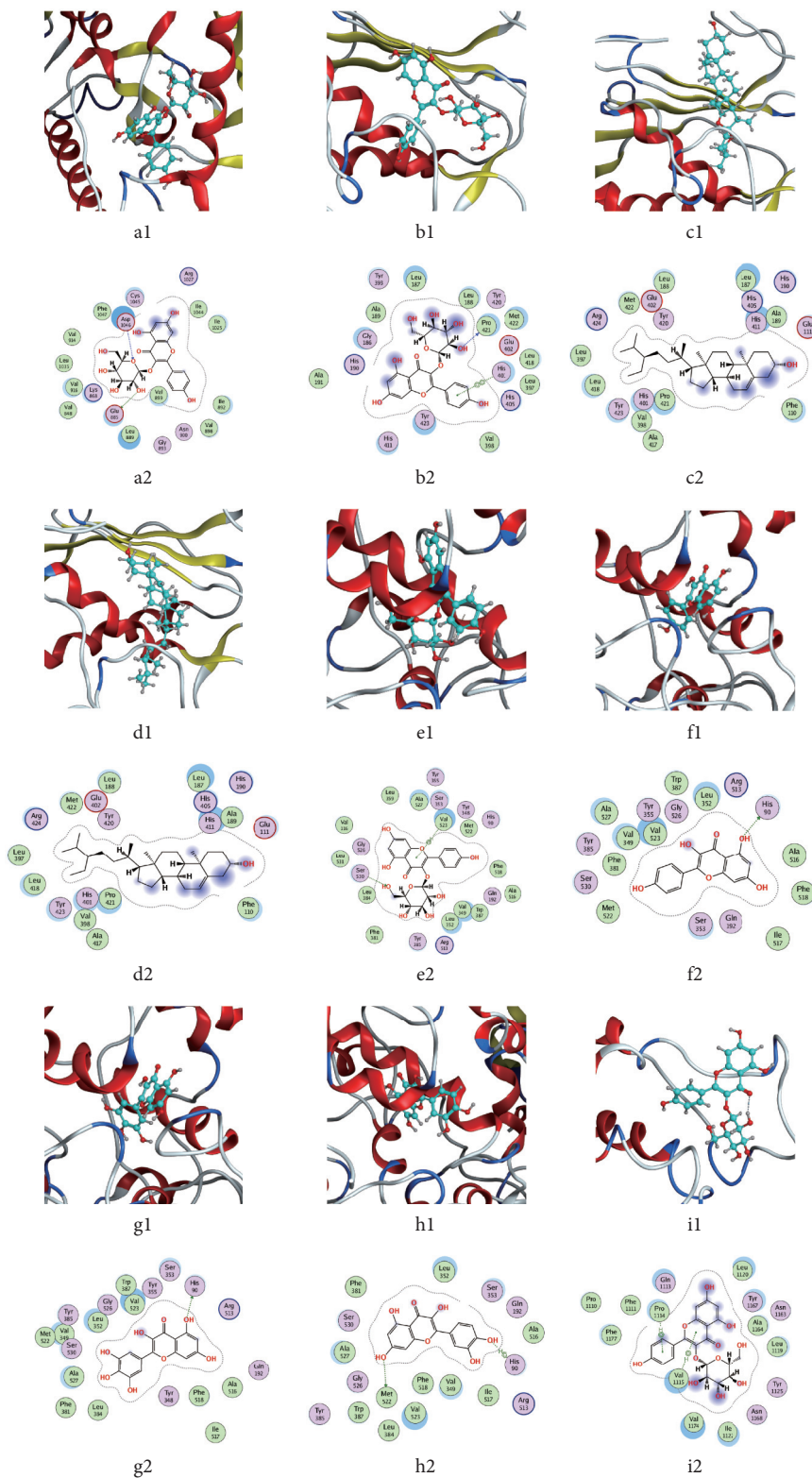


FIGURE 7: Molecular docking model. In the 3D structure of ligand-protein complexes, the protein backbone is represented as a cartoon (α -helices in red and β -sheets in green), peptide chains are coloured differently, and ligands are displayed in blue. The 2D interaction model shows amino acids circled differently according to their propensity for water; green: hydrophobic residues; purple: polar residues. (a) KDR-6gqq-astragalinal; (b) MMP9-1gkc-astragalinal; (c) MMP9-1gkc-beta-diosgenin; (d) MMP9-1gkc-beta-sitosterol; (e) PTGS2-5ikq-astragalinal; (f) PTGS2-5ikq-kaempferol; (g) PTGS2-5ikq-myricetin; (h) PTGS2-5ikq-quercetin; (i) tp53-1jsp-astragalinal.

extract of *Morus alba* Root Bark inhibits the proliferation and migration of vascular smooth muscle cells induced by PDGF. It stimulates the formation of nitric oxide (NO) in endothelial cells [67]. NO is a vital gaseous signalling molecule that participates in the growth and remodelling of essential biochemical and molecular reactions necessary for regulating angiogenesis. The NO-induced activation of soluble guanylate cyclase increases cyclic guanosine monophosphate formation and protein kinase G activity to modulate signalling cascades by phosphorylation MAPKs, which successively phosphorylate and activate downstream proteins such as ERK1/2 [68,69]. These events regulate the proliferation and migration of endothelial cells, resulting in angiogenesis. Forsythiae Fructus aqueous extract triggers the inhibition of oxidative stress and inflammation via the MAPKs/Nrf2/HO-1 signalling pathway and inhibits cancer cell proliferation and angiogenesis [70].

Traditional Chinese medicines can be classified based on the four natures, five flavours, and meridians. Information about these factors can be related to efficacy and utility in a clinical setting [71]. In this study, the most prevalent natures were found to be warm and cold. According to Chapter 74 of the *Zhizhenyao Dalunpian: Discussion on the Most Important and Abstruse Theory - Plain Questions*, which describes the rules of using traditional Chinese medicine in treatment, diseases caused by cold are treated with warm-natured therapy, and heat syndromes are treated with cold-natured therapy.

The core function of warm is to activate blood, replenish qi, and prevent the inhibition of water. It is usually used in treating yang deficiency or problems in fluid transformation such as heart failure. In some studies, it is shown that the extract of the warm-natured drugs such as Allicin [72] and astragaloside IV [73], through regulating sarcoplasmic reticulum Ca²⁺ pump, improved the distribution and expression of PECAM-1, enhanced the migration and angiogenesis ability of cardiac microvascular endothelial cells, promoted angiogenesis, protected myocardial ischemia, inhibited cardiac hypertrophy and fibrosis, and reduced myocardial cell apoptosis. The primary function of cold is heat-clearing, detoxicating, and draining fire. It inhibited the release of inflammatory factors to treat the diseases caused by inflammation [74] such as cancer. Some extracts of the cold-natured drugs such as tetrandrine [75], artemisinin [76], and andrographolide [77] inhibited endothelial cell proliferation, adhesion, invasion, and tube formation by targeting vascular endothelial growth factor and blocking angiogenesis and invasion of cancer cells

Moreover, the highest-ranked flavours were acrid, bitter, and sweet. Acrid promotes diffusion and outthrust with dissipation—it is favourable for treating blood-stasis, blockage, and accumulations, such as ischemic stroke and cancer. Galangin and tetramethylpyrazine were extracted and isolated from traditional Chinese medicine with acrid flavours. Galangin ameliorated neurological scores, cerebral infarct volume, and cerebral edema through improving the neurovascular microenvironment [78]. Tetramethylpyrazine restrains angiogenesis by suppressing the ERK1/2 and Akt pathways and promotes apoptosis of tumour cells [24].

Furthermore, the bitter flavour and cold-natured drugs exerted a similar effect on draining fire, but the bitterness was better to dry dampness and drain fire downward. It also has an excellent therapeutic effect on diseases caused by inflammation. The primary function of sweet is to supplement and harmonize the centre and relax tension. It is appropriate for patients who are in pain and asthenia. Under the Chinese medicine theory, diabetic retinopathy was often classified as the pattern of dual vacuity of qi and yin and was influential in treating diabetic retinopathy by boosting qi and nourishing, clearing heat, and breeding body fluids [79]. Plantaginis semen belongs to the extract of sweet medicinals, which ameliorated diabetic retinopathy through increasing vascular permeability and retinal vessel diameter and restrained retinal vascular dilation [80].

The theory of channel tropism posits that medicines have selective therapeutic effects in different Zang-fu organs. This study shows that the top two meridians related to the studied traditional medicines were the liver and lungs. The liver is a crucial organ that regulates blood, including its storage, filtration, and bleeding. In contrast, the lungs control the qi and are intimately related to the qi of the chest. They also play an essential role in the blood and qi movement in circulation in the body. Thus, the liver and lungs closely collaborate in regulating the qi and blood. Because of the above, it can be presumed that impaired angiogenesis, according to the basic theory of Chinese medicine, is associated with the failure of the liver and lungs to perform their functions. Qi stagnation and blood stasis cause poor circulation of blood, which leads to the collection of water-humour, with the stagnant qi being transformed into heat. Therefore, traditional Chinese medicine's fundamental treatment principles are to warm the yang, rectify the qi, and activate the blood. In cases of long-time ailment, efforts should be made to eliminate dampness and clear heat.

5. Conclusions

In this study, we used network pharmacology to identify proteins related to angiogenesis through databases and documentation. Also, we constructed a target-compound-traditional Chinese medicine network, which was explored and analysed for the potential compounds and mechanisms of traditional Chinese medicine that participated in angiogenesis. The findings of this study can effectively narrow the scope of screening, improve scientific research efficiency, and reduce economic costs in the research of therapeutic agents to treat angiogenesis. However, this study is preliminary and is based on database analysis; therefore, it does not fully demonstrate the actual situation or verify the participation of traditional Chinese medicine in angiogenesis *in vivo*. The specific molecular mechanism still needs to be explored through subsequent experimental research.

Abbreviations

ECM: Extracellular matrix
ETCM: Encyclopedia of Traditional Chinese Medicine
HIF: Hypoxia-inducible factor

OMIM: Online Mendelian Inheritance in Man
 PDGF: Platelet-derived growth factor
 ROS: Reactive oxygen species
 TTD: Therapeutic Target Database
 VEGF: Vascular endothelial cell growth factor.

Data Availability

The data and materials used for this study will be made available by the corresponding author Qingyong He upon reasonable request.

Disclosure

Wenchao Dan is the co-first author. An earlier version of this paper has been presented as a preprint in “Research Square” for scholars to comment on (<https://www.researchsquare.com/article/rs-104137/v1>). The funders had no role in the study design, data collection and analysis, decision to publish, or preparation of the manuscript.

Conflicts of Interest

The authors declare that they have no conflicts of interest.

Authors' Contributions

Wingyan Yun, Jinlei Liu, Xinyuan Guo, and Min Li collected the related targets of angiogenesis and related molecular compounds. Wingyan Yun and Wenchao Dan performed the network pharmacology analysis and molecular docking, and Wingyan Yun wrote the manuscript. Wenchao Dan and Qingyong He revised the manuscript. All authors were responsible for reviewing data and read and approved the final manuscript.

Acknowledgments

The authors gratefully acknowledge Jianliang Li and Jianbo Guo (Beijing University of Chinese Medicine) for the study design and overall guidance. This study was supported by the Beijing Science and Technology Rising Star (Z181100006218035), the National Natural Science Foundation of China (81202803), and the National Administration of TCM Project Fund (G2T-FJS- 2019-203).

References

- [1] P. Lenzi, G. Bocci, and G. Natale, John Hunter and the origin of the term “angiogenesis”, 2016.
- [2] J. Folkman, “Tumor Angiogenesis: therapeutic Implications,” *New England Journal of Medicine*, vol. 285, no. 21, pp. 1182–1186, 1971.
- [3] M. A. Gimbrone, S. B. Leapman, R. S. Cotran, and J. Folkman, “Tumor dormancy in vivo by prevention of neo-vascularization,” *The Journal of Experimental Medicine*, vol. 136, no. 2, pp. 261–276, 1972.
- [4] D. Ribatti, “Judah Folkman, a pioneer in the study of angiogenesis,” *Angiogenesis*, vol. 11, no. 1, pp. 3–10, 2008.
- [5] J. Folkman, *Angiogenesis In Biology Of Endothelial Cells*, pp. 412–428, Springer, Heidelberg, Germany, 1984.
- [6] J. Folkman and C. Haudenschild, “Angiogenesis in vitro,” *Nature*, vol. 288, no. 5791, pp. 551–556, 1980.
- [7] N. Warmke, A. M. N. Walker, and R. M. Cubbon, “Angiogenesis,” *Encyclopedia of Cardiovascular Research and Medicine*, pp. 85–96, 2018.
- [8] F. Hillen and A. W. Griffioen, “Tumour vascularization: sprouting angiogenesis and beyond,” *Cancer and Metastasis Reviews*, vol. 26, pp. 3–4, 2007.
- [9] W. Risau, “Mechanisms of angiogenesis,” *Nature*, vol. 386, no. 6626, pp. 671–674, 1997.
- [10] S. J. Mentzer and M. A. Konerding, “Intussusceptive angiogenesis: expansion and remodeling of microvascular networks,” *Angiogenesis*, vol. 17, no. 3, pp. 499–509, 2014.
- [11] A. N. Makanya, R. Hlushchuk, and V. G. Djonov, “Intussusceptive angiogenesis and its role in vascular morphogenesis, patterning, and remodeling,” *Angiogenesis*, vol. 12, no. 2, pp. 113–123, 2009.
- [12] S. Krishna Priya, R. P. Nagare, V. S. Sneha et al., “Tumour angiogenesis-Origin of blood vessels,” *International Journal of Cancer*, vol. 139, no. 4, pp. 729–735, 2016.
- [13] F. Shojaei and N. Ferrara, “Role of the microenvironment in tumor growth and in refractoriness/resistance to anti-angiogenic therapies,” *Drug Resistance Updates*, vol. 11, no. 6, pp. 219–230, 2019.
- [14] F. Shojaei, “Anti-angiogenesis therapy in cancer: current challenges and future perspectives,” *Cancer Letters*, vol. 320, no. 2, pp. 130–137, 2018.
- [15] E. A. Kuczynski and A. R. Reynolds, “Vessel co-option and resistance to anti-angiogenic therapy,” *Angiogenesis*, vol. 23, no. 1, pp. 55–74, 2019.
- [16] Y. Haibe, M. Kreidieh, H. El Hajj et al., “Resistance mechanisms to anti-angiogenic therapies in cancer,” *Frontiers in Oncology*, vol. 10, 2021 pages, 2020.
- [17] A. Chandra, J. Rick, G. Yagnik, and M. K. Aghi, *Autophagy as a Mechanism for Anti-angiogenic Therapy Resistance Seminars In Cancer Biology*, Elsevier, Amsterdam, Netherlands, 2019.
- [18] Y. Crawford and N. Ferrara, “Tumor and stromal pathways mediating refractoriness/resistance to anti-angiogenic therapies,” *Trends in Pharmacological Sciences*, vol. 30, no. 12, pp. 624–630, 2009.
- [19] R. Ronca, M. Benkheil, S. Mitola, S. Struyf, and S. Liekens, “Tumor angiogenesis revisited: regulators and clinical implications,” *Medicinal Research Reviews*, vol. 37, no. 6, pp. 1231–1274, 2017.
- [20] C. Viallard and B. Larrivée, “Tumor angiogenesis and vascular normalization: alternative therapeutic targets,” *Angiogenesis*, vol. 20, no. 4, pp. 409–426, 2018.
- [21] C. Widakowich, G. De Castro, E. De Azambuja, P. Dinh, and A. Awada, “Side effects of approved molecular targeted therapies in solid cancers,” *The oncologist*, vol. 12, no. 12, pp. 1443–1455, 2013.
- [22] H.-P. Lee, Y.-C. Liu, P.-C. Chen et al., “Tanshinone IIA inhibits angiogenesis in human endothelial progenitor cells in vitro and in vivo,” *Oncotarget*, vol. 8, no. 65, Article ID 109217, 2017.
- [23] L.-Q. Yang, R.-Y. Li, X.-Y. Yang et al., “Co-administration of shexiang baixin pill and chemotherapy drugs potentiated cancer therapy by vascular-promoting strategy,” *Frontiers in Pharmacology*, vol. 10, p. 565, 2019.
- [24] L. Zou, X. Liu, J. Li et al., “Tetramethylpyrazine enhances the antitumor effect of paclitaxel by inhibiting angiogenesis and inducing apoptosis,” *Frontiers in Pharmacology*, vol. 10, 10707 pages, 2019.

- [25] S. Wang, Z. Zheng, Y. Weng et al., "Angiogenesis and anti-angiogenesis activity of Chinese medicinal herbal extracts," *Life sciences*, vol. 74, no. 20, pp. 2467–2478, 2004.
- [26] Y. Dong, B. Lu, X. Zhang et al., "Cucurbitacin E, a tetracyclic triterpenes compound from Chinese medicine, inhibits tumor angiogenesis through VEGFR2-mediated Jak2-STAT3 signaling pathway," *Carcinogenesis*, vol. 31, no. 12, pp. 2097–2104, 2015.
- [27] S. Zhang, D. Tang, W. Zang et al., "Synergistic inhibitory effect of traditional Chinese medicine astragaloside IV and curcumin on tumor growth and angiogenesis in an orthotopic nude-mouse model of human hepatocellular carcinoma," *Anticancer Research*, vol. 37, no. 2, pp. 465–474, 2017.
- [28] L. Shao and B. Zhang, "Traditional Chinese medicine network pharmacology: theory, methodology and application," *Chinese Journal of Natural Medicines*, vol. 11, no. 2, pp. 110–120, 2013.
- [29] S. Li, B. Zhang, and N. Zhang, "Network target for screening synergistic drug combinations with application to traditional Chinese medicine," *BMC Systems Biology*, vol. 5, no. 1, pp. 1–13, 2013.
- [30] G.-B. Zhang, Q.-Y. Li, Q.-L. Chen, and S.-B. Su, "Network pharmacology: a new approach for Chinese herbal medicine research," *Evidence-Based Complementary and Alternative Medicine*, vol. 2013, Article ID 621423, 9 pages, 2013.
- [31] M. Safran, I. Dalah, J. Alexander et al., "GeneCards Version 3: the human gene integrator," *Database*, vol. 2010, 2010.
- [32] Y. Wang, S. Zhang, F. Li et al., "Therapeutic target database: enriched resource for facilitating research and early development of targeted therapeutics," *Nucleic Acids Research*, vol. 48, pp. D1031–D1041, 2020.
- [33] J. S. Amberger, C. A. Bocchini, F. Schiettecatte, A. F. Scott, and A. Hamosh, "OMIM.org: Online Mendelian Inheritance in Man (OMIM®), an online catalog of human genes and genetic disorders," *Nucleic Acids Research*, vol. 43, pp. D789–D798, 2020.
- [34] D. S. Wishart, Y. D. Feunang, A. C. Guo et al., "DrugBank 5.0: a major update to the DrugBank database," *Nucleic Acids Research*, vol. 46, pp. D1074–D1082, 2018.
- [35] J. Piñero, J. M. Ramirez-Anguaita, J. Saüch-Pitarch et al., "The DisGeNET knowledge platform for disease genomics update," *Nucleic Acids Research*, vol. 48, pp. D845–D855, 2019.
- [36] U. Consortium, "UniProt: the universal protein knowledgebase," *Nucleic Acids Research*, vol. 46, no. 5, p. 2699, 2017.
- [37] J. Ru, P. Li, J. Wang et al., "TCMSP: a database of systems pharmacology for drug discovery from herbal medicines," *Journal of Cheminformatics*, vol. 6, no. 1, p. 13, 2014.
- [38] H.-Y. Xu, Y.-Q. Zhang, Z.-M. Liu et al., "ETCM: an encyclopaedia of traditional Chinese medicine," *Nucleic Acids Research*, vol. 47, pp. D976–D982, 2019.
- [39] P. Shannon, A. Markiel, O. Ozier et al., "Cytoscape: a software environment for integrated models of biomolecular interaction networks," *Genome Research*, vol. 13, no. 11, pp. 2498–2504, 2003.
- [40] C. P. Commission, *Chinese Pharmacopoeia (2020 Edition)*, China Medical Science Press, Beijing, China, 2020.
- [41] Z.-X. Zhou and D.-C. Tang, "13th five-year plan textbook of Traditional Chinese Medicine Pharmacy," *China Press of Traditional Chinese Medicine*, vol. 2, no. 2, pp. 53–59, 2016.
- [42] C. Peng, *Chinese Dictionary of Clinical Drugs*, China Medical Science Press, Beijing, China, 2018.
- [43] O. Trott and A. J. Olson, "AutoDock Vina: improving the speed and accuracy of docking with a new scoring function, efficient optimization, and multithreading," *Journal of Computational Chemistry*, vol. 31, no. 2, pp. 455–461, 2010.
- [44] L. J. Le, I. W. Chao, H. Q. Yong, X. B. Wen, and Q. Yi, "Molecular mechanism of diyu shengbai tablets in treatment of leukopenia based on network pharmacology," *Modern Chinese Medicine*, vol. 22, no. 9, pp. 1–16, 2007.
- [45] M. A. Iñiguez, A. Rodríguez, O. V. Volpert, M. Fresno, and J. M. Redondo, "Cyclooxygenase-2: a therapeutic target in angiogenesis," *Trends in Molecular Medicine*, vol. 9, no. 2, pp. 73–78, 2005.
- [46] R. S. Apte, D. S. Chen, and N. Ferrara, "VEGF in signaling and disease: beyond discovery and development," *Cell*, vol. 176, no. 6, pp. 1248–1264, 2019.
- [47] J. E. Rundhaug, "Matrix metalloproteinases and angiogenesis," *Journal of Cellular and Molecular Medicine*, vol. 9, no. 2, pp. 267–285, 2005.
- [48] M. Hollborn, C. Stathopoulos, A. Steffen, P. Wiedemann, L. Kohen, and A. Bringmann, "Positive feedback regulation between MMP-9 and VEGF in human RPE cells," *Investigative Ophthalmology & Visual Science*, vol. 48, no. 9, p. 4360, 2007.
- [49] I. Stamenkovic, "Extracellular matrix remodelling: the role of matrix metalloproteinases," *The journal of Pathology: a Journal of the Pathological Society of Great Britain and Ireland*, vol. 200, no. 4, pp. 448–464, 2003.
- [50] A. Yabluchanskiy, Y. Ma, R. P. Iyer, M. E. Hall, and M. L. Lindsey, "Matrix metalloproteinase-9: many shades of function in cardiovascular disease," *Physiology*, vol. 28, no. 6, pp. 391–403, 2013.
- [51] H. Huang, "Matrix metalloproteinase-9 (MMP-9) as a cancer biomarker and MMP-9 biosensors: recent advances," *Sensors*, vol. 18, no. 10, p. 3249, 2021.
- [52] Z. Ma, T. Piao, Y. Wang, and J. Liu, "Astragalin inhibits IL-1 β -induced inflammatory mediators production in human osteoarthritis chondrocyte by inhibiting NF- κ B and MAPK activation," *International Immunopharmacology*, vol. 25, no. 1, pp. 83–87, 2015.
- [53] N. Azoitei, A. Becher, K. Steinestel et al., "PKM2 promotes tumor angiogenesis by regulating HIF-1 α through NF- κ B activation," *Molecular Cancer*, vol. 15, no. 1, 2016.
- [54] M. Imran, B. Salehi, J. Sharifi-Rad et al., "Kaempferol: a key emphasis to its anticancer potential," *Molecules*, vol. 24, no. 12, 2277 pages, 2017.
- [55] Y.-W. Kim and T. V. Byzova, "Oxidative stress in angiogenesis and vascular disease," *Blood*, vol. 123, no. 5, pp. 625–631, 2014.
- [56] W. N. Duran, J. W. Breslin, and F. A. Sanchez, "The NO cascade, eNOS location, and microvascular permeability," *Cardiovascular Research*, vol. 87, no. 2, pp. 254–261, 2010.
- [57] J. Lu, L. V. Papp, J. Fang, S. Rodriguez-Nieto, B. Zhivotovskiy, and A. Holmgren, "Inhibition of mammalian thioredoxin reductase by some flavonoids: implications for myricetin and quercetin anticancer activity," *Cancer Research*, vol. 66, no. 8, pp. 4410–4418, 2006.
- [58] J. Lu and A. Holmgren, "The thioredoxin antioxidant system," *Free Radical Biology and Medicine*, vol. 66, pp. 75–87, 2014.
- [59] D. Lee, I. M. J. Xu, D. K. C. Chiu et al., "Induction of oxidative stress through inhibition of thioredoxin reductase 1 is an effective therapeutic approach for hepatocellular carcinoma," *Hepatology*, vol. 69, no. 4, pp. 1768–1786, 2019.
- [60] J. Zhang, J. Yao, S. Peng, X. Li, and J. Fang, "Securinin disturbs redox homeostasis and elicits oxidative stress-mediated apoptosis via targeting thioredoxin reductase," *Biochimica et Biophysica Acta (BBA) Molecular Basis of Disease*, vol. 1863, no. 1, pp. 129–138, 2017.

- [61] M. A. Abdelsaid, S. Matragoon, and A. B. El-Remessy, "Thioredoxin-Interacting protein expression is required for VEGF-mediated angiogenic signal in endothelial cells," *Antioxidants & Redox Signaling*, vol. 19, no. 18, pp. 2199–2212, 2013.
- [62] L. L. Dunn, A. M. Buckle, J. P. Cooke, and M. K. C. Ng, "The emerging role of the thioredoxin system in angiogenesis," *Arteriosclerosis, Thrombosis, and Vascular Biology*, vol. 30, no. 11, pp. 2089–2098, 2010.
- [63] Q. Yang, D. Yu, and Y. Zhang, " β -Sitosterol attenuates the intracranial aneurysm growth by suppressing TNF- α -mediated mechanism," *Pharmacology*, vol. 104, no. 6, pp. 302–310.
- [64] W.-H. Hu, G. K.-L. Chan, J.-S. Lou et al., "The extract of *Polygoni Cuspidati Rhizoma et Radix* suppresses the vascular endothelial growth factor-induced angiogenesis," *Phytomedicine*, vol. 42, pp. 135–143, 2019.
- [65] P. Abeyrathna and Y. Su, "The critical role of Akt in cardiovascular function," *Vascular Pharmacology*, vol. 74, pp. 38–48, 2019.
- [66] Q. Zhang, S. Lu, T. Li et al., "ACE2 inhibits breast cancer angiogenesis via suppressing the VEGFa/VEGFR2/ERK pathway," *Journal of Experimental & Clinical Cancer Research*, vol. 38, no. 1, 2019.
- [67] N. Panth, K. R. Paudel, D.-S. Gong, and M.-H. Oak, "Vascular protection by ethanol extract of *Morus alba* Root Bark: endothelium-dependent relaxation of rat aorta and decrease of smooth muscle cell migration and proliferation," *Evidence-Based Complementary and Alternative Medicine*, vol. 2018, Article ID 7905763, 8 pages, 2018.
- [68] S. C. Bir, Y. Xiong, C. G. Kevil, and J. Luo, "Emerging role of PKA/eNOS pathway in therapeutic angiogenesis for ischaemic tissue diseases," *Cardiovascular Research*, vol. 95, no. 1, pp. 7–18, 2012.
- [69] J. R. Molina and A. A. Adjei, "The ras/raf/MAPK pathway," *Journal of Thoracic Oncology*, vol. 1, no. 1, pp. 7–9, 2006.
- [70] J. Bao, R. Ding, L. Zou et al., "Forsythiae fructus inhibits B16 melanoma growth involving MAPKs/Nrf2/HO-1 mediated anti-oxidation and anti-inflammation," *The American Journal of Chinese Medicine*, vol. 44, no. 5, pp. 1043–1061, 2016.
- [71] J. Nugent-Head, "Returning our focus to the flavour and nature of herbs," *The Journal of Chinese Medicine*, vol. 105, p. 30, 1870.
- [72] P. Shi, Y. Cao, J. Gao et al., "Allicin improves the function of cardiac microvascular endothelial cells by increasing PECAM-1 in rats with cardiac hypertrophy," *Phytomedicine*, vol. 51, pp. 241–254, 2018.
- [73] Y. Zang, J. Wan, Z. Zhang, S. Huang, X. Liu, and W. Zhang, "An updated role of astragaloside IV in heart failure," *Biomedicine & Pharmacotherapy*, vol. 126, Article ID 110012, 2020.
- [74] Q. Wang, C.-P. Su, H.-M. Zhang, Y.-L. Ren, W. Wang, and S.-Z. Guo, "Anti-inflammatory mechanism of heat-clearing and detoxifying Chinese herbs," *China journal of Chinese Materia Medica*, vol. 43, no. 18, pp. 3787–3794, 2018.
- [75] T. Liu, X. Liu, and W. Li, "Tetrandrine, a Chinese plant-derived alkaloid, is a potential candidate for cancer chemotherapy," *Oncotarget*, vol. 7, no. 26, Article ID 40800, 2016.
- [76] R. Mancuso, M. Foglio, and S. O. Saad, "Artemisinin-type drugs for the treatment of hematological malignancies," *Cancer Chemotherapy and Pharmacology*, vol. 87, no. 1, pp. 1–22, 2021.
- [77] J. C. W. Lim, T. K. Chan, D. S. Ng, S. R. Sagineedu, J. Stanslas, and W. F. Wong, "Andrographolide and its analogues: versatile bioactive molecules for combating inflammation and cancer," *Clinical and Experimental Pharmacology and Physiology*, vol. 39, no. 3, pp. 300–310, 2012.
- [78] C. Wu, J. Chen, C. Chen et al., "Wnt/ β -catenin coupled with HIF-1 α /VEGF signaling pathways involved in galangin neurovascular unit protection from focal cerebral ischemia," *Scientific Reports*, vol. 5, no. 1, pp. 1–11, 2015.
- [79] X. Ai, P. Yu, Y. Hou et al., "A review of traditional Chinese medicine on treatment of diabetic retinopathy and involved mechanisms," *Biomedicine & Pharmacotherapy*, vol. 132, Article ID 110852, 2020.
- [80] T.-F. Tzeng, W. Y. Liu, S.-S. Liou, T.-Y. Hong, and I.-M. Liu, "Antioxidant-rich extract from plantaginis semen ameliorates diabetic retinal injury in a streptozotocin-induced diabetic rat model," *Nutrients*, vol. 8, no. 9, p. 572, 2011.

Research Article

Computer-Aided Drug Discovery Identifies Alkaloid Inhibitors of Parkinson's Disease Associated Protein, Prolyl Oligopeptidase

Apoorva M. Kulkarni, Shailima Rampogu, and Keun Woo Lee 

*Division of Life Sciences, Division of Applied Life Science (BK21 Plus),
Plant Molecular Biology and Biotechnology Research Center (PMBBRC), Research Institute of Natural Science (RINS),
Gyeongsang National University (GNU), 501 Jinju-daero, Jinju 52828, Republic of Korea*

Correspondence should be addressed to Keun Woo Lee; kwlee@gnu.ac.kr

Received 17 November 2020; Revised 25 December 2020; Accepted 19 February 2021; Published 9 April 2021

Academic Editor: Siba Shanak

Copyright © 2021 Apoorva M. Kulkarni et al. This is an open access article distributed under the Creative Commons Attribution License, which permits unrestricted use, distribution, and reproduction in any medium, provided the original work is properly cited.

Parkinson's disease is a common neurodegenerative disorder marked by the accumulation of the protein alpha synuclein. Studies have indicated the role of prolyl oligopeptidase (POP), a serine protease, in alpha synuclein accumulation. Therefore, POP emerges as an attractive medicinal target. Traditionally, most of the early medicines have been plant-based owing to their ready availability and negligible side effects. Alkaloids owing to their neurotransmitter modulatory, anti-amyloid, anti-oxidant, and anti-inflammatory activities have shown potential in neurodegenerative disease. In this work, we computationally evaluated alkaloid class of phytochemicals for their therapeutic efficacy against POP. Alkaloids were retrieved from the publically available database, Chemical Entities of Biological Interest (ChEBI), and screened for their drug likeness (Lipinski's rule of 5) and absorption, distribution, metabolism, and excretion, and toxicity (ADMET) in Discovery Studio by ensuring parameters suitable for a central nervous system disease such as blood-brain barrier (BBB) level set to ≤ 2 , absorption level set to 0 and solubility level permitted set to 2, 3, or 4. Next, molecular docking was performed to learn about the affinity of the filtered alkaloids with the POP. Subsequently, molecular dynamic simulations were conducted to assess the reliability and stability of the alkaloid-protein complex. Our study identified metergoline, pipericalosine, celacinnine, lobeline, cystodytin G, lycoperine A, hookerianamide J, and martefragin A as putative lead compounds against POP. Among these, metergoline, pipericalosine, hookerianamide J, and lobeline showed the most promising results. These compounds demonstrated better or equivalent molecular docking scores in comparison to three POP inhibitors that had reached clinical trials, i.e., Z-321, S-17092, and JTP-4819. MD simulations indicated that these compounds remained intact at the active site while adhering to the binding mode and interaction patterns as that of the reported inhibitors. The research conducted here, therefore, provides evidence for conducting in vitro POP inhibitory studies of these newly identified plant-based POP inhibitors.

1. Introduction

Parkinson's disease (PD) is a chronic and progressive neurodegenerative central nervous system (CNS) disorder. Affected individuals experience difficulty in walking, tremors, stiffness in limbs, or impaired balance (<https://www.ninds.nih.gov/disorders/patient-caregiver-education/hope-through-research/parkinsons-disease-hope-through-research>, last accessed December 20, 2019). Largely an age-related disease, PD can be either sporadic or genetic. It is characterized by the presence of Lewy bodies which are clusters of alpha synuclein and other

proteins [1]. In 2008, research done by Brandt et al. indicated that prolyl oligopeptidase (POP) stimulates the aggregation of alpha synuclein [2]. Also, Hannula and colleagues identified that POP generally co-localizes with alpha synuclein and this interaction is stronger in PD brains [3]. Therefore, POP emerges as an attractive pharmacological target.

POP (also known as PREP or prolyl endopeptidase; EC 3.4.21.26) is a large 80 kDa intracellular enzyme belonging to serine protease family. It is capable of cleaving peptides shorter than 30 amino acids after a proline residue [4]. POP is majorly expressed in brain areas populated with

neuropeptide receptors [5] and influences CNS-related activities like memory, learning, and mood responses [6, 7].

POP in entirety assumes a cylindrical shape and is comprised of two domains: peptidase or catalytic domain (residues 1–72 and 428–710) containing the alpha/beta hydrolase fold, and a 7-bladed β -propeller domain (residues 73–427) containing seven-fold repeat of four stranded antiparallel β sheets. The catalytic triad consisting of Ser554, His680, and Asp641 is found at the interface of these domains. Several sub-sites form part of active site: the S1 specificity pocket comprises Phe476, Asn555, Val580, Trp595, Tyr599, and Val644 residues thus forming a hydrophobic environment for the ease of accommodating the proline or aromatic rings present in inhibitors, the less specific S2 pocket containing the guanidium ring of Arg643, and the hydrophobic S3 pocket comprising non-polar residues such as Phe173, Met235, Cys255, Ile591, and Ala594. Hydrogen bonds interactions of the residues Trp595 and Arg643 with the POP inhibitors have been shown to be of vital importance [8].

Although several research groups have focused on POP inhibition [9–11], three inhibitors Z-321, S-17092, and JTP-4819 were considered for clinical trials [12]. Crossing of blood brain barrier (BBB) poses a major concern for POP inhibitors [13]. Besides this, safety is a perennial question in drug discovery projects. In this regard, plant-based therapeutics are alluring as they have been used long in history without any adverse side effects. Berberine and baicalein were identified as natural product inhibitors of POP with IC50 values of $145 \pm 19 \mu\text{M}$ and $12 \pm 3 \mu\text{M}$ [14, 15]. Cyclotide psysol 2 isolated from *Psychotria solitudinum* was found to inhibit POP [16]. Despite the identification of these natural product POP inhibitors, no advancement has been done and there are currently no clinically approved POP inhibitors in the market. This urges for identification of safe and novel therapeutics effective against POP. There have been reports on activity of various alkaloids in PD and other neurodegenerative diseases [17–19]. Therefore, here we have computationally evaluated alkaloids to screen for the best prospective drug candidate against POP and elucidate their mechanism of action.

2. Materials and Methods

In brief, structures of the alkaloids and target protein (POP) were retrieved. Alkaloids were screened for their drug likeness and ADMET properties, following which molecular docking was performed in order to access their binding to POP. Lastly, molecular dynamics simulations were conducted to evaluate the stability of the prospective drug candidates when bound to POP.

2.1. Structure Retrieval and Preparation of Target Protein. Structure of POP bearing PDB id: 3DDU [20] was downloaded from Protein Data Bank (PDB). Using Discovery studio v18 (DS) [21], the protein structure was cleaned by deleting heteroatoms and water molecules. Hydrogen atoms were added. Missing loops were added based on the sequence obtained from Uniprot identifier P48147 [22].

2.2. Alkaloids Retrieval, Drug Likeness, and ADMET Prediction. The list of alkaloid compounds was downloaded from ChEBI (Chemical Entities of Biological Interest) (<https://www.ebi.ac.uk/chebi/init.do>) by using the search term “alkaloid.” Retrieved compounds were first subjected to absorption, distribution, metabolism, and excretion, and toxicity (ADMET) studies. For this, DS’s ADMET tool was used with a value of 0 as cutoff for ADMET_ABSORPTION_LEVEL and a value of 2, 3, or 4 as cutoff for ADMET_SOLUBILITY_LEVEL and a cutoff value of 0, 1, or 2 was used for ADMET_BBB_LEVEL. Compounds that passed ADMET were subjected to “Filter by Lipinski and Veber Rules” using the default parameters. After this, the alkaloids were minimized using “full minimization tool” in DS for carrying out the molecular docking studies with the target protein.

2.3. Molecular Docking. To predict the binding affinity of the filtered alkaloids with POP, molecular docking was performed using Genetic Optimisation for Ligand Docking (GOLD) version 5.2.2 [23]. The ligand binding co-ordinates were calculated by inbound co-crystal (GSK552) using “Define and edit binding site” module of DS. GoldScore fitness was used as the default scoring function. GoldScore fitness comprises hydrogen bond and van der Waals energy of protein ligand, ligand internal van der Waals energy, and ligand torsional strain energy. The best docked pose of the alkaloid with the protein was selected based on the following: it should be part of the largest cluster that obeys the co-crystal’s binding mode, should have a better GoldScore fitness value than reference compounds, and should demonstrate interactions with key residues in the active site. In order to validate our docking parameters, GSK552 from PDB structure was docked and root mean square deviation (RMSD) was checked for.

2.4. Molecular Dynamics Simulations. To determine the reliability and consistency of the binding of the prospective drug candidates to the target protein, molecular dynamics (MD) simulations were performed using GROningen MAchine for Chemical Simulations (GROMACS) v5.0.6 package [24] and using CHARMM27 [25] as desired force field. Ligand topology was generated using SwissParam [26]. Dodecahedron system solvated with TIP3P water model was utilized for solvation. Na^+ ions were added to neutralize the negative charge of the system. Steepest Descent was used for energy minimization. Equilibration of the system was carried out in two phases: constant number N, volume V, and temperature T (NVT) and constant number N, pressure P, and temperature T (NPT). NVT ensemble was performed at 300 K for 1 ns and NPT ensemble at 1 bar pressure for 1 ns with a Parrinello–Rahman barostat [27]. Once the system was well equilibrated, MD was carried out for 50 ns (metergoline) or 20 ns (other identified alkaloid inhibitors). MD analysis was performed using Visual Molecular Dynamics (VMD) and DS.

3. Results

3.1. Drug Likeness and ADMET. ChEBI search resulted in the retrieval of 565 alkaloid compounds (accessed on 14th August 2019). To ensure a good pharmacokinetic profile of the potential drug candidates, ADMET tests were carried out in DS. By setting 0 as cutoff value for ADMET_ABSORPTION_LEVEL, it was ensured that potential inhibitors had a good intestinal absorption. Filtering of compounds where ADMET_SOLUBILITY_LEVEL was either 2, 3, or 4 ensured that the potential inhibitors were neither too soluble nor insoluble in water. The most important factor in identifying drug for neurological diseases is their ability to penetrate blood brain barrier. Usage of 0, 1, or 2 as cutoff for ADMET_BBB_LEVEL ensured only the compounds that could pass blood brain barrier would be retained. 190 of the initial 565 compounds passed the ADMET test. Drug likeness of these 190 compounds was accessed using “Filter by Lipinski and Veber Rules” with default parameters. Lipinski’s rule states that a drug-like molecule should not have more than 5 hydrogen bond donors and 10 hydrogen bond acceptors, molecular weight should not exceed 500 daltons, and LogP should not be more than 5 [28]. 189 compounds that passed drug-likeness criteria were retained and were subjected to further study.

3.2. Molecular Docking to Access Binding Affinity with POP. In order to determine whether the candidate inhibitors bind to POP, molecular docking was performed by employing Z-321 and S-17092 as reference 1 (Ref1) and reference 2 (Ref2), respectively.

RMSD measures the average distance between the atoms of superimposed proteins and is used to measure the quality of reproduction of a known binding pose. Therefore, the lower the RMSD, the lesser the deviation from the known binding pose. The docked pose of co-crystal, i.e., GSK552 with POP resulted in an RMSD of 0.094 nm. The low RMSD ensured the credibility of our docking protocol. Using the affirmed docking parameters of GSK552, 189 candidate inhibitors were docked at the active site of POP. From the largest cluster obeying the binding mode of the co-crystal, best pose was selected based on higher score than that of reference compounds and interaction with key residues. GoldScore fitness for Ref1 and Ref2 was 70.5265 and 68.4808, respectively. Metergoline with a GoldScore fitness of 72.6547 was the only compound to score better than both Ref1 and Ref2. Pipericallosine with a GoldScore fitness of 68.6628 attained a slightly higher docking score than that of Ref2 (68.4808). Additionally, since JTP-4819 was also considered in clinical trials as POP inhibitor, we also docked it against POP. The GoldScore fitness value for JTP-4819 against POP was 60.0431. Apart from metergoline and pipericallosine, six other alkaloids, celacinnine, lobeline, cystodytin G, lycoperine A, hookerianamide J, and marte-fragin A, fared better than JTP-4819. These collectively will be referred to as hit candidates from now on. The docking

scores of all these compounds are tabulated in Supplementary Table 1.

After gaining knowledge on binding affinity via docking scores, we explored the interaction pattern of the hit candidates and reference compounds with POP. Because of its high docking score, we were mainly interested in learning about metergoline’s interaction with POP active site residues. “Show 2d diagram” of DS was utilized to inspect the molecular interactions with POP. Ref1, Ref2, and metergoline all interacted with the active site residues. Ref1 formed hydrogen bond with Trp595 and Arg643 and Ref2 formed hydrogen bond with Trp595, Tyr599, and Arg643. Metergoline like Ref1 and Ref2 was involved in hydrogen bond formation with Arg643 and Trp595, thus maintaining the necessary hydrogen bond interactions. These hydrogen bond interactions are depicted in Figures 1(a)–1(c). Ref1 and Ref2 demonstrated non-covalent π interactions with Phe173, Met235, Cys255, Phe476, Val580, Ala594, Trp595, and Val644 with Ref1 showing an additional interaction with Ile591. Metergoline formed π interactions with Phe173, Met235, Arg252, Cys255, Phe476, Val580, Ile591, Ala594, and Trp595. van der Waals interactions were formed by both Ref1 and Ref2 with Arg252, Gly254, Tyr473, Ile478, Asn555, and His680 residues of POP. Ref1 and Ref2 developed an additional van der Waals interaction with Tyr599 and Ile591, respectively. Both Ref1 and Ref2 displayed a carbon-hydrogen bond with Ser554. Additionally, Ref2 formed a carbon-hydrogen bond with Arg643 also. Metergoline established van der Waals bonds with Ser174, Cys175, Asn188, Gln208, Gly236, Gly237, Ser250, Gly254, Tyr473, Ser554, Asn555, Tyr599, Val644, and His680 residues. Metergoline also formed a carbon-hydrogen bond with Met235. All these interactions are presented in Figures 1(d)–1(f).

We also performed interaction analysis of JTP-4819 and other hit compounds (pipericallosine, celacinnine, lobeline, cystodytin G, lycoperine A, hookerianamide J, and marte-fragin A) with POP. JTP-4819 demonstrated four hydrogen bonds: one each with Arg128 and Cys255 and two with Arg643. π interactions were seen between Phe173, Phe476, Ile591, Ala594, Trp595, and JTP-4819. With the other active site residues such as Met235, Asn555, Val580, Tyr599, and Val644, JTP-4819 established van der Waals interactions. Pipericallosine established one hydrogen bond with Arg643. Cystodytin G demonstrated a total of three hydrogen bonds, two with Cys255 and one with Tyr473. Lobeline, lycoperine A, and hookerianamide J established two hydrogen bonds. Lobeline and hookerianamide J established hydrogen bonds, one each with Cys255 and Arg643, whereas lycoperine A established hydrogen bonds, one each with Cys255 and Tyr473. Interestingly, marte-fragin A demonstrated 5 hydrogen bonds: a bifurcated hydrogen bond with Ser554 and His680 and one each with Cys255, Tyr473, and Arg643. However, celacinnine did not display any hydrogen bonds. All the hit compounds interacted with all the active site residues except for cystodytin G which did not demonstrate any interaction with the active site residue Ala594. It

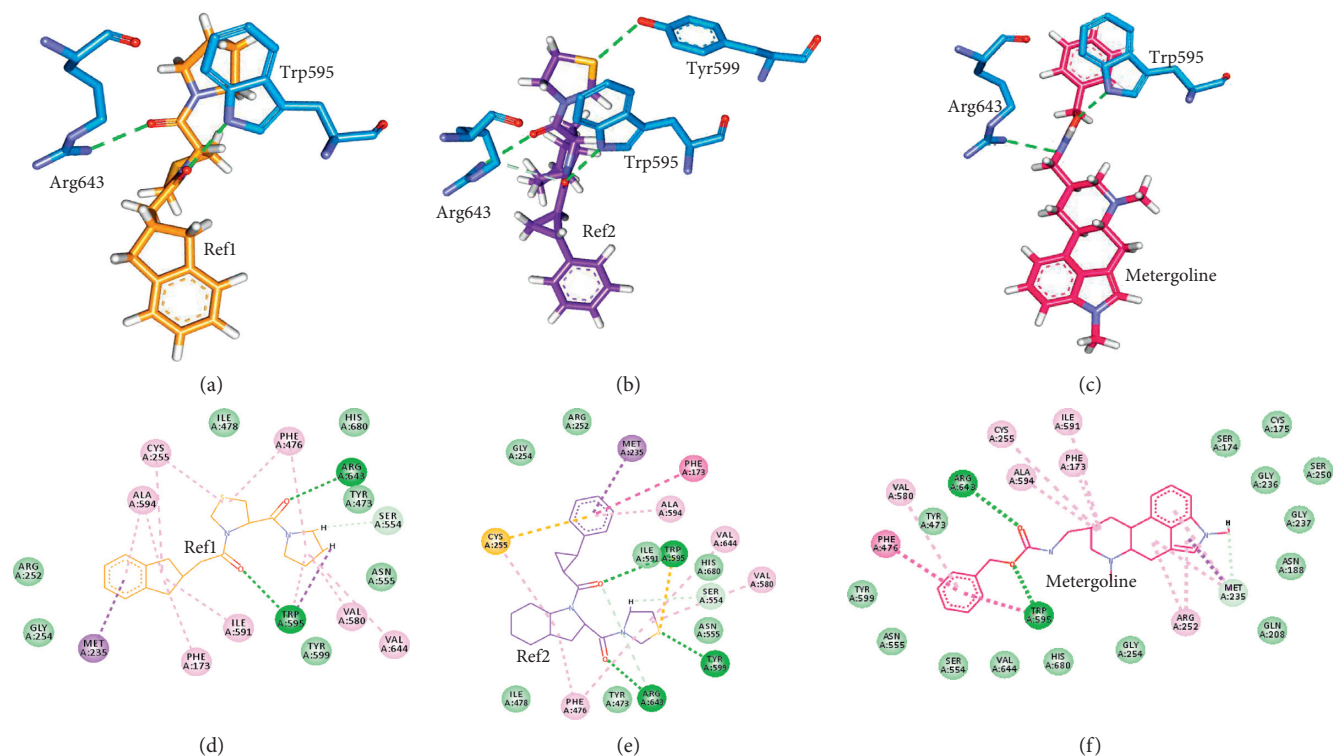


FIGURE 1: Molecular docking based intermolecular interactions. Upper panel (a–c) demonstrates hydrogen bond interactions of POP residues (blue) with (a) Ref1, (b) Ref2, and (c) metergoline. Lower panel (d–f) is the 2D representation of all the molecular interactions between POP and (d) Ref1, (e) Ref2, and (f) metergoline. Green dashed lines in upper and lower panel represent hydrogen bond. All the other dashed lines represent various types of π bonds. Light green colored spheres indicate the residues participating in van der Waals interactions.

however displayed interactions with all the other active site residues. These interactions are demonstrated in Supplementary Figure 1.

3.3. Molecular Dynamic Simulations for Binding Stability.

We performed a 50 ns MD simulation using GROMACS in order to access the binding stability of POP when bound to Ref1, Ref2, and metergoline. RMSD for backbone atoms and potential energy calculations were executed to determine the stability of protein-ligand complex. As illustrated in Figure 2(a), very low average backbone RMSDs of 0.12 nm, 0.13 nm, and 0.13 nm for Ref1, Ref2, and metergoline, respectively, indicated that the protein-ligand complexes were stable. Also, the potential energy profile for all the three systems remained largely unvaried throughout the simulation as depicted in Figure 2(b).

As the RMSD and potential energy profiles were reflecting stability of protein-ligand complexes, reference structures for all the three systems from last 5 ns were extracted and superimposed to check if the binding mode was retained. This analysis, as depicted in Figure 3, revealed that metergoline was retained at the active site while holding onto the binding mode of the reference molecules.

Further, hydrogen bond interactions sustained for Ref1 and Ref2 with Trp595 and Arg643. In case of metergoline, hydrogen bond with Trp595 was persistent and a new π interaction was established with Arg643. Additionally, metergoline also formed a carbon-hydrogen bond with Phe173. Ref1 and Ref2 interacted with all the active site residues. Apart from the interactions with Asn555, Val580, and Tyr599, interactions with all the other active site residues were maintained in case of metergoline. However, metergoline additionally formed van der Waals interactions with other residues. Figure 4 displays all these interactions.

For JTP-4819 and other hit compounds, we performed 20 ns MD simulation with POP. The average RMSD for pipercolosine, lobeline, martefragin A, lycoperine A, cystodytin G, and celacinnine was observed to be 0.11 nm and for JTP-4819 and hookerianamide J, the average RMSD value was 0.12 nm. The RMSD profiles of all these systems were below the accepted value of 0.15 nm thus indicating stability when bound to POP. Potential energy profiles of these compounds with POP also strengthened and supported the stability observation. The RMSD and potential energy profiles are depicted in Supplementary Figure 2.

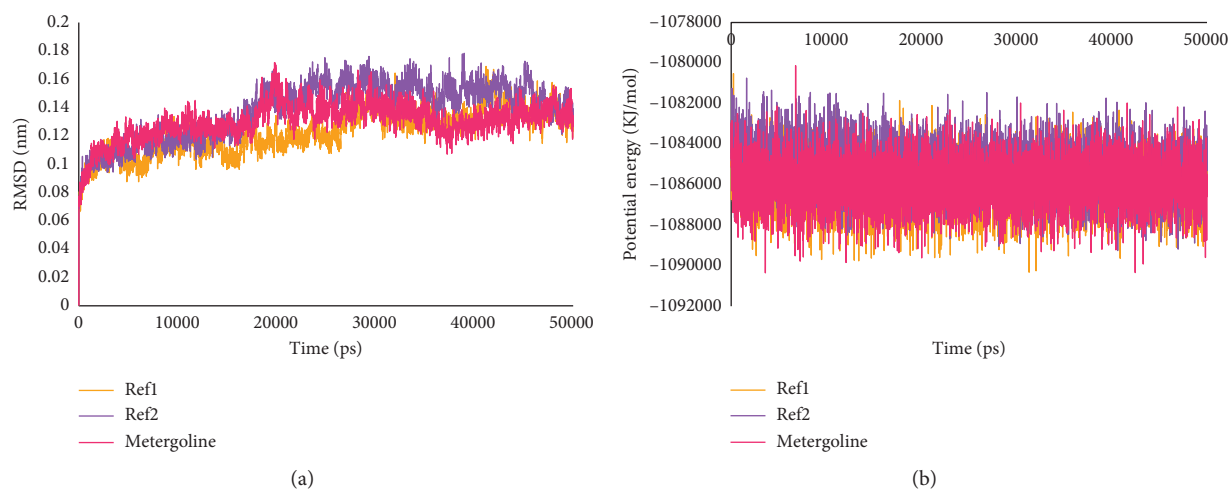


FIGURE 2: Stability analysis from MD insights. (a) RMSD profiles for POP with Ref1, Ref2, and metergoline; (b) potential energy profiles for POP with Ref1, Ref2, and metergoline.

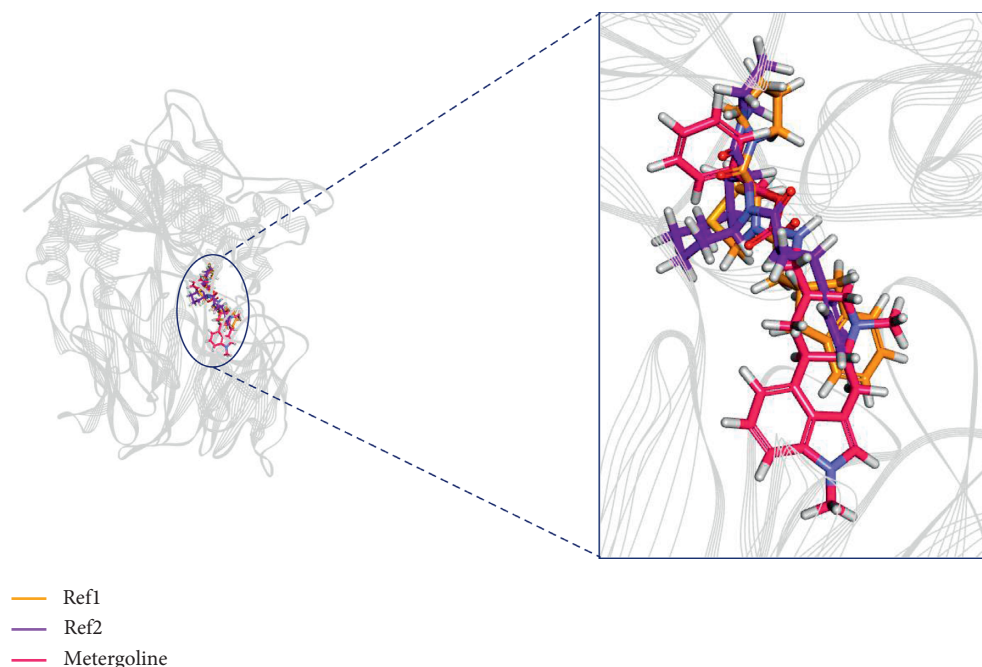


FIGURE 3: Binding mode analysis of POP with Ref1, Ref2, and metergoline. (a) Superimposed image of representative structures; (b) enlarged view. Protein is shown in grey wire model and compounds are depicted in stick models.

Owing to the stability conferred by the protein-ligands complexes, the representative structure was picked from the last 5 ns. These representative structures were aligned and superimposed. All the hit molecules remained at the active site. Although martefragin A, lycoperine A, and cystodytin G largely remained at the active site, compared to other molecules, a slight drift was observed. The aligned and superimposed representative structures of JTP-4819 along

with other hit compounds are shown in Supplementary Figure 3. Upon checking for the hydrogen bond interactions after MD simulations, it was learnt that JTP-4819 lost hydrogen bond interactions with Arg128 and Arg643. However, hydrogen bond interaction with Cys255 persisted. Interestingly, pipercollosine which had demonstrated only one hydrogen bond interaction with Arg643 prior to MD formed an additional hydrogen bond with Trp595.

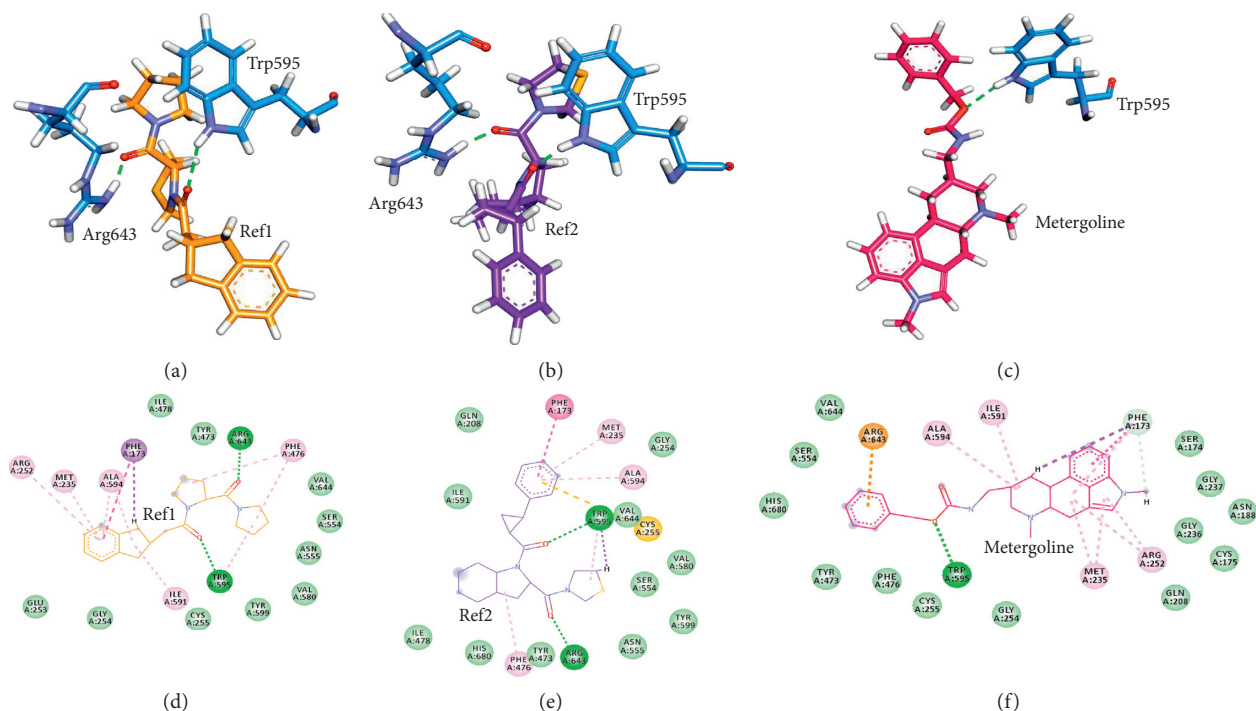


FIGURE 4: Post-MD intermolecular interactions. Upper panel (a–c) demonstrates hydrogen bond interactions of POP residues (blue) with (a) Ref1, (b) Ref2, and (c) metergoline. Lower panel (d–f) is the 2D representation of all the molecular interactions between POP and (d) Ref1, (e) Ref2, and (f) metergoline. Green dashed lines in upper and lower panel represent hydrogen bonds. All the other dashed lines represent various types of π bonds. Light green colored spheres indicate the residues participating in van der Waals interactions.

Hookerianamide J retained its hydrogen bond with Arg643. Although its interaction with Cys255 was lost, hookerianamide J formed a new hydrogen bond interaction with Trp595. Lobeline maintained its hydrogen bond interaction with Arg643. Surprisingly, all the hydrogen bond interactions observed in the docked pose of martefragin A were lost after MD and a new hydrogen bond was formed with Gly254. Cystodytin G and lycoperine A did not demonstrate any hydrogen bond. Similar to the interactions before MD, celacinnine failed to show any hydrogen bond interaction. These hydrogen bonds along with the other π and van der Waals interactions formed by the hit compounds with POP are detailed in Supplementary Figure 4.

4. Discussion

Due to POP's ability to alter several aspects and function of CNS such as learning, memory, mood, and hypertension [29] and its involvement in alpha synuclein accumulation, POP surfaces out as an appealing target for PD. Although the initial clinical trials results were promising for Z-321, S 17092, and JTP-4819, these were discontinued [12]. JTP-4819 had demonstrated poor BBB permeability [30]. Moreover, safety-related concerns always exist in drug discovery processes. Plants harbor a major reserve of pharmaceutically active compounds and accordingly, interest in natural products based drugs discovery is on the

rise. Owing to the therapeutic ability of alkaloids in PD mentioned in the introduction, our work was aimed at exploiting them against POP, computationally. The results demonstrate the POP inhibitory ability of certain alkaloids with metergoline, pipericallosine, hookerianamide J, and lobeline emerging out as notable potential POP inhibitors.

Metergoline is an ergoline alkaloid obtained from taxa such as fungi and some higher plants [31]. There are studies reporting the various therapeutic roles of metergoline: for anti-microbial activity [32, 33] and as antidepressant in seasonal affective disorders [34]. Of interest in relation to Parkinson's disease where the dopamine receptor level is seen to be imbalanced [35], metergoline has been shown to have high affinity for D1 and D4 dopamine receptors [36]. In addition to this, it has been shown that voltage-gated sodium channels have a role in cognitive impairments of PD in rats [37] and Lee and colleagues have recently identified the role of metergoline in inhibiting neural Na^+ channels [38]. Pipericallosine is an alkaloid enamide isolated from various *Piper* species [39–41]. It is an active apoptosis inducer [41]. Hookerianamide J is a steroid alkaloid obtained from *Sarcococca hookeriana*. It is shown to possess antileishmanial and antibacterial activity and is an effective cholinesterase inhibitor [42]. Lobeline is an optically active piperidine alkaloid obtained from plants particularly in Genus *lobelia*. It binds to and activates a nicotinic acetylcholine receptor and has been shown to be useful in protection of

dopaminergic neurons and in reducing the symptoms of parkinsons disease [17, 43].

Upon performing molecular docking of POP with prospective compounds, the GoldScore fitness of Z-321, S-17092, and JTP-4819 was 70.5265, 68.4808, and 60.0431, respectively. Metergoline with a GoldScore fitness of 72.6547 surpassed all the above mentioned inhibitors, while piper-callosine showed a slightly higher GoldScore fitness value of 68.6628 as compared to S-17092. Celacinnine, lobeline, cystodytin G, lycoperine A, hookerianamide J, and marte-fragin A showed higher GoldScore fitness as compared to JTP-4819 (Supplementary Table 1). Additionally, we also docked berberine against POP which resulted in Goldscore fitness value of 49.319. It was observed that berberine formed interactions with fewer active site residues (Cys255, Phe476, Asn555, Val580, Trp595, Arg643, and Val644) as compared to our hit molecules (data not shown). All our identified alkaloid hits have achieved much higher score than berberine and because berberine has already been tested in vitro for POP inhibitory activity, we believe our compounds will have a greater edge over demonstrating in vitro POP inhibition.

Phe476, Asn555, Val580, Trp595, Tyr599, and Val644 form the S1 Subsite of active site, Arg643 forms the S2 subsite and S3 subsite is formed by Phe173, Met235, Cys255, Ile591, and Ala594. The best docked poses of all our hits molecules demonstrated interactions with all these residues, except only for cystodytin G which apart from Ala594 interacted with all the residues. Interaction monitoring after MD analysis of these hit compounds with POP revealed that metergoline, piper-callosine, hookerianamide J, and lobeline demonstrated crucial hydrogen bond interaction with either Trp595 or Arg643 or with both. Piper-callosine and hookerianamide J both showed both Trp595 and Arg643 hydrogen bond interactions. Metergoline and lobeline demonstrated hydrogen bond interaction with Trp595 and Arg643, respectively. All these compounds were retained at the active site as was observed from the aligned and superimposed MD poses (Figure 3 and Supplementary Figure 3). Because metergoline has demonstrated the best molecular docking scores and docked pose had indicated hydrogen bond interactions with Arg643, which was lost after MD, we looked for reasons behind this loss. It was learnt that this hydrogen bond was formed by HH11 (hydrogen) of Arg643 from POP with O25 (oxygen) of metergoline. We compared the metergoline-POP complex profiles at 0, 25, and 49 ns as depicted in Figure 5. Firstly, it was learnt that Arg643 was part of a loop; therefore, it had freedom to move. Secondly, it was observed that the benzene ring in metergoline had moved during the course of simulation. Owing to these reasons, the distance between HH11 of Arg643 and O25 of metergoline had moved from an initial distance of 3.005 Å

at 0 ns to 3.188 Å at 25 ns and to 3.450 Å by the end of simulation, thus resulting in loss of the hydrogen bond. However, interaction with Arg643 was pursued in the form of π -cation interaction.

GSK552 docking with POP resulted in a GoldScore fitness value of 73.88. Additionally, interaction analysis of docked pose of GSK552 also demonstrated hydrogen bonds with Trp595 and Arg643. We also performed a 20 ns MD for GSK552 in complex with POP. The average RMSD was observed to be 0.09 nm (Supplementary Figure 2). Trp595 and Arg643 hydrogen bonds were preserved and interactions with all the other active site residues were also observed. The 2D representation of the docked pose and MD representative structure of GSK552 are indicated in Supplementary Figures 1 and 4, respectively.

It has been reported that, for a drug to efficiently cross BBB, its molecular weight should be in the range of 314–420 Da, it should be highly lipophilic, i.e., logP should be in the range of 0.66–6, PSA less than 60–70 Å², H-bond donors should be <2, H-bond acceptors should be less than <6, and total number of nitrogen + oxygen atoms should be less than 6 [30, 44].

Literature survey indicated that while Ref1, Ref2 [30], and berberine [45] were capable of crossing BBB, JTP-4819 demonstrated poor BBB permeability [30]. Table 1 compares the properties of Ref1, Ref2, and JTP4819 with metergoline, piper-callosine, hookerianamide J, and lobeline. While Ref1 and Ref2 satisfied the conditions of crossing BBB, with a logP of 0.527, PSA of 89.94, and total number of N + O atoms exceeding 6, JTP-4819 did not satisfy the conditions of BBB permeability, probably which is why it was not able to cross the BBB in clinical trials. Metergoline, piper-callosine, and lobeline satisfied all these conditions of crossing BBB. While hookerianamide J satisfied all the other conditions, its molecular weight is slightly higher (442.677 Da) than the accepted range of efficient BBB crossers, i.e., 314–420 Da. These results further strengthen our proposal for testing them as prospective CNS drugs. Properties pertaining to effective BBB crossing for GSK552, berberine, and other compounds are given in Supplementary Table 2.

Although this research was started keeping Parkinson's disease in mind, literature survey during the process highlighted the role of POP inhibitors not just in PD but in various other disorders such as schizophrenia [30], autism [46], Huntington disease [47], hepatocyte steatosis [48], and acute myeloid leukemia [49]. The role of POP in Alzheimer's disease is contradictory, where certain studies have reported increased POP activity in AD [50] and others have reported decreased POP activity [51, 52]. Based on this, we speculate that the identified hit compounds might be potential pharmaceutical candidates in host of other diseases as well.

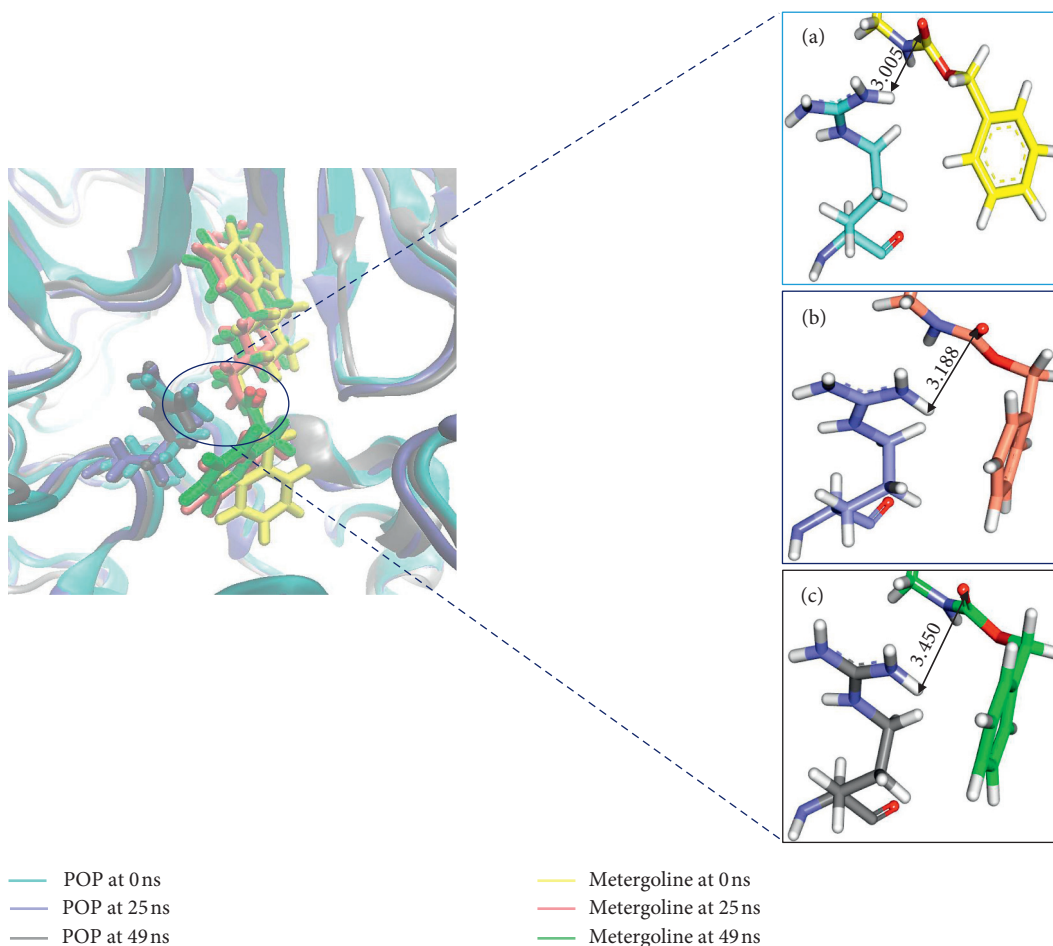


FIGURE 5: Left image displays superimposed metergoline-POP complex at 0, 25, and 49 ns. Right panel displays the enlarged view of Arg643 and metergoline while highlighting the distance between HH11 of Arg643 with O25 of metergoline at (a) 0 ns, (b) 25 ns, and (c) 49 ns.

TABLE 1: Comparison of BBB permeability properties.

Properties	Ref1	Ref2	JTP-4819	Metergoline	Pipercollosine	Hookerianamide J	Lobeline
Molecular weight (Da)	344.5	384.5	359.185	403.517	329.433	442.677	337.455
logP	2.378	3.203	0.527	4.249	4.758	4.935	3.933
Polar surface area (\AA^2)	65.92	65.92	89.94	46.5	47.56	52.57	40.54
Hydrogen bond donor	0	0	2	1	1	2	1
Hydrogen bond acceptor	3	3	4	3	3	3	3
N + O atoms	4	4	7	5	4	4	3

5. Conclusion

Safety of potential drug candidates is of utmost importance in development of new drugs. Due to their abundance and relative low toxicity, research in identifying plant-based drugs has seen an uptrend. Additionally, crossing of BBB is a major roadblock but an absolute necessary requirement for development of CNS drugs. Using in silico approaches, this work unravels the likely ability of alkaloids in inhibiting prolyl oligopeptidase, which has been indicated as therapeutic target in many diseases. By comparing POP inhibitors that had reached clinical trials, our work

displayed better affinity of metergoline, pipercollosine, hookerianamide J, and lobeline for POP. Finally, MD simulations confirmed their stability in complex with POP. Therefore, the research conducted here provides promising results for further investigation of metergoline, pipercollosine, hookerianamide J, and lobeline as effective POP inhibitors.

Data Availability

The datasets generated or analyzed in the current study are available from the corresponding author upon request.

Conflicts of Interest

The authors declare no conflicts of interest.

Acknowledgments

This research was supported by the Bio & Medical Technology Development Program of the National Research Foundation (NRF) and funded by the Korean Government (MSIT) (no. NRF-2018M3A9A7057263). The authors would like to thank Dr. Rabia Mukhtar Rana and Ms. Shraddha Parate for the insightful discussions during the course of this research.

Supplementary Materials

Supplementary Table 1: docking scores of hit compounds and reference inhibitors. Supplementary Figure 1: molecular docking-based intermolecular interactions of JTP-4819, GSK552, and other hit compounds. Supplementary Figure 2: RMSD and potential energy profiles of JTP-4819, GSK552, and other hit compounds. Supplementary Figure 3: binding mode analysis of POP with JTP-4819, GSK552, and other hit compounds. Supplementary Figure 4: post-MD intermolecular interactions of JTP-4819, GSK552, and other hit compounds. Supplementary Table 2: BBB permeability properties of celastrol, cystodytin G, lycoperine A, martepragin A, berberine, and GSK552. Supplementary Figure 5: chemical structures of the proposed inhibitors. (*Supplementary Materials*)

References

- [1] K. Wakabayashi, K. Tanji, F. Mori, and H. Takahashi, "The Lewy body in Parkinson's disease: molecules implicated in the formation and degradation of α -synuclein aggregates," *Neuropathology*, vol. 27, no. 5, p. 494, 2007.
- [2] I. Brandt, M. Gérard, K. Sergeant et al., "Prolyl oligopeptidase stimulates the aggregation of α -synuclein," *Peptides*, vol. 29, no. 9, p. 1472, 2008.
- [3] M. J. Hannula, T. T. Myöhänen, J. Tenorio-laranga, P. T. Männistö, and J. A. Garcia-horsman, "Corrigendum to "prolyl oligopeptidase colocalizes with α -synuclein, β -amyloid, tau protein and astroglia in the post-mortem brain samples with Parkinson's and Alzheimer's diseases" [neuroscience 242 (2013) 140–150]," *Neuroscience*, vol. 248, p. 344, 2013.
- [4] Z. Szeltner and L. Polgár, "Structure, function and biological relevance of prolyl oligopeptidase," *Current Protein & Peptide Science*, vol. 9, no. 1, pp. 96–107, 2008.
- [5] G. Bellemère, H. Vaudry, L. Mounien, I. Boutelet, and S. Jégou, "Localization of the mRNA encoding prolyl endopeptidase in the rat brain and pituitary," *Journal of Comparative Neurology*, vol. 471, no. 2, p. 128, 2004.
- [6] J. P. Huston and R. U. Hasenöhr, "The role of neuropeptides in learning: focus on the neurokinin substance P," *Behavioural Brain Research*, vol. 66, no. 1–2, pp. 117–127, 1995.
- [7] D. F. Cunningham and B. O'Connor, "Proline specific peptidases," *Biochimica et Biophysica Acta*, vol. 1343, no. 2, pp. 160–186, 1997.
- [8] R. Kumar, R. Bavi, M. G. Jo et al., "New compounds identified through in silico approaches reduce the α -synuclein expression by inhibiting prolyl oligopeptidase in vitro," *Scientific Reports*, vol. 7, no. 1, 2017.
- [9] R. Svarcbahts, U. H. Julku, and T. T. Myöhänen, "Inhibition of prolyl oligopeptidase restores spontaneous motor behavior in the α -synuclein virus vector-based Parkinson's disease mouse model by decreasing α -synuclein oligomeric species in mouse brain," *The Journal of Neuroscience*, vol. 36, no. 49, p. 12485, 2016.
- [10] R. Svarcbahts, U. H. Julku, S. Norrbacka, and T. T. Myöhänen, "Removal of prolyl oligopeptidase reduces alpha-synuclein toxicity in cells and in vivo," *Scientific Reports*, vol. 8, no. 1, 2018.
- [11] T. Myöhänen, M. Hannula, R. Van Elzen et al., "A prolyl oligopeptidase inhibitor, KYP-2047, reduces α -synuclein protein levels and aggregates in cellular and animal models of Parkinson's disease," *British Journal of Pharmacology*, vol. 166, no. 3, p. 1097, 2012.
- [12] R. Svarcbahts, U. Julku, T. Kilpeläinen, M. Kyyrö, M. Jäntti, and T. T. Myöhänen, "New tricks of prolyl oligopeptidase inhibitors—a common drug therapy for several neurodegenerative diseases," *Biochemical Pharmacology*, vol. 161, p. 113, 2019.
- [13] S. Guardiola, R. Prades, L. Mendieta et al., "Targeted covalent inhibition of prolyl oligopeptidase (POP): discovery of sulfonylfluoride peptidomimetics," *Cell Chemical Biology*, vol. 25, no. 8, pp. 1031–1037, 2018.
- [14] T. Tarrago, N. Kichik, J. Seguí, and E. Giralt, "The natural product berberine is a human prolyl oligopeptidase inhibitor," *ChemMedChem*, vol. 2, no. 3, p. 354, 2007.
- [15] T. Tarragó, N. Kichik, B. Claasen, R. Prades, M. Teixidó, and E. Giralt, "Baicalin, a prodrug able to reach the CNS, is a prolyl oligopeptidase inhibitor," *Bioorganic & Medicinal Chemistry*, vol. 16, no. 15, p. 7516, 2008.
- [16] R. Hellinger, J. Koehbach, A. Puigpinós et al., "Inhibition of human prolyl oligopeptidase activity by the cyclotide psysol 2 isolated from *Psychotria solitudinum*," *Journal of Natural Products*, vol. 78, no. 5, p. 1073, 2015.
- [17] G. Hussain, A. Rasul, H. Anwar et al., "Role of plant derived alkaloids and their mechanism in neurodegenerative disorders," *International Journal of Biological Sciences*, vol. 14, no. 3, p. 341, 2018.
- [18] S. Girdhar, A. Girdhar, S. K. Verma, V. Lather, and D. Pandita, "Plant derived alkaloids in major neurodegenerative diseases: from animal models to clinical trials," *Journal of Ayurvedic and Herbal Medicine*, vol. 1, no. 3, pp. 91–100, 2015.
- [19] Y. Bi, P.-C. Qu, Q.-S. Wang et al., "Neuroprotective effects of alkaloids from *Piper longum* in a MPTP-induced mouse model of Parkinson's disease," *Pharmaceutical Biology*, vol. 53, no. 10, p. 1516, 2015.
- [20] C. D. Haffner, C. J. Diaz, A. B. Miller et al., "Pyrrolidinyl pyridone and pyrazinone analogues as potent inhibitors of prolyl oligopeptidase (POP)," *Bioorganic & Medicinal Chemistry Letters*, vol. 18, no. 15, p. 4360, 2008.
- [21] BIOVIA, *Discovery Studio Modeling Environment*, Dassault Systèmes, San Diego, CA, USA, 2016.
- [22] The UniProt Consortium, "UniProt: a worldwide hub of protein knowledge the UniProt consortium," *Nucleic Acids Research*, vol. 47, pp. 506–515, 2019.
- [23] M. L. Verdonk, J. C. Cole, M. J. Hartshorn, C. W. Murray, and R. D. Taylor, "Improved protein-ligand docking using GOLD," *Proteins: Structure, Function, and Bioinformatics*, vol. 52, no. 4, p. 609, 2003.

- [24] M. J. Abraham, T. Murtola, R. Schulz et al., "Gromacs: high performance molecular simulations through multi-level parallelism from laptops to supercomputers," *SoftwareX*, vol. 1-2, p. 19, 2015.
- [25] X. Zhu, P. E. M. Lopes, and A. D. Mackerell, "Recent developments and applications of the CHARMM force fields," *WIREs Computational Molecular Science*, vol. 2, no. 1, p. 167, 2012.
- [26] V. Zoete, M. A. Cuendet, A. Grosdidier, and O. Michielin, "SwissParam: a fast force field generation tool for small organic molecules," *Journal of Computational Chemistry*, vol. 32, no. 11, p. 2359, 2011.
- [27] M. Parrinello and A. Rahman, "Polymorphic transitions in single crystals: a new molecular dynamics method," *Journal of Applied Physics*, vol. 52, no. 12, p. 7182, 1981.
- [28] I. Franc, A. Lipinski, and P. J. Feeney, "Lipinski rule," *Advanced Drug Delivery Reviews*, vol. 23, no. 1-3, 1997.
- [29] J. Lawandi, S. Gerber-Lemaire, L. Juillerat-Jeanerret, and N. Moitessier, "Inhibitors of prolyl oligopeptidases for the therapy of human diseases: defining diseases and inhibitors," *Journal of Medicinal Chemistry*, vol. 53, no. 9, p. 3423, 2010.
- [30] A. López, L. Mendieta, R. Prades, S. Royo, T. Tarragó, and E. Giral, "Peptide POP inhibitors for the treatment of the cognitive symptoms of schizophrenia," *Future Medicinal Chemistry*, vol. 5, no. 13, p. 1509, 2013.
- [31] A. Markert, N. Steffan, K. Ploss et al., "Biosynthesis and accumulation of ergoline alkaloids in a mutualistic association between *Ipomoea asarifolia* (Convolvulaceae) and a clavicipitalean fungus," *Plant Physiology*, vol. 147, no. 1, 2008.
- [32] K. Kang, K.-S. Wong, C. Jayampath Seneviratne, L. P. Samaranyake, W.-P. Fong, and P. W.-K. Tsang, "In vitro synergistic effects of metergoline and antifungal agents against *Candida krusei*," *Mycoses*, vol. 53, no. 6, p. 495, 2010.
- [33] M. J. Ellis, C. N. Tsai, J. W. Johnson et al., "A macrophage-based screen identifies antibacterial compounds selective for intracellular *Salmonella typhimurium*," *Nature Communications*, vol. 10, no. 1, 2019.
- [34] E. H. Turner, P. J. Schwartz, C. H. Lowe et al., "Double-blind, placebo-controlled study of single-dose metergoline in depressed patients with seasonal affective disorder," *Journal of Clinical Psychopharmacology*, vol. 22, no. 2, p. 216, 2002.
- [35] M. J. Hurley and P. Jenner, "What has been learnt from study of dopamine receptors in Parkinson's disease?" *Pharmacology & Therapeutics*, vol. 111, no. 3, p. 715, 2006.
- [36] J. M. Hooker, S. W. Kim, A. T. Reibel, D. Alexoff, Y. Xu, and C. Shea, "Evaluation of [¹¹C]metergoline as a PET radiotracer for 5HTR in nonhuman primates," *Bioorganic & Medicinal Chemistry*, vol. 18, no. 22, p. 7739, 2010.
- [37] Z. Wang, Y. Lin, W. Liu et al., "Voltage-gated sodium channels are involved in cognitive impairments in Parkinson's disease-like rats," *Neuroscience*, vol. 418, p. 231, 2019.
- [38] J.-h. Lee, J. Liu, M. Shin, M. Hong, S.-y. Nah, and H. Bae, "Metergoline inhibits the neuronal Nav1.2 voltage-dependent Na⁺ channels expressed in *Xenopus* oocytes," *Acta Pharmacologica Sinica*, vol. 35, no. 7, p. 862, 2014.
- [39] G.-H. Tang, D.-M. Chen, B.-Y. Qiu et al., "Cytotoxic amide alkaloids from *Piper boehmeriaefolium*," *Journal of Natural Products*, vol. 74, no. 1, p. 45, 2011.
- [40] N. Choudhary and V. Singh, "A census of *P. longum*'s phytochemicals and their network pharmacological evaluation for identifying novel drug-like molecules against various diseases, with a special focus on neurological disorders," *PLoS One*, vol. 13, no. 1, Article ID e0191006, 2018.
- [41] L. Pan, S. Matthew, D. D. Lantvit et al., "Bioassay-guided isolation of constituents of *Piper sarmentosum* using a mitochondrial transmembrane potential assay," *Journal of Natural Products*, vol. 74, no. 10, p. 2193, 2011.
- [42] K. P. Devkota, B. N. Lenta, J. D. Wansi et al., "Bioactive 5 α -pregnane-type steroidal alkaloids from *Sarcococca hookeriana*," *Journal of Natural Products*, vol. 71, no. 8, p. 1481, 2008.
- [43] C.-Y. Li, L.-M. Zhao, X.-W. Shi, and J.-D. Zhang, "Lobeline shows protective effects against MPTP-induced dopaminergic neuron death and attenuates behavior deficits in animals," *Experimental and Therapeutic Medicine*, vol. 7, no. 2, p. 375, 2014.
- [44] E. H. Kerns and L. Di, *Drug-like Properties: Concepts, Structure Design and Methods*, Academic Press, Cambridge, MA, USA, 2008.
- [45] W. Jiang, S. Li, and X. Li, "Therapeutic potential of berberine against neurodegenerative diseases," *Science China Life Sciences*, vol. 58, no. 6, pp. 564-569, 2015.
- [46] N. Momeni, B. M. Nordström, V. Horstmann, H. Avarseji, and B. V. Sivberg, "Alterations of prolyl endopeptidase activity in the plasma of children with autistic spectrum disorders," *BMC Psychiatry*, vol. 5, no. 1, 2005.
- [47] D. Mantle, G. Falkous, S. Ishiura, P. J. Blanchard, and E. K. Perry, "Comparison of proline endopeptidase activity in brain tissue from normal cases and cases with Alzheimer's disease, Lewy body dementia, Parkinson's disease and Huntington's disease," *Clinica Chimica Acta*, vol. 249, no. 1-2, pp. 129-139, 1996.
- [48] D. Zhou, B.-H. Li, J. Wang et al., "Prolyl oligopeptidase inhibition attenuates steatosis in the L02 human liver cell line," *PLoS One*, vol. 11, no. 10, Article ID e0165224, 2016.
- [49] H. Cao, X. Zhao, S. Lu, and Z. Wang, "Prolyl oligopeptidase inhibitor suppresses the upregulation of ACSDKP in patients with acute myeloid leukemia," *Experimental and Therapeutic Medicine*, vol. 15, pp. 5431-5435, 2018.
- [50] T. Aoyagi, T. Wada, M. Nagai et al., "Increased γ -aminobutyrate aminotransferase activity in brain of patients with Alzheimer's disease," *Chemical & Pharmaceutical Bulletin*, vol. 38, no. 6, p. 1748, 1990.
- [51] A. M. Gibson, J. A. Edwardson, and J. R. McDermott, "Post mortem levels of some brain peptidases in Alzheimer's disease: reduction in proline endopeptidase activity in cerebral cortex," *Neuroscience Research Communications*, vol. 9, pp. 73-81, 1991.
- [52] D. Terwel, J. Bothmer, E. Wolf, F. Meng, and J. Jolles, "Affected enzyme activities in Alzheimer's disease are sensitive to antemortem hypoxia," *Journal of the Neurological Sciences*, vol. 161, no. 1, pp. 47-56, 1998.

Research Article

The Use of Traditional Chinese Medicine in Relieving EGFR-TKI-Associated Diarrhea Based on Network Pharmacology and Data Mining

Shuaihang Hu ^{1,2}, Wenchao Dan ^{1,2}, Jinlei Liu ^{1,2}, Peng Ha,³ Tong Zhou,¹ Xinyuan Guo ⁴, and Wei Hou ¹

¹Guang'anmen Hospital, China Academy of Chinese Medical Sciences, Beijing 100053, China

²Beijing University of Chinese Medicine, Beijing 100029, China

³University of Leicester, University Road, Leicester LE1 7RH, UK

⁴Cancer Hospital Chinese Academy of Medical Sciences, Beijing 100021, China

Correspondence should be addressed to Wei Hou; houwei1964@163.com

Received 14 February 2021; Accepted 23 March 2021; Published 1 April 2021

Academic Editor: Akhilesh K. Tamrakar

Copyright © 2021 Shuaihang Hu et al. This is an open access article distributed under the Creative Commons Attribution License, which permits unrestricted use, distribution, and reproduction in any medium, provided the original work is properly cited.

In this study, the role of traditional Chinese medicine (TCM) in relieving epidermal growth factor receptor-tyrosine kinase inhibitor- (EGFR-TKI-) associated diarrhea was discussed by network pharmacology and data mining. Prediction of drug targets by introducing the EGFR-TKI molecular structures into the SwissTargetPrediction platform and diarrhea-related targets in the DrugBank, GeneCards, DisGeNET, and OMIM databases were obtained. Compounds in the drug-disease target intersection were screened by absorption, distribution, metabolism, and excretion parameters and Lipinski's rule in Traditional Chinese Medicine Systems Pharmacology. TCM-containing compounds were selected, and information on the property, taste, and meridian tropism of these TCMs was summarized and analyzed. A target-compound-TCM network diagram was constructed, and core targets, compounds, and TCMs were selected. The core targets and components were docked by AutoDock Vina (Version 1.1.2) to explore the target combinations of related compounds and evaluate the docking activity of related targets and compounds. Twenty-three potential therapeutic TCM targets for the treatment of EGFR-TKI-related diarrhea were obtained. There were 339 compounds acting on potential therapeutic targets, involving a total of 402 TCMs. The results of molecular docking showed good binding between the core targets and compounds, and the binding between the core targets and compounds was similar to that of the core target and the recommended drug loperamide. TCMs have multitarget characteristics and are present in a variety of compounds used for relieving EGFR-TKI-associated diarrhea. Antitumor activity and the efficacy of alleviating diarrhea are the pharmacological basis of combining TCMs with EGFR-TKI in the treatment of non-small-cell lung cancer. The core targets, compounds, and TCMs can provide data to support experimental and clinical studies on the relief of EGFR-TKI-associated diarrhea in the future.

1. Background

Primary bronchial lung cancer is the most common malignant tumor in the world, of which approximately 80–85% are non-small-cell lung cancer (NSCLC), and nearly 70% of NSCLC patients are in the locally advanced stage or have metastatic lesions at the primary diagnosis [1]. Although chemotherapy was once considered the first-line treatment for NSCLC, advancements in targeted gene research have

given rise to epidermal growth factor receptor-tyrosine kinase inhibitors (EGFR-TKIs), such as erlotinib and gefitinib, to replace chemotherapy as the first-line therapy for NSCLC patients who are positive for the relevant driver genes [2, 3]. The adverse reactions to EGFR-TKI are different from those to chemotherapy, which include myelosuppression, nausea, and vomiting; the administration of EGFR-TKI is prone to causing rashes, diarrhea, and other adverse reactions, which have a negative impact on the patients'

quality of life and can even lead to drug discontinuation. Therefore, it is essential to prevent and control adverse reactions during targeted therapy.

In clinical practice, common EGFR-TKI drugs are divided into three generations: the first generation includes gefitinib, erlotinib, and icotinib; the second includes afatinib; the third includes osimertinib. All these drugs can cause varying degrees of adverse reactions, and these common adverse reactions to EGFR-TKI treatment limit the application of EGFR-TKI; the mechanism by which these adverse reactions occur is not clear, but studies have shown that it is related to the secretion of chloride [4]. According to a previously published EGFR-TKI phase III clinical study, the overall incidence of diarrhea is 9.5–95.2%. EGFR-TKI treatment should be suspended if Grade 2 diarrhea lasts more than 48 hours, and for Grade 3 or higher diarrhea, EGFR-TKI treatment should be stopped until the grade of diarrhea is reduced to 1 or below. If symptoms are not relieved in 14 days, the administration of EGFR-TKI should be discontinued. Loperamide is often used in the clinical treatment of severe diarrhea, but there are few studies on the corresponding precautionary measures [5].

TCM has a long history of use for the treatment of diarrhea and has advantages in treating EGFR-TKI-related diarrhea, because besides relieving diarrhea, it can regulate the gastrointestinal function of patients, increase appetite, and prevent the reoccurrence of diarrhea [6]. TCM combined with targeted drugs can enhance efficacy, reduce toxicity, and reverse drug resistance, improving the quality of life for patients. The mechanism of action for TCM mainly involves the regulation of the immune function of lung cancer patients, thereby enhancing the migration of T cells. At the same time, it can inhibit the proliferation of tumor cells and induce tumor cell apoptosis [7, 8].

The synergistic effect of drugs on the human body can be explored through the analysis of network topology and nodes. Andrew Hopkins combined systems biology, pharmacology, information networks, and computer science to put forward network pharmacology, which demonstrates mutual complex disease-gene-target-drug relationships by applying a professional visual network analysis software in the form of network signals, allowing these relationships to be analyzed through the topology of the network and nodes [9]. Due to the pharmacodynamic material basis of TCM, the mechanisms and toxicological effects of compounds containing TCM are still not clear; as the quality of medicinal materials is difficult to control, it is different to study them on an integral level compared to a molecular level [10]. As TCM is characterized by “multiple components, multiple targets, low affinity, low selectivity”, and its effective constituents can be applied to various targeted diseases, it has obvious advantages in the treatment of multiple factors of a polygenic disease. Therefore, using network pharmacology to study multiple ways of regulating signaling pathways and to explain and explore how to effectively improve the efficacy of drugs is more in line with the ideals of TCM compounds. In this study, by screening drug and disease targets and using a variety of databases to screen compounds containing TCM, a target-compound-TCM relationship network was

constructed. This network was then used to explore potential therapeutic targets and related compounds and identify TCMs that can relieve EGFR-TKI-associated diarrhea and have certain antitumor effects. These results can provide a scientific molecular basis for the clinical application of TCM in combination with EGFR-TKI. The specific process of the study is shown in Figure 1.

2. Materials and Methods

2.1. Screening of Drugs and Targets of the Disease. Through a literature search, the molecular formulae of gefitinib, erlotinib, icotinib, afatinib, and osimertinib were obtained. Their molecular structures were downloaded separately in SDF format using the PubChem database (pubchem.ncbi.nlm.nih.gov) and uploaded onto the SwissTargetPrediction (<http://www.swisstargetprediction.ch>) platform [11, 12], with species set to “*Homo sapiens*”, to predict the target of drug action. The results from the SwissTargetPrediction platform were supplemented by consulting the literature.

To obtain the targets of diseases related to diarrhea, a search through the GeneCards (<http://www.genecards.org>) [13], OMIM (omim.org) [14], DisGeNET (<http://www.disgenet.org>) [15], and DrugBank (<http://www.drugbank.ca>) [16] databases was performed using “diarrhea”, “diarrhoea”, and “diarrheas” as keywords. Drug and disease targets were converted into standard gene names through the UniProt database (<https://www.uniprot.org/>) [17]. The targets from the intersection of drug prediction targets and disease targets were obtained.

2.2. Screening Target-Related Compounds and Potential Therapeutic Targets. A search was conducted for the compounds related to the intersection targets through the database of Traditional Chinese Medicine Systems Pharmacology (TCMSP; <http://tcmssp.com/index.php>) [18] and filtered by absorption, distribution, metabolism, and excretion (ADME) parameters and Lipinski’s rule [19–22]: oral bioavailability: $\geq 30\%$; drug-likeness: ≥ 0.18 ; the number of bonds which allow free rotation around themselves ≤ 10 ; topological polar surface area $\leq 60 \text{ \AA}^2$; and molecular weight: 180–500 Da.

As some of the data provided by the TCMSP database may be inconsistent with actual applications, compounds that were filtered out were checked one by one to supplement the related compounds. The screened compounds were mapped to the intersection targets of diseases and drugs, with targets not containing active ingredients excluded and potential therapeutic targets screened out, and a potential therapeutic target-compound network diagram was drawn using Cytoscape 3.7.2 [23]. Core therapeutic targets were screened out after performing an analysis of the characteristics of the network using a network analyzer.

2.3. Screening and Analysis of TCMs. The TCMSP database provided a list of TCMs that corresponded to the compounds, and the corresponding TCMs were screened out through the relevant compounds. To make the research

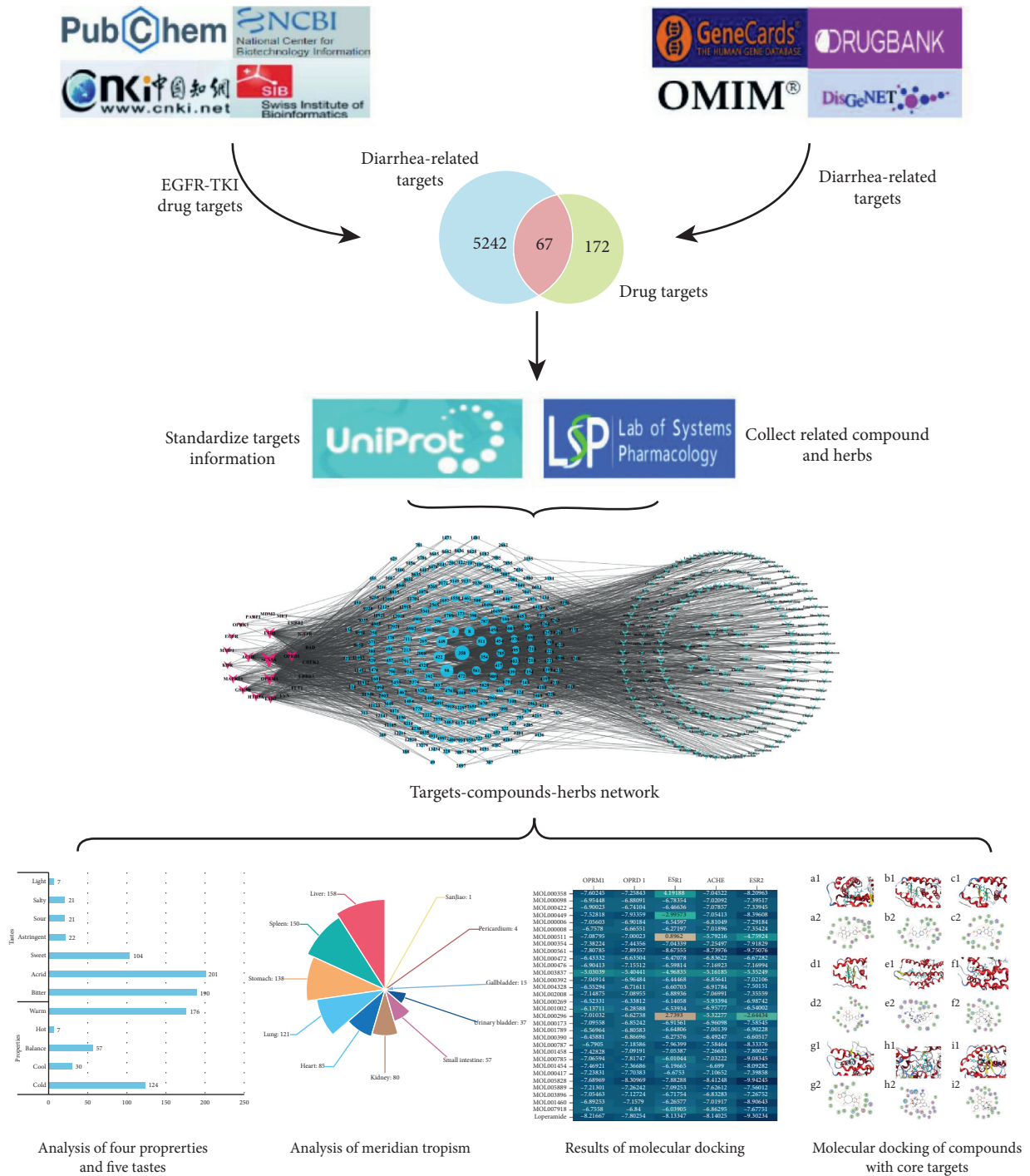


FIGURE 1: Framework of network pharmacology and data mining.

results standardized and practical, TCMs not listed in the “Pharmacopoeia of the People’s Republic of China 2015 Edition” [24] were excluded. According to the “Pharmacopoeia of the People’s Republic of China 2015 Edition” and the textbook “Chinese Pharmacy” in the “Thirteenth Five-Year Plan” [25], this study carried out frequency analysis on the components containing TCM.

2.4. Construction of Target-Compound-TCM Network. A target-compound-TCM network from the potential therapeutic targets and the corresponding compounds, as well as the TCMs contained in the candidate compound, was constructed using the software Cytoscape 3.7.2, and the network characteristics were analyzed by a network analyzer. The degree value indicates the number of connections a

particular target has. The more related compounds there are in a single TCM and the more related targets the related compounds act on, the higher the degree value, based on the core compounds and TCMs selected [26].

2.5. Molecular Docking between Target and Compound.

To confirm the credibility of the interaction between the core targets and the core components in the target-compound-TCM network and obtain a new drug-target combination, we selected five targets with a high median degree value in the target-compound-TCM network as receptors and used the recommended therapeutic drug, loperamide, as the ligand for molecular docking [6].

The crystal structures of the five selected targets were obtained from the Protein Data Bank (<http://www.rcsb.org>), a protein crystal database, and saved in PDB format. The 3D chemical structures of the candidate compounds were downloaded from the PubChem database and saved in SDF format; the output documents were converted to PDB format for subsequent molecular docking. The coordinate documents of the receptor and ligand were prepared using AutoDock Tools 1.5.6, with the water molecules deleted from the ligand, the ligand and receptor separated, nonpolar hydrogen added, and the Gasteiger charge calculated after it was saved in PDBQT format. The potential core ligand was subjected to the treatment of energy minimization, obtaining the ligand atom type after calculation, and finally saved in PDBQT format. The AutoDock Vina software was used for the calculation of docking of semisoft molecules. Compared with AutoDock4, AutoDock Vina 1.1.2 adopts a complex gradient algorithm and multithreading technology and performs molecular docking scoring to evaluate the matching degree and activity between the target and the ligand. A docking score of < -4.25 indicates binding activity between the ligand and the target, a score of < -5.0 indicates better binding activity, and a score of < -7.0 indicates strong docking activity [27].

3. Results

3.1. Drug-Disease Target Intersection. The probability value obtained from the SwissTargetPrediction platform to predict drug effect targets represents the probability that the query molecule targets the protein. From a total of 239 drug targets, the top 100, as ranked by probability, were selected after those with a probability of 0 were removed, and 5 drug targets were obtained after eliminating duplicates.

A total of 5245 diarrhea-related disease targets were obtained by searching the disease databases, merging the data, and removing duplicate values. A total of 67 targets were obtained from the intersection of drug and disease targets, as shown in Figure 2.

3.2. Screening of Target-Related Compounds and Potential Therapeutic Targets. A total of 67 targets were obtained from the intersection of EGFR-TKI and diarrhea and imported into the TCMSP database; 29 targets and 834 compounds of relevance were retrieved. After the selection of the ADME

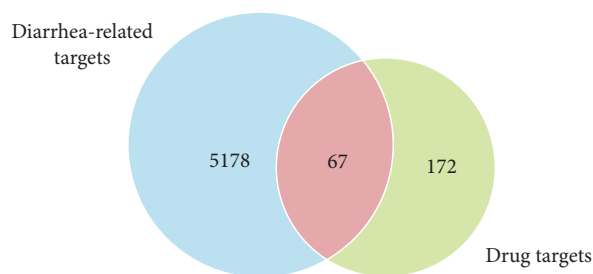


FIGURE 2: Intersection targets of EGFR-TKI and diarrhea.

parameters and Lipinski's rule, 293 compounds were obtained. The compounds excluded by the ADME parameters and Lipinski's rule were checked individually for the purpose of rigor, and 46 compounds associated with tumor treatment and adverse diarrhea effects were added, leading to a total of 339 compounds. There were 23 targets that met the 339 compounds at the intersection of EGFR-TKI and diarrhea; these were identified as the potential therapeutic targets for the treatment of adverse reactions of EGFR-TKI diarrhea with TCM (Table 1).

A network diagram of the final 339 compounds included with 23 potential therapeutic targets was constructed (Figure 3). To ensure a clear network diagram, the prefixes "MOL" and "0" of the compound name were deleted, leaving only the compound number. The network feature analysis was performed through a network analyzer plug-in, where the degree value determines the number of node connections and the role of the reaction nodes in the network is positively correlated with the target size in the diagram. Sodium channel protein type 5 subunit alpha (SCN5A), OPRM1, OPRD1, ESR1, ACHE, and ESR2 were core targets with large degree values of 280, 158, 128, 121, 90, and 55, respectively. The compounds with large degree values all had multiple potential therapeutic targets, suggesting that the selection of the compounds corresponded to the ideals of TCM and had extensive therapeutic value.

3.3. Compounds Corresponding to TCM. The final 339 compounds included in the network diagram were imported into the TCMSP platform to obtain 432 kinds of TCMs contained in the compounds. Following the deletion of 30 kinds of TCMs that were not recorded in the "Pharmacopoeia of the People's Republic of China 2015 Edition", a total of 402 kinds of TCMs were incorporated.

The property, taste, and meridian tropism of the 402 TCMs were summarized and their frequency was analyzed. Acrid and bitter drugs had the highest frequencies, accounting for 35.51% and 33.56% of the selected TCMs, respectively. Drugs that were warm in property were the most frequently occurring, accounting for 44.67% of the selected TCMs, followed by those cold in property, which accounted for 31.47%. The frequency analysis of meridian tropism showed that the frequency of liver, spleen, and stomach was the highest in the included TCMs, accounting for 52.71% of the total, while 14.3% were attributed to the lungs. It is evident that most of the TCMs included were

TABLE 1: Potential therapeutic targets of TCM for the treatment of EGFR-TKI-related diarrhea.

ID	GeneSymbol	Uniprot ID	Protein name
1	SCN5A	Q14524	Sodium channel protein type 5 subunit alpha
2	PARP1	P09874	Poly [ADP-ribose] polymerase 1
3	OPRM1	P35372	Mu-type opioid receptor
4	OPRK1	P41145	Kappa-type opioid receptor
5	OPRD1	P41143	Delta-type opioid receptor
6	MMP1	P03956	Interstitial collagenase
7	MET	P08581	Hepatocyte growth factor receptor
8	MDM2	Q00987	E3 ubiquitin-protein ligase Mdm2
9	MAPK14	Q16539	Mitogen-activated protein kinase 14
10	KDR	P35968	Vascular endothelial growth factor receptor 2
11	IGF1R	P08069	Insulin-like growth factor 1 receptor
12	HTR3A	P46098	5-Hydroxytryptamine receptor 3A
13	GSK3B	P49841	Glycogen synthase kinase-3 beta
14	FYN	P06241	Tyrosine-protein kinase fyn
15	FLT1	P17948	Vascular endothelial growth factor receptor 1
16	ESR2	Q92731	Estrogen receptor beta
17	ESR1	P03372	Estrogen receptor
18	ERBB3	P21860	Receptor tyrosine-protein kinase erbB-3
19	ERBB2	P04626	Receptor tyrosine-protein kinase erbB-2
20	EGFR	P00533	Epidermal growth factor receptor
21	CHEK2	O96017	Serine/threonine-protein kinase Chk2
22	BAD	Q92934	Bcl2-associated agonist of cell death
23	ACHE	P22303	Acetylcholinesterase

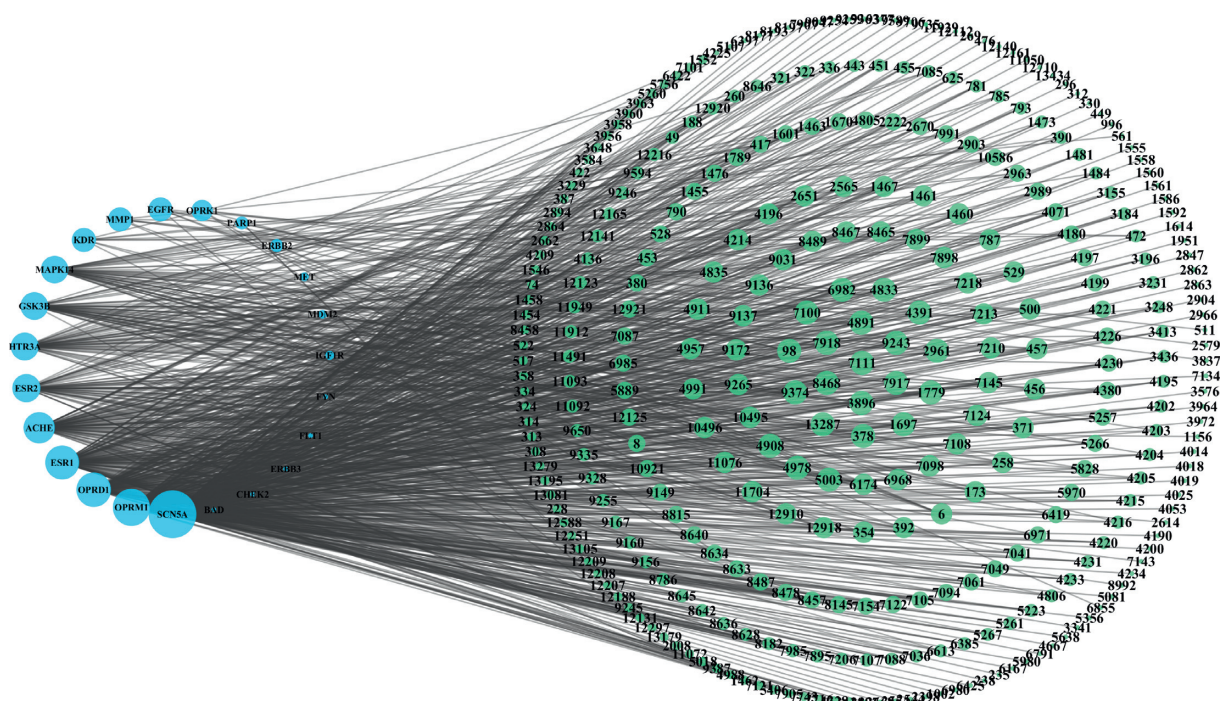


FIGURE 3: Target-compound network. (The network diagram consisted of 362 points and 1022 edges, with the potential therapeutic targets shown in blue and the compound targets shown in green.)

closely related to the liver, spleen, and stomach, followed by the lungs. These findings are consistent with the TCM theory of treating diarrhea and are related to the TCM theory of the digestive system (Figures 4 and 5).

3.4. Construction of the Target-Compound-TCM Network and Selection of Core Components. A network diagram of 23 potential therapeutic targets, 339 compounds, and 402 kinds of TCMs was constructed, with 764 nodes and 2707 edges.

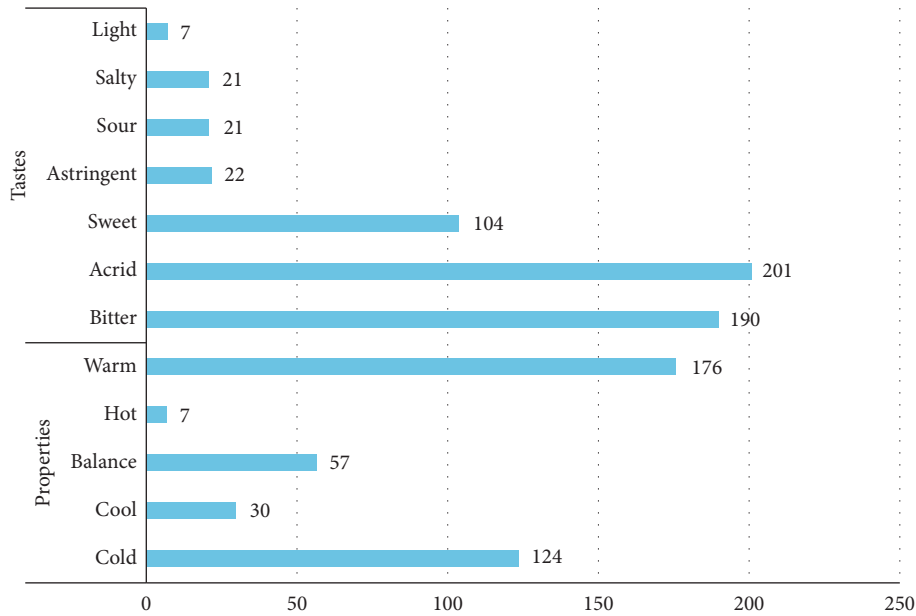


FIGURE 4: Analysis of four properties and five tastes.

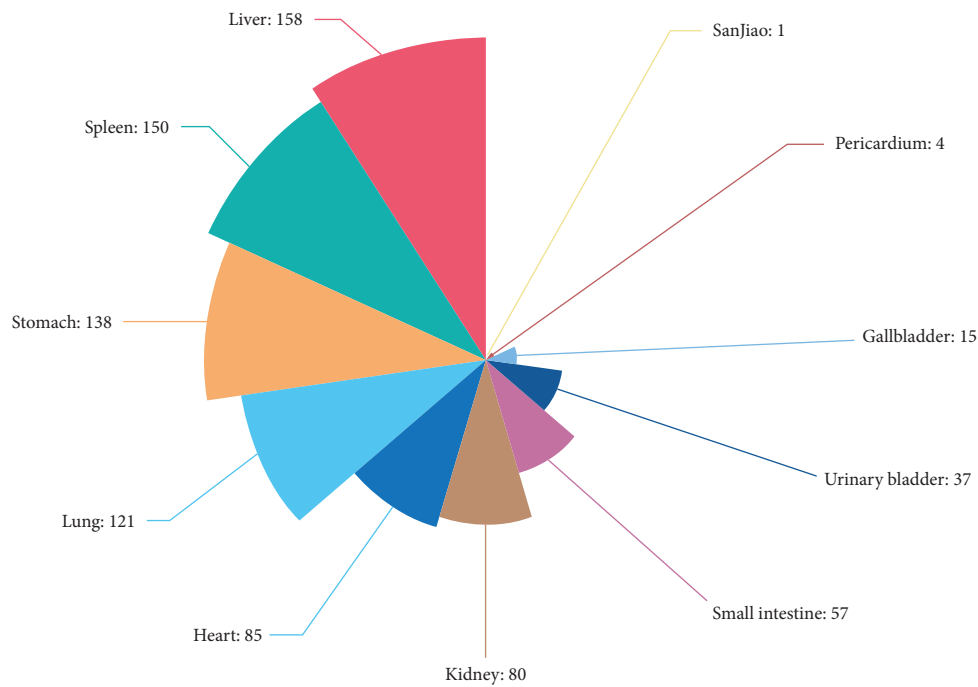


FIGURE 5: Analysis of meridian tropism.

For a clearer visual representation of the network relationships, only compounds and TCMs with degree values higher than the median (degree ≥ 4) were kept in the network (Figure 6).

The top 10 TCMs based on degree value in the target-compounds-TCM network diagram were Yanhusuo, Danshen, Gancao, Wuzhuyu, Huangbo, Guanhuangbo, Leigongteng, Baiqcai, Gouteng, and Huangqi, as candidate compounds 38, 28, 26, 16, 16, 13, 13, 12, 12, and 11, respectively. Using the connection relationship between the

related compounds and the targets in TCM, the potential targets of the TCMs for the treatment of EGFR-TKI-related diarrhea were collected. It was indicated that Yinyanghuo, Gaoliangjiang, Huangqi, Huzhang, Ziwan, Gancao, Jinqiaomai, Juhua, Yinxingye, and Heye were related to more targets, acting on 20, 18, 18, 18, 18, 17, 17, 17, 17, and 16 targets, respectively, showing that these TCMs had a strong modulating function on diarrhea as an adverse effect of EGFR-TKI. The core compounds were selected with a median degree value of 4 and a standard of 8, which was

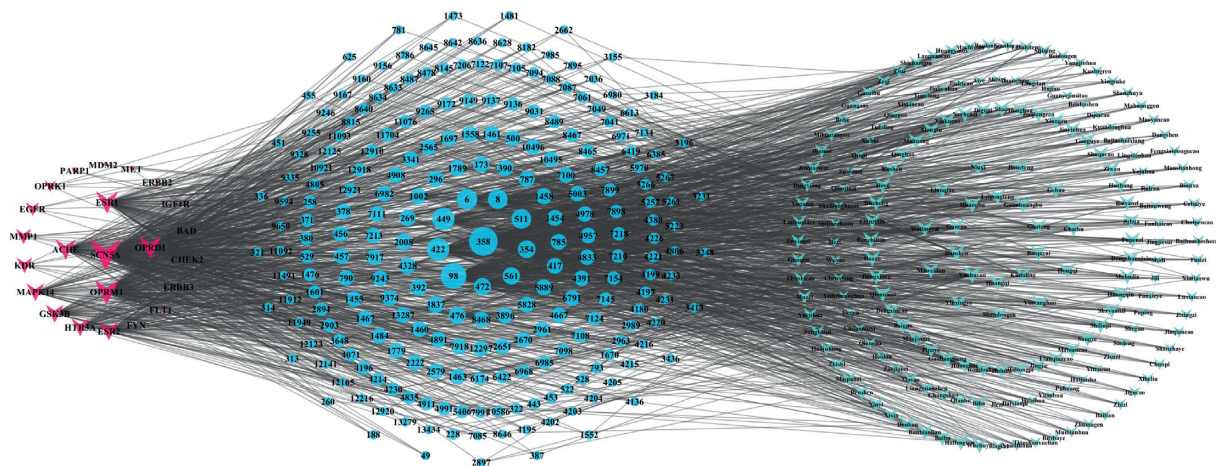


FIGURE 6: Target-compound-TCM network (compound degree ≥ 4 ; TCM degree ≥ 4 ; the network diagram consisted of 362 points and 1022 edges, with the potential therapeutic targets being shown in blue and the compound targets being shown in green).

greater than twice the median of the degree value. The top 10 compounds based on the degree value of the compounds were β -sitosterol, quercetin, kaempferol, stigmasterol, luteolin, apigenin, ursolic acid, isorhamnetin, astragaloside, and emodin (Table 2).

3.5. Molecular Docking Results. The molecular docking of five core targets, OPRM1 (PDBID: 4DKL), OPRD1 (PDBID: 4N6H), ESR1 (PDBID: 1A52), ACHE (PDBID: 1ODC), and ESR2 (PDBID: 1L2J), with 31 core compounds and the commonly used therapeutic drug loperamide, resulted in a total of 186 receptor-ligand docking results (Figure 7). There were 38 combinations in the target-compound network with the highest docking score of -9.9424 kcal/mol from MOL005828(nobiletin)-ESR2 and the lowest docking score of -6.0104 kcal/mol from MOL000785(astragaloside)-ESR1. The average score of -7.0956 kcal/mol for the intranetwork combination implies good binding activity between the core targets and the core compounds, further proving the reliability of the therapeutic relationship between the compounds and the targets. Meanwhile, there were 117 new combinations outside the target-compound network. The top 3 combinations ranked according to affinity were MOL000561 (palmatine)-ESR2 with a score of -9.7507 kcal/mol, MOL001460(berberine)-ESR2 with a score of -8.9064 kcal/mol, and MOL000561(palmatine)-ACHE with a score of -8.7397 . The average score of the off-net combination was -6.7672 kcal/mol. The docking results showed that there were still drug-target combinations that were not included in the TCMSP, and the effects of the compounds in TCM on the adverse reactions to EGFR-TKI in the form of diarrhea need to be further studied. The core targets and docking of loperamide can be summarized as follows: -8.2166 kcal/mol with OPRM1, -7.8025 kcal/mol with OPRD1, -9.3023 kcal/mol with ESR2, -8.1334 kcal/mol with ESR1, and -8.1402 kcal/mol with ACHE. This research has demonstrated that the potential therapeutic targets and drugs have good binding activity and have verified that the core targets selected in this study are of great significance for

the treatment of diarrhea. The above-mentioned docking results offer reliable data support for further exploration of effective TCM ingredients and can serve as the theoretical reference for selecting effective targets and ingredients in future tests.

Taking into account the affinity values for molecular docking and the degree values of the target-compound-TCM network, the docking patterns with affinity < -10 in the target-compound-TCM network and the top 4 ranked by affinity values outside the network were presented as 2D and 3D molecular docking pattern plots. As shown in Figure 8, each ligand was inserted into the active pocket of the target and reacted with a number of residues of the target via hydrophobic interaction and hydrogen bond formation.

4. Discussion

At present, for NSCLC patients who are positive for EGFR gene mutations, using EGFR-TKI as the first-line treatment leads to better progression-free survival, especially in the Asia-Pacific region and Russia, where EGFR gene mutations are present in 49.3% of the total number of patients with NSCLC [28, 29]. However, diarrhea is a common adverse event of EGFR-TKI drug use; if not taken correctly, it may lead to dehydration, forced reduction in drug dose, or even the interruption of treatment. The mechanism leading to such adverse reactions is not yet clear. It may involve imbalances in the ion transport system and abnormal secretion of chlorides, leading to secretory diarrhea [30], which lack effective preventive drugs. Although diarrhea is a common adverse reaction to all EGFR-TKIs, data show that second-generation inhibitors with a wider range of activities and targets cause a higher incidence of diarrhea [31]. Therefore, it is particularly important to explore the therapeutic targets related to EGFR-TKI and the drug-target relationship to investigate how EGFR-TKI may lead to adverse reactions such as diarrhea and to find effective therapeutic targets and drugs. Many studies have confirmed that TCM combined with EGFR-TKI treatment can improve the therapeutic effects and reduce toxicity by decreasing the incidence of

TABLE 2: Core compounds (degree ≥ 8).

MolID	MolName	CAS	Degree
MOL000358	Beta-sitosterol	83-46-5	234
MOL000098	Quercetin	117-39-5	185
MOL000422	Kaempferol	520-18-3	128
MOL000449	Stigmasterol	83-48-7	124
MOL000006	Luteolin	491-70-3	91
MOL000008	Apigenin	520-36-5	78
MOL000511	Ursolic acid	77-52-1	77
MOL000354	Isorhamnetin	480-19-3	43
MOL000561	Astragalin	480-10-4	36
MOL000472	Emodin	518-82-1	32
MOL000476	Physcion	521-61-9	30
MOL003837	Esculetin	305-01-1	26
MOL000392	Formononetin	485-72-3	23
MOL004328	Naringenin	153-18-4	23
MOL002008	Myricetin	529-44-2	22
MOL000269	Elemicin	487-11-6	20
MOL001002	Ellagic acid	476-66-4	18
MOL000296	Hederagenin	465-99-6	17
MOL000173	Wogonin	632-85-9	15
MOL001789	Isoliquiritigenin	961-29-5	15
MOL000787	Fumarine	130-86-9	14
MOL000390	Daidzein	486-66-8	14
MOL001458	Coptisine	3486-66-6	13
MOL000785	Palmatine	3486-67-7	12
MOL001454	Berberine	633-66-9	12
MOL005828	Nobiletin	478-01-3	11
MOL005889	Rhamnetin	90-19-7	11
MOL000417	Calycosin	20575-57-9	11
MOL003896	7-Methoxy-2-methyl isoflavone	19725-44-1	10
MOL001460	Cryptopin	482-74-6	9
MOL004891	Shinpterocarpin	157414-04-5	9
MOL007918	2-Hydroxy-7-methoxy-1,8-dimethyl-5-ethenyl-9,10-dihydrophenanthrene	—	9
MOL008468	Methyl (E)-2-[(2S, 3Z, 12bS)-3-ethylidene-2,4,6,7,12,12b-hexahydro-1h-indolo[3,2-h]quinolizin-2-yl]-3-methoxyprop-2-enoate	—	9
MOL000500	Vestitol	20879-05-4	8
MOL001461	Dihydrochelerythrine	6880-91-7	8

diarrhea as an adverse reaction [32–34], indicating that TCM has certain advantages in the treatment of diarrhea. It can also enhance the therapeutic effects, but the research on related drugs and molecular mechanisms is still insufficient and lacks specific TCM intervention in studies of EGFR-TKI use with diarrhea as an adverse reaction. Therefore, it is of great clinical significance to assess effective therapeutic ingredients and targets in TCM. This research used network pharmacology to explore the mechanisms behind multi-component and multitarget TCMs, to identify effective therapeutic targets, related compounds, and related TCMs, and to provide data support for using TCM to further improve the therapeutic effect of EGFR-TKI and reduce the incidence of diarrhea.

4.1. Core Targets. After screening the potential therapeutic targets, those with a high degree 294 value were screened for certain antitumor and antidiarrhea effects, such as OPRM1

and OPRD1. Opioids that act through such targets can reduce gastrointestinal propulsive peristaltic contractions and increase circular muscle tension and intraluminal pressure [35]. Endogenous opioids maintain gastrointestinal homeostasis. The activation of intestinal opioid receptors such as μ receptors and δ receptors reduces epithelial secretion and increases water/electrolyte absorption, producing an antidiarrheal effect [36]. As a synthetic opioid receptor agonist, loperamide, a recommended drug for the treatment of diarrhea as an adverse reaction to EGFR-TKI, not only acts through μ receptors in the muscular plexus of the intestinal wall but also inhibits the release of acetylcholine, thus reducing intestinal peristaltic activity [37]. Antidiarrheal drugs based on such targets are under continuous development [38, 39]. The neurotransmitter acetylcholine participates in various activities mainly through nicotinic and muscarinic receptors, of which M3 receptors are widely distributed in the gastrointestinal tract. It plays an



FIGURE 7: Results of molecular docking.

important role in maintaining the contraction of gastrointestinal smooth muscle [40]. ACHE, which is one of the core therapeutic targets identified in this study, can convert acetylcholine to choline and acetic acid, thereby preventing the contraction effect of acetylcholine on the smooth muscles of the gastrointestinal tract and producing a specific antidiarrheal effect. This feature has the same effect as loperamide in inhibiting the release of acetylcholine.

ESR1 and ESR2 are estrogen receptors, and studies have confirmed that there is a significant correlation between ESR1 expression and the overall survival of patients with NSCLC. Estrogen-induced growth of transplanted cells in vitro correlated closely with acute hormonal activation of mitogen-activated protein kinase signaling, and treatment with the antiestrogen drug Faslodex can reduce its growth. ESR1 expression is considered an independent prognostic factor for metastatic NSCLC [41, 42]. The single nucleotide polymorphisms of ESR2 are closely related to lung cancer in nonsmoking women [43], and studies have shown that nonsmoking women in Asia have a higher mutation rate of the EGFR gene [44]. We believe that ESR2 is correlated with EGFR's effect on metabolism during the treatment of NSCLC. However, at present, there are few studies on this kind of research, and its mechanism is not clear.

SCN5A is mainly responsible for the initiation and propagation of cardiac action potentials, thereby generating cardiac excitability and electrical stimulation to the cardiac muscles. Dysfunction of this target will cause excess sodium

to enter the cardiomyocytes through abnormal channels, which leads to long QT syndrome [45]. Related studies have shown that QT interval prolongation is a relatively rare adverse event of several TKIs such as osimertinib and crizotinib, and it is believed that the heart should be monitored during the treatment of axitinib in patients with a previous family history of heart disease [46].

Mok et al. observed advanced NSCLC patients with the EGFR T790M mutation after an EGFR-TKI treatment of oral axitinib plus cisplatin or carboplatin. Among them, 4% of patients taking osimertinib experienced QT interval prolongation, with 1% classified as having grade III adverse events [47]. At present, there are few studies on cardiotoxicity caused by TKIs. The SCN5A target identified in this study was predicted from the molecular structure of osimertinib on the SwissTargetPrediction platform. There were no such targets identified from other drug structures, so it is speculated that the adverse reaction of axitinib in prolonging QT interval may be related to this target, which provides new research ideas for the future exploration of TKI leading to adverse cardiac reactions.

4.2. Core Compounds. To better synergize with EGFR-TKI treatment, the selected compounds should not only alleviate the adverse reaction of diarrhea but also have an antitumor effect. Through topological analysis of the target-compound-TCM network, core compounds with higher degree values were identified and included β -sitosterol, quercetin,

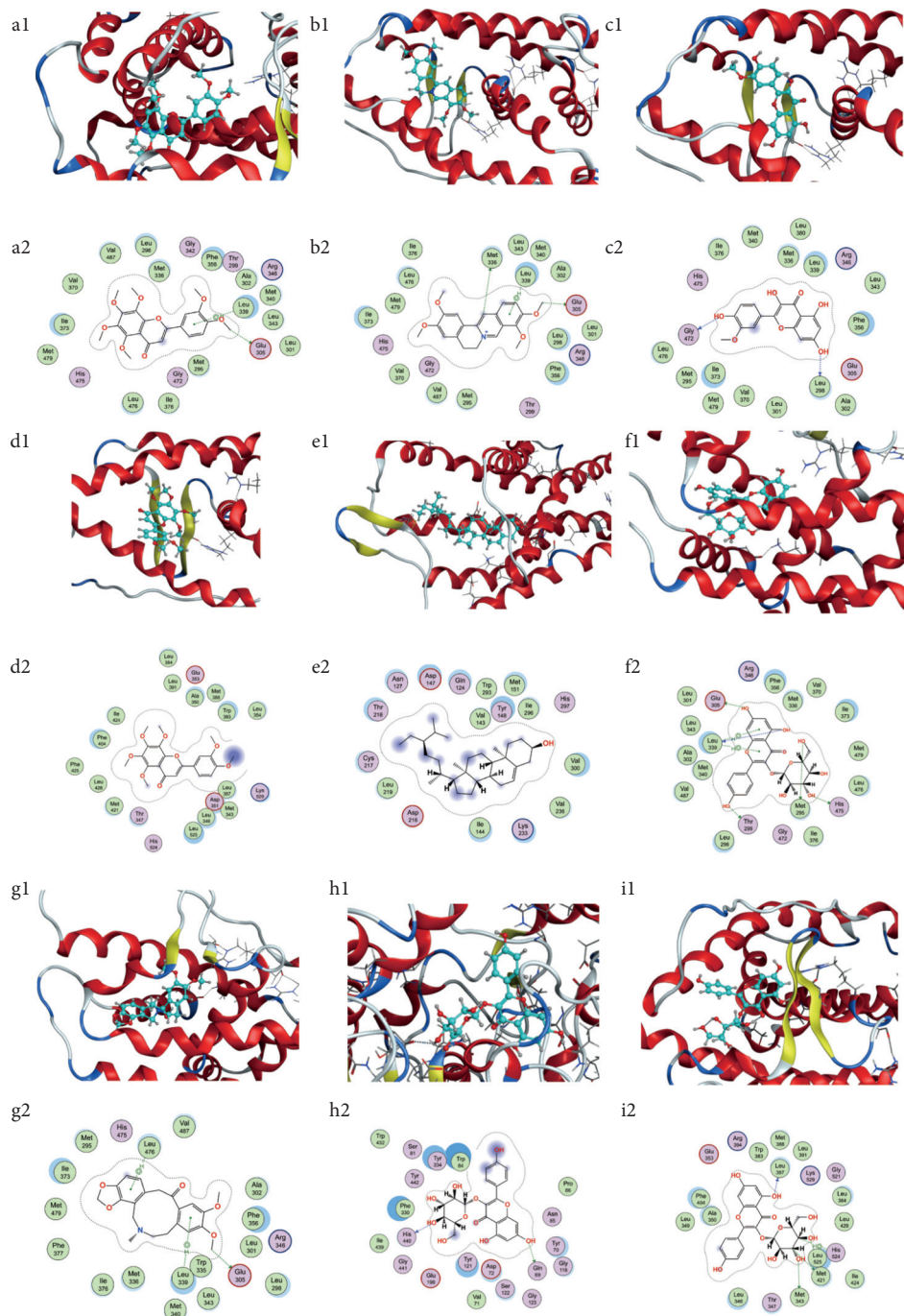


FIGURE 8: Molecular docking structure. (A) The overall 3D structure of the ligand-protein complex. The backbone of the protein was rendered as tubes and colored by chains. The ligands were rendered as sticks and colored in blue. (B) The 2D protein-ligand interaction diagrams of ligand-protein complexes. Protein residues were rendered as circles and colored based on their properties: green, hydrophobic residue; purple, polar residue (a: ESR2-nobiletin; b: ESR2-astragalin; c: ESR2-formononetin; d: ESR1-nobiletin; e: OPRM1-daidzein; f: ESR2-palmatine; g: ESR2-berberine; h: ACHE-palmatine; i: ESR1-palmatine).

kaempferol, stigmasterol, luteolin, and apigenin. All of them have antitumor effects and can relieve the adverse reaction of diarrhea to a certain extent.

β -Sitosterol, which is widely present in various plants [48], can interfere with various cell signaling pathways and affect the cell cycle, thereby inhibiting tumor cell proliferation. It has anticancer properties against breast, prostate,

colon, lung, and gastric cancers [49]. β -Sitosterol can also inhibit the growth of A549 cells in a dose- and time-dependent manner, arresting the cell cycle of the tumor cells in the G2/M phase. In vivo toxicity experiments show that β -sitosterol is nontoxic and reduces the absorption of cholesterol in the intestinal tract. It is a potential drug for the treatment of lung cancer [50].

Quercetin has various pharmacological properties such as having antitumor effects, conveying protection to the blood vessels, having anti-inflammatory and antioxidative properties, and being involved in immune regulation. Its main antitumor mechanism is related to the induction of apoptosis by inhibiting the cellular signal proteins regulated by antiapoptotic proteins, such as B-cell lymphoma-2 (Bcl-2), and upregulating proapoptotic proteins. It also inhibits cell proliferation by blocking the progression of the cell cycle from G0/G1 to G2/M and inhibits angiogenesis and metastasis [51]. A study has shown that quercetin promotes the apoptosis of A549 cells by downregulating the expression of matrix metalloproteinase 9 (MMP-9) and transforming growth factor- β (TGF- β) [52]. Li et al. [53] used various concentrations of quercetin and gemcitabine to treat lung cancer alone or in combination and found that quercetin, when combined with gemcitabine treatment, could act as a chemosensitizer by downregulating heat shock protein 70 (HSP70). However, its poor water solubility and low bioavailability limit further clinical use [54]. Phycophyllin also has good antitumor activity, and as the most active anti-diarrheal ingredient in guava, it can inhibit the invasion of gastrointestinal diseases caused by *Escherichia coli* and *Shigella flexneri* in HEP-2 cells. Its anti-inflammatory and antioxidative effects can eliminate oxygen free radicals in the intestinal tract, reduce the loss of intestinal water and electrolytes, inhibit intestinal peristalsis caused by inflammation, and restore normal intestinal mechanical activity [55, 56].

Kaempferol can block the cell cycle through a variety of mechanisms, thus inhibiting the proliferation of cancer cells. It can inhibit the concentration of cyclin-dependent kinase (CDK), arresting cells in the G2/M phase [57]. The overexpression of the cell myelomatosis virus oncogene (cMyc) in most cancers leads to excessive cell proliferation. Kaempferol can reduce the level of the cMyc mRNA and increase the level of the CDKN1A mRNA in cancer cells. The combination of cyclin-dependent kinase inhibitor 1A (CDKN1A) and the CDK complex inactivates CDK and blocks the cell cycle [58]. Kaempferol inhibits the secretion of vascular endothelial growth factor (VEGF) and inhibits angiogenesis [59]. Kaempferol and quercetin have synergistic antiproliferation effects on cancer cells through the decrease of the nuclear proliferating antigen Ki67 [60]. Inflammation is closely related to the occurrence and development of acute and chronic diarrhea. Kaempferol can regulate the activity of proinflammatory enzymes and inhibit transcription factors, adhesion molecules, and inhibit the expression of proliferation-related genes. At present, as the mechanisms behind diarrhea caused by EGFR-TKI are not clear, kaempferol, with the antitumor and anti-inflammatory properties, can provide a reference for the development of new drugs to alleviate the adverse reaction of diarrhea and strengthen EGFR-TKI therapy [61].

The other core components, such as stigmaterol, luteolin, apigenin, and ursolic acid, also have antitumor and anti-inflammatory effects. Stigmaterol inhibits cancer cell metastasis and arrests cell cycle in the G2/M phase [62]. It has also been shown to significantly decrease the expression

of cyclooxygenase-2 (COX-2) and colony-stimulating factor-1, which could reduce the severity of colitis [63]. Luteolin can effectively inhibit the proliferation of NSCLC A549 cells by inducing apoptosis and inhibiting proinflammatory cytokines (IL-1 β , IL-6, IL-8, and TNF- α) and VEGF, thus inhibiting angiogenesis [64]. A study has shown that luteolin has significant antitumor effects on EGFR with the L858R/T790M mutation and erlotinib-corrected NSCLC at the organism and cellular levels [65]. Luteolin is also a good antioxidant, scavenging free radicals and producing an anti-inflammatory effect [66]. Apigenin and ursolic acid are also good anti-inflammatory and antitumor drugs. Ursolic acid and its derivatives can induce tumor cell apoptosis, inhibit angiogenesis, tumor cell invasion, and metastasis, and can exert an anti-inflammatory effect by inhibiting COX-2 [67]. Apigenin can block the cell cycle in the G1/S and G2/M phases, induce apoptosis, and has anti-inflammation and antioxidation properties [68]. It can inhibit the proliferation of A549 lung cancer cells and the transcriptional activation of VEGF, thus inhibiting tumor neovascularization [69].

At present, the mechanism behind diarrhea as an adverse reaction to EGFR-TKI is not clear. However, some studies have suggested that diarrhea is caused by the decrease of intestinal epithelial growth and repair due to the inhibition of signal transduction in intestinal epithelial cells by EGFR-TKI [70]; EGFR-TKI causes the toxicity of the intestinal epithelium and intestinal inflammation, which in turn can increase the exfoliation and apoptosis of the intestinal epithelium [71]. The core compounds identified in this study include several flavonoids, such as quercetin, kaempferol, luteolin, and apigenin. As effective antioxidants, flavonoids have good anti-inflammatory and anticancer activities. Some studies have confirmed a correlation between the intake of flavonoids and lung cancer [72]. Therefore, the core compounds identified in this study can be used as potential therapeutic drugs for lung cancer, and their anti-inflammatory activities can provide a pharmacological reference for alleviating the adverse reaction of diarrhea to EGFR-TKI.

4.3. Molecular Docking. The results of molecular docking activity showed that in the target-compound-TCM network, the highest binding activity was between nobiletin and ESR2. Nobiletin, as a flavonoid compound contained in the TCM citrus peel, has good anticancer and antioxidant pharmacological effects. Nobiletin and its main metabolites, such as 4'-demethylnobiletin and 3'-desmethylnobiletin, can significantly inhibit the occurrence of lung cancer in mice by blocking the cell cycle and inducing apoptosis [73]. Nobiletin combined with paclitaxel, carboplatin, and other chemotherapeutic drugs can significantly inhibit the growth of subcutaneous A549 tumor xenotransplants in mice and enhance the sensitivity of A549 cells to chemotherapeutic drugs by regulating various signaling pathways such as the Akt/GSK3 β /MYCN pathway [74, 75]. Nobiletin's good anti-inflammatory activity can alleviate the occurrence of diarrhea. Related studies have shown that nobiletin can protect the intestinal epithelium barrier by reducing inflammatory cytokines and can reduce duodenal retraction to treat

inflammatory bowel disease by inhibiting tumor necrosis factor- α (TNF- α) and the expression of COX-2. It thus has potential intestinal protective function [76, 77].

In the past, there were few studies on the relationship between ESR2 and lung cancer. It is also widely believed that ESR2 is closely related to the occurrence and development of breast cancer [78]. However, studies have also found that ESR2 may be a new therapeutic target for lung adenocarcinoma in the future, as its downregulation reduces matrix metalloproteinase 2 (MMP-2) and MMP-9 expression, inhibiting the progression of lung adenocarcinoma through the MEK/ERK signaling pathway [79]. From the above, it can be seen that the targets and related compounds identified in this study have antitumor effects and can relieve the adverse reaction of diarrhea.

The target-compound-TCM network contains 117 target and compound docking combinations, including many compounds with good pharmacological activity, such as palmatine and berberine, which have high docking scores. Palmatine has anticancer, antioxidant, anti-inflammatory, neuroprotective, antibacterial, antiviral, and other pharmacological effects [80]. Berberine is used clinically to treat a variety of diseases with good pharmacological activity; it not only inhibits the proliferation, invasion, and metastasis of cancer cells but also has an excellent inhibitory effect on toxins and bacteria, including *Helicobacter pylori*. Its ability to protect the intestinal epithelial barrier from injury is used in the treatment of a variety of digestive system diseases [81]. The results of molecular docking showed that the selected compounds and the drug loperamide had good docking activity with their targets, with many compounds having a docking score higher than that of loperamide. It showed that the compounds selected in this study have good medicinal reference value, and the results of molecular docking can provide related compound and target references for the future study of good therapeutic drugs that can be combined with EGFR-TKI treatment.

4.4. Core Chinese Medicine. The core Chinese medicines identified through network pharmacology and data mining were mainly acrid and warm, and their meridian tropism mostly covered the liver, spleen, stomach, and lungs. The characteristics of these core Chinese medicines reflect the characteristics of the TCM theory for treating diarrhea by “warming yang and transforming dampness”. The theory of TCM believes that diarrhea originates in the spleen, and the transportation of the water in one’s diet cannot be separated from the rise and fall of the spleen and stomach and the adjustment of liver gas. The location of lung cancer is mainly the lungs, and the meridian tropism of these core Chinese medicines aligns with the treatment theory of TCM, which provides a theoretical reference for clinical treatment with TCM.

The core TCMs obtained in this study were Yanhusuo, Danshen, Gancao, Wuzhuyu, Huangbo, Yinyanghuo, Gaoliangjiang, and Huangqi. Modern pharmacology has shown that Yanhusuo extracts contain 13-methyl-palmatine, which has antitumor activities and can inhibit the

proliferation of lung cancer A549 cells by blocking the activation of the EGFR and MAPK signaling pathways [82]. Studies have confirmed that Yanhusuo alkaloid extracts can inhibit the VEGF signaling pathways, thereby producing antiangiogenic effects, and are expected to be used as antiangiogenic drugs [83]. Yanhusuo extracts also contain berberine, which not only inhibits the proliferation of cancer cells [84] but also can be used in the treatment of inflammatory bowel disease by protecting the intestinal epithelial barrier, regulating the transcription of intestinal inflammatory cytokines, and reducing proinflammatory cytokines such as TNF- α , IL-13, IL-6, IL-8, and IFN- γ [85]. Therefore, the core Chinese medicine Yanhusuo, when combined with EGFR-TKI treatment, not only has an antitumor effect but also reduces the incidence of diarrhea.

Other selected Chinese medicines also have such effects. The extract of Danshen contains cryptotanshinone, which can inhibit the proliferation of NSCLC cells through the miR-146a-5p/EGFR axis, block the G0/G1 phase of the cell cycle, and promote apoptosis [86, 87]. Tanshinone IIA combined with cisplatin treatment for NSCLC can prevent cancer cell migration and invasion, block the cell cycle in the S phase, and induce A549 cell apoptosis [88]. Gancao, as a widely used TCM, contains a variety of flavonoid compounds and has a variety of pharmaceutical effects, such as antioxidative, anti-inflammatory, antibacterial, antitussive, antiviral, anticancer, and antimutagenic effects [89]. Evodiamine, found in the extract of Wuzhuyu, can inhibit the proliferation of cancer cells through various methods, such as blocking the cell cycle and inhibiting the proliferation of A549 cells. It can induce protective autophagy in Lewis lung carcinoma cells and has good anticancer activity against many kinds of cancer cells [90]. Evodiamine can also effectively inhibit excessive gastrointestinal motility, providing a basis for the treatment of adverse reactions of diarrhea [91]. In summary, the core Chinese medicines screened in this study are closely related to antitumor effects and can alleviate adverse reactions. Their good pharmacological activity provides a reference for the mining and utilization of related TCMs and provides a theoretical basis for related experimental research and the better use of TCM combined with EGFR-TKI in the treatment of NSCLC in the future.

5. Conclusion

In this study, using network pharmacology and data mining, the role of TCM in alleviating EGFR-TKI-associated diarrhea was explored; core targets, compounds, and TCMs were screened using the relevant topological analysis parameters, and the pharmacological activities of the included targets and compounds were further evaluated by molecular docking. Core targets such as OPRM1, OPRD1, and ESR1 were screened, and the related targets of rare adverse reactions such as SCN5A were identified. The core components selected included β -sitosterol, quercetin, kaempferol, and stigmasterol. The core TCMs selected included Yanhusuo, Danshen, Gancao, and Wuzhuyu. Not only were the relevant targets and compounds consistent with existing research, but also the meridian tropism covered by the core

TCMs selected was consistent with the theory of TCM. These results can provide data support for the study of the anti-tumor effect of TCMs and their potential in alleviating diarrhea as an adverse reaction to EGFR-TKI treatment in the future and provide a basis for exploring TCM combined with EGFR-TKI in the treatment of NSCLC.

The advantage of this study is that the relevant data were obtained from an authoritative database. However, a disadvantage is that some of the data may be outdated. Another disadvantage is that the research results depend on the calculation of the software used. There are also certain limitations as the contents of each component of the TCMs are not exactly defined. The results still need to be verified by subsequent animal and clinical trials.

Data Availability

The datasets supporting the conclusions of this study are included within the article.

Conflicts of Interest

All authors declare no conflicts of interest.

Authors' Contributions

HSH and DWC were involved in the design of the study. Data collection and analysis are done by HSH and DWC together, and the pictures in this article are drawn. The article was jointly drafted by HSH and DWC. ZT and GXY review the data of the article one by one to make sure the data is correct. HW, HP, and LJJ provided critical comments and revised the manuscript. All the authors read and approved the final version of the manuscript.

Acknowledgments

The authors sincerely thank Zheng Li (China Academy of Chinese Medical Sciences) for his contribution to the data analysis of this study. This study was supported by the project Priority Theme Setting and Evidence-Based Research Scheme Design of Traditional Chinese Medicine for Malignant Tumor (K858).

References

- [1] J. R. Molina, P. Yang, S. D. Cassivi, S. E. Schild, and A. A. Adjei, "Non-small cell lung cancer: epidemiology, risk factors, treatment, and survivorship," *Mayo Clinic Proceedings*, vol. 83, no. 5, pp. 584–594, 2008.
- [2] R. S. Herbst, D. Morgensztern, and C. Boshoff, "The biology and management of non-small cell lung cancer," *Nature*, vol. 553, no. 7689, pp. 446–454, 2018.
- [3] O. Kawano, H. Sasaki, K. Endo et al., "PIK3CA mutation status in Japanese lung cancer patients," *Lung Cancer*, vol. 54, no. 2, pp. 209–215, 2006.
- [4] A. Harandi, A. S. Zaidi, A. M. Stocker, and D. A. Laber, "Clinical efficacy and toxicity of anti-EGFR therapy in common cancers," *Journal of Oncology*, vol. 2009, Article ID 567486, , 2009.
- [5] R. Califano, N. Tariq, and S. Compton, "Expert consensus on the management of adverse events from EGFR tyrosine kinase inhibitors in the UK," 2015.
- [6] Chinese Society, "EGFR-TKI ADR management Chinese expert consensus," *Chinese Journal of Lung Cancer*, vol. 22, no. 2, pp. 57–81, 2019.
- [7] S. Chen, A. Flower, A. Ritchie et al., "Oral Chinese herbal medicine (CHM) as an adjuvant treatment during chemotherapy for non-small cell lung cancer: a systematic review," *Lung Cancer*, vol. 68, no. 2, pp. 137–145, 2010.
- [8] J. Gao, W. A. Morgan, A. Sanchez-Medina, and O. Corcoran, "The ethanol extract of *Scutellaria baicalensis* and the active compounds induce cell cycle arrest and apoptosis including upregulation of p53 and Bax in human lung cancer cells," 2011.
- [9] A. L. Hopkins, "Network pharmacology: the next paradigm in drug discovery," *Nature Chemical Biology*, vol. 4, no. 11, pp. 682–690, 2008.
- [10] D. Yan and X. Xiao, "Investigation on pattern and methods of quality control for Chinese materia medica based on dao-di herbs and bioassay-bioassay for *Coptis chinensis*," 2011.
- [11] D. Gfeller, O. Michielin, and V. Zoete, "Shaping the interaction landscape of bioactive molecules," *Bioinformatics*, vol. 29, no. 23, pp. 3073–3079, 2013.
- [12] A. Daina, O. Michielin, and V. Zoete, "Swiss target prediction: updated data and new features for efficient prediction of protein targets of small molecules," *Nucleic Acids Research*, vol. 47, no. W1, pp. W357–W364, 2019.
- [13] M. Safran, I. Dalah, J. Alexander et al., "GeneCards Version 3: the human gene integrator," *Database*, vol. 2010, p. baq020, 2010.
- [14] J. S. Amberger, C. A. Bocchini, F. Schiettecatte, A. F. Scott, and A. Hamosh, "OMIM.org: online Mendelian Inheritance in Man (OMIM), an online catalog of human genes and genetic disorders," *Nucleic Acids Research*, vol. 43, no. D1, pp. D789–D798, 2015.
- [15] J. Piñero, J. M. Ramírez-Anguita, J. Saüch-Pitarch et al., "The DisGeNET knowledge platform for disease genomics: 2019 update," *Nucleic Acids Research*, vol. 48, no. D1, pp. D845–D855, 2020.
- [16] D. S. Wishart, Y. D. Feunang, A. C. Guo et al., "DrugBank 5.0: a major update to the DrugBank database for 2018," *Nucleic Acids Research*, vol. 46, no. D1, pp. D1074–D1082, 2018.
- [17] T. UniProt Consortium, "UniProt: the universal protein knowledgebase," *Nucleic Acids Research*, vol. 46, no. 5, p. 2699, 2018.
- [18] J. Ru, P. Li, and J. Wang, "TCMSP: a database of systems pharmacology for drug discovery from herbal medicines," *Journal of Cheminformatics*, vol. 6, p. 13, 2014.
- [19] X. Xu, W. Zhang, C. Huang et al., "A novel chemometric method for the prediction of human oral bioavailability," *International Journal of Molecular Sciences*, vol. 13, no. 6, pp. 6964–6982, 2012.
- [20] D. F. Veber, S. R. Johnson, H.-Y. Cheng, B. R. Smith, K. W. Ward, and K. D. Kopple, "Molecular properties that influence the oral bioavailability of drug candidates," *Journal of Medicinal Chemistry*, vol. 45, no. 12, pp. 2615–2623, 2002.
- [21] W. Tao, X. Xu, X. Wang et al., "Network pharmacology-based prediction of the active ingredients and potential targets of Chinese herbal *Radix Curcumae* formula for application to cardiovascular disease," *Journal of Ethnopharmacology*, vol. 145, no. 1, pp. 1–10, 2013.
- [22] P. Ertl, B. Rohde, and P. Selzer, "Fast calculation of molecular polar surface area as a sum of fragment-based contributions

- and its application to the prediction of drug transport properties,” *Journal of Medicinal Chemistry*, vol. 43, no. 20, pp. 3714–3717, 2000.
- [23] P. Shannon, A. Markiel, and O. Ozier, “Cytoscape: a software environment for integrated models of biomolecular interaction networks,” *Genome Research*, vol. 13, no. 11, pp. 2498–2504, 2003.
- [24] C. P. Commission, *Pharmacopoeia of People’s Republic of China (2015 Edition)*: 北京, China Medical Science Press, Beijing, China, 2015.
- [25] G. Zhong, *Chinese Medicine (New Century)*: 北京, China Press of Traditional Chinese Medicine, Beijing, China, 4th edition, 2016.
- [26] M. Yang, J. Chen, L. Xu, and G. Ji, “Navigating traditional Chinese medicine network pharmacology and computational tools,” *Evidence-Based Complementary And Alternative Medicine : ECAM*, vol. 2013, Article ID 731969, 2013.
- [27] K. Hsin, S. Ghosh, and H. Kitano, “Combining machine learning systems and multiple docking simulation packages to improve docking prediction reliability for network pharmacology,” *PLoS One*, vol. 8, no. 12, Article ID e83922, 2013.
- [28] J. Greenhalgh, K. Dwan, and A. Boland, “First-line treatment of advanced epidermal growth factor receptor (EGFR) mutation positive non-squamous non-small cell lung cancer,” *The Cochrane Database of Systematic Reviews*, vol. 5, Article ID D10383, 2016.
- [29] B. Han, S. Tjulandin, K. Hagiwara et al., “EGFR mutation prevalence in Asia-Pacific and Russian patients with advanced NSCLC of adenocarcinoma and non-adenocarcinoma histology: the IGNITE study,” *Lung Cancer*, vol. 113, pp. 37–44, 2017.
- [30] K. E. Barrett, “Epithelial transport in digestive diseases - mice, monolayers and mechanisms: 2019 hans using distinguished lecture article,” *American Journal of Physiology. Cell Physiology*, vol. 318, no. 6, 2020.
- [31] H. S. Rugo, J. A. Di Palma, D. Tripathy et al., “The characterization, management, and future considerations for ErbB-family TKI-associated diarrhea,” *Breast Cancer Research and Treatment*, vol. 175, no. 1, pp. 5–15, 2019.
- [32] L. Jiao, J. Xu, and J. Sun, “Chinese herbal medicine combined with EGFR-TKI in EGFR mutation-positive advanced pulmonary adenocarcinoma (CATLA): a multicenter, randomized, double-blind, placebo-controlled trial,” *Frontiers in Pharmacology*, vol. 10, p. 732, 2019.
- [33] M. Tang, S. Wang, and B. Zhao, “Traditional Chinese medicine prolongs progression-free survival and enhances therapeutic effects in epidermal growth factor receptor tyrosine kinase inhibitor (EGFR-TKI) treated non-small-cell lung cancer (NSCLC) patients harboring EGFR mutations,” *Medical Science Monitor International Medical Journal of Experimental And Clinical Research*, vol. 25, no. 614, pp. 8430–8437, 2019.
- [34] Z.-l. Liu, W.-r. Zhu, W.-c. Zhou et al., “Traditional Chinese medicinal herbs combined with epidermal growth factor receptor tyrosine kinase inhibitor for advanced non-small cell lung cancer: a systematic review and meta-analysis,” *Journal of Integrative Medicine*, vol. 12, no. 4, pp. 346–358, 2014.
- [35] G. W. Pasternak and Y.-X. Pan, “Mu opioids and their receptors: evolution of a concept,” *Pharmacological Reviews*, vol. 65, no. 4, pp. 1257–1317, 2013.
- [36] A. Jarmuż, M. Zielińska, K. Leń, M. Banaszek, M. Storr, and J. Fichna, “Review: the role of MOP and DOP receptors in treatment of diarrheapredominant irritable bowel syndrome,” *Mini Reviews in Medicinal Chemistry*, vol. 16, no. 18, pp. 1462–1469, 2016.
- [37] K. J. Lee, “Pharmacologic agents for chronic diarrhea,” *Intestinal Research*, vol. 13, no. 4, pp. 306–312, 2015.
- [38] M. Corsetti and P. Whorwell, “New therapeutic options for IBS: the role of the first in class mixed μ -opioid receptor agonist and δ -opioid receptor antagonist (mudelta) eluxadoline,” *Expert Review of Gastroenterology & Hepatology*, vol. 11, no. 4, pp. 285–292, 2017.
- [39] J. Pannemans and M. Corsetti, “Opioid receptors in the GI tract: targets for treatment of both diarrhea and constipation in functional bowel disorders?” *Current Opinion in Pharmacology*, vol. 43, pp. 53–58, 2018.
- [40] F. J. Ehler, R. S. Ostrom, and G. W. Sawyer, “Subtypes of the muscarinic receptor in smooth muscle,” *Life Sciences*, vol. 61, no. 18, pp. 1729–1740, 1997.
- [41] A. Atmaca, S.-E. Al-Batran, R. M. Wirtz et al., “The validation of estrogen receptor 1 mRNA expression as a predictor of outcome in patients with metastatic non-small cell lung cancer,” *International Journal of Cancer*, vol. 134, no. 10, pp. 2314–2321, 2014.
- [42] R. Pietras, D. Márquez, H. Chen, E. Tsai, O. Weinberg, and M. Fishbein, “Estrogen and growth factor receptor interactions in human breast and non-small cell lung cancer cells,” *Steroids*, vol. 70, no. 5–7, pp. 372–381, 2005.
- [43] J. Y. Song, J. M. Siegfried, B. Diergaarde et al., “Genetic variation in ESR2 and estrogen receptor-beta expression in lung tumors,” *Cancer Epidemiology*, vol. 37, no. 4, pp. 518–522, 2013.
- [44] S.-H. I. Ou, “Republished: lung cancer in never-smokers. does smoking history matter in the era of molecular diagnostics and targeted therapy?” *Postgraduate Medical Journal*, vol. 90, no. 1062, pp. 228–235, 2014.
- [45] A. A. M. Wilde and A. S. Amin, “Clinical spectrum of SCN5A mutations,” *JACC: Clinical Electrophysiology*, vol. 4, no. 5, pp. 569–579, 2018.
- [46] M. Schiefer, L. E. L. Hendriks, T. Dinh, U. Lalji, and A. C. Dingemans, “Current perspective: osimertinib-induced QT prolongation: new drugs with new side-effects need careful patient monitoring,” 2018.
- [47] T. S. Mok, Y. Wu, and M. Ahn, “Osimertinib or platinum-pemetrexed in EGFR T790M-positive lung cancer,” 2017.
- [48] A. Leone, A. Spada, A. Battezzati, A. Schiraldi, J. Aristil, and S. Bertoli, “Moringa oleifera seeds and oil: characteristics and uses for human health,” *International Journal of Molecular Sciences*, vol. 17, no. 12, 2016.
- [49] M. S. Bin Sayeed and S. S. Ameen, “Beta-sitosterol: a promising but orphan nutraceutical to fight against cancer,” *Nutrition and Cancer*, vol. 67, no. 8, pp. 1214–1220, 2015.
- [50] T. Rajavel, R. Mohankumar, G. Archunan, K. Ruckmani, and K. P. Devi, “Beta sitosterol and Daucosterol (phytosterols identified in *Grewia tiliaefolia*) perturbs cell cycle and induces apoptotic cell death in A549 cells,” *Scientific Reports*, vol. 7, no. 1, p. 3418, 2017.
- [51] D. Kashyap, S. Mittal, K. Sak, P. Singhal, and H. S. Tuli, “Molecular mechanisms of action of quercetin in cancer: recent advances,” *Tumor Biology*, vol. 37, no. 10, pp. 12927–12939, 2016.
- [52] X. Zhao and J. Zhang, “Mechanisms for quercetin in prevention of lung cancer cell growth and metastasis,” *Zhong nan da xue xue bao. Yi xue ban = Journal of Central South University. Medical sciences*, vol. 40, no. 6, pp. 592–597, 2015.
- [53] S. H. Lee, E. J. Lee, K. H. Min et al., “Quercetin enhances chemosensitivity to gemcitabine in lung cancer cells by

- inhibiting heat shock protein 70 expression,” *Clinical Lung Cancer*, vol. 16, no. 6, pp. e235–e243, 2015.
- [54] A. Massi, O. Bortolini, and D. Ragno, “Research progress in the modification of quercetin leading to anticancer agents,” *Molecules (Basel, Switzerland)*, vol. 22, no. 8, 2017.
- [55] T. Birdi, P. Daswani, S. Brijesh, P. Tetali, A. Natu, and N. Antia, “Newer insights into the mechanism of action of Psidium guajava L. leaves in infectious diarrhoea,” *BMC Complementary and Alternative Medicine*, vol. 10, no. 671, p. 33, 2010.
- [56] G. D’Andrea, “Quercetin: a flavonol with multifaceted therapeutic applications?” *Fitoterapia*, vol. 106, pp. 256–271, 2015.
- [57] W.-W. Huang, S.-C. Tsai, S.-F. Peng et al., “Kaempferol induces autophagy through AMPK and AKT signaling molecules and causes G2/M arrest via downregulation of CDK1/cyclin B in SK-HEP-1 human hepatic cancer cells,” *International Journal of Oncology*, vol. 42, no. 6, pp. 2069–2077, 2013.
- [58] A. Y. Chen and Y. C. Chen, “A review of the dietary flavonoid, kaempferol on human health and cancer chemoprevention,” *Food Chemistry*, vol. 138, no. 4, pp. 2099–2107, 2013.
- [59] H. Luo, G. O. Rankin, N. Juliano, B.-H. Jiang, and Y. C. Chen, “Kaempferol inhibits VEGF expression and in vitro angiogenesis through a novel ERK-NF κ B-cMyc-p21 pathway,” *Food Chemistry*, vol. 130, no. 2, pp. 321–328, 2012.
- [60] M. L. Ackland, S. van de Waarsenburg, and R. Jones, “Synergistic antiproliferative action of the flavonols quercetin and kaempferol in cultured human cancer cell lines,” *In Vivo (Athens, Greece)*, vol. 19, no. 1, pp. 69–76, 2005.
- [61] K. P. Devi, D. S. Malar, S. F. Nabavi et al., “Kaempferol and inflammation: from chemistry to medicine,” *Pharmacological Research*, vol. 99, pp. 1–10, 2015.
- [62] K. Li, D. Yuan, R. Yan, L. Meng, Y. Zhang, and K. Zhu, “Stigmasterol exhibits potent antitumor effects in human gastric cancer cells mediated via inhibition of cell migration, cell cycle arrest, mitochondrial mediated apoptosis and inhibition of JAK/STAT signalling pathway,” *Journal of B.U.ON. : Official Journal of the Balkan Union of Oncology*, vol. 23, no. 5, pp. 1420–1425, 2018.
- [63] S. Feng, Z. Dai, A. Liu et al., “ β -Sitosterol and stigmasterol ameliorate dextran sulfate sodium-induced colitis in mice fed a high fat Western-style diet,” *Food & Function*, vol. 8, no. 11, pp. 4179–4186, 2017.
- [64] M. Imran, A. Rauf, and T. Abu-Izneid, “Luteolin, a flavonoid, as an anticancer agent: a review,” *Biomedicine & Pharmacotherapy = Biomedicine & Pharmacotherapie*, vol. 112, Article ID 108612, 2019.
- [65] L. Bai, Y. Nong, Y. Shi et al., “Luteolin inhibits hepatitis B virus replication through extracellular signal-regulated kinase-mediated down-regulation of hepatocyte nuclear factor 4 α expression,” *Molecular Pharmaceutics*, vol. 13, no. 2, pp. 568–577, 2016.
- [66] G. Seelinger, I. Merfort, and C. Schempp, “Anti-oxidant, anti-inflammatory and anti-allergic activities of luteolin,” *Planta Medica*, vol. 74, no. 14, pp. 1667–1677, 2008.
- [67] S. Mlala, A. O. Oyedeji, M. Gondwe, and O. O. Oyedeji, “Ursolic acid and its derivatives as bioactive agents,” *Molecules (Basel, Switzerland)*, vol. 24, no. 15, 2019.
- [68] A. Kowalczyk, A. Bodalska, M. Miranowicz, and K. Karłowicz-Bodalska, “Insights into novel anticancer applications for apigenin,” *Advances in Clinical and Experimental Medicine*, vol. 26, no. 7, pp. 1143–1146, 2017.
- [69] Z.-D. Li, L.-Z. Liu, X. Shi, J. Fang, and B.-H. Jiang, “Benzo[a]pyrene-3,6-dione inhibited VEGF expression through inducing HIF-1 α degradation,” *Biochemical And Biophysical Research Communications*, vol. 357, no. 2, pp. 517–523, 2007.
- [70] J. M. Bowen, “Mechanisms of TKI-induced diarrhea in cancer patients,” *Current Opinion in Supportive & Palliative Care*, vol. 7, no. 2, pp. 162–167, 2013.
- [71] L. Vereecke, R. Beyaert, and G. van Loo, “Enterocyte death and intestinal barrier maintenance in homeostasis and disease,” *Trends in Molecular Medicine*, vol. 17, no. 10, pp. 584–593, 2011.
- [72] P. Knekt, R. Järvinen, R. Seppänen et al., “Dietary flavonoids and the risk of lung cancer and other malignant neoplasms,” *American Journal of Epidemiology*, vol. 146, no. 3, pp. 223–230, 1997.
- [73] Y. Sun, Y. Han, M. Song et al., “Inhibitory effects of nobiletin and its major metabolites on lung tumorigenesis,” *Food & Function*, vol. 10, no. 11, pp. 7444–7452, 2019.
- [74] S. Uesato, H. Yamashita, R. Maeda et al., “Synergistic anti-tumor effect of a combination of paclitaxel and carboplatin with nobiletin from Citrus depressa on non-small-cell lung cancer cell lines,” *Planta Medica*, vol. 80, no. 06, pp. 452–457, 2014.
- [75] J. Y. Moon, L. V. Manh Hung, T. Unno, and S. K. Cho, “Nobiletin enhances chemosensitivity to adriamycin through modulation of the akt/GSK3 β/β catenin/MYCN/MRP1 signaling pathway in A549 human non-small-cell lung cancer cells,” *Nutrients*, vol. 10, no. 12, 2018.
- [76] X. Wen, H. Zhao, L. Wang et al., “Nobiletin attenuates DSS-induced intestinal barrier damage through the HNF4 α -claudin-7 signaling pathway,” *Journal of Agricultural and Food Chemistry*, vol. 68, no. 16, pp. 4641–4649, 2020.
- [77] W. He, Y. Li, and M. Liu, “Citrus aurantium L. and its flavonoids regulate TNBS-induced inflammatory bowel disease through anti-inflammation and suppressing isolated jejunum contraction,” *International Journal of Molecular Sciences*, vol. 19, no. 10, 2018.
- [78] Z. Dai, T. Tian, and M. Wang, “Genetic polymorphisms of estrogen receptor genes are associated with breast cancer susceptibility in Chinese women,” *Cancer Cell International*, vol. 19, p. 11, 2019.
- [79] W. Chen, B. Xin, H. Pang et al., “Downregulation of estrogen receptor β inhibits lung adenocarcinoma cell growth,” *Oncology Reports*, vol. 41, no. 5, pp. 2967–2974, 2019.
- [80] J. Long, J. Song, L. Zhong, Y. Liao, L. Liu, and X. Li, “Palmitate: a review of its pharmacology, toxicity and pharmacokinetics,” *Biochimie*, vol. 162, pp. 176–184, 2019.
- [81] D. Song, J. Hao, and D. Fan, “Biological properties and clinical applications of berberine,” *Frontiers of Medicine*, vol. 14, no. 5, pp. 564–582, 2020.
- [82] J. Chen, X. Lu, C. Lu et al., “13-Methyl-palmatrubine induces apoptosis and cell cycle arrest in A549 cells in vitro and in vivo,” *Oncology Reports*, vol. 36, no. 5, pp. 2526–2534, 2016.
- [83] L. Wan, Y. Zhao, and Q. Zhang, “Alkaloid extract of Corydalis yanhusuo inhibits angiogenesis via targeting vascular endothelial growth factor receptor signaling,” *BMC Complementary and Alternative Medicine*, vol. 19, no. 1, p. 359, 2019.
- [84] L. M. G. Ortiz, P. Lombardi, M. Tillhon, and A. I. Scovassi, “Berberine, an epiphany against cancer,” *Molecules (Basel, Switzerland)*, vol. 19, no. 8, pp. 12349–12367, 2014.
- [85] K. Zou, Z. Li, Y. Zhang et al., “Advances in the study of berberine and its derivatives: a focus on anti-inflammatory and anti-tumor effects in the digestive system,” *Acta Pharmacologica Sinica*, vol. 38, no. 2, pp. 157–167, 2017.
- [86] P. Qi, Y. Li, X. Liu et al., “Cryptotanshinone suppresses non-small cell lung cancer via microRNA-146a-5p/EGFR axis,”

- International Journal of Biological Sciences*, vol. 15, no. 5, pp. 1072–1079, 2019.
- [87] S. Kim, O. Kang, and D. Kwon, “Cryptotanshinone induces cell cycle arrest and apoptosis of NSCLC cells through the PI3K/Akt/GSK-3 β pathway,” *International Journal of Molecular Sciences*, vol. 19, no. 9, 2018.
- [88] X. Z. Liao, Y. Gao, S. Huang et al., “Tanshinone IIA combined with cisplatin synergistically inhibits non-small-cell lung cancer in vitro and in vivo via down-regulating the phosphatidylinositol 3-kinase/Akt signalling pathway,” *Phytotherapy Research*, vol. 33, no. 9, pp. 2298–2309, 2019.
- [89] G. Pastorino, L. Cornara, S. Soares, F. Rodrigues, and M. B. P. P. Oliveira, “Liquorice (*Glycyrrhiza glabra*): a phytochemical and pharmacological review,” *Phytotherapy Research*, vol. 32, no. 12, pp. 2323–2339, 2018.
- [90] X. Hu, D. Li, and C. Chu, “Antiproliferative effects of alkaloid evodiamine and its derivatives,” *International Journal of Molecular Sciences*, vol. 19, no. 11, 2018.
- [91] H. X. Ren, Q. C. Tang, L. Yan, H. Xia, and H. S. Luo, “Evodiamine inhibits gastrointestinal motility via CCK and CCK1 receptor in water-avoidance stress rat model,” *Life Sciences*, vol. 209, pp. 210–216, 2018.

Research Article

Virtual Screening of Cablin Patchouli Herb as a Treatment for Heat Stress: A Study Based on Network Pharmacology, Molecular Docking, and Experimental Verification

Yan Xu,¹ Lizhong Ding,² Zhongtian Wang,¹ Yanbo Wang ¹ and Liping Sun ¹

¹Changchun University of Chinese Medicine, Changchun, 130117, China

²Affiliated Hospital, Changchun University of Chinese Medicine, Changchun, Jilin 130021, China

Correspondence should be addressed to Yanbo Wang; 14463798@qq.com and Liping Sun; slpcczyydx@sina.com

Received 11 July 2020; Revised 21 February 2021; Accepted 26 February 2021; Published 10 March 2021

Academic Editor: Hilal Zaid

Copyright © 2021 Yan Xu et al. This is an open access article distributed under the Creative Commons Attribution License, which permits unrestricted use, distribution, and reproduction in any medium, provided the original work is properly cited.

Heat-related diseases have long been known to damage the structure and function of essential macromolecules such as proteins, lipids, and nucleic acids, thereby compromising the integrity of cells and tissues and the physiological functions of the entire organism. Heat stress is the physical discomfort caused by overheating the body and is also the initial manifestation of heat-related diseases. Cablin patchouli herb (CPB) has been used in China for two thousand years and has been used to treat heat stress, but to date, no related mechanistic research is available. In this study, KEGG and PPI networks and the TCMSP and GEO databases were used to explore the components of CPB in relation to heat stress: quercetin, genkwanin, irisolidone, 3,23-dihydroxy-12-oleanen-28-oic acid, and quercetin 7-O- β -D-glucoside. The targets identified were EGFR, NCOA1, FOS, HIF1A, NFKBIA, and NCOA2; these proteins were verified by molecular docking and experimental verification. In short, our research represents the first report on the use of the traditional Chinese medicine CPB to treat heat stress and thus has pioneering significance.

1. Introduction

As global warming intensifies, heat-related diseases have become a major public health issue during heat waves around the world, even in areas traditionally considered to be temperate and cold. In July 1995, a heat wave in the United States killed more than 700 people in less than 7 days, and more than 3,000 people visited the emergency room [1]. In 2003 and 2010, two severe heat waves affected Western Europe and Russia, respectively, causing 70,000 deaths and 55,000 deaths [2, 3]. More seriously, children account for almost half of the total population suffering from heat-related diseases (47.6%) [4].

Heat-related diseases have been known since ancient times; they reflect the relationship between the human body and heat imbalance [5], and long-term exposure to excessive heat or certain drugs that cause fever are the main drivers of heat-related diseases [6]. Heat can damage the structure and function of essential macromolecules such as proteins,

lipids, and nucleic acids, thereby compromising the integrity of cells and tissues and the physiological functions of the entire organism, especially the central nervous system [7–10]. Heat-related conditions can be categorized into heat rash, heat cramps, heat stress, heat exhaustion, and heat stroke according to their severity; all these conditions have fever in common [4, 6]. In this study, we focused on exploring heat stress, an early manifestation of heat-related diseases. The symptoms of heat stress include prolonged fever, excess sweating or thirst, tiredness, and cramps; however, tachycardia and nervous system damage do not manifest.

Cablin patchouli herb (CPB) was first published in “Mingyi Bielu,” a medical book of the Han Dynasty, more than 2,000 years ago. It has the effect of “dispelling heat and dampness” and is recognized as a cure for heat stress. The Chinese patent medicine Huoxiang Zhengqi water, which uses CPB as its main medicinal material, was described in the textbook “Internal Medicine of Traditional Chinese

Medicine” in China, and it is also considered to exhibit excellent effects in treating heat stress (yin-related heat-related diseases). It should be noted that according to the Chinese Yin-Yang Theory, the scope of heat-related diseases is broad and can be divided into Yin and Yang. Heat stress is usually biased towards yin-related heat-related diseases that is relatively less harmful to the human body. Heat exhaustion and heat stroke are generally regarded as yang-related heat-related diseases that are more harmful to the human body. CPB is usually used to treat heat stress (i.e., yin-related heat-related diseases). At present, reports on CPB treatment of heat stress are concentrated in the Chinese literature. Fusen used scraping therapy combined with Huoxiang Zhengqi water (for which the main component is CPB) to treat 48 cases of yin-related heat stroke and achieved good results [11]. Li used Huoxiang Zhengqi water to treat 240 cases of pediatric fever and found that children’s heat-related symptoms were significantly reduced 3-4 hours after treatment [12]. Gu Fang and Rinan also used Huoxiang Zhengqi water to treat 18 cases of pediatric heat rash, a rash caused by heat. The effective rate for the treatment group reached 94.4%, which was significantly better than that of the control group [13]. Chaobin and Wanzhou elaborated on the theoretical basis of traditional Chinese medicine for the treatment of yin-related heat stroke with CPB. They believed that CPB can also treat fever and diarrhea [14]. There are some studies on the treatment of diarrhea [15, 16]. In short, since 2000, Chinese people have reliably used CPB to treat heat-related diseases, and its therapeutic effects are very good. However, with the strong development of science in the modern era, a great deal of interest has arisen in understanding such traditional disease treatment methods. It is necessary to study specific treatment mechanisms and to clarify their specific ingredients and targets.

However, there is a major difficulty in exploring the treatment mechanism of CPB: the complexity of Chinese medicine components and the multiplicity of pharmacological effects make it difficult to conduct comprehensive and systematic research in the context of Chinese medicine [17]. To solve this problem, after decades of research, Li Shao proposed in 1999 that there may be a connection between TCM syndrome and molecular networks [18–23]. Based on the rapid development of systems biology and computer technology, network pharmacology was born. Network pharmacology is based on the herb network-biological network-phenotype network interaction network [20]. Through network analysis, we can systematically observe the interventions and impacts of drugs on diseases and reveal the mysteries of drug molecules synergistically acting on the human body. This is the same as the core concept of traditional Chinese medicine: the principle of multicomponent, multipathway, and multitarget synergistic effects. Network pharmacology is also rapidly becoming a frontier research field in current drug research and next-generation drug research models [18].

Based on the above information, in this study, we used network pharmacology and molecular docking and experimental verification methods to explore the specific mechanisms by which CPB treats heat stress. Our goal was to

enable people outside China to recognize and accept CPB and to help patients with heat-related diseases worldwide.

2. Materials and Methods

2.1. The Composition and Targets of CPB. The TCMSP database (<http://tcmsp.com/tcmssp.php>) [24] was used to identify the active ingredients and targets of CPB. Oral bioavailability (OB), drug-like properties (DL), relative molecular mass (MV), octanol-water partition coefficient (AlogP), number of H-bond coordination electron donors (Hdon), and number of H-bond coordination electron acceptors (Hacc) were used as indicators to compare the physical and chemical properties of the CPB components and to study the similarities and differences between the components.

2.2. Genes Differentially Expressed during Heat Stress. Differentially expressed genes were obtained from NCBI-GEO, a free public microarray/gene profile database. GEO accession number GSE90763 includes the transcriptome information of 15 volunteers who were subjected to heat stress. The data before exposure (T0) and at the end of heat exposure (T1) were selected for comparison. These data were analyzed using the GEO2R online tool, and 1,789 differentially expressed genes were identified using $|\log_{2}FC| \geq 1$ and P value < 0.05 as criteria.

2.3. Disease-Drug-Target Network. After the composition of CPB was obtained using $OB > 30\%$ and $DL > 0.18$, the targets of CPB components were downloaded from the TCMSP database, and the target elements were entered into the UniProt database one by one (<https://www.UniProt.org/>, currently the most complete nonredundant protein sequence database with the most complete sequence data and the richest annotation information in the world) for correction and conversion to GeneSymbol. Next, differentially expressed genes were used to intersect the corrected CPB target and were imported into Cytoscape (version: 3.6.1) and used to construct the CPB ingredient-target-disease network.

2.4. Molecular Docking. The protein data for P-gp (PDB ID: 4XWK), CYP3A4 (PDB ID: 3NXU), EGFR (PDB ID: 2ITW), FOS (PDB ID: 1A02), HIF1A (PDB ID: 1H2M), NCOA1 (PDB ID: 1K4W), NCOA2 (PDB ID: 2ZZZ), and NFKBIA (PDB ID: 6Y1J) were downloaded from the PDB database (<http://www.rcsb.org/>). Then, MGLTools 1.5.6 was used to process the protein data, simulate hydrogenation, calculate the charge, merge the nonpolar hydrogen, and save the results as a pdbqt file. According to each protein’s ligand, the active site was defined, the grid box coordinates were set, and the box size was defined as $40 \times 40 \times 40$ grid points; the distance between the small grid points was 0.1 nm. AutoDock Vina 1.1.2 was used to simulate the docking of molecules and proteins. The affinity was less than 0, indicating that the receptor and ligand can spontaneously bind.

2.5. PPI Network Enrichment and KEGG Analyses. The protein-protein interaction (PPI) network was analyzed using the Search Tool for the Retrieval of Interacting Genes (STRING, <http://string.embl.de/>) database (organism: *Homo sapiens*). Kyoto Encyclopedia of Genes and Genomes (KEGG) pathway enrichment analyses were performed using the clusterProfiler package in R (3.6.1) software with $p\text{-valuecutoff} = 0.05$ and $q\text{-valuecutoff} = 0.05$ [25].

2.6. CPB Animal Experiment Verification

2.6.1. Drugs and Materials. CPB was purchased from Jiangyin Tianjiang Pharmaceutical Co., Ltd. (production batch number: 19086254) and diluted to 10 mg/mL, 20 mg/mL, and 40 mg/mL with normal saline (NS) for use. Ibuprofen suspension (production batch number: H19991011) was purchased from Shanghai Johnson Pharmaceutical Co., Ltd. and was used at 0.6 g/kg and diluted with NS. The NCOA1 (MD696513) kit, RIPA lysis buffer (article number: MD912016), BCA protein concentration determination kit (article number: MD913053), SDS-PAGE precast gel kit (article number: MD911919), and Rabbit Anti-Mouse antibody (MD912566) were purchased from Beijing Biotek Biomedical Technology Co., Ltd. PVDF membrane (Millipore, USA, ISEQ00010) and medium protein molecular weight marker (26617) were purchased from Thermo, USA, and EGFR antibody (ab32077) and C-FOS antibody (ab134122) were purchased from Abcam, USA. SDS-PAGE system (U.S. BIO-Rad company, model Mini-PROTEAN), protein wet transfer instrument (U.S. BIO-Rad company, model Mini Trans-Blot), and western blot imaging system (U.S. BIO-Rad company, model 170-8280) were employed.

2.6.2. Animals and Models. Forty-two specific pathogen-free (SPF) rats (female, 3-5 weeks old, 50-70 g) were purchased from Liaoning Changsheng Biotechnology Co., Ltd. (experimental animal production license number: NO.SCXX (Liao) 2020-0001) and subjected to the following conditions: rearing temperature— $(24 \pm 3)^{\circ}\text{C}$, relative humidity— $(40 \pm 5)\%$, illumination—alternating light and dark, noise $<55\text{Db}$, free water and food, and twice-weekly litter change. The animal experimentation was approved by the Animal Ethics Committee of Changchun University of Traditional Chinese Medicine (No. 20190116). The basal body temperature of SD rats was measured 3 days before the experiment, and the average value of the rectal temperature measured at three time points in the morning, midnight, and evening was used as the basal body temperature of the experimental animal. The rats were divided into 7 groups, 6 in each group, and fasted 6 hours before the experiment. Except for the blank group and the blank + NS group, the other 5 groups were subcutaneously injected with 10% dry yeast suspension (10 mL/kg) on the backs of rats. Body temperature was measured every 1 hour after modeling. After successful modeling ($\Delta T > 0.8^{\circ}\text{C}$, approximately 5 hours), each group was given intragastric administration: the blank + NS and model group were given 31 mL/kg NS, and the CPB treatment group and the ibuprofen group were

given different concentrations of CPB and 31 mL/kg ibuprofen. After the administration, the body temperature was measured every 1 h, a total of 10 times, and the body temperature change value was calculated. Ten hours after the dry yeast group was modeled, a microcapillary was used to collect blood from the fundus venous plexus of the rats in each group. After standing at room temperature for 30 minutes, the blood samples were centrifuged at 4°C and 300 r/min for 10 minutes, the upper serum was drawn and stored in a -80°C refrigerator for use, and IL- 1β , IL-6, TNF- α , and NCOA1 were detected in serum according to the instructions of the ELISA kit. After blood collection, the rats were anesthetized by intraperitoneal injection of 10% chloral hydrate (4 mL/kg). The skin was then cut along the costal arches on both sides, the abdominal cavity was opened, and curved scissors were used to create a small cut at the junction of the diaphragm and the sternum stem; this cut was then extended to both sides, the diaphragm and ribs were cut, the heart was fully exposed, and intravenous drip with a needle was used. The apex of the left ventricle was entered and fixed with a vascular clamp. NS (room temperature) was quickly instilled while cutting the right atrial appendage. When the blood color of the outflow liquid was light and almost clear, the perfusion was stopped. The brain was decapitated immediately, and the hypothalamus was removed from the center of the optic chiasm and gray nodules. The hypothalamus was quickly frozen in liquid nitrogen for 20 minutes and then stored at -80°C .

2.6.3. Western Blot Detection. Each experimental group included an equal mass of hypothalamic samples. RIPA buffer was added to produce lysate, and each sample was shaken with a tissue homogenizer for 5 minutes, centrifuged at 12,000 r/min for 15 minutes to obtain the supernatant, and the protein concentration was measured by BCA. After mixing with the loading buffer, samples were boiled in a boiling water bath for 5 minutes, and SDS-PAGE was employed. The protein was transferred to PVDF membrane by the wet transfer method, and 5% skimmed milk powder was sealed at room temperature for 2 hours. The primary antibody was incubated overnight at 4°C . After washing the membrane with TBST, the secondary antibody was added to incubate at 37°C for 1 hour. After washing the membrane with TBST, the color developed.

2.7. Statistics. The data were expressed as the mean \pm SD ($n \geq 3$) and analyzed by GraphPad Prism 6.0 (GraphPad Software) using Student's *t*-test ($*p < 0.05$ and $**p < 0.01$).

3. Results

3.1. General Description of CPB. The TCMSP database was used to collect CPB composition information and produce statistical descriptions based on the OB, DL, MV, AlogP, Hdon, and Hacc parameters, as shown in Table 1. The average value of OB was 37.90 (20.22), and the average value of DL was 0.20 (0.22), higher than the value range found by

TABLE 1: Physical and chemical properties of CPB components.

Index	Result
<i>n</i>	94
OB (mean (SD))	37.90 (20.22)
DL (mean (SD))	0.20 (0.22)
MW (mean (SD))	253.41 (118.93)
AlogP (mean (SD))	3.27 (1.77)
Hdon (mean (SD))	1.18 (2.12)
Hacc (mean (SD))	2.76 (3.82)

The values are expressed as the mean (SD).

previous studies (OB > 30%, DL > 0.18) [26]. This shows that CPB has good oral availability and drug-like properties.

3.2. Further Screening of CPB Components. To eliminate possible false-positive components, OB > 30% and DL > 0.18 were also used as screening indices [26], and the CPB components were screened more stringently. As shown in Table 2, a total of 11 components satisfied the new screening conditions.

3.3. Eleven Active Ingredients Docked with P-gp and CYP3A4 Molecules. The absorption, distribution, metabolism, and excretion of CPB in the human body are affected by many factors. Among them, the interaction between P-gp and cytochrome CYP3A4 plays a key role [35]. P-gp is widely distributed and expressed in intestinal epithelial cells, hepatocytes, and capillary endothelial cells and plays an important role in the process by which most heterologous compounds pass through the blood-brain barrier and the blood-testis barrier [35, 36]. CYP3A4 is the most important metabolic enzyme in the P450 enzyme system and contributes to the metabolism of 1/3 of oral drugs [35, 37]. P-gp and CYP3A4 can synergistically restrict the entry of foreign substances into the human body in the intestine [35, 38]. To explore whether the active ingredients of CPB can enter the human body and play pharmacological roles, the molecular docking method was used for verification, as shown in Figure 1.

P-gp and CPB molecular docking showed that the 11 active ingredients could successfully dock and that their affinity values were less than 0. In addition, the docking results of CYP3A4 and CPB with the active ingredient molecules also showed that they could successfully dock, with the exception of acanthoside B. Given this result, acanthoside B was removed from the list of main active ingredients, and the subsequent steps examined only the remaining ingredients.

3.4. Drug-Ingredient-Target-Disease Network. Genes differentially expressed in heat stress were identified through the GEO database. Using $|\log_{2}FC| > 1$ and P value < 0.05 as criteria, a total of 1,789 differentially expressed genes were obtained (Supplementary Table 1). The CPB component targets were then downloaded from the TCMSMP database, and UniProt database correction was performed to remove some targets that have not been manually annotated and

reviewed. After correction, only 85 targets with 8 components (Supplementary Table 2) were obtained. Immediately afterwards, the differentially expressed genes of heat-related diseases and the corrected CPB targets were used for intersection, and a drug-component-target-disease network was generated, as shown in Figure 2. Only 5 molecules and their corresponding targets corresponded to heat stress genes. The molecules were quercetin, genkwanin, irisolidone, 3,23-dihydroxy-12-oleanen-28-oic acid, and quercetin 7-O- β -D-glucoside. Studies have shown that quercetin can increase secretion in cherry tomato fruit in a hot environment and can increase disease resistance [39]. It is worth mentioning that similar to quercetin, those molecules are also found in several other medicinal plants, such as kales, onions, berries, apples, red grapes, broccoli, and cherries as well as tea and red wine [40]. However, the content differs for each medicinal plant. In addition, existing technology cannot make specific judgments about complex chemical reactions that occur simultaneously in different molecules in plants. After a Chinese medicine enters the body, there are also complicated processes of absorption, distribution, metabolism, and excretion. Therefore, we hypothesize that although different Chinese medicines may have some of the same molecules, based on the complex characteristics of multiple components and multiple targets of traditional Chinese medicine, it is still believed that each traditional Chinese medicine, and even each molecule, corresponds with a distinct biological process in the body.

3.5. KEGG Enrichment Analysis. In the previous drug-component-target-disease network, we obtained 7 targets for possible treatments: EGFR, FOS, HIF1A, IRF1, NCOA1, NCOA2, and NFKBIA. However, the physiological and metabolic effects of CPB in the body were still unknown. Therefore, we performed KEGG enrichment analyses, as shown in Figure 3. Notably, in the KEGG enrichment analysis, we found that pathways related to PD-L1 expression and the PD-1 checkpoint pathway in cancer and estrogen signaling pathway were the most enriched.

The occurrence and development of tumors is accompanied by the formation of a special tumor immune microenvironment. Tumor cells can escape immune surveillance and destroy the host's immune checkpoints through various methods, thus avoiding elimination from the host's immune system [41]. Under normal physiological conditions, immune checkpoint molecules are in a balanced state such that the immune response of T cells maintains an appropriate intensity and scope in order to minimize damage to surrounding normal tissues and avoid autoimmune reactions [42]. However, cancer uses a variety of methods to upregulate negative signals through cell surface molecules, thereby inhibiting T cell activation or inducing apoptosis and promoting cancer progression and metastasis [43]. The immunotherapy method that uses antagonistic antibodies to block the immune checkpoint pathway can release cancer suppression and promote antitumor activity, thereby achieving the purpose of treating cancer. Programmed death 1 (PD-1) and its ligands PD-L1 (B7H1) and

TABLE 2: The 11 main components of CPB.

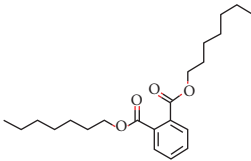
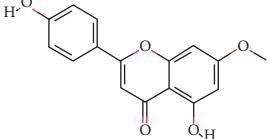

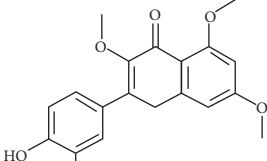
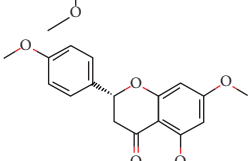
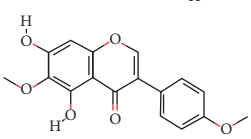
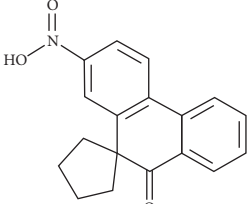
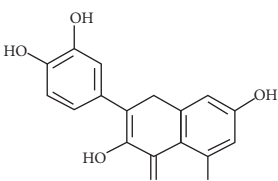
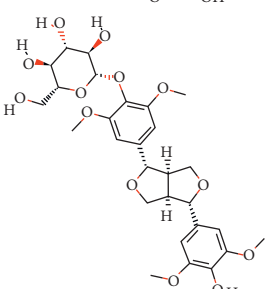
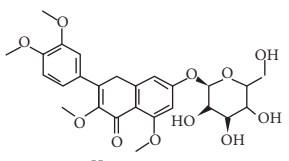
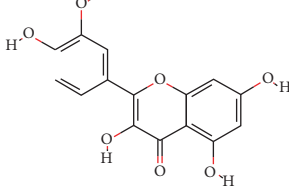
No.	MolID	MolName	OB	DL	Molecular structure	Reference
1	MOL002879	Diop	43.59	0.39		[27]
2	MOL005573	Genkwanin	37.13	0.24		[27]
3	MOL005884	Patchoulan 1, 12-diol	38.17	0.25		[27, 28]
4	MOL005890	Pachypodol	75.06	0.4		[29, 30]
5	MOL005911	5-Hydroxy-7, 4'-dimethoxyflavanone	51.54	0.27		[31]
6	MOL005916	Irisolidone	37.78	0.3		[27]
7	MOL005918	Phenanthrone	38.7	0.33		[27, 32]
8	MOL005921	Quercetin 7-O-β-D-glucoside	49.57	0.27		[31]
9	MOL005922	Acanthoside B	43.35	0.77		[27]

TABLE 2: Continued.

No.	MolID	MolName	OB	DL	Molecular structure	Reference
10	MOL005923	3, 23-Dihydroxy-12-oleanen-28-oic acid	30.86	0.86		[27, 33]
11	MOL000098	Quercetin	46.43	0.28		[31, 34]

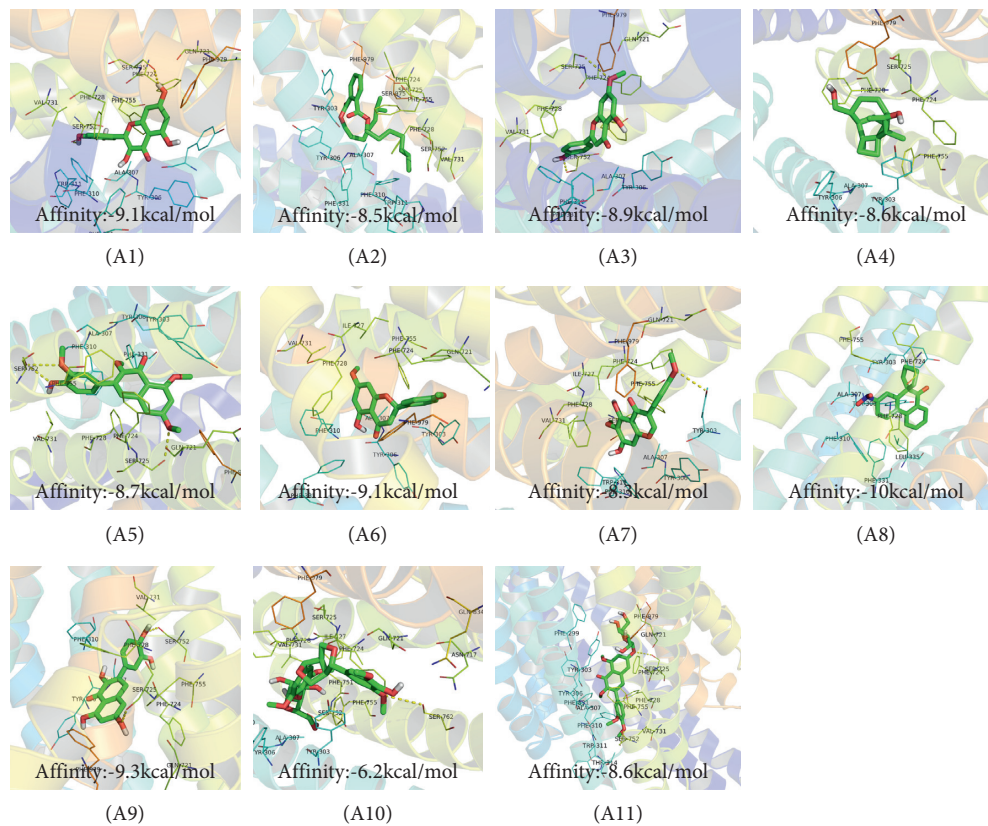


FIGURE 1: Continued.

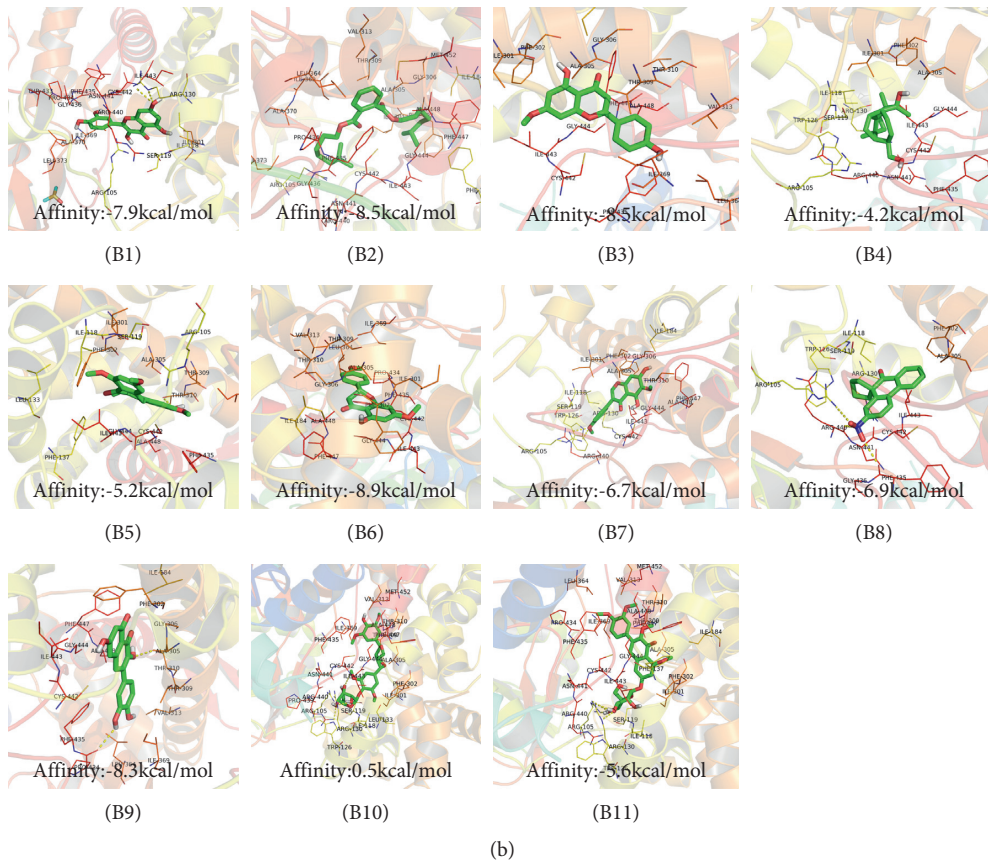


FIGURE 1: The 11 active components of CPB docked with P-gp and CYP3A4 molecules. (a) P-gp. (b) CYP3A4. 1, quercetin; 2, Diop; 3, genkwanin; 4; patchoulan 1,12-diol; 5, pachypodol; 6, 5-hydroxy-7,4'-dimethoxyflavanone; 7, irisolidone; 8, phenanthrone; 9, quercetin 7-O-β-D-glucoside; 10, acanthoside B; 11, 3,23-dihydroxy-12-oleanen-28-oic acid. A1, A3, A5, A7, A9, A10, A11, B1, B5, B7, B8, B9, B10, and B11 are hydrogen bond links and short-range van der Waals forces or π interaction forces. A2, A4, A6, A8, B2, B3, B4, and B6 are short-range van der Waals forces or π interaction force connections.

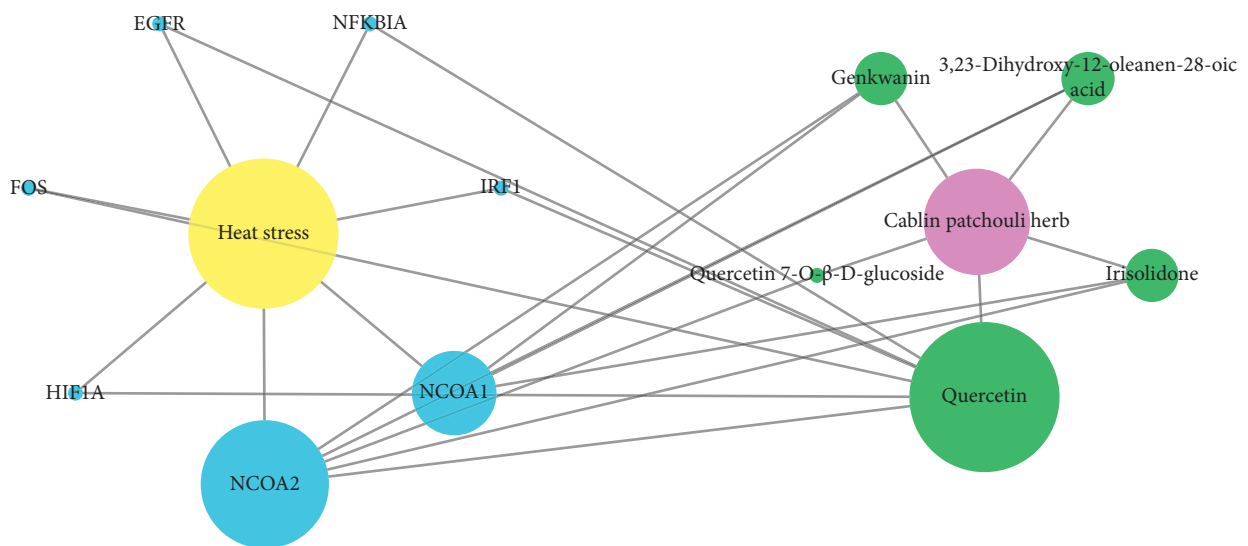


FIGURE 2: Drug-component-target-disease network. Blue represents targets, green represents drug molecules, magenta represents the drug, and yellow represents the disease. The size of each node represents its degree value: the larger the node is, the greater the degree value is.

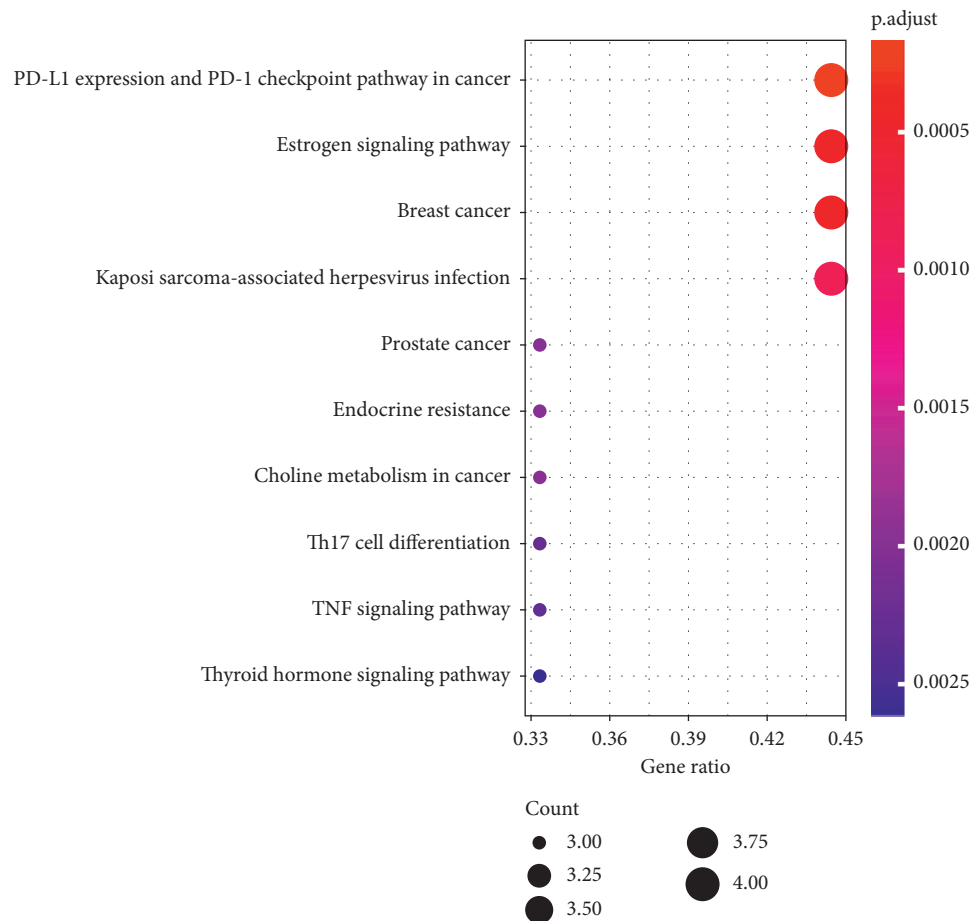


FIGURE 3: KEGG enrichment of CPB targets.

PD-L2 (B7-DC) represent the current main research directions with respect to immune checkpoint molecules [44]. The expression of PD-L1 is induced by a variety of proinflammatory factors (including type I and type II IFN- γ , IL-1 β , TNF- α , LPS, and so on) [45, 46]. Proinflammatory factors are indispensable factors in the process of tumor formation and the main factors that cause fever in the human body. In conclusion, our research found that CPB may exert a certain regulatory effect on PD-L1 expression and the PD-1 checkpoint in cancer pathway.

Estrogen is a female steroid compound secreted by organs such as the ovaries and placenta. There are mainly three forms: estrone, estradiol, and estriol [47]. Previous studies have shown that estrogen can not only regulate reproductive behavior through estrogen receptors but also exert an important effect on the central nervous system [48]. Although the specific mechanism remains unclear, studies have shown that estrogen has a huge effect on body temperature regulation. The evidence includes the following: estrogen or related estrogen receptor ligand therapy can lower core temperature [49]; compared with ovariectomized rats that received estrogen, the temperature of skin vasodilation in ovariectomized rats was 4° lower [50]; the state of estrogen deficiency will increase the sensitivity of the thermal defense pathway, leading to the activation of heat loss effect factors at lower ambient temperatures [51].

3.6. PPI Network. As the agents of cell activity and function, proteins do not exist independently. The interactions between proteins play important roles in each stage of life and maintain the steady state of the internal environment. To analyze the interaction modes of the CPB target proteins and the targets of the two signaling pathways enriched by the KEGG analysis, the cancer and estrogen signaling pathways, a PPI network of the CPB target proteins was constructed, as shown in Figure 4.

Among them, EGFR, NCOA1, and FOS are involved in two pathways. Epidermal growth factor receptor (EGFR) is a transmembrane glycoprotein that is one of the four members of the ErbB family of tyrosine kinase receptors. The activation of EGFR leads to the autophosphorylation of receptor tyrosine kinase, which triggers a series of downstream signaling pathways and participates in the regulation of cell proliferation, differentiation, and survival. EGFR is abnormally activated through various mechanisms, such as receptor overexpression, mutation, ligand-dependent receptor dimerization, and ligand-independent activation, and is associated with the occurrence of various human cancers. EGFR inhibition is one of the key targets of cancer chemotherapy [52]. Nuclear receptor coactivators (NCOAs) are multifunctional transcriptional coregulators of a growing number of signal-activated transcription factors. The members of the p160 family (NCOA1/2) are increasingly

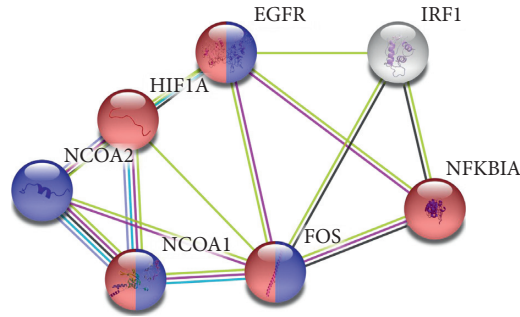


FIGURE 4: CPB target PPI network. Red indicates target proteins involved in cancer-related pathways; blue indicates target proteins involved in estrogen signaling.

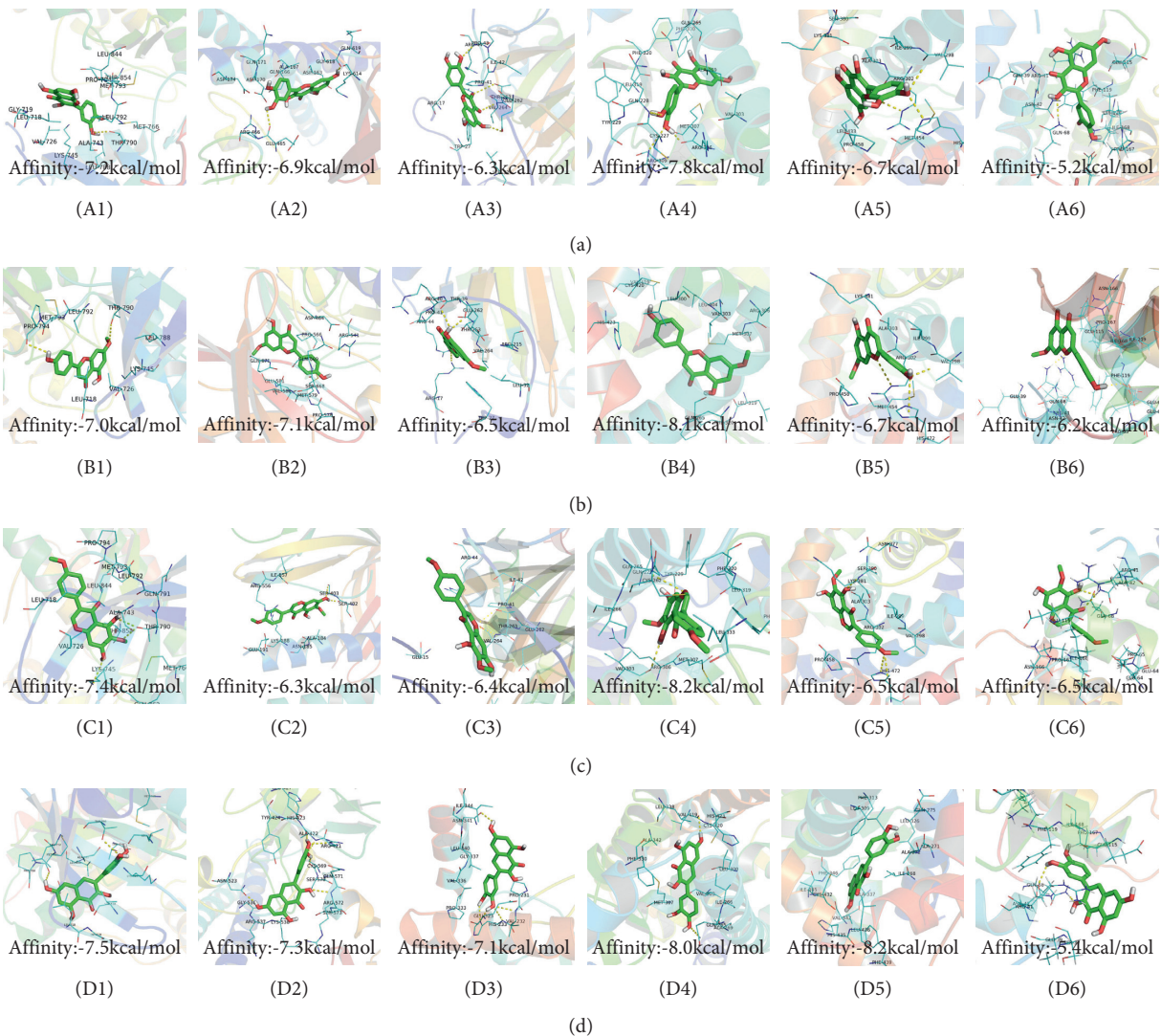


FIGURE 5: Continued.

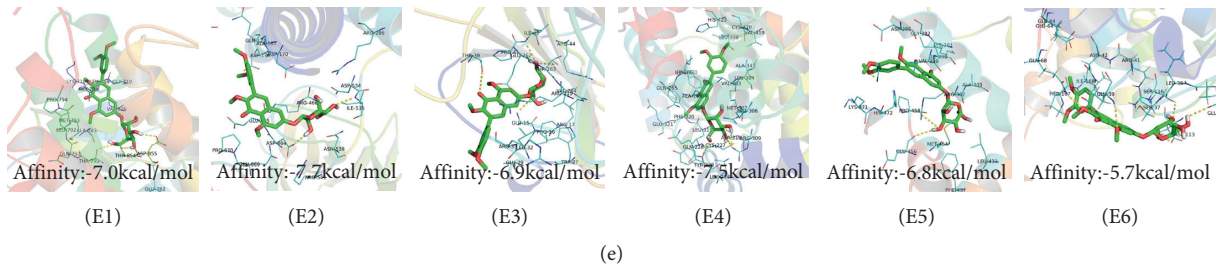


FIGURE 5: Docking results of CPB components and target molecules. (a) Quercetin. (b) Genkwanin. (c) Irisolidone. (d) Quercetin 7-O-β-D-glucoside. (e) 3,23-Dihydroxy-12-oleanen-28-oic acid. 1, EGFR; 2, FOS; 3, HIF1A; 4, NCOA1; 5, NCOA2; 6, NFKBIA. A1, A2, A3, A4, A5, A6, B1, B3, B5, B6, C1, C2, C3, C4, C5, C6, D1, D2, D3, D4, D6, E1, E2, E3, E4, E5, and E6 are hydrogen bond links and short-range van der Waals forces or π interaction forces. B2, B4, and D5 are short-range van der Waals forces or π interaction force connections.

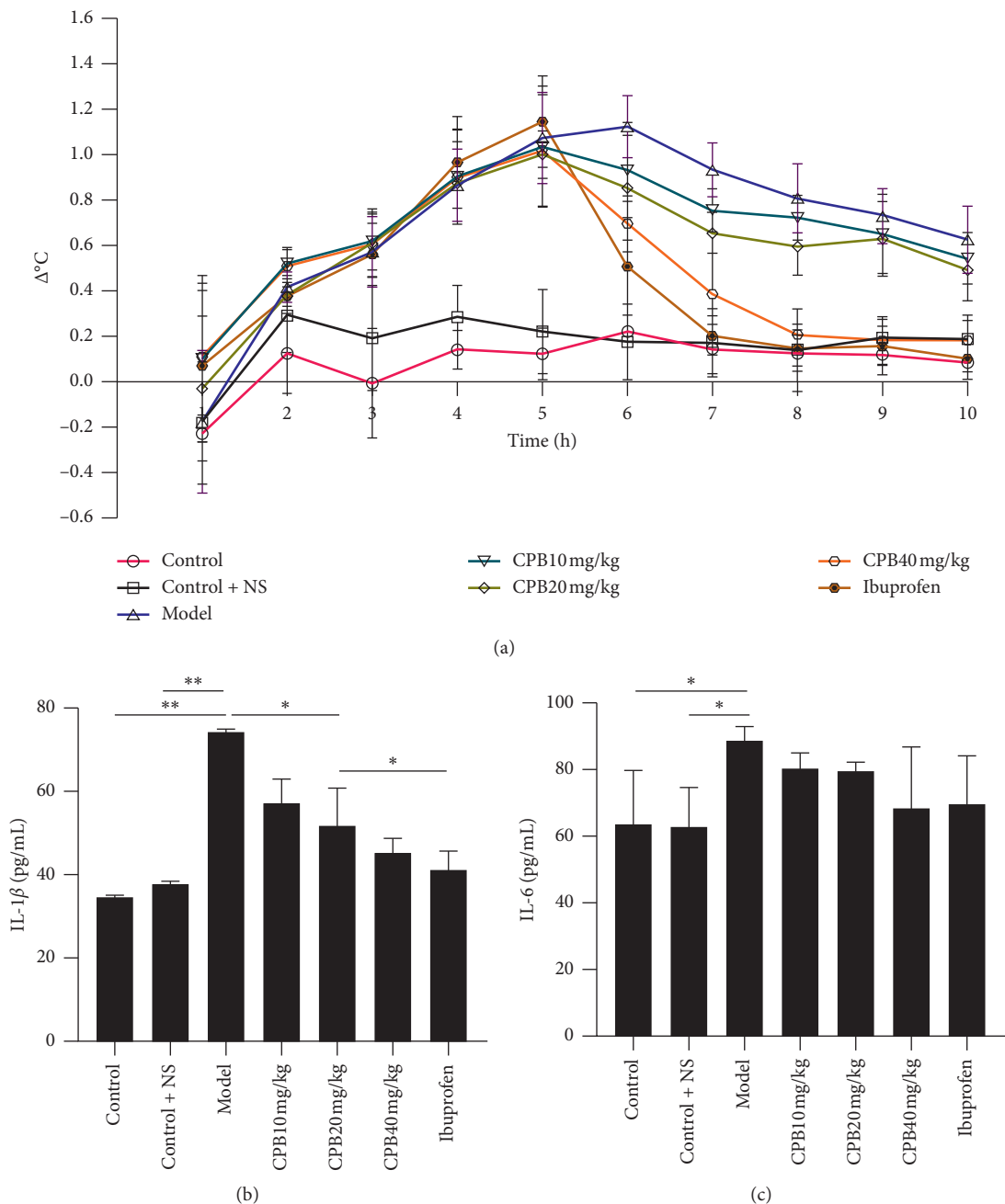


FIGURE 6: Continued.

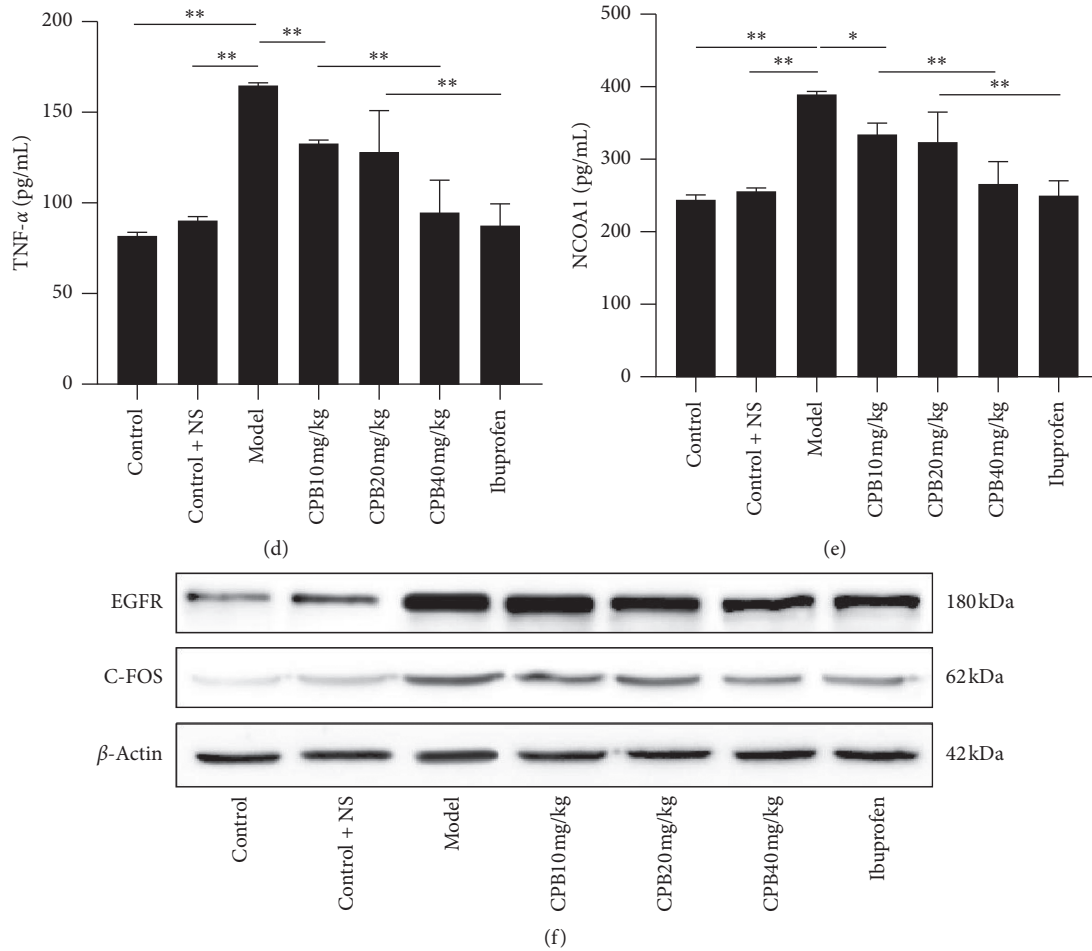


FIGURE 6: The effect of CPB on rats. (a) CPB on the body temperature of rats. (b) CPB on the amount of IL-1 β in rat serum. (c) CPB on the amount of IL-6 in rat serum. (d) CPB on the amount of TNF- α in rat serum. (e) CPB on the amount of NCOA1 in rat serum. (f) CPB on EGFR and C-FOS protein.

recognized as essential and nonredundant players in a number of physiological processes [53]. This family has been shown to be related to cancer [54] and inflammation and metabolism [53]. FOS is a nuclear phosphoprotein encoded by mature mRNA transcribed from the *c-fos* gene and is closely related to seizures [55] and cancer [56]. Hypoxia-inducible factor 1-alpha (HIF1A) is an oxygen-dependent transcriptional activator that plays key roles in tumor angiogenesis and mammalian development [57]. Finally, NFKBIA encodes inhibitors of nuclear factor- κ B (NF- κ B) that regulate the translation of genes involved in inflammatory and immune reactions [58, 59]. In conclusion, our results demonstrate that EGFR, NCOA1, FOS, HIF1A, NFKBIA, and NCOA2 may be the main targets of CPB.

3.7. Molecular Docking Verification. In the above, we showed that quercetin, genkwanin, irisolidone, 3,23-dihydroxy-12-oleanen-28-oic acid, and quercetin 7-O- β -D-glucoside are the main components of CPB. EGFR, NCOA1, FOS, HIF1A, NFKBIA, and NCOA2 are the main target proteins, which we analyzed to more clearly verify whether the components and the targets can actually interact. We

continued to use molecular docking technology for verification, and the results are shown in Figure 5. In short, the molecular docking verification of the 5 main components of CPB and the 6 main target proteins was successful.

3.8. Animal Experiment Verification. To further prove the availability of CPB, a rat model of fever was used to study CPB intragastric treatment. As shown in Figure 6(a), CPB at a concentration of 40 mg/kg showed a significant antipyretic effect after treatment. At the same time, we also measured the values of IL-1 β , IL-6, TNF- α , and NCOA1 in the blood. As shown in Figures 6(b), 6(d), and 6(e), CPB can reduce the levels of IL-1 β , TNF- α , and NCOA1 in rat serum. In Figure 6(c), the amount of IL-6 also seems to decrease, although it is not statistically significant. To further verify the conclusions we have reached, we used the protein expression in the rat hypothalamus to perform western blot verification. As shown in Figure 6(f), the expression of EGFR and C-FOS proteins in rats increased after modeling, but after CPB treatment, the expression of EGFR and C-FOS proteins decreased. In short, all animal experiments have successfully verified the conclusions we have reached.

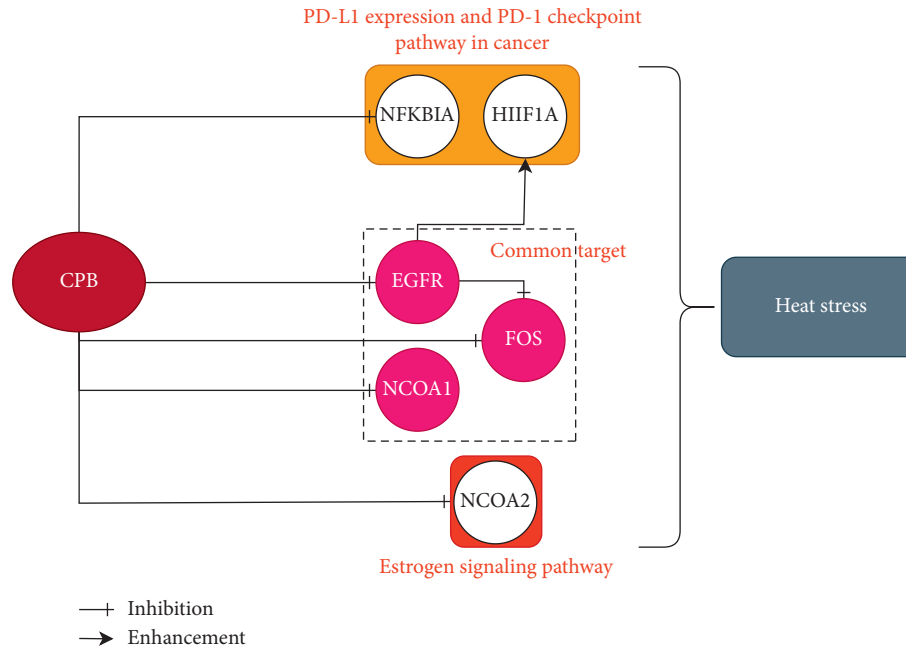


FIGURE 7: The target map of CPB for the treatment of heat stress.

4. Discussion

This study used network pharmacology combined with molecular docking. First, we collected the components and targets of CPB and screened them. Then, the ingredients were used for molecular docking with P-gp and CYP3A4 to initially verify that the active ingredients can be absorbed by the body. Then, we obtained genes which are differentially expressed during heat stress from the GEO database, constructed a drug-component-target-disease network, and further identified quercetin, genkwanin, irisolidone, 3,23-dihydroxy-12-oleanen-28-oic acid, and quercetin 7-O- β -D-glucoside as the main ingredients of CPB. We also constructed KEGG and PPI networks based on target information and proved that EGFR, NCOA1, FOS, HIF1A, NFKBIA, and NCOA2 are the main targets. Finally, the 5 active compounds were used to verify molecular docking with the 6 main targets.

To enhance the level of evidence for CPB in the treatment of heat stress, we continued to use febrile rats for experimental verification. We first proved that CPB can reduce the body temperature of febrile rats. The values of IL-1 β , TNF- α , and NCOA1 in the blood of rats also decreased. Western blot detection also found that EGFR and C-FOS proteins in the hypothalamus were reduced. We have also produced a map of the targets of CPB, as shown in Figure 7.

In conclusion, our study shows that the main components of CPB as a treatment for heat stress are quercetin, genkwanin, irisolidone, 3,23-dihydroxy-12-oleanen-28-oic acid, and quercetin 7-O- β -D-glucoside. Its main targets are EGFR, NCOA1, FOS, HIF1A, NFKBIA, and NCOA2. Our study is the first network pharmacology study and experimental verification of the use of the traditional Chinese medicine CPB to treat heat stress; thus, this research has pioneering significance.

Data Availability

The research data used to support the findings of this study are included within the supplementary information files.

Conflicts of Interest

The authors declare that they have no conflicts of interest.

Authors' Contributions

Yan Xu and Lizhong Ding contributed equally to this study.

Acknowledgments

This study was supported by the National Key Research and Development Program of China (2017YFC1703202), the Jilin Scientific and Technological of Chinese Medicine Program (2019023), the Inheritance and Innovation of Chinese Medicine "Millions of Standouts" Project (the Project of Qihuang), the Inheritance Workroom of the Chinese Medicine Master Wang Lie, and the Jilin Scientific and Technological Program of Sanitation and Population Control (2018J106).

Supplementary Materials

Supplementary Table 1: 1789 heat stress differentially expressed genes. Supplementary Table 2: the CPB components and targets after correction. (*Supplementary Materials*)




References

- [1] J. C. Semenza, C. H. Rubin, K. H. Falter et al., "Heat-related deaths during the July 1995 heat wave in Chicago," *New England Journal of Medicine*, vol. 335, no. 2, pp. 84–90, 1996.
- [2] J.-M. Robine, S. L. K. Cheung, S. Le Roy et al., "Death toll exceeded 70,000 in Europe during the summer of 2003," *Comptes Rendus Biologies*, vol. 331, no. 2, pp. 171–178, 2008.
- [3] D. Barriopedro, E. M. Fischer, J. Luterbacher, R. M. Trigo, and R. García-Herrera, "The hot summer of 2010: redrawing the temperature record map of Europe," *Science*, vol. 332, no. 6026, pp. 220–224, 2011.
- [4] C. W. Mangus and T. L. Canares, "Heat-related illness in children in an era of extreme temperatures," *Pediatrics in Review*, vol. 40, no. 3, pp. 97–107, 2019.
- [5] D. J. Casa, L. E. Armstrong, R. Carter, R. Lopez, B. McDermott, and K. Scriber, "Historical perspectives on medical care for heat stroke, Part 1: ancient times through the nineteenth century," *Athletic Training & Sports Health Care*, vol. 2, no. 3, pp. 132–138, 2010.
- [6] C. R. Gomez, "Disorders of body temperature," *Neurologic Aspects of Systemic Disease Part II*, vol. 120, pp. 947–957, 2014.
- [7] A. Bouchama and J. P. Knochel, "Heat stroke," *New England Journal of Medicine*, vol. 346, no. 25, pp. 1978–1988, 2002.
- [8] J. R. Lepock, "Cellular effects of hyperthermia: relevance to the minimum dose for thermal damage," *International Journal of Hyperthermia*, vol. 19, no. 3, pp. 252–266, 2003.
- [9] D. Kültz, "Molecular and evolutionary basis of the cellular stress response," *Annual Review of Physiology*, vol. 67, no. 1, pp. 225–257, 2005.
- [10] K. Richter, M. Haslbeck, and J. Buchner, "The heat shock response: life on the verge of death," *Molecular Cell*, vol. 40, no. 2, pp. 253–266, 2010.
- [11] L. fusen, "Scraping and huoxiang zhengqi water for 48 cases of yin and heat," *Chinese Folk Remedies*, vol. 12, pp. 23–24, 1999.
- [12] X. Li, "Observation on the curative effect of Huoxiangzhengqi water rubbing the back to treat children with high fever (Chinese)," *Contemporary Clinical Medicine*, vol. 28, no. 3, pp. 1387–1388, 2015.
- [13] L. Y. Gu Fang and C. Rinan, "Huoxiang zhengqi water in treating 18 cases of children's heat rash (Chinese)," *Chinese Practical Journal of Rural Doctors*, vol. 9, 2005.
- [14] L. Chaobin and G. Wanzhou, "Discussion on huoxiang zhengqi water in treating heat stroke(Chinese)," *Shaanxi Traditional Chinese Medicine*, vol. 31, no. 12, p. 1668, 2010.
- [15] H. J. Zhao, L. P. Guo, F. W. Yang et al., "[Huoxiang Zhengqi formulas for treatment of gastrointestinal type cold:a systematic review and Meta-analysis]," *China Journal of Chinese Materia Medica*, vol. 42, no. 8, pp. 1495–1499, 2017.
- [16] Y. Liu, W. Liu, Q. X. Peng, J. L. Peng, L. Z. Yu, and J. L. Hu, "Protective effect of huoxiang zhengqi oral liquid on intestinal mucosal mechanical barrier of rats with postinfectious irritable bowel syndrome induced by acetic Acid," *Evidence-based Complementary and Alternative Medicine*, vol. 2014, Article ID 218383, 10 pages, 2014.
- [17] Z. Xu, "Modernization: one step at a time," *Nature*, vol. 480, no. 7378, pp. S90–S92, 2011.
- [18] S. Li and B. Zhang, "Traditional Chinese medicine network pharmacology: theory, methodology and application," *Chinese Journal of Natural Medicines*, vol. 11, no. 2, pp. 110–120, 2013.
- [19] S. Li, Z. Q. Zhang, L. J. Wu, X. G. Zhang, Y. D. Li, and Y. Y. Wang, "Understanding ZHENG in traditional Chinese medicine in the context of neuro-endocrine-immune network," *IET Systems Biology*, vol. 1, no. 1, pp. 51–60, 2007.
- [20] S. Li, "Network systems underlying traditional Chinese medicine syndrome and herb formula," *Current Bioinformatics*, vol. 4, no. 3, 2009.
- [21] S. Li, "[Network target: a starting point for traditional Chinese medicine network pharmacology]," *China Journal of Chinese Materia Medica*, vol. 36, no. 15, pp. 2017–2020, 2011.
- [22] S. Li, B. Zhang, and N. Zhang, "Network target for screening synergistic drug combinations with application to traditional Chinese medicine," *BMC Systems Biology*, vol. 5, no. 1, p. S10, 2011.
- [23] H. Li, L. Zhao, B. Zhang et al., "A network pharmacology approach to determine active compounds and action mechanisms of ge-gen-qin-lian decoction for treatment of type 2 diabetes," *Evidence-based Complementary and Alternative Medicine*, vol. 2014, Article ID 495840, 12 pages, 2014.
- [24] J. Ru, P. Li, J. Wang et al., "TCMSP: a database of systems pharmacology for drug discovery from herbal medicines," *Journal of Cheminformatics*, vol. 6, p. 13, 2014.
- [25] G. Yu, L.-G. Wang, Y. Han, and Q.-Y. He, "clusterProfiler: an R package for comparing biological themes among gene clusters," *OMICS: A Journal of Integrative Biology*, vol. 16, no. 5, pp. 284–287, 2012.
- [26] Z. F. Wang, Y. Q. Hu, Q. G. Wu, and R. Zhang, "Virtual screening of potential anti-fatigue mechanism of polygonati rhizoma based on network pharmacology," *Combinatorial Chemistry & High Throughput Screening*, vol. 22, no. 9, pp. 612–624, 2019.
- [27] M. Chuan, P. Cheng, L. Xinrui, X. liang, and Z. Qinmei, "Research progress on chemical constituents and pharmacological activities of patchouli (Chinese)," *Journal of Chengdu University of Traditional Chinese Medicine*, vol. 43, no. 1, pp. 72–80, 2020.
- [28] M. Pertino, J. A. Rodriguez, C. Theoduloz, I. Razmilic, and G. Schmeda-Hirschmann, "Gastroprotective activity and cytotoxic effect of cyperenoic acid derivatives," *The Journal of Pharmacy and Pharmacology*, vol. 58, no. 11, 2006.
- [29] Q. M. Zhou, C. Peng, X. H. Li, L. Guo, L. Xiong, and D. S. Lin, "[Study on constituents of the aerial parts of Pogostemon cablin]," *Journal of Chinese Medicinal Materials*, vol. 36, no. 6, pp. 915–918, 2013.
- [30] M. Swamy and U. Sinniah, "A comprehensive review on the phytochemical constituents and pharmacological activities of pogostemon cablin benth.: an aromatic medicinal plant of industrial importance," *Molecules: A Journal of Synthetic Chemistry and Natural Product Chemistry*, vol. 20, no. 5, 2015.
- [31] S. N. Ruan, Y. Lu, and D. F. Chen, "[Anti-complementary constituents of Pogostemon cablin]," *China Journal of Chinese Materia Medica*, vol. 38, no. 13, pp. 2129–2135, 2013.
- [32] M. Ramar, M. G. Rao, S. Veerappan, and B. Pemaiah, "Pogostemon hirsutus oil, rich in abietane diterpenes," *Natural Product Communications*, vol. 8, no. 12, 2013.
- [33] M. Miyazawa, Y. Okuno, S. Nakamura, and H. Kosaka, "Antimutagenic activity of flavonoids from Pogostemon cablin," *Journal of Agricultural and Food Chemistry*, vol. 48, no. 3, 2000.
- [34] V. Kumar, V. Shriram, R. Bhagat, T. Khare, S. Kapse, and N. Kadoo, "Phytochemical profile, anti-oxidant, anti-inflammatory, and anti-proliferative activities of Pogostemon deccanensis essential oils," *3 Biotech*, vol. 9, no. 1, p. 31, 2019.
- [35] Y. Yao, X. Zhang, Z. Wang et al., "Deciphering the combination principles of Traditional Chinese Medicine from a systems pharmacology perspective based on Ma-huang

- Decoction," *Journal of Ethnopharmacology*, vol. 150, no. 2, pp. 619–638, 2013.
- [36] M. Varma, Y. Ashokraj, C. S. Dey, and R. Panchagnula, "P-glycoprotein inhibitors and their screening: a perspective from bioavailability enhancement," *Pharmacological Research*, vol. 48, no. 4, pp. 347–359, 2003.
- [37] F. P. Guengerich, "Cytochrome P-450 3A4: regulation and role in drug metabolism," *Annual Review of Pharmacology and Toxicology*, vol. 39, no. 1, pp. 1–17, 1999.
- [38] Y. S. Kumar, D. Adukondalu, D. Sathish et al., "P-Glycoprotein- and cytochrome P-450-mediated herbal drug interactions," *Drug Metabolism And Drug Interactions*, vol. 25, no. 1-4, pp. 3–16, 2010.
- [39] Y. Wei, D. Zhou, J. Peng, L. Pan, and K. Tu, "Hot air treatment induces disease resistance through activating the phenylpropanoid metabolism in cherry tomato fruit," *Journal of Agricultural and Food Chemistry*, vol. 65, no. 36, pp. 8003–8010, 2017.
- [40] D. Xu, M. Hu, Y. Wang, and Y. Cui, "Antioxidant activities of quercetin and its complexes for medicinal application," *Molecules: A Journal of Synthetic Chemistry and Natural Product Chemistry*, vol. 24, no. 6, 2019.
- [41] T. Sjöblom, S. Jones, L. D. Wood et al., "The consensus coding sequences of human breast and colorectal cancers," *Science*, vol. 314, no. 5797, pp. 268–274, 2006.
- [42] T. R. Mosmann and S. Sad, "The expanding universe of T-cell subsets: Th1, Th2 and more," *Immunology Today*, vol. 17, no. 3, pp. 138–146, 1996.
- [43] W. Zou, "Immunosuppressive networks in the tumour environment and their therapeutic relevance," *Nature Reviews Cancer*, vol. 5, no. 4, pp. 263–274, 2005.
- [44] B. T. Fife and J. A. Bluestone, "Control of peripheral T-cell tolerance and autoimmunity via the CTLA-4 and PD-1 pathways," *Immunological Reviews*, vol. 224, no. 1, pp. 166–182, 2008.
- [45] A. Kondo, T. Yamashita, H. Tamura et al., "Interferon- γ and tumor necrosis factor- α induce an immunoinhibitory molecule, B7-H1, via nuclear factor- κ B activation in blasts in myelodysplastic syndromes," *Blood*, vol. 116, no. 7, pp. 1124–1131, 2010.
- [46] M. Sznol and L. Chen, "Antagonist antibodies to PD-1 and B7-H1 (PD-L1) in the treatment of advanced human cancer," *Clinical Cancer Research*, vol. 19, no. 5, pp. 1021–1034, 2013.
- [47] B. Li, J. Zhao, J. Lv et al., "Additive antidepressant-like effects of fasting with imipramine via modulation of 5-HT₂ receptors in the mice," *Progress in Neuro-Psychopharmacology and Biological Psychiatry*, vol. 48, pp. 199–206, 2014.
- [48] J.-Å. Gustafsson, "What pharmacologists can learn from recent advances in estrogen signalling," *Trends in Pharmacological Sciences*, vol. 24, no. 9, pp. 479–485, 2003.
- [49] T. A. Roepke, M. A. Bosch, E. A. Rick et al., "Contribution of a membrane estrogen receptor to the estrogenic regulation of body temperature and energy homeostasis," *Endocrinology*, vol. 151, no. 10, pp. 4926–4937, 2010.
- [50] P. A. Dacks and N. E. Rance, "Effects of estradiol on the thermoneutral zone and core temperature in ovariectomized rats," *Endocrinology*, vol. 151, no. 3, pp. 1187–1193, 2010.
- [51] N. E. Rance, P. A. Dacks, M. A. Mittelman-Smith, A. A. Romanovsky, and S. J. Krajewski-Hall, "Modulation of body temperature and LH secretion by hypothalamic KNDy (kisspeptin, neurokinin B and dynorphin) neurons: a novel hypothesis on the mechanism of hot flushes," *Frontiers in Neuroendocrinology*, vol. 34, no. 3, pp. 211–227, 2013.
- [52] D. Singh, B. Kumar Attri, R. Kaur Gill, and J. Bariwal, "Review on EGFR inhibitors: critical updates," *Mini-Reviews in Medicinal Chemistry*, vol. 16, no. 14, pp. 1134–1166, 2016.
- [53] D. A. Rollins, M. Coppo, and I. Rogatsky, "Minireview: nuclear receptor coregulators of the p160 family: insights into inflammation and metabolism," *Molecular Endocrinology*, vol. 29, no. 4, pp. 502–517, 2015.
- [54] S. A. Oñate, S. Y. Tsai, M. J. Tsai, and B. W. O'Malley, "Sequence and characterization of a coactivator for the steroid hormone receptor superfamily," *Science (New York, N.Y.)*, vol. 270, no. 5240, pp. 1354–1357, 1995.
- [55] D. G. Herrera and H. A. Robertson, "Activation of c-fos in the brain," *Progress in Neurobiology*, vol. 50, no. 2-3, pp. 83–107, 1996.
- [56] A. Krishna, M. Bhatt, V. Singh et al., "Differential expression of c-fos proto-oncogene in normal oral mucosa versus squamous cell carcinoma," *Asian Pacific Journal of Cancer Prevention: APJCP*, vol. 19, no. 3, pp. 867–874, 2018.
- [57] J.-W. Lee, S.-H. Bae, J.-W. Jeong, S.-H. Kim, and K.-W. Kim, "Hypoxia-inducible factor (HIF-1) α : its protein stability and biological functions," *Experimental & Molecular Medicine*, vol. 36, no. 1, pp. 1–12, 2004.
- [58] G. L. Zhang, Y. F. Zou, X. L. Feng et al., "Association of the NFKBIA gene polymorphisms with susceptibility to autoimmune and inflammatory diseases: a meta-analysis," *Inflammation research: official journal of the European Histamine Research Society*, vol. 60, no. 1, pp. 11–18, 2011.
- [59] M. Zhang, J. Huang, X. Tan et al., "Common polymorphisms in the NFKBIA gene and cancer susceptibility: a meta-analysis," *Medical Science Monitor*, vol. 21, pp. 3186–3196, 2015.

Research Article

Design and Synthesis of 4-O-Podophyllotoxin Sulfamate Derivatives as Potential Cytotoxic Agents

Ammar Bader ¹, **Majdi M. Bkhaitan** ^{1,2}, **Ashraf N. Abdalla** ¹,
Qasem M. A. Abdallah ^{3,4}, **Hamed I. Ali** ⁵, **Dima A. Sabbah** ⁶, **Ghadeer Albadawi** ⁶,
and **Ghassan M. Abushaikha** ⁶

¹Umm Al-Qura University, Makkah 21955, Saudi Arabia

²Biomedical Sciences Unit, Arab American University, Jenin, State of Palestine

³Department of Pharmacology and Toxicology, College of Pharmacy, Taif University, Taif, Saudi Arabia

⁴Faculty of Pharmacy and Medical Sciences, University of Petra, Amman, Jordan

⁵Rangel College of Pharmacy, Health Science Center, Texas A&M University, Kingsville, TX 78363, USA

⁶Department of Pharmacy, Al-Zaytoonah University of Jordan, P.O. Box 130, Amman 11733, Jordan

Correspondence should be addressed to Ammar Bader; ammarosio@yahoo.it

Received 13 November 2020; Revised 25 December 2020; Accepted 9 January 2021; Published 27 January 2021

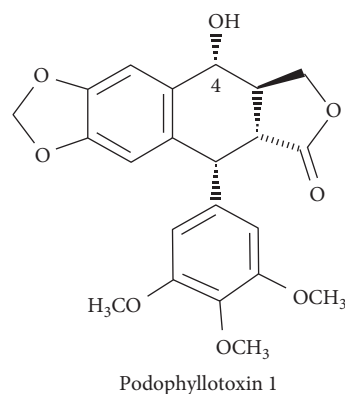
Academic Editor: Akhilesh K. Tamrakar

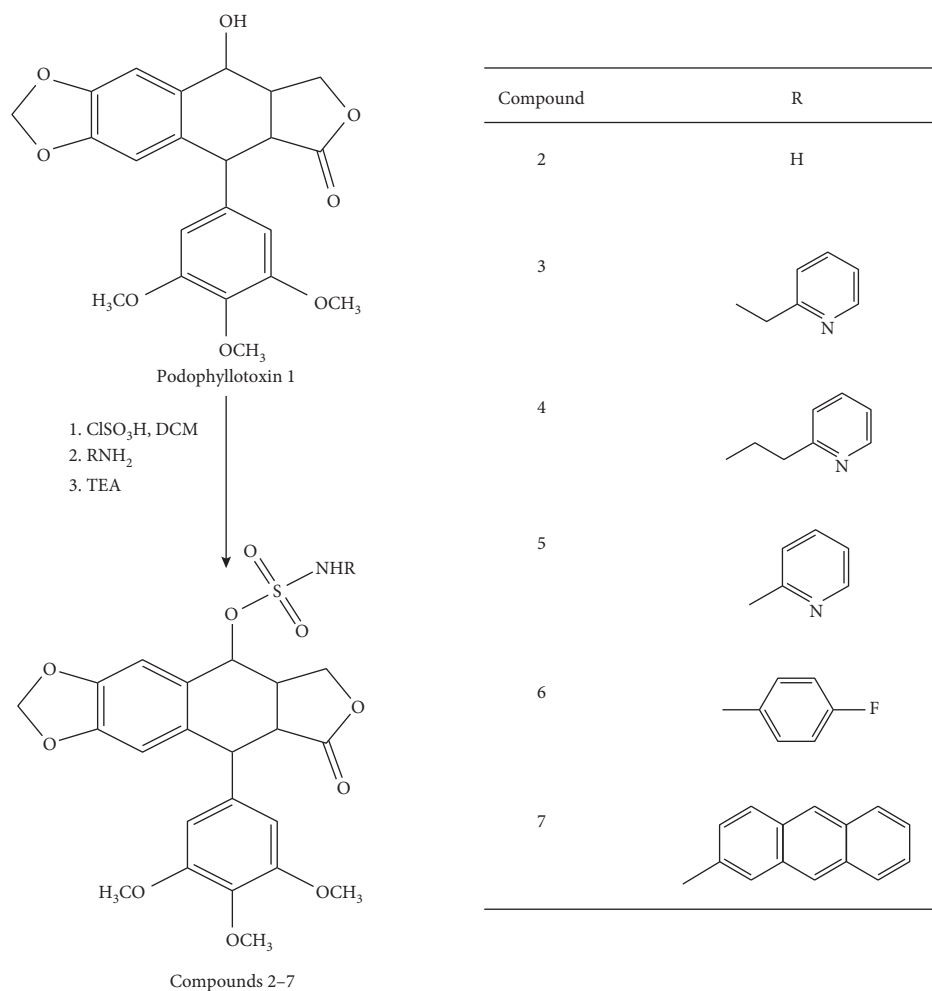
Copyright © 2021 Ammar Bader et al. This is an open access article distributed under the Creative Commons Attribution License, which permits unrestricted use, distribution, and reproduction in any medium, provided the original work is properly cited.

4-O-Podophyllotoxin sulfamate derivatives were prepared using the natural lignan podophyllotoxin. The prepared compounds were afforded by reacting O-sulfonyl chloride podophyllotoxin with ammonia or aminoaryl/heteroaryl motif. Biological evaluation was performed in human breast cancer (MCF7), ovarian cancer (A2780), colon adenocarcinoma (HT29), and normal lung fibroblast (MRC5) cell lines. Compound 3 exhibited potent inhibitory activity and good selectivity margin. Compounds 2, 3, and 7 exerted apoptotic effect in MCF7 cells in a dose-dependent manner. The cytotoxicity of the verified compounds was inferior to that of podophyllotoxin.

1. Introduction

Podophyllotoxin 1 (PPT) is a natural lignan of the aryl tetralin class and the main component of *Podophyllum peltatum* L., and it was used in folk medicine since remote times [1, 2]. It is generally considered as an effective anti-cancer agent with the ability to inhibit microtubules assembly by interacting with the tubulin proteins at the same binding site of colchicine, preventing the formation of the mitotic spindle [3, 4].





SCHEME 1: Synthesis of compounds 2-7.

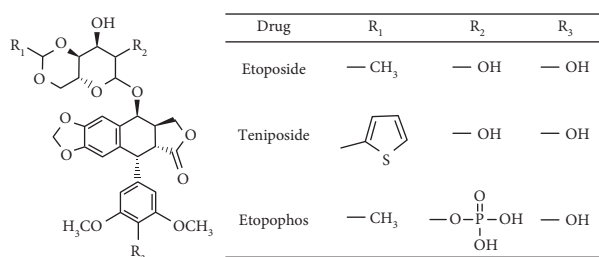


FIGURE 1: Podophyllotoxin derivatives in clinical use.

Serious adverse effects, including nausea, vomiting, diarrhea, abdominal pain, thrombocytopenia, leucopenia, cytotoxicity, and lack of oocytes maturation, were documented for PPT [5-7]. In addition, PPT suffers from poor water solubility and poor pharmacokinetic properties, limiting its wide spread in clinical use [8]. Nevertheless, due to its extraordinary biological activity and longtime use in traditional medicine, PPT and 4'-demethylpodophyllotoxin will continue to represent an important lead in the development of new active entities [9-13].

Multiple structural modifications were made on podophyllotoxin structure to improve the potency and

pharmacokinetic properties as well as to overcome drug resistance. In particular, the C-4 position has represented a primary target for these modifications [8, 11]. As a matter of fact, multiple in vitro and in silico studies have demonstrated that C-4 molecular area is suitable to lodge significant structural varieties [10, 14]. These efforts were crowned by the preparation and introduction of potent derivatives such as the highly prescribed anticancer drugs etoposide, teniposide, and the prodrug etopophos (Figure 1) [15].

It is worth mentioning that the cytotoxic mechanism of these derivatives is linked to their inhibition of topoisomerase II (topo II), inducing cell death, by enhancing the topo II-mediated DNA cleavage through the stabilization of the transitory DNA/topo II cleavage complex [16]. These agents including etoposide were associated with numerous limitations such as cytotoxicity toward normal cells, drug resistance, and poor bioavailability [17, 18].

Recently, the design of 4-substituted podophyllotoxin derivatives containing sulfonamide groups was reported [19]. This study exploited the diverse physical, chemical, and biological properties of reported derivatives, in particular, compound (A) in Figure 2; an *N*-(aminosulfonyl)-4-podophyllotoxin carbamate derivative demonstrated high in vitro

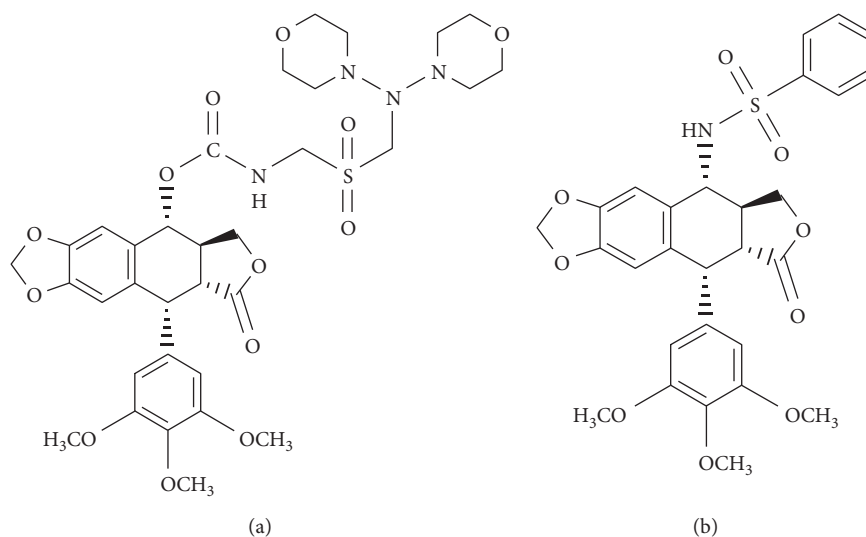


FIGURE 2: (a) *N*-(aminosulfonyl)-4-podophyllotoxin carbamate derivative; (b) 4-sulphonamide derivatives.

antiproliferative activity against tumor cell lines such as cervix carcinoma (HeLa), lung carcinoma (A-549), ileocecal carcinoma (HCT-8), and liver carcinoma (HepG2) cell lines, whereas low toxicity against the normal lung (WI-38) cell line. Biological data showed that the derivatives inhibit tubulin polymerization and microtubule assembly in HeLa cells [19]. In another study, 4-sulfonylamino derivatives exemplified by compound B in Figure 2 exerted highly potent cytotoxicity against human prostate (DU145), colon (HT29), breast (MCF7), multidrug-resistant breast (MCF7/ADR), lung (NCI-H460), and brain (U251) cancer cell lines [20]. In addition, a novel series of C-4 β -disulfide/trisulfide-containing podophyllotoxin derivatives showed good anticancer activity against oral cancer (KB/VCR) cell lines superior to that of etoposide [21]. This work reports the design and synthesis of 4-O-podophyllotoxin sulfamate derivatives having various substituents to afford more potent and less toxic compounds.

2. Materials and Methods

2.1. Chemicals. All chemicals, reagents, and solvents were of analytical grade and used directly without extra purification. Chloroform, methanol, cyclohexane, ethylacetate, dichloromethane (DCM), and triethylamine (TEA) were purchased from Fisher Scientific (UK) and Tedia Company (USA). Podophyllotoxin, chlorosulfonic acid, ammonia, 2-picolylamine(2-aminomethyl pyridine), 2-(2-aminoethyl) pyridine, 2-amino pyridine, 4-fluoroaniline, and 2-amino anthracene were purchased from Sigma-Aldrich (Germany).

2.2. Instruments. Nuclear Magnetic Resonance (NMR) charts were recorded by BRUKER 500 MHz Avance III. Chemical shifts are reported in ppm related to tetramethylsilane (TMS), internal standard. Deuterated chloroform (CDCl₃) was used as a solvent in sample preparation. ¹H-NMR data are reported as following: chemical shift (ppm), multiplicity, coupling constant (Hz), number of protons, and their corresponding proton(s). For initial identification of compounds, infrared (IR) spectra

were recorded using Shimadzu 8400 FT-IR spectrophotometer (Japan). All tested compounds were triturated with potassium bromide (KBr) and compressed into thin film discs (ACros, Belgium). The melting point (m.p) was measured using Gallenkamp melting point apparatus (Gallenkamp, UK). Thin layer chromatography (TLC) was performed on 20 × 20 cm aluminum plates precoated fluorescent silica gel GF254 (ALBET, Germany). The TLC was visualized under UV lamp, Spectroline® cabinet, Model CX-20 (USA), at 254 and/or 360 nm. For the efficient and gentle removal of solvents from the samples, Rotavapor model R-114 (Buchi, Switzerland) was used.

2.3. Synthesis

2.3.1. General Procedure for the Synthesis of Compounds 2–7.

To a stirred solution of **1** (1.0 mmol) in dry dichloromethane (CH₂Cl₂) (10 mL) cooled in ice bath, chlorosulfonic acid (ClSO₃H) (1.5 mmol) solution in dry CH₂Cl₂ (10 mL) was added cautiously drop wise. After stirring for 1 h at room temperature, ammonia or aryl amines (2.0 mmol) were added. The mixture was reacted for 1–4 h at room temperature. Then, triethylamine (TEA) (3.0 mmol) was added and filtered. The filtrate was evaporated to dryness, and the crude residue was purified by column chromatography on silica gel with cyclohexane-ethylacetate to afford compounds 2–7, Scheme 1.

2.3.2. 4-O-Podophyllotoxin Sulfamate (2). White powder (44%); m.p 234°C; *R*_f = 0.7 in (chloroform: methanol, 98 : 2); ¹H-NMR (400 Hz, CDCl₃): δ = 3.23 (m, 1H), 3.74 (s, 6H, 2xOCH₃), 3.80 (s, 3H, OCH₃), 4.60 (m, 1H), 5.70 (m.1H), 4.77 (d, *J* = 5.20 Hz, 1H), 5.95 (br s, 2H, NH₂), 6.20 (d, *J* = 7.20 Hz, 2H), 6.35 (s, 2H, methylenedioxy), 6.50 (s, 1H, Ar-H), 7.17 (s, 2H, Ar-H), 7.32 (s, 1H, Ar-H) ppm; ¹³C-NMR (CDCl₃): δ = 29.7 (1C), 45.0 (1C), 46.5 (1C), 50.6 (1C), 56.0 (1C), 56.3 (2C), 60.9 (1C), 62.2 (1C), 101.2 (1C), 106.1 (2C), 106.6 (1C), 112.0 (1C), 128, 8 (1C), 134.5 (1C), 140.0

(1C), 146.1 (1C), 147.6 (1C), 150.1 (1C), 153.3 (1C), 178.4 (1C) ppm; IR (KBr disc): $\nu = 3350$ (NH₂ sulfamate), 1730 (CO-g-lactone), 1600 (OSO₂), 1430 (OSO₂) cm⁻¹.

2.3.3. 4-N-(2-Pyridinylmethyl)podophyllotoxin Sulfamate (3). White powder (31%); m.p 230°C; $R_f = 0.75$ in (chloroform: methanol, 98 : 2); ¹H-NMR (400 Hz, CDCl₃): $\delta = 3.0$ (s, 2H), 3.15 (m, 1H), 3.74 (s, 6H, 2xOCH₃), 3.80 (s, 3H, OCH₃), 4.60 (m, 1H), 5.55 (m, 1H), 4.77 (d, $J = 5.18$ Hz, 1H), 5.75 (br s, 1H, NH), 6, 15 (m, 1H), 6.20 (d, $J = 7.15$ Hz, 2H), 6.25 (m, 1H), 6.35 (s, 2H, methylenedioxy), 6.50 (s, 1H, Ar-H), 7.07 (s, 2H, Ar-H), 7.15 (s, 1H, Ar-H), 7.40 (m, 1H), 7, 45 (m, 1H) ppm; ¹³C-NMR (CDCl₃): $\delta = 24$ (1C), 29.7 (1C), 45.0 (1C), 46.5 (1C), 50.6 (1C), 56.2 (1C), 57.9 (2C), 60.9 (1C), 67.4 (1C), 101.5 (1C), 108.3 (2C), 109.6 (1C), 111.0 (1C), 128.8 (1C), 134.5 (1C), 137.2 (1C), 140.0 (1C), 143.6 (1C), 146.1 (1C), 147.6 (1C), 148.2 (1C), 150.1 (1C), 152.5 (1C), 153, 1 (1C), 154.0 (1C), 175.0 (1C) ppm; IR (KBr disc): $\nu = 3310$ (NH₂ sulfamate), 1710 (CO-g-lactone), 1570 (OSO₂), 1410 (OSO₂) cm⁻¹.

2.3.4. 4-N-(2-Pyridinylethyl)podophyllotoxin Sulfamate (4). White powder (20%); m.p 225°C; $R_f = 0.8$ in (chloroform: methanol, 98 : 2); ¹H-NMR (400 Hz, CDCl₃): $\delta = 2.05$ (m, 2H), 2.78 (m, 2H), 3.05 (m, 1H), 3.74 (s, 6H, 2xOCH₃), 3.80 (s, 3H, OCH₃), 4.50 (m, 1H), 5.25 (m, 1H), 4.77 (m, 1H), 5.75 (br s, 1H, NH), 6, 10 (m, 1H), 6.15 (m, 2H), 6.17 (m, 1H), 6.30 (s, 2H, methylenedioxy), 6.41 (s, 1H, Ar-H), 6.90 (s, 2H, Ar-H), 7.0 (s, 1H, Ar-H), 7.23 (m, 1H), 7, 30 (m, 1H) ppm; ¹³C-NMR (CDCl₃): $\delta = 14.1$ (1C), 22.7 (1C), 29.2 (1C), 42.8 (1C), 46.1 (1C), 50.3 (1C), 56.2 (1C), 56.3 (2C), 60.8 (1C), 67.1 (1C), 101.3 (1C), 107.7 (2C), 109.6 (1C), 111.0 (1C), 128.8 (1C), 134.5 (1C), 137.2 (1C), 140.0 (1C), 143.6 (1C), 146.1 (1C), 147.3 (1C), 148.0 (1C), 150.1 (1C), 152.3 (1C), 153.0 (1C), 153.2 (1C), 167.0 (1C) ppm; IR (KBr disc): $\nu = 3300$ (NH₂ sulfamate), 1700 (CO-g-lactone), 1566 (OSO₂), 1410 (OSO₂) cm⁻¹.

2.3.5. 4-N-(2-Pyridinyl)podophyllotoxin Sulfamate (5). White powder (35%); m.p 230°C decomp.; $R_f = 0.73$ in (chloroform: methanol, 98 : 2); ¹H-NMR (400 Hz, CDCl₃): $\delta = 3.32$ (m, 1H), 3.80 (s, 6H, 2xOCH₃), 3.85 (s, 3H, OCH₃), 4.70 (m, 1H), 5.95 (m, 1H), 4.77 (m, 1H), 6.55 (br s, 1H, NH), 6.27 (m, 1H), 6.32 (m, 2H), 6.35 (m, 1H), 6.43 (s, 2H, methylenedioxy), 6.65 (s, 1H, Ar-H), 7.20 (s, 2H, Ar-H), 7.30 (s, 1H, Ar-H), 7.64 (m, 1H), 7, 75 (m, 1H) ppm; ¹³C-NMR (CDCl₃): $\delta = 31$ (1C), 45.5 (1C), 46.9 (1C), 52 (1C), 57 (1C), 58.7 (2C), 63 (1C), 68.2 (1C), 101.7 (1C), 108.8 (2C), 110.7 (1C), 112.0 (1C), 129.4 (1C), 134.9 (1C), 137.7 (1C), 140.6 (1C), 144.4 (1C), 147 (1C), 148.3 (1C), 149 (1C), 150.4 (1C), 153.3 (1C), 154 (1C), 154.7 (1C), 177.2 (1C) ppm; IR (KBr disc): $\nu = 3390$ (NH₂ sulfamate), 1730 (CO-g-lactone), 1620 (OSO₂), 1460 (OSO₂) cm⁻¹.

2.3.6. 4-N-(4-Fluorophenyl)podophyllotoxin Sulfamate (6). White powder (20%); m.p 220°C; $R_f = 0.8$ in (chloroform: methanol, 98 : 2); ¹H-NMR (400 Hz, CDCl₃): $\delta = 3.0$ (m, 1H), 3.76 (s, 6H, 2xOCH₃), 3.82 (s, 3H, OCH₃), 4.64 (m, 1H), 5.62 (m, 1H), 4.74 (m, 1H), 5.95 (br s, 1H, NH), 6.30 (m, 1H), 6.27

(d, $J = 5.30$ Hz, 2H), 6.32 (d, $J = 6.10$ Hz, 2H, Ar-H), 6.40 (s, 2H, methylenedioxy), 6.55 (d, $J = 6.15$ Hz, 2H, Ar-H), 7.10 (s, 2H, Ar-H), 7.21 (s, 1H, Ar-H) ppm; ¹³C-NMR (CDCl₃): $\delta = 30.7$ (1C), 45.4 (1C), 46.8 (1C), 51 (1C), 56.6 (1C), 58.3 (2C), 61.2 (1C), 67.8 (1C), 102.3 (1C), 108.6 (2C), 109.9 (1C), 111.3 (1C), 129.2 (1C), 134.8 (1C), 137.6 (1C), 140.9 (1C), 144 (1C), 146.5 (1C), 148.2 (1C), 148.7 (1C), 150.1 (1C), 152.7 (1C), 153.4 (1C), 154.3 (1C), 156.7 (1C), 176.0 (1C) ppm; IR (KBr disc): $\nu = 3330$ (NH₂ sulfamate), 1710 (CO-g-lactone), 1570 (OSO₂), 1430 (OSO₂) cm⁻¹. This compound was unstable, and it was excluded from the biological assay.

2.3.7. 4-N-(2-Anthracenyl)podophyllotoxin Sulfamate (7). White powder (58%); m.p 246°C decomp.; $R_f = 0.89$ in (chloroform: methanol, 98 : 2); ¹H-NMR (400 Hz CDCl₃): $\delta = 3.08$ (m, 1H), 3.77 (s, 6H, 2xOCH₃), 3.81 (s, 3H, OCH₃), 4.64 (m, 1H), 4.89 (m, 1H), 3.81 (m, 1H), 5.96 (br s, 1H, NH), 4.64 (m, 2H), 6.25 (m, 1H, Ar-H), 6.35 (s, 2H, methylenedioxy), 6.55 (s, 1H), 6.83 (m, 2H, Ar-H), 7.09 (s, 1H), 7.43 (m, 1H), 7.52 (m, 2H), 7.82 (m, 1H), 7.91 (m, 2H), 8.11 (s, 1H, Ar-H), 8.26 (s, 1H, Ar-H) ppm; ¹³C-NMR (CDCl₃): $\delta = 29.7$ (1C), 45.9 (1C), 46.2 (1C), 50.3 (1C), 56.3 (1C), 58.0 (2C), 60.8 (1C), 69.0 (1C), 101.6 (1C), 108.4 (2C), 109.6 (1C), 110.8 (1C), 105.6 (1C), 120.9 (1C), 121 (1C), 123 (1C), 125.1 (1C), 125.8 (1C), 126, 5 (1C), 127 (1C), 128.4 (1C), 128.9 (1C), 129.2 (1C), 131.9 (1C), 133.6 (1C), 134.8 (1C), 137.6 (1C), 146.5 (1C), 148.2 (1C), 148.7 (1C), 150.1 (1C), 152.4 (1C), 152.9 (1C), 171.0 (1C) ppm; IR (KBr disc): $\nu = 3310$ (NH₂ sulfamate), 1680 (CO-g-lactone), 1575 (OSO₂), 1410 (OSO₂) cm⁻¹.

2.4. Cell Culture. Three cancer cell lines, human breast adenocarcinoma (MCF7), human ovary adenocarcinoma (A2780), and human colon adenocarcinoma (HT29), in addition the normal human fetal lung fibroblast (MRC5), were used. All cell lines were obtained from the ATCC. The three cancer cells were subcultured in RPMI-1640 media (10% FBS), while MRC5 was maintained in Eagles minimum essential medium (EMEM, 10% FBS), all at 37°C, 5% CO₂, and 100% relative humidity [22].

2.5. Cytotoxicity Assay. As previously reported [23, 24], the cytotoxicity of the six compounds, including podophyllotoxin as reference, was evaluated by the MTT assay. The three cell lines and one normal fibroblast cells were separately cultured in 96-well (3 × 10³/well) and incubated at 37°C overnight. Final compound concentrations are as follows: 0, 0.005, 0.050, 0.500, 5.000, and 25.000 μM (DMSO 0.1%; $n = 3$). Plates were incubated for 72 h, followed by addition of MTT to each well. Plates were incubated for 3 hr, supernatant was aspirated, and DMSO was added to each well. The absorbance was read on multiplate reader. The optical density of the purple formazan A₅₅₀ is proportional to the number of viable cells. Compound concentration causing 50% inhibition (IC₅₀) compared to control cell growth (100%) was determined. GraphPad Prism version 5.00 for

TABLE 1: Cytotoxic activity of the verified compounds (2, 3, 4, 5, and 7) (MTT 72 h, IC50 \pm SD μ M).

Compound	MCF7	A2780	HT29	MRC5
2	0.648 \pm 0.087	0.729 \pm 0.363	1.343 \pm 0.637	7.507 \pm 1.510
3	0.150 \pm 0.060*	0.179 \pm 0.010*	0.222 \pm 0.098*	2.027 \pm 0.250
4	0.212 \pm 0.010*	0.456 \pm 0.180*	0.228 \pm 0.075*	0.048 \pm 0.003**
5	0.184 \pm 0.052*	0.132 \pm 0.012*	1.048 \pm 0.005	0.047 \pm 0.042**
7	2.120 \pm 0.989	3.652 \pm 1.939	5.082 \pm 0.673	9.076 \pm 1.010
Podophyllotoxin	0.004 \pm 0.001***	0.007 \pm 0.001***	0.002 \pm 0.001***	0.043 \pm 0.060**

Data are representation of three independent experiments ($n=4$). Statistical difference (one-way ANOVA, Tukey's post hoc): $p < 0.05^*$, $p < 0.01^{**}$, and $p < 0.001^{***}$ were considered significant.

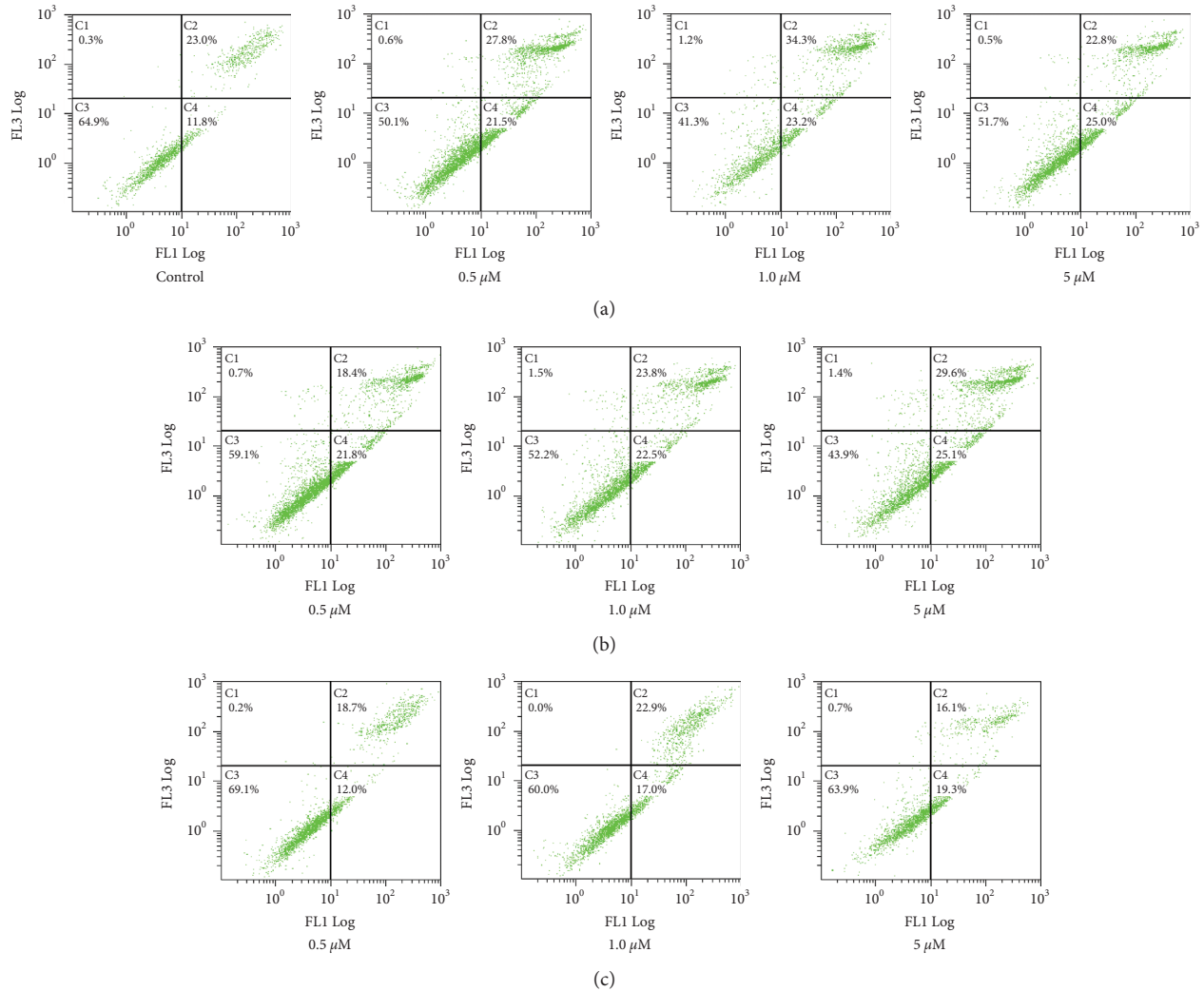


FIGURE 3: Histogram showing different phases of staining MCF7 cells with annexin V FITC/PI treated with vehicle control. Compounds (a) 2, (b) 3, and (c) 7, each in three concentrations, 24 h. X-axis: annexin (V); y-axis: PI. C1: (necrosis death, PI+/annexin V-); C2: (late apoptosis, PI+/annexin V+); C3: (living cells, PI-/annexin V-); C4: (early apoptosis, PI-/annexin V+). Experiment was repeated 2x.

Windows, GraphPad Software, San Diego California, USA, was used for analysis.

2.6. Annexin V FITC/PI Apoptosis Assay. Annexin V FITC/PI assay was used to evaluate possible ability to induce apoptosis [25]. MCF7 cells were cultured in 6 well plates

(1×10^5 cells/well) overnight at 37°C . Compounds **2**, **3**, and **7** were used to treat cells (0, 0.5, 1.0, and $5.0 \mu\text{M}$). After 24 h, the supernatant of treated cells was collected in tubes and kept in ice, and cells were trypsinized and incubated at 37°C before being added to the tubes. MCF7 cells were centrifuged (2000 rpm) and washed with PBS (x1), and pellets resuspended in the binding buffer ($100 \mu\text{L}$) and annexin V FITC

(10 μL). Tubes were incubated at room temperature in dark for 20 min, before adding binding buffer (400 μL) and 10 μL propidium iodide (PI). Analysis was performed by flow cytometry (BC, FC500, USA). Different cell populations (early apoptotic, late apoptotic, and necrotic cells) were identified by annexin V and PI staining.

3. Results and Discussion

3.1. Chemistry. The synthesis of podophyllotoxin sulfamates, compounds 2–7, was achieved by reaction of podophyllotoxin (1) with chlorosulfonic acid in dry dichloromethane (DCM) (Scheme 1). Then, the podophyllotoxin sulfonyl chloride intermediate derivatives were immediately treated with ammonia or with the corresponding aryl and heteroaryl amines in the presence of triethylamine (TEA). The structures of the target compounds 2–7 were identified by IR, $^1\text{H-NMR}$, and $^{13}\text{C-NMR}$ spectral analysis.

3.2. Cytotoxicity Assay. The cytotoxicity of the new podophyllotoxin derivatives against breast, ovarian, and colon cancer cells was evaluated using MTT assay. Additionally, one normal cell line was tested to assess the selectivity of the new derivatives. Compound 3 shows the highest activity against the three cell lines (0.150–0.220 μM), and it was 9.1–13.5-fold more selective against MCF7, A2780, and HT29 compared to MRC5 cells. Compound 2 also showed ≤ 1 μM activity against MCF7, A2780, and HT29, and it was less cytotoxic against MRC5 cells. Compounds 4 and 5 showed similar activity to 3, but they showed no selectivity against MRC5. Finally, compound 7 was the least active (IC_{50} : 2.120–5.082 μM), but it showed 2–4-fold selectivity against the normal cells. Compound 3 showed the comparable activity to podophyllotoxin (Table 1).

3.3. Annexin V FITC/PI Apoptosis Assay. Compounds 2, 3, and 7 were selected for further investigations to explain their mechanism of action. Annexin V FITC/PI assay was used to evaluate whether they can induce apoptosis or not in MCF7 cells, following 24 h treatment. Compounds 2, 3, and 7 increased the early apoptotic MCF7 cell populations in a dose-dependent manner (1.7–2.2-fold, compared to control), as shown in Figure 3.

The desired podophyllotoxin sulfamate derivatives were successfully prepared in a one-pot reaction in good yields. This novel method was developed in our lab applying the coupling reaction between the alcohol podophyllotoxin with excess chlorosulfonic acid affording a highly reactive O-sulfonyl chloride intermediates that are immediately subjected to sulfonamidation reactions with ammonia or amino/heteroaryl derivatives. The obtained compounds were identified by IR and ^1H and $^{13}\text{C-NMR}$ spectral data. The prepared compounds were evaluated for their cytotoxic activity against MCF7, A2780, and HT29, in addition to MRC5. All tested compounds showed cytotoxicity in the micromolar range but were less potent than podophyllotoxin, which was used as a reference. Compound 3 was the most potent derivative, and it exhibited a good selectivity

margin; in fact, it showed 9.1–13.5 times more cytotoxicity in cancer cells compared to normal MRC5 cells. Compounds 2 and 7 showed cytotoxicity with moderate selectivity. Consequently, compounds 2, 3, and 7 were also evaluated for their apoptotic inducing ability on MCF7 cells and showed activity in a dose-dependent manner that partially explains the mechanism of their activity. These results indicate that podophyllotoxin sulfamate derivatives are valid candidates for further development as anticancer agents.

4. Conclusion

Derivatives of 4-O-podophyllotoxin sulfamate were synthesized through a simple and direct one-pot methodology developed in our laboratory. The synthesized derivatives showed cytotoxicity in the micromolar concentrations. Compounds (2, 3, and 7) showed a dose dependent increase in apoptotic events. Yet, the activity of all compounds was inferior to that of podophyllotoxin. We are looking for optimizing the core structure of this scaffold and exploring the activity of these derivatives *in vivo* study to get insights about the efficacy and tolerability in animal models.

Data Availability

Data used to support the findings of this study are available from the corresponding author upon request.

Conflicts of Interest

The authors declare that they have no conflicts of interest pertaining to the publication of this paper.

Acknowledgments

This project was funded by the National Plan for Science, Technology, and Innovation (MAARIFAH), King Abdulaziz City for Science and Technology, Kingdom of Saudi Arabia (award number 12-MED2310-10), through Science and Technology Unit (STU) at Umm Al-Qura University.

Supplementary Materials

$^1\text{H-NMR}$ spectrum (500 MHz, CDCl_3) of podophyllotoxin and its derivatives: 2–7. Page 2: $^1\text{H-NMR}$ of compound 1: podophyllotoxin. Page 3: $^1\text{H-NMR}$ of compound 2: 4-O-podophyllotoxin sulfamate. Page 4: $^1\text{H-NMR}$ of compound 3: 4-N-(2-pyridinylmethyl)-podophyllotoxin sulfamate. Page 5: $^1\text{H-NMR}$ of compound 4: 4-N-(2-pyridinylethyl)-podophyllotoxin sulfamate. Page 6: $^1\text{H-NMR}$ of compound 5: 4-N-(2-pyridinyl)-podophyllotoxin sulfamate. Page 7: $^1\text{H-NMR}$ of compound 6: 4-N-(4-fluorophenyl)-podophyllotoxin sulfamate. Page 8: $^1\text{H-NMR}$ of compound 7: 4-N-(2-anthracenyl)-podophyllotoxin sulfamate. (*Supplementary Materials*)

References

- [1] D. E. Jackson and P. M. Dewick, "Aryltetralin lignans from *Podophyllum hexandrum* and *Podophyllum peltatum*," *Phytochemistry*, vol. 23, no. 5, pp. 1147–1152, 1984.

- [2] R. M. Moraes, E. Bedir, C. Burandt, C. Canel, and I. A. Khan, "Evaluation of *Podophyllum peltatum* accessions for podophyllotoxin production," *Planta Medica*, vol. 68, no. 4, pp. 341–344, 2002.
- [3] M. Jordan and K. Kamath, "How do microtubule-targeted drugs work? An overview," *Current Cancer Drug Targets*, vol. 7, no. 8, pp. 730–742, 2007.
- [4] J. D. Loike, C. F. Brewer, H. Sternlicht, W. J. Gensler, and S. B. Horwitz, "Structure-activity study of the inhibition of microtubule assembly in vitro by podophyllotoxin and its congeners," *Cancer Research*, vol. 38, no. 9, pp. 2688–2693, 1978.
- [5] W.-F. Kao, D.-Z. Hung, W.-J. Tsai, K.-P. Lin, and J.-F. Deng, "Podophyllotoxin intoxication: toxic effect of Bajiaolian in herbal therapeutics," *Human and Experimental Toxicology*, vol. 11, no. 6, pp. 480–487, 1992.
- [6] B. Meyer, N. Ferrigni, J. Putnam, L. Jacobsen, D. Nichols, and J. McLaughlin, "Brine shrimp: a convenient general bioassay for active plant constituents," *Planta Medica*, vol. 45, no. 5, pp. 31–34, 1982.
- [7] L. L. Hu, X. Zhou, H. L. Zhang et al., "Exposure to podophyllotoxin inhibits oocyte meiosis by disturbing meiotic spindle formation," *Scientific Reports*, vol. 8, pp. 1–8, 2018.
- [8] Y. Yang, J. Bteich, and S.-D. Li, "Current update of a carboxymethylcellulose-PEG conjugate platform for delivery of insoluble cytotoxic agents to tumors," *The AAPS Journal*, vol. 19, no. 2, pp. 386–396, 2017.
- [9] Y.-Q. Liu, J. Tian, K. Qian et al., "Recent progress on C-4-Modified podophyllotoxin analogs as potent antitumor agents," *Medicinal Research Reviews*, vol. 35, no. 1, pp. 1–62, 2015.
- [10] Z.-Z. Wang, W.-X. Sun, X. Wang et al., "Design, synthesis, biological evaluation, and 3D-QSAR analysis of podophyllotoxin-dioxazole combination as tubulin targeting anticancer agents," *Chemical Biology and Drug Design*, vol. 90, no. 2, pp. 236–243, 2017.
- [11] X. Zhang, K. P. Rakesh, C. S. Shantharam et al., "Podophyllotoxin derivatives as an excellent anticancer aspirant for future chemotherapy: a key current imminent needs," *Bioorganic and Medicinal Chemistry*, vol. 26, no. 2, pp. 340–355, 2018.
- [12] M. Bkhaitan, S. K. Bardaweel, G. Abushaikha, A. Z. Mirza, and K. A. Sweidan, "Synthesis and antiproliferative activity of 4 β -O -substituted, 4 β -N -substituted deoxypodophyllotoxin derivatives, and 4 β -O H- 4'-O -substituted podophyllotoxin," *ChemistrySelect*, vol. 5, no. 47, pp. 14924–14929, 2020.
- [13] L. Zhang, F. Chen, J. Wang et al., "Novel isatin derivatives of podophyllotoxin: synthesis and cytotoxic evaluation against human leukaemia cancer cells as potent anti-MDR agents," *RSC Advances*, vol. 5, no. 118, pp. 97816–97823, 2015.
- [14] M. M. Bkhaitan, A. Z. Mirza, H. Shamshad et al., "Identification of potent virtual leads and ADME prediction of isoxazolidine podophyllotoxin derivatives as topoisomerase II and tubulin inhibitors," *Journal of Molecular Graphics and Modelling*, vol. 73, pp. 74–93, 2017.
- [15] R. Ali, P. Hilgard, S. Florentine et al., "Current development of podophyllotoxins," *Cancer Chemotherapy and Pharmacology*, vol. 7, pp. 93–98, 1982.
- [16] E. Baldwin and N. Osheroff, "Etoposide, topoisomerase II and cancer," *Current Medicinal Chemistry-Anti-Cancer Agents*, vol. 5, no. 4, pp. 363–372, 2005.
- [17] T. F. Imbert, "Discovery of podophyllotoxins," *Biochimie*, vol. 80, no. 3, pp. 207–222, 1998.
- [18] M. Guerram, Z.-Z. Jiang, and L.-Y. Zhang, "Podophyllotoxin, a medicinal agent of plant origin: past, present and future," *Chinese Journal of Natural Medicines*, vol. 10, no. 3, pp. 161–169, 2012.
- [19] X.-H. Xu, X.-W. Guan, S.-L. Feng, Y.-Z. Ma, S.-W. Chen, and L. Hui, "One-pot synthesis and biological evaluation of N-(aminosulfonyl)-4-podophyllotoxin carbamates as potential anticancer agents," *Bioorganic & Medicinal Chemistry Letters*, vol. 27, no. 13, pp. 2890–2894, 2017.
- [20] A. Kamal, B. Ashwini Kumar, M. Arifuddin, and S. G. Dastidar, "Synthesis of 4 β -amido and 4 β -sulphonamido analogues of podophyllotoxin as potential antitumour agents," *Bioorganic and Medicinal Chemistry*, vol. 11, no. 23, pp. 5135–5142, 2003.
- [21] S.-J. Zhu, H.-Z. Ying, Y. Wu et al., "Design, synthesis and biological evaluation of novel podophyllotoxin derivatives bearing 4 β -disulfide/trisulfide bond as cytotoxic agents," *RSC Advances*, vol. 5, no. 125, pp. 103172–103183, 2015.
- [22] A. N. Abdalla, U. Shaheen, Q. M. A. Abdallah et al., "Proapoptotic activity of *Achillea membranacea* essential oil and its major constituent 1,8-cineole against A2780 ovarian cancer cells," *Molecules*, vol. 25, no. 7, p. 1582, 2020.
- [23] A. Bader, Q. M. A. Abdallah, M. I. S. Abdelhady et al., "Cytotoxicity of some plants of the asteraceae Family: anti-proliferative activity of *psadia punctulata* root sesquiterpenes," *Records of Natural Products*, vol. 13, pp. 307–315, 2018.
- [24] M. M. Bkhaitan, M. Alarjah, A. Z. Mirza, A. N. Abdalla, H. M. El-Said, and H. S. Faidah, "Preparation and biological evaluation of metronidazole derivatives with monoterpenes and eugenol," *Chemical Biology and Drug Design*, vol. 92, no. 6, pp. 1954–1962, 2018.
- [25] U. Shaheen, E. A. Ragab, A. N. Abdalla, and A. Bader, "Triterpenoidal saponins from the fruits of *Gleditsia caspica* with proapoptotic properties," *Phytochemistry*, vol. 145, pp. 168–178, 2018.

Research Article

Use of Network Pharmacology to Investigate the Mechanism by Which Allicin Ameliorates Lipid Metabolism Disorder in HepG2 Cells

Bijun Cheng , Tianjiao Li , and Fenglin Li 

Jilin Agricultural Science and Technology University, Jilin, China

Correspondence should be addressed to Tianjiao Li; litianjiao@jlnku.edu.cn and Fenglin Li; lifenglin@jlnku.edu.cn

Received 25 July 2020; Revised 16 December 2020; Accepted 26 December 2020; Published 12 January 2021

Academic Editor: Akhilesh K. Tamrakar

Copyright © 2021 Bijun Cheng et al. This is an open access article distributed under the Creative Commons Attribution License, which permits unrestricted use, distribution, and reproduction in any medium, provided the original work is properly cited.

Allicin has been well documented to exhibit a wide spectrum of biological activities, especially lipid-lowering activity, as a promising candidate for the management of nonalcoholic fatty liver disease (NALFD). However, the mechanisms underlying the therapeutic effects of allicin require further investigation. It is tempting to think of combining network pharmacology and experimental validation to investigate the mechanism by which allicin ameliorates lipid metabolism disorder in HepG2 cells. We established a cell model of hepatic steatosis induced by PA to investigate the antisteatotic effects of allicin. The studies showed that allicin reduced PA-induced lipid accumulation using Nile red staining and TC and TG assays. Then, 219 potential targets of allicin were successfully predicted by PharmMapper. According to Reactome Pathway Analysis, 44 potential targets related to lipid metabolism were screened out. Molecular signaling cascades mediated by allicin included PPARA, PPARG, FABP4, and FABP6 by cytoHubba and qPCR analysis. Results revealed that allicin activated the gene expression of PPARA and FABP6 and suppressed the gene expression of FABP4 and PPARG. Thus, the present study united the methods of network pharmacology and experimental validation to investigate the protein targets of allicin on PA-induced lipid metabolism disorders to supply a reference for related application for the first time.

1. Introduction

Lipid metabolism disorders are common pathological processes in various clinical diseases and are characterized by abnormal changes in the content and/or arrangement of various kinds of lipoprotein [1], including elevations in total cholesterol (TC) and triglycerides (TG) [2]. Substantial evidence has demonstrated the association between lipid accumulation and systemic conditions, such as NALFD [3], hyperlipaemia [2], and type 2 diabetes mellitus [4]. Adjusting abnormal lipid metabolism is a practical procedure to slow or prevent the degeneration of systemic conditions. Simultaneously, it is recommended that advantageous dietetic components make an important impact on the prevention and therapy of lipid metabolism disorder [5].

Natural products have more and more widespread applications in medicine and green agriculture due to their mild and largely harmless properties in comparison with chemical agents. Allicin is produced by an enzymatic reaction when raw garlic is crushed or chopped. As an active constituent of garlic, allicin has been found to possess generous pharmacological activities, such as anticancer [6], antibacterial, antihypertensive, antihypolipidemic, and antihypoglycemic activities [7]. In addition, allicin also showed antioxidant role on Nile tilapia and stem cells. It has been proved in our previous research that allicin could reduce lipid droplets induced by 1,3-DCP in HepG2 cells, recommending allicin as a potential candidate for handling of abnormal lipid metabolism [8]. However, the mechanisms underlying the therapeutic effects of allicin require further investigation.

In this work, we aim to find the pharmacological mechanisms by which allicin ameliorates lipid metabolism disorder in HepG2 cells. First of all, we established a cell model of hepatic steatosis induced by PA to investigate the antisteatotic effects of allicin. Then, we predicted potential targets of allicin by PharmMapper, a free online tool applied to seek the target proteins for allicin on the basis of reverse pharmacophore mapping [8]. Furthermore, we conducted GO enrichment and pathway analysis for the potential targets of allicin. Moreover, protein–protein interaction (PPI) relationship between the target proteins was constructed by STRING. Then, the potential target proteins were further analyzed via qPCR. In the present study, we made an effort to elucidate the biological mechanisms by which allicin exhibits a lipid lowering activity using a combination of experimental operation and network pharmacology.

2. Materials and Methods

2.1. Reagents. Allicin and palmitic acid (PA) were purchased from Sigma Chemical Co. (St. Louis, MO, USA).

2.2. Cell Culture Experiments. HepG2 cells were purchased from ATCC. Cells were cultured under standard cell cultured conditions (DMEM, 10% FBS) at 37°C in a 5% CO₂ atmosphere.

2.3. Cell Viability Assays. The cytotoxicity of PA and allicin was detected using CCK8 assays. 8×10^3 cells per well were seeded in triplicate in 96-well plates overnight. First, cells were treated with various doses of PA and allicin for 22 h. Next, cells were treated with CCK-8 (Shangbao, China) for 2 h. The absorbance value of the culture solution in the plate was detected by a microplate reader (Bio Tek, USA) at 450 nm.

2.4. Determination of TC and TG Levels. TC and TG levels were analyzed by an enzymatic kit (Beckman Coulter, Inc.) and indicated as mM of TC and TG per milligram of cellular protein. The operations were performed following the kit manufacturer's instructions.

2.5. Nile Red Staining Assay. Briefly, 8×10^3 cells per well were seeded in a 24-well plate overnight. Then, cells were treated with various doses of PA and allicin for 24 h. Nile red staining of cells was performed referring to the methods reported in the literature [9]. Cells were observed and pictured by a fluorescence microscope (BX53, Olympus, Japan).

2.6. Targets Predicted by PharmMapper. PharmMapper is a web server for potential drug target identification based on the use of a pharmacophore mapping approach. We obtained the sdf structure format of allicin from the PubChem database (CID: 65036). The molecular file of allicin was uploaded to the PharmMapper server. The search started using the maximum generated conformations at 300 by

selecting “Human Protein Targets Only (v2010, 2241)” option and default value of 300 for the number of reserved matched targets as described previously [9, 10]. “Default Mode” was chosen for other parameters.

2.7. Functional Enrichment Analysis. DAVID provides a comprehensive set of functional annotation tools for investigators to understand the biological meaning behind a large list of genes. FunRich is a software mainly used for gene functional classification that provides a comprehensive set of functional annotation for researchers to understand biological characteristics [11]. In the present study, gene ontology (GO) function and Kyoto Encyclopedia of Genes and Genomes (KEGG) pathway enrichment analyses of allicin were performed through FunRich (version 3.1.3 for Windows) and DAVID databases (version 6.8).

2.8. PPI Network Construction. The Search Tool for the Retrieval of Interacting Genes (STRING; <http://string.embl.de/>) is a biological database designed to construct a PPI network of allicin based on the known and predicted PPIs and then analyze the functional interactions between proteins. Based on the STRING online tool in Cytoscape software (version 3.7.1), we obtained the PPI network data of proteins with a confidence score ≥ 0.7 . Subsequently, the plug-in of cytoHubba in Cytoscape software was applied to explore the significant proteins in PPI network. The default settings were used for advanced options.

2.9. mRNA Analysis. Briefly, 5×10^5 cells per well were seeded in a 6-well plate overnight. Then, cells were treated with various doses of PA and allicin for 24 h. RNA from cells was isolated using TRIZOL reagent (Invitrogen, Carlsbad CA, USA). RNA concentration was determined by the absorbance at 260/280 nm. cDNA was synthesized from 2 μ g of total RNA by 5 \times All-In-OneMasterMix (abm, Canada). The primer sequences were designed using Oligo7 software (Table 1) and synthesized by Sangon Biotech Co. (Shanghai, China). The qRT-PCR reactions were set up by EvaGreen 2X qPCR MasterMix-No Dye (abm, Canada) according to the manufacturer's instructions. qPCR was performed by Bio-Rad CFX96 Touch Real-Time PCR detection system with the following cycle: 95°C for 10 min, followed by 95°C for 15 sec and 60°C for 60 sec for 40 cycles. At last, the dissolution curve was determined. The relative gene expression value was statistically evaluated by the $2^{-\Delta\Delta C_t}$ method.

2.10. Statistical Analysis. Statistical significance of difference in measured variables was performed by SPSS 19.0 software (SPSS Inc., Chicago, IL, USA). All data were analyzed by one-way ANOVA. Data are expressed as mean \pm SEM and plotted in histograms with GraphPad Prism 5.0.

3. Results

3.1. Allicin Inhibits PA-Induced Hepatocyte Injury. First, we determined the concentration dependence of the cytotoxic

TABLE 1: Primer sequences used for qPCR.

Gene name	QRT-PCR primers	
RXRA	Forward	TCCTTCTCCCACCGCTCCATC
	Reverse	CAGCTCCGTCTTGTCCATCTG
PPARA	Forward	ATCCCATCACTCTCTCTGTG
	Reverse	AACTACCTGCTCAGGACTCA
PPARG	Forward	GCACTGCCTATGAGCACTTC
	Reverse	CCATTGGGTCAGCTCTTGTG
FABP4	Forward	TGGTGTTGGAATGCGTCAT
	Reverse	GGTCAACGTCCCTTGGCTTA
FABP6	Forward	AGCACCACCCATTCTCCTCA
	Reverse	AAGTGAAGTCTGCCATCCT

effect of allicin in the absence or presence of 400 μM PA for 24 h in HepG2 cells by using CCK8 assay. As shown in Figure 1(a), allicin (0–500 μM) had no cytotoxic effect on HepG2 cells. As shown in Figure 1(b), allicin (50–200 μM) prevented PA-induced cell death in HepG2 cells. Based on these results, concentrations from 50 μM to 200 μM were applied in the following studies.

3.2. Allicin Reduced Lipid Accumulation in PA-Induced Steatotic HepG2 Cells. To investigate the antisteatotic effect of allicin in HepG2 cells, HepG2 cells were exposed to various concentrations of allicin (50–200 μM) in presence of a PA mixture at a concentration of 400 μM for 24 h. Total intracellular lipid levels in HepG2 cells were measured after Nile red staining, and the TG and TC contents were assayed using enzymatic kits.

From Figure 2(a), it is clear that cellular oil droplets were apparently increased by 400 μM PA treatment and decreased in a concentration-dependent response of allicin treatment. In addition, the data of TC and TG validated the results of Nile red staining. A very significant reduction of TC and TG was observed in presence of allicin. The inhibitory effect of allicin on PA-induced lipogenesis of HepG2 cells was dose-dependent (Figures 2(b) and 2(c)).

3.3. Construction of the Interaction Network and Network Analysis. Ranked by fit score in descending order, 219 potential targets were predicted by PharmMapper. According to Reactome Pathway Analysis, 44 potential targets were found to be related to lipid metabolism. Subsequently, 44 potential targets were used for further investigation (Table 2).

3.4. GO Enrichment and Pathway Analysis for Potential Targets of Allicin. As a GO Term statistical analysis method, GO enrichment analysis focused on the biological function, molecular function, and cellular component [12, 13]. We imported the selected potential 44 target genes into the FunRich for GO enrichment. GO analysis results revealed that the functions of these potential targets were related to many biological processes that may be important for lipid metabolism, such as metabolism, energy pathways, transport, cell communication, and signal transduction. A total of

10 molecular functions were enriched, mainly involving transporter activity, catalytic activity, and ligand-dependent nuclear receptor activity. Cellular components related to lipid metabolism were also identified, including cytoplasm, nucleus, exosomes, extracellular region, and cytosol (Table 3).

Then, we imported the selected potential 44 target genes into the DAVID for pathway analysis. A total of 16 pathways were obtained by KEGG analysis, from which we acquired the top thirteen pathways that met the criterion of $p < 0.05$. These pathways contained PPAR signaling pathway, arachidonic acid metabolism, metabolism of xenobiotics by cytochrome P450, steroid hormone biosynthesis, chemical carcinogenesis, bile secretion, metabolic pathways, linoleic acid metabolism, thyroid cancer, insulin resistance, hepatitis C, non-small cell lung cancer, and nonalcoholic fatty liver disease (NAFLD). Among them, the most important enriched KEGG pathways were metabolic pathways and PPAR signaling pathway. The screened pathways suggested that allicin could play a role in the treatment with disorder of lipid metabolism by participating in the aforementioned pathways (Figure 3). In addition, genes involved in each pathway are listed in Table 4.

3.5. Protein-Protein Interaction Network (PPI) Analysis. The selected potential 44 target genes were imported into the STRING version 11.0 database in Cytoscape to construct a PPI network. The network complex included 40 nodes and 109 edges (Figure 4). Then, we applied cytoHubba in Cytotype to evaluate a node with a degree, which denotes the number of edges between a node and other nodes in a network. A high-degree node was the most influential node in the network, and a hub node was a component of a network with a high-degree node. In this study, we selected the top 10 hub nodes: ALB (degree = 19), RXRA (degree = 15), PPARA (degree = 11), CYP2C9 (degree = 10), SULT2A1 (degree = 9), PPARG (degree = 9), FABP4 (degree = 9), FABP6 (degree = 9), HPGDS (degree = 8), and AKR1C3 (degree = 8). The hub nodes maintain the stability of the network and show the metabolism of lipid, which involves multiple genes and multidimensional regulation. Among the hub nodes, RXRA, PPARA, PPARG, FABP4, and FABP6 belong to PPAR signaling pathway, which plays an important role in lipid metabolism (Figure 5). Therefore, RXRA, PPARA, PPARG, FABP4, and FABP6 were selected for subsequent analysis.

3.6. Validation of Potential Targets. The effects of allicin on five candidate targets (RXRA, PPARA, PPARG, FABP4, and FABP6) were further investigated in HepG2 cells. We found no statistically significant difference in expression of RXRA mRNA. However, PPARA and FABP6 mRNA levels were significantly decreased by 400 μM PA treatment ($p < 0.01$), while administration of allicin showed a concentration-dependent increase compared with PA group. Treatment with PA increased the expression of FABP4 and PPARG mRNA significantly, while administration of allicin lowered

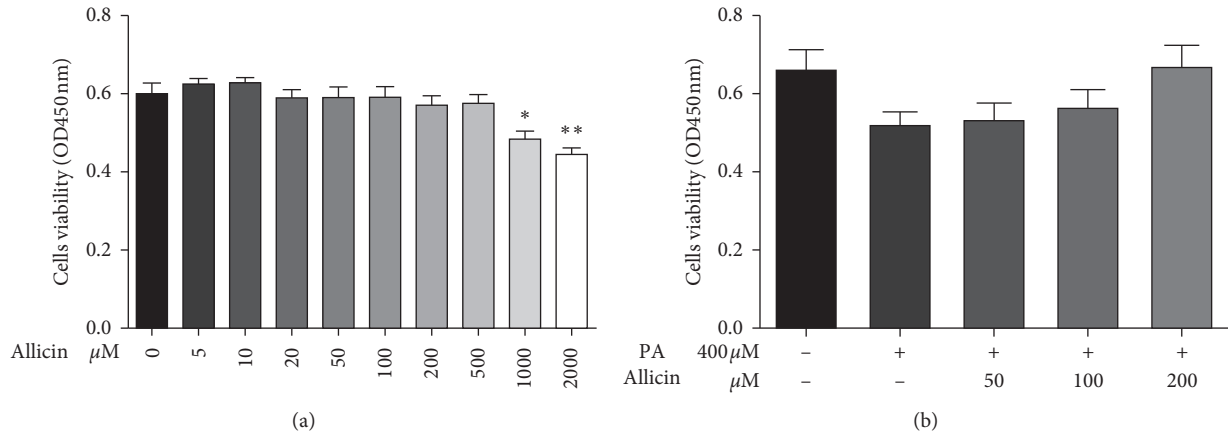


FIGURE 1: The effects of allicin and PA on cell viability in HepG2 cells. Cell viability was determined by CCK8 assays. The results were expressed as means ± S.D. of three independent experiments. * $p < 0.05$, ** $p < 0.01$ vs. control; [#] $p < 0.05$ vs. PA-treated cells.

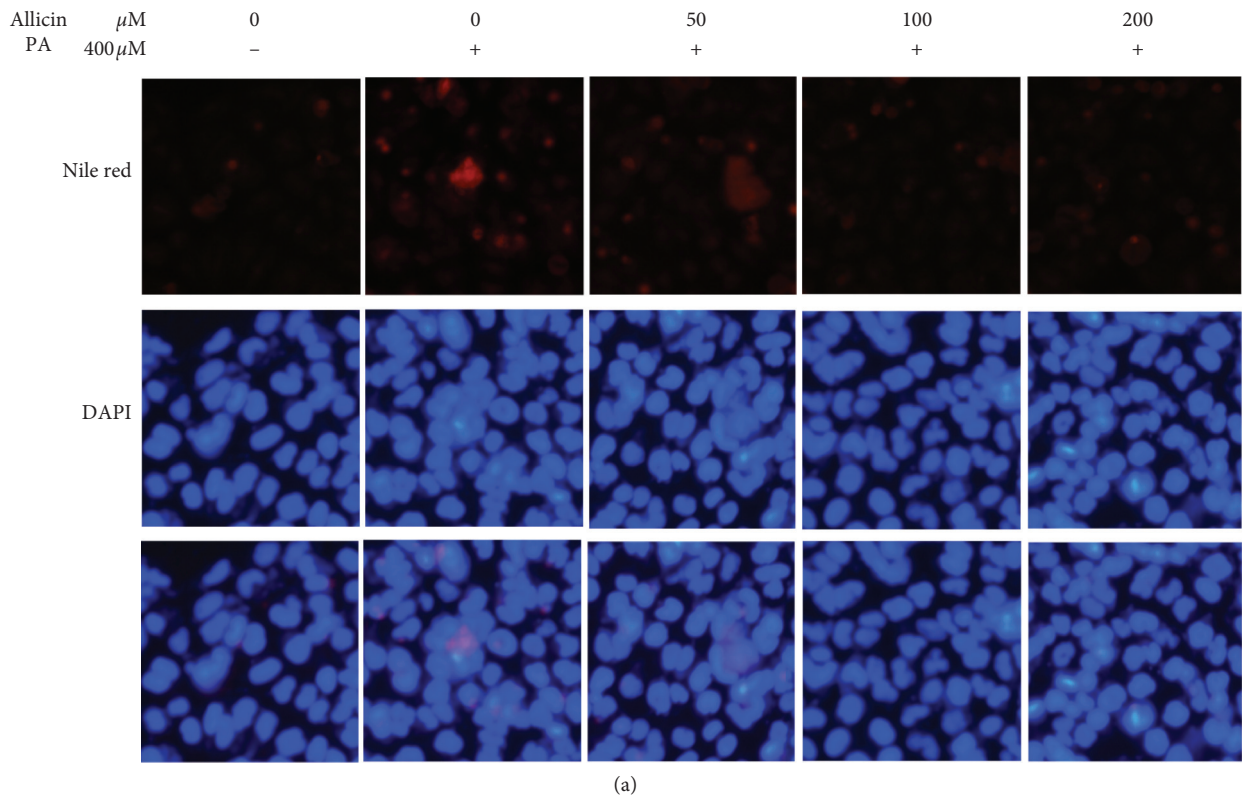


FIGURE 2: Continued.

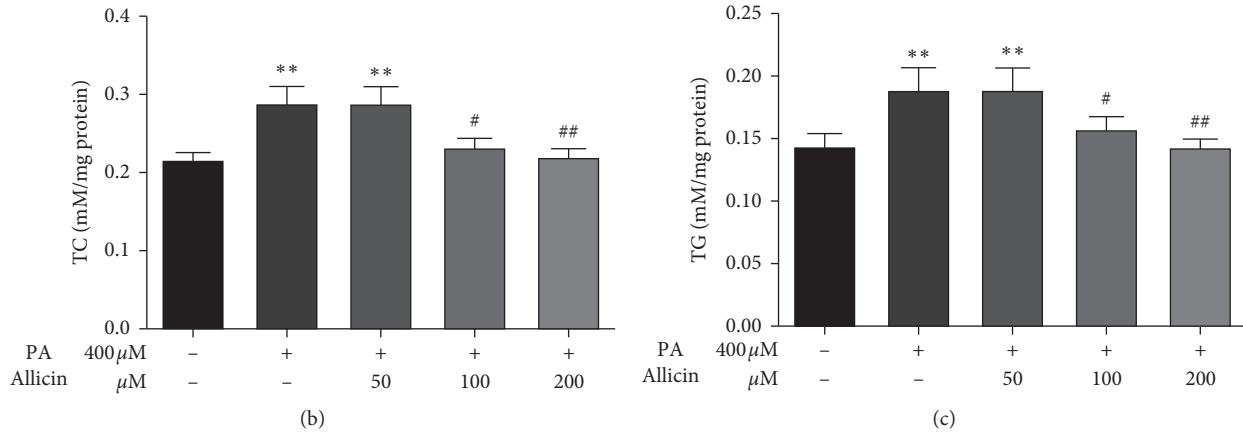


FIGURE 2: Inhibition of PA-induced lipid accumulation by allicin in HepG2 cells. (a) HepG2 cells were stained by Nile red and assessed by fluorescence microscopy (captured by microscope at 400X magnification). ((b) and (c)) TC and TG level were measured as described in the Materials and Methods section. The results are expressed as means \pm S.D. of three independent experiments. ** $p < 0.01$ vs. control; # $p < 0.05$, ## $p < 0.01$ vs. PA-treated HepG2 cells.

TABLE 2: Information of potential targets related to lipid metabolism.

Gene name			
FABP6	AKR1B1	AKR1C1	VDR
APOA2	LSS	NR1H2	HPGDS
ESRRA	PIK3R1	STS	HMGCR
FABP7	HSD17B1	CYP2C9	LTA4H
GM2A	ALB	PLA2G2A	DPEP1
FABP4	HSD11B1	MAPKAPK2	PCTP
FABP3	NR1H4	RXR	PPARG
PPARA	NR1H3	BCHE	RORA
PPARD	AKR1C2	RXRA	PLA2G10
CBR1	AKR1C3	GC	PNMT
SULT2A1	EPHX2	GSTM1	GSTM2

TABLE 3: GO enrichment analysis of the potential targets.

Term	Genes
Metabolism	GM2A; CBR1; SULT2A1; AKR1B1; LSS; HSD17B1; HSD11B1; NR1H4; AKR1C2; AKR1C3; EPHX2; AKR1C1; STS; CYP2C9; PLA2G2A; BCHE; GSTM1; GSTM2; HPGDS; HMGCR; PLA2G10; PNMT
Energy pathways	GM2A; CBR1; SULT2A1; AKR1B1; LSS; HSD17B1; AKR1C3; EPHX2; AKR1C1; STS; CYP2C9; PLA2G2A; BCHE; GSTM1; GSTM2; HPGDS; HMGCR; PLA2G10; PNMT
Bone remodeling	RORA
Transport	FABP6; APOA2; FABP7; FABP3; ALB; AKR1C2; GC; PCTP
Xenobiotic metabolism	GSTM1
Transcription	PPARD
Regulation of gene expression, epigenetic	VDR
Cell communication	FABP4; PIK3R1; NR1H4; NR1H3; NR1H2; MAPKAPK2; RXR; RXRA
Signal transduction	FABP4; PIK3R1; NR1H4; NR1H3; NR1H2; MAPKAPK2; RXR; RXRA
Protein metabolism	LTA4H; DPEP1

TABLE 3: Continued.

	Term	Genes
Molecular function	Ligand-dependent nuclear receptor activity	PPARA; NR1H4; NR1H3; NR1H2; RXRB; RXRA
	Transporter activity	FABP6; APOA2; FABP7; GM2A; FABP3; ALB; AKR1C2; GC; PCTP
	Catalytic activity	LSS; HSD17B1; HSD11B1; AKR1C3; AKR1C1; STS; CYP2C9; HMGCR
	Glutathione transferase activity	GSTM1; GSTM2
	Phospholipase activity	PLA2G2A; PLA2G10
	Oxidoreductase activity	CBR1; AKR1B1; AKR1C2
	Hydrolase activity	EPHX2; BCHE; LTA4H
	Transcription factor activity	PPARD; VDR; PPARG
	Protein serine/threonine kinase activity	MAPKAPK2
	DNA binding	RORA
Cellular component	Extracellular region	APOA2; ALB; PLA2G2A; BCHE; GC; PLA2G10
	Cytoplasm	FABP6; APOA2; FABP7; FABP4; FABP3; PPARA; CBR1; SULT2A1; AKR1B1; PIK3R1; HSD17B1; ALB; AKR1C3; EPHX2; AKR1C1; NR1H2; PLA2G2A; MAPKAPK2; GC; GSTM1; GSTM2; VDR; HPGDS; LTA4H; PCTP; PPARG
	Cytosol	SULT2A1; AKR1B1; PIK3R1; AKR1C2; EPHX2; AKR1C1; MAPKAPK2; PCTP; PNMT
	Exosomes	APOA2; GM2A; FABP3; CBR1; AKR1B1; ALB; EPHX2; GSTM2; LTA4H; DPEP1; PPARG
	Extracellular	APOA2; GM2A; FABP3; AKR1B1; ALB; PLA2G2A; BCHE; GC; HMGCR; PLA2G10
	Endoplasmic reticulum	LSS; HSD11B1; STS; CYP2C9; PLA2G2A; HMGCR; DPEP1
	Lysosome	APOA2; GM2A; CBR1; AKR1B1; LSS; HSD17B1; ALB; STS
	Extracellular space	AKR1B1; ALB; PLA2G2A
	Nucleus	ESRRA; PPARA; PPARD; PIK3R1; ALB; NR1H4; NR1H3; AKR1C3; NR1H2; MAPKAPK2; RXRB; RXRA; VDR; LTA4H; PPARG; RORA
	Plasma membrane	PIK3R1; STS; GC

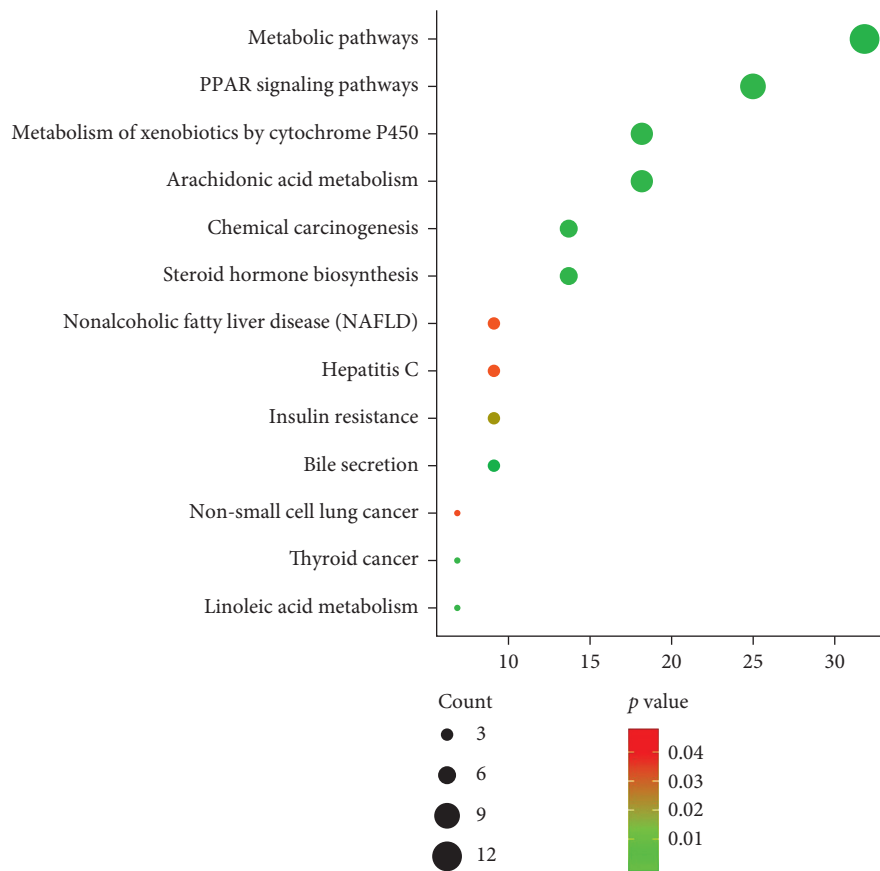


FIGURE 3: KEGG pathway enrichment of the potential targets.

TABLE 4: Genes involved in each pathway.

Term	Count	Genes
Metabolic pathways	14	PLA2G10, PNMT, HSD17B1, HMGCR, CYP2C9, EPHX2, LSS, AKR1C3, CBR1, AKR1B1, HSD11B1, PLA2G2A, LTA4H, HPGDS
PPAR signaling pathway	11	PPARA, APOA2, PPARD, RXRB, RXRA, PPARG, FABP3, FABP4, FABP7, FABP6, NR1H3
Arachidonic acid metabolism	8	AKR1C3, CBR1, PLA2G10, CYP2C9, PLA2G2A, EPHX2, LTA4H, HPGDS
Metabolism of xenobiotics by cytochrome P450	8	GSTM1, GSTM2, AKR1C2, CBR1, SULT2A1, CYP2C9, HSD11B1, AKR1C1
Steroid hormone biosynthesis	6	AKR1C3, AKR1C2, STS, HSD17B1, HSD11B1, AKR1C1
Chemical carcinogenesis	6	GSTM1, GSTM2, CBR1, SULT2A1, CYP2C9, HSD11B1
Bile secretion	4	SULT2A1, HMGCR, RXRA, NR1H4
Insulin resistance	4	NR1H2, PPARA, PIK3R1, NR1H3
Hepatitis C	4	PPARA, RXRA, PIK3R1, NR1H3
Nonalcoholic fatty liver disease (NAFLD)	4	PPARA, RXRA, PIK3R1, NR1H3
Linoleic acid metabolism	3	PLA2G10, CYP2C9, PLA2G2A
Thyroid cancer	3	RXRB, RXRA, PPARG
Non-small cell lung cancer	3	RXRB, RXRA, PIK3R1

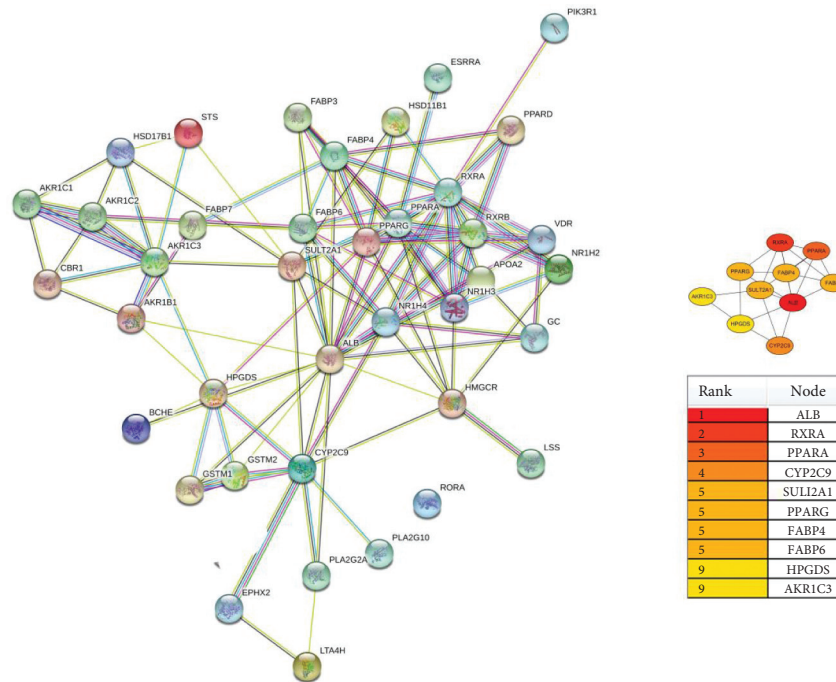


FIGURE 4: Candidate target proteins identified in the PPI network constructed using Cytoscape software.

the expression of FABP4 and PPARG mRNA in a dose-dependent response (Figure 6).

4. Discussion

PharmMapper server is a freely accessed web server designed to identify potential target candidates for the given small molecules (drugs, natural products, or other newly discovered compounds with unidentified binding targets) using pharmacophore mapping approach [8, 9, 14]. The results of the network pharmacology method provide a basis for understanding the mechanism of action of allicin.

In the present study, we investigated the role of allicin in lipid metabolism. We found that allicin reduced lipid accumulation in a dose-dependent response in HepG2 cells. Then, using network pharmacology prediction, we successfully predicted 219 potential targets of allicin. According to Reactome Pathway Analysis, 44 potential targets related to lipid metabolism were screened out. Then, 44 potential targets were subjected to GO and KEGG pathway enrichment analyses.

GO analytical data suggested that the potential targets mainly referred to metabolism, energy pathways, transport, and cell communication. These biological processes were

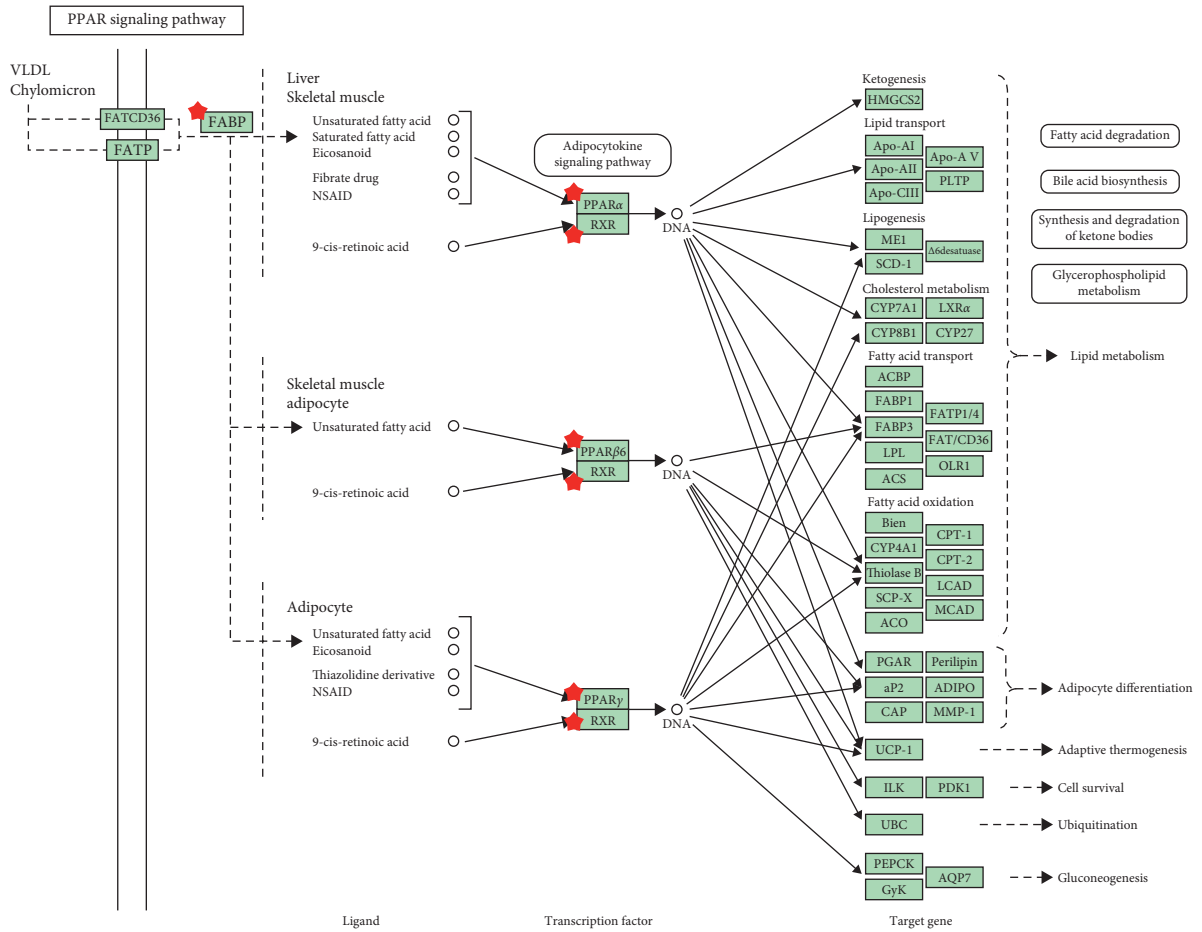


FIGURE 5: PPAR signaling pathway of potential targets of allicin.

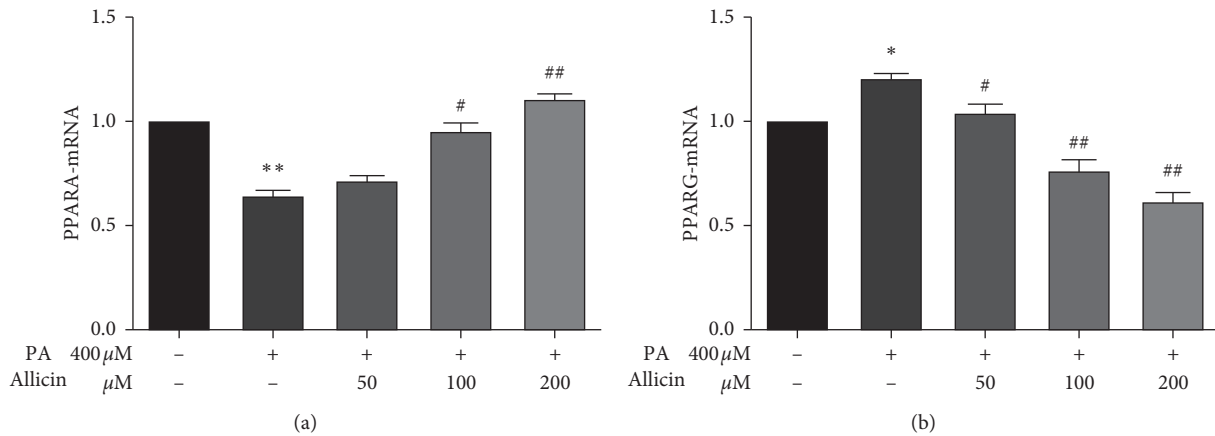


FIGURE 6: Continued.

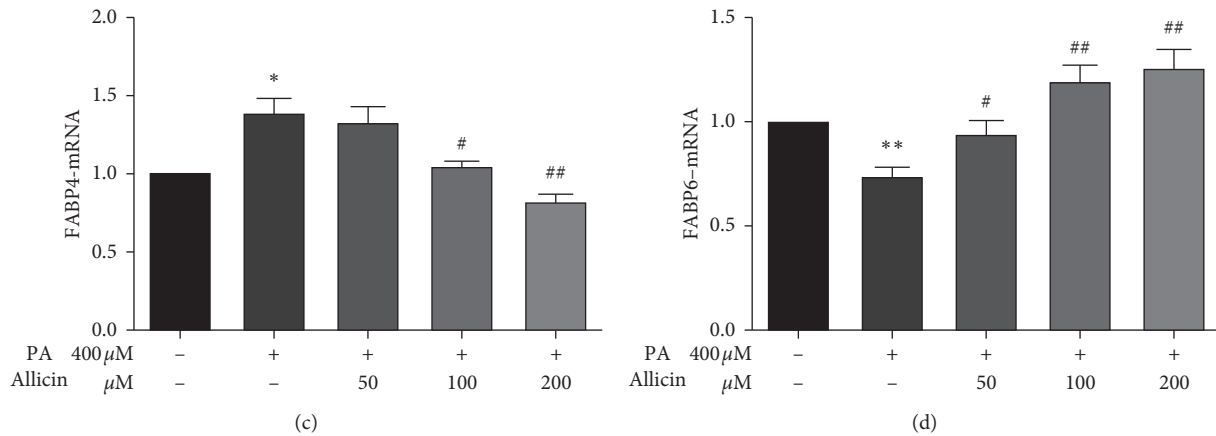


FIGURE 6: Effect of allicin on the relative gene expression in HepG2 cells. Values given are the mean \pm SEM ($n = 3$). ** $p < 0.01$, * $p < 0.05$ vs. control; # $p < 0.05$, ## $p < 0.01$ vs. PA-treated HepG2 cells.

related to NAFLD and lipid metabolism, which were consistent with the literature [15, 16]. Therefore, the potential targets of allicin participated in multiple biological processes and played pivotal roles in lipid metabolism.

Based on the KEGG pathway analysis, potential targets were mainly involved in 16 pathways. Among them, PPAR signaling was an extremely important pathway. The PPAR signaling pathway has been considered to be related to the pathological processes of fatty liver development in rats with acute pancreatitis [17]. PPARA was a nuclear hormone receptor and important regulator of lipid metabolism in the liver. PPARA was considered to be an important regulator of lipid metabolism, which, upon activation, accelerated not only transport, binding, and β -oxidation of fatty acids, but also lipogenesis [18]. PPARA was mainly activated by ligand binding, which required heterodimer formation with RXR [19]. Another part of the PPAR family, PPARG, was a nuclear hormone receptor, which played an important role in the metabolism of lipids. In addition, it was also related to a variety of diseases, including diabetes, obesity, atherosclerosis, and cancer [20, 21]. It had been reported that PPARG could also be activated by fatty acids and played an important part in insulin sensitivity and fat production [22]. Therefore, in the present study, PPAR signaling pathway was supposed to serve crucial roles in the lipid metabolism regulated by allicin.

STRING database can analyze the interaction relationship between some proteins [23–25]. cytoHubba can identify hub objects and subnetworks from a complex interactome. Then, using of STRING database and cytoHubba suggested 10 hub targets, which play important roles in the PPI. Among them, RXRA, PPARA, PPARG, FABP4, and FABP6 belong to PPAR signaling pathway, which plays an important role in lipid metabolism. Therefore, RXRA, PPARA, PPARG, FABP4, and FABP6 included in PPAR signaling pathway were selected for further exploration by qPCR analysis. The present results revealed that allicin activated the gene expression of PPARA and FABP6 and suppressed the gene expression of FABP4 and PPARG. Findings are aligned with the previous studies. It was found that

treatment with garlic essential oil (GEO) and diallyl disulfide (DADS) significantly upregulated the hepatic PPARA and CPT-1 expression levels in HFD-fed mice compared with HFD-fed mice without treatment [26]. A recent study also confirmed that PPARA activation enhances mitochondrial β -oxidation activity accelerating FA degradation in the liver [27]. A study performed confirmed the association between PPARG and obesity. It was reported that PPARG activation could normalize epigenetic and transcriptional regulation primarily related to lipid metabolism [28]. Moreover, PPARG induces the expression level of FABP4 leading to hepatic adipogenesis; the increase of fat is related to the upregulation of PPARG and FABP4 mRNA and downregulation of FABP6 mRNA [29–32]. Consistent with previous studies, our results indicate that allicin may alleviate the PA-induced lipid accumulation in HepG2 cells through activating the gene expression of PPARA and FABP6 and suppressing the gene expression of FABP4 and PPARG.

5. Conclusions

In conclusion, the underlying inhibitory mechanism of allicin on PA-induced lipogenesis of HepG2 cells was explored in this study by combining experimental operation and network pharmacology prediction. Moreover, the potential targets (PPARA, PPARG, FABP4, and FABP6) were successfully selected based on this practical strategy. Overall, our findings indicated that allicin might alleviate lipid accumulation in HepG2 cells, at least in part, through the PPAR signaling pathway.

Abbreviations

CCK-8:	Cell counting kit-8
TC:	Total cholesterol
TG:	Triglycerides
NALFD:	Nonalcoholic fatty liver disease
PPARA:	Peroxisome proliferator-activated receptor alpha
PPARG:	Peroxisome proliferator-activated receptor gamma

FABP4: Fatty acid-binding protein
 FABP6: Gastrotropin
 qPCR: Quantitative real-time PCR.

Data Availability

The data used to support the findings of this study are available from the corresponding author upon request.

Conflicts of Interest

The authors declare that there are no conflicts of interest associated with the manuscript.

Authors' Contributions

Bijun Cheng was responsible for data curation and writing and original draft preparation; Fenlin Li designed the research. Tianjiao Li was responsible for writing and review and editing and funding acquisition. All authors have read and agreed to the published version of the manuscript.

Acknowledgments

This study was supported by the Science and Technology Research Project of the Education Department of Jilin Province during the Thirteenth Five-Year Plan Period (no. JJKH20200389KJ).

References

- [1] C. M. Hales, M. D. Carroll, C. D. Fryar, and C. L. Ogden, "Prevalence of obesity among adults and youth: United States, 2015-2016," *NCHS Data Brief*, vol. 288, p. 1, 2017.
- [2] C. K. Glass and J. L. Witztum, "Atherosclerosis. the road ahead," *Cell*, vol. 104, no. 4, pp. 503-516, 2001.
- [3] P. R. Afolabi, E. Scorletti, D. E. Smith, A. A. Almeahadi, P. C. Calder, and C. D. Byrne, "The characterisation of hepatic mitochondrial function in patients with non-alcoholic fatty liver disease (NAFLD) using the C-13-ketoisocaproate breath test," *Journal of Breath Research*, vol. 12, 2018.
- [4] K. Raghunathan, "History of diabetes from remote to recent times," *Bulletin of the Indian Institute of History of Medicine*, vol. 6, pp. 167-182, 1976.
- [5] C. Diling, Y. Xin, Z. Chaoqun et al., "Extracts from *Hericium erinaceus* relieve inflammatory bowel disease by regulating immunity and gut microbiota," *Oncotarget*, vol. 8, no. 49, pp. 85838-85857, 2017.
- [6] Y.-L. Chu, C.-T. Ho, J.-G. Chung, R. Raghu, Y.-C. Lo, and L.-Y. Sheen, "Allicin induces anti-human liver cancer cells through the p53 gene modulating apoptosis and autophagy," *Journal of Agricultural and Food Chemistry*, vol. 61, no. 41, pp. 9839-9848, 2013.
- [7] J. Borlinghaus, F. Albrecht, M. Gruhlke, I. Nwachukwu, and A. Slusarenko, "Allicin: chemistry and biological properties," *Molecules*, vol. 19, no. 8, pp. 12591-12618, 2014.
- [8] J. Lu, B. Cheng, B. Fang et al., "Protective effects of allicin on 1,3-DCP-induced lipid metabolism disorder in HepG2 cells," *Biomedicine & Pharmacotherapy*, vol. 96, pp. 1411-1417, 2017.
- [9] P. Spiekermann, B. H. A. Rehm, R. Kalscheuer, D. Baumeister, and A. Steinbüchel, "A sensitive, viable-colony staining method using Nile red for direct screening of bacteria that accumulate polyhydroxyalkanoic acids and other lipid storage compounds," *Archives of Microbiology*, vol. 171, no. 2, pp. 73-80, 1999.
- [10] X. Liu, S. Ouyang, B. Yu et al., "PharmMapper server: a web server for potential drug target identification using pharmacophore mapping approach," *Nucleic Acids Research*, vol. 38, no. 2, pp. W609-W614, 2010.
- [11] M. Pathan, S. Keerthikumar, C.-S. Ang et al., "FunRich: an open access standalone functional enrichment and interaction network analysis tool," *Proteomics*, vol. 15, no. 15, pp. 2597-2601, 2015.
- [12] K. Glass and M. Girvan, "Annotation enrichment analysis: an alternative method for evaluating the functional properties of gene sets," *Scientific Reports*, vol. 4, p. 4191, 2014.
- [13] L. Cheng, H. Lin, Y. Hu, J. Wang, and Z. Yang, "Gene function prediction based on the Gene Ontology hierarchical structure," *PLoS One*, vol. 9, Article ID e107187, 2014.
- [14] X. Wang, C. Pan, J. Gong, X. Liu, and H. Li, "Enhancing the enrichment of pharmacophore-based target prediction for the polypharmacological profiles of drugs," *Journal of Chemical Information and Modeling*, vol. 56, no. 6, pp. 1175-1183, 2016.
- [15] H. Rafiei, K. Omidian, and B. Bandy, "Dietary polyphenols protect against oleic acid-induced steatosis in an in vitro model of NAFLD by modulating lipid metabolism and improving mitochondrial function," *Nutrients*, vol. 11, 2019.
- [16] B. Favreau, M. Denis, R. Ployet et al., "Distinct leaf transcriptomic response of water deficient *Eucalyptus grandis* submitted to potassium and sodium fertilization," *PLoS One*, vol. 14, Article ID e0218528, 2019.
- [17] Q. Wang, H. Yan, G. Wang et al., "RNA sequence analysis of rat acute experimental pancreatitis with and without fatty liver: a gene expression profiling comparative study," *Scientific Reports*, vol. 7, p. 734, 2017.
- [18] J. A. van Diepen, P. A. Jansen, D. B. Ballak et al., "PPAR-alpha dependent regulation of vanin-1 mediates hepatic lipid metabolism," *Journal of Hepatology*, vol. 61, no. 2, pp. 366-372, 2014.
- [19] C. N. A. Palmer, M.-H. Hsu, K. J. Griffin, and E. F. Johnson, "Novel sequence determinants in peroxisome proliferator signaling," *Journal of Biological Chemistry*, vol. 270, no. 27, pp. 16114-16121, 1995.
- [20] A. Berger, I. Monnard, M. Baur, C. Charbonnet, I. Safonova, and A. Jomard, "Epidermal anti-inflammatory properties of 5,11,14 20:3: effects on mouse ear edema, PGE2 levels in cultured keratinocytes, and PPAR activation," *Lipids in Health and Disease*, vol. 1, no. 1, p. 5, 2002.
- [21] J. N. Feige, L. Gelman, L. Michalik, B. Desvergne, and W. Wahli, "From molecular action to physiological outputs: peroxisome proliferator-activated receptors are nuclear receptors at the crossroads of key cellular functions," *Progress in Lipid Research*, vol. 45, no. 2, pp. 120-159, 2006.
- [22] C.-H. Lee, P. Olson, A. Hevener et al., "PPAR regulates glucose metabolism and insulin sensitivity," *Proceedings of the National Academy of Sciences*, vol. 103, no. 9, pp. 3444-3449, 2006.
- [23] Y. Gao, Q. Li, J. Zhang et al., "Bead-string-shaped DNA nanowires with intrinsic structural advantages and its potential for biomedical applications," *ACS Applied Materials & Interfaces*, vol. 12, 2019.
- [24] E. Akkaya, K. Sozener, J. Rixe et al., "Venous access closure using a purse-string suture without heparin antagonism or additional compression after MitraClip implantation," *Catheterization and Cardiovascular Interventions*, vol. 96, 2019.

- [25] M. S. Bahovadinov, O. Gülseren, and J. Schnack, "Local entanglement and string order parameter in dimerized models," *Journal of Physics: Condensed Matter*, vol. 31, no. 50, Article ID 505602, 2019.
- [26] Y.-S. Lai, W.-C. Chen, C.-T. Ho et al., "Garlic essential oil protects against obesity-triggered nonalcoholic fatty liver disease through modulation of lipid metabolism and oxidative stress," *Journal of Agricultural and Food Chemistry*, vol. 62, no. 25, pp. 5897–5906, 2014.
- [27] T. Nagaya, N. Tanaka, T. Kimura et al., "Mechanism of the development of nonalcoholic steatohepatitis after pancreaticoduodenectomy," *BBA Clinical*, vol. 3, pp. 168–174, 2015.
- [28] E. Legchenko, P. Chouvarine, P. Borchert et al., "PPAR γ agonist pioglitazone reverses pulmonary hypertension and prevents right heart failure via fatty acid oxidation," *Science Translational Medicine*, vol. 10, Article ID eaao0303, 2018.
- [29] Y.-C. Kim, Y.-K. Cho, W.-Y. Lee et al., "Serum adipocyte-specific fatty acid-binding protein is associated with nonalcoholic fatty liver disease in apparently healthy subjects," *The Journal of Nutritional Biochemistry*, vol. 22, no. 3, pp. 289–292, 2011.
- [30] A. Stefanska, G. Sypniewska, B. Blaszkiewicz, I. Ponikowska, and M. Cwiklinska-Jurkowska, "Comparison between C-reactive protein and adipocyte fatty acid-binding protein as a component of metabolic syndrome in middle-aged women," *Clinical Biochemistry*, vol. 44, no. 4, pp. 304–306, 2011.
- [31] K. E. Andersson, A. Chawade, N. Thuresson et al., "Whole-grain oat diet changes the expression of genes associated with intestinal bile acid transport," *Molecular Nutrition & Food Research*, vol. 61, no. 7, Article ID 1600874, 2017.
- [32] G. Floresta, V. Pistarà, E. Amata et al., "Adipocyte fatty acid binding protein 4 (FABP4) inhibitors. A comprehensive systematic review," *European Journal of Medicinal Chemistry*, vol. 138, pp. 854–873, 2017.

Research Article

Diarylalkanooids as Potent Tyrosinase Inhibitors from the Stems of *Semecarpus caudata*

Phu H. Dang ^{1,2} Tho H. Le ^{1,2} Truong N. V. Do ^{1,2} Hai X. Nguyen ^{1,2}
Mai T. T. Nguyen ^{1,2,3} and Nhan T. Nguyen ^{1,2,3}

¹Faculty of Chemistry, University of Science, 227 Nguyen Van Cu Street, Ward 4, District 5, Ho Chi Minh City, Vietnam

²Vietnam National University, Quarter 6, Linh Trung Ward, Thu Duc District, Ho Chi Minh City, Vietnam

³Cancer Research Laboratory, University of Science, 227 Nguyen Van Cu Street, District 5, Ho Chi Minh City, Vietnam

Correspondence should be addressed to Nhan T. Nguyen; ntnhan@hcmus.edu.vn

Received 2 October 2020; Revised 5 November 2020; Accepted 16 December 2020; Published 4 January 2021

Academic Editor: Siba shanak

Copyright © 2021 Phu H. Dang et al. This is an open access article distributed under the Creative Commons Attribution License, which permits unrestricted use, distribution, and reproduction in any medium, provided the original work is properly cited.

From a CHCl_3 -soluble extract of the stems of *Semecarpus caudata* (Anacardiaceae), two new diarylalkanooids, semedienone (**1**) and semetrienone (**2**), were isolated. Their structures were elucidated based on NMR spectroscopic data interpretation. These compounds possess strong tyrosinase inhibitory activity with the IC_{50} values of 0.033 and 0.11 μM , respectively. Docking studies of **1** and **2** with *oxy*-tyrosinase were carried out to analyze their interactions. Accordingly, semedienone (**1**) showed good interactions with the peroxide group and amino acid residues. The biosynthesis of the isolated diarylalkanooids was proposed.

1. Introduction

Melanin is a pigment that is essential for protecting human skin against UV radiation. However, the abnormal accumulation of melanin induced skin pigmentation disorders. Melanogenesis is a complex process to produce melanin under control of tyrosinase. Tyrosinase (EC 1.14.18.1) is a binuclear copper-containing monooxygenase, which catalyzes the oxidation of phenol to the corresponding *o*-quinone [1,2]. Tyrosinase is the main factor causing some dermatological diseases including freckles, age spots, and melasma. Hydroquinone, arbutin, kojic acid, azelaic acid, L-ascorbic acid, ellagic acid, and tranexamic acid are commercial tyrosinase inhibitors, which have been used as skin-whitening agents, but these compounds have certain drawbacks [3]. Thus, the finding of new efficient and safe antityrosinase agents is necessary for anti-hyperpigmentation drug development.

A previous study on the chemical constituents of *Semecarpus caudata* (Anacardiaceae), collected at Dong Nai Province in Vietnam, led to the isolation of six flavonoid derivatives and the evaluation of their tyrosinase inhibitory activity [4]. Our continued phytochemical study on the

stems of *S. caudata* was carried out, leading to the isolation of seven compounds (**1**–**7**) including two new diarylalkanooids named semedienone (**1**) and semetrienone (**2**). These compounds were found to possess tyrosinase inhibitory activity. Semedienone (**1**) showed a strong effect with an IC_{50} value of 0.033 μM , which makes it 1300 times more potent than that of kojic acid (IC_{50} , 44.6 μM). In addition, molecular docking studies of **1** and **2** with the *oxy*-form of the copper-bound *Streptomyces castaneoglobisporus* tyrosinase were performed.

2. Materials and Methods

2.1. General Experimental Procedures. Optical values were measured on a Shimadzu UV-1800 spectrophotometer (Shimadzu Pte., Ltd., Singapore). IR spectra were measured with a Shimadzu IR-408 infrared spectrometer (Shimadzu Pte., Ltd., Singapore). NMR spectra were acquired on a Bruker Avance III 500 spectrometer (Bruker BioSpin AG, Bangkok, Thailand). Chemical shifts are expressed as δ values. HRESIMS data were acquired on Bruker micrOTOF-QII mass spectrometer (Bruker Singapore Pte., Ltd., Singapore). Column chromatography was carried out using

silica gel 60, 0.06–0.2 mm (Scharlau, Barcelona, Spain) and LiChroprep RP-18, 40–63 μm (Merck KGaA, Darmstadt, Germany). Kieselgel 60 F₂₅₄ or RP-18 F₂₅₄ plates for TLC were purchased from Merck (Merck KGaA, Darmstadt, Germany). Tyrosinase (EC 1.14.18.1) from mushroom (3933 U·mL⁻¹) and L-dihydroxyphenylalanine (L-DOPA) were obtained from Sigma-Aldrich (Sigma-Aldrich Pte., Ltd., Singapore). Other chemicals were of the highest grade available.

2.2. Plant Material. The stems of *Semecarpus caudata* were collected in the Ma Da Forest, Dong Nai Culture and Nature Reserve, Dong Nai Province, Vietnam, in April 2014. The plant was identified by Assoc. Prof. Dr. Hop Tran, Institute of Tropical Biology, Ho Chi Minh City, Vietnam. A voucher sample (MCE0002) has been deposited at the Division of Medicinal Chemistry, Faculty of Chemistry, University of Science, Ho Chi Minh City, Vietnam.

2.3. Extraction and Isolation. The dried powdered stems of *S. caudata* (7.0 kg) were exhaustively extracted in a Soxhlet extractor with MeOH (20 L, 3 h \times 3) to yield MeOH-soluble extract (700 g). This extract was suspended in H₂O (5 L) and successively partitioned with *n*-hexane (2 L) and CHCl₃ (3 L) to give *n*-hexane (37 g)- and CHCl₃ (500 g)-soluble fractions. The CHCl₃-soluble fraction was chromatographed by silica gel column chromatography (15 \times 150 cm) and eluted with EtOAc-*n*-hexane (0:100 \rightarrow 100:0) and MeOH-CHCl₃ (0:100 \rightarrow 20:80) to afford 12 fractions (Fr.1–Fr.12). Fraction Fr.3 (4.5 g) was subjected to further silica gel column chromatography and was eluted with EtOAc-*n*-hexane (0–100%) to yield 4 sub-fractions (Fr.3.1–Fr.3.4). Subfractions Fr.3.2 (1.1 g) and Fr.3.3 (540 mg) were chromatographed over a silica gel column with EtOAc-*n*-hexane (0–100%) and purified by preparative TLC with EtOAc-*n*-hexane (20:80) and EtOAc-CHCl₃ (10:90) to afford **5** (5.0 mg) and **7** (6.0 mg), respectively. Fraction Fr.5 (5.2 g) was separated by silica gel column chromatography with EtOAc-*n*-hexane (0–100%) and MeOH-CHCl₃ (0–20%) to yield 5 subfractions (Fr.5.1–Fr.5.5). Subfraction Fr.5.3 (850 mg) was subjected to further silica gel column chromatography, eluted with Me₂CO-CHCl₃ (0–80%) to give **4** (5.0 mg). Fraction Fr.6 (0.9 g) was separated by normal-phase chromatography with EtOAc-*n*-hexane (0:100 \rightarrow 80:20) and MeOH-CHCl₃ (0:100 \rightarrow 5:95) and reversed phase chromatography with H₂O-MeOH (0–100%) and then purified by preparative TLC with AcOH-EtOAc-PhMe (4:16:80) to obtain **3** (4.0 mg) and **6** (4.0 mg). Fraction Fr.8 (4.5 g) was loaded onto a silica gel column and eluted with CHCl₃-Me₂CO (0–80%) and CHCl₃-MeOH (0–20%) to yield 5 subfractions (Fr.8.1–Fr.8.5). Subfraction Fr.8.2 (630 mg) was further purified using a silica gel column with EtOAc-CHCl₃ (0–80%) and preparative TLC with MeOH-CHCl₃ (5:95) to give **1** (2.0 mg) and **2** (2.0 mg).

2.3.1. Semedienone (1). Yellow, amorphous solid; IR ν_{max} (CHCl₃): 3455, 1620, 1485, 1250, 1091 cm⁻¹; ¹H and ¹³C NMR (500 MHz, acetone-*d*₆, see Table 1); HRESIMS *m/z* 321.0752 [M + Na]⁺ (calcd. for C₁₇H₁₄O₅Na, 321.0739).

2.3.2. Semetrienone (2). Yellow, amorphous solid; IR ν_{max} (CHCl₃): 3305, 1650, 1430, 1245, 1085 cm⁻¹; ¹H and ¹³C NMR (500 MHz, acetone-*d*₆, see Table 1); HRESIMS *m/z* 347.0902 [M + Na]⁺ (calcd. for C₁₉H₁₆O₅Na, 347.0895).

2.4. Synthesis of 2,4,2',4'-Tetrahydroxychalcone (8). 2,4-Dihydroxybenzaldehyde (276.3 mg, 2.0 mmol) and 2',4'-dihydroxyacetophenone (152.1 mg, 1.0 mmol) were dissolved in 1 mL H₂O, and then 1 mL KOH 14 M was added. The resulting mixture was kept in the ultrasonic water bath at 80°C for 8 h. This reaction was monitored by TLC using MeOH-CHCl₃ (1:9) mixture. After completion, the reaction mixture was quenched by acidification with HCl 3 M to pH \sim 5 and cooled to 0°C to precipitate crude product, which was recrystallized with MeOH-H₂O (1:3) mixture to afford pure chalcone. It was identified as 2,4,2',4'-tetrahydroxychalcone (**8**), by comparison with authentic sample.

2.5. Tyrosinase Inhibitory Assay. All pure compounds were dissolved in DMSO and tested at concentrations ranging from 0.01 to 100 μM . Assay mixtures in 0.1 M phosphate buffer pH 6.8 were prepared immediately before use, consisting of 100 μL of tyrosinase solution (15 U/mL) and 1900 μL of test solution. These mixtures were preincubated at room temperature for 30 min, followed by addition of 1000 μL of L-DOPA 1.5 mM in pH 6.8 phosphate buffer and incubated at room temperature for 7 min. The absorbances (*A*) at 475 nm were acquired on Shimadzu UV-1800 spectrophotometer. The inhibitory percentage (*I*%) was calculated according to the formula: $I\% = ((A_{\text{control}} - A_{\text{sample}}) / A_{\text{control}}) \times 100\%$. Data were represented as means \pm standard error (*n* = 3). The IC₅₀ values were determined by using GraphPad Prism software with multivariate nonlinear regression and $R^2 > 0.9$. Kojic acid was used as positive control.

2.6. Molecular Docking. Docking studies of **1**, **2**, **8**, and the positive reference (kojic acid) were performed with Molecular Operating Environment 2016 (MOE 2016.0802) suite. The structures of these compounds were constructed by using the Builder module. Subsequently, all compounds were minimized up to 0.0001 gradients using the Amber12:EHT force field. The crystal structure of the *oxy*-tyrosinase was taken from the Protein Data Bank (PDB code 1WX2). The caddie protein (ORF378) and water molecules were removed. The enzyme structure was prepared using the QuickPrep module. The binding site was determined based on the PLB (Propensity for Ligand Binding) score in the Site Finder module. The molecular docking was performed by Dock module, using Triangle Matcher placement, Induced Fit refinement, London dG, and GBVI/WSA dG scoring methods. Five top poses showed up based on the negative binding free energy value (*S* value). The best pose was selected to analyze the receptor-ligand interactions by using BIOVIA Discovery Studio Visualizer 2016.

3. Results and Discussion

3.1. Extraction and Isolation. The dried powdered stems of *S. caudata* were exhaustively extracted in a Soxhlet extractor

TABLE 1: ^1H (500 MHz) and ^{13}C (125 MHz) NMR data (acetone- d_6) for compounds **1** and **2**.

Position	1		2	
	δ_{C} , type C	δ_{H} (J, Hz)	δ_{C} , type C	δ_{H} (J, Hz)
1'	114.5, C		114.9, C	
2'	167.6, C		167.4, C	
3'	103.8, CH	6.35, d (2.4)	103.8, CH	6.35, d (2.4)
4'	165.5, C		165.9, C	
5'	108.7, CH	6.45, dd (8.9, 2.4)	108.8, CH	6.45, dd (8.9, 2.4)
6'	132.9, CH	7.94, d (8.9)	132.6, CH	7.92, d (8.9)
C=O	192.8, C		192.6, C	
α	122.1, CH	7.27, d (14.5)	122.8, CH	7.26, d (14.5)
β	147.3, CH	7.68, dd (14.5, 11.3)	145.8, CH	7.61, dd (14.5, 11.5)
γ	125.0, CH	7.17, dd (15.6, 11.3)	129.4, CH	6.62, dd (13.7, 11.5)
δ	139.5, CH	7.35, d (15.6)	145.8, CH	7.00, m
ϵ			126.1, CH	7.00, m
ζ			134.3, CH	7.13, d (14.6)
1	116.5, C		116.6, C	
2	158.5, C		157.8, C	
3	103.7, CH	6.47, d (2.4)	103.7, CH	6.45, d (2.4)
4	161.0, C		161.0, C	
5	108.9, CH	6.42, dd (8.5, 2.4)	108.8, CH	6.39, dd (8.5, 2.4)
6	130.2, CH	7.43, d (8.5)	129.3, CH	7.39, d (8.5)
OH-2'		13.68, s		13.64, s

with MeOH to yield MeOH-soluble extract (700 g). This extract was successively partitioned to give the *n*-hexane (37 g)- and CHCl_3 (500 g)-soluble fractions. The CHCl_3 -soluble extract of stems of *S. caudata* was repeatedly chromatographed using silica gel CC and preparative TLC to obtain seven compounds including two new diarylalkanoids named semedienone (**1**) and semetrienone (**2**). The known compounds were identified as 2,6-dimethoxybenzoquinone (**3**) [5], *p*-coumaric acid (**4**) [6], methyl *p*-coumarate (**5**) [7], *trans*-4-(3,4-dihydroxyphenyl)but-3-en-2-one (**6**) [8], and ferulic acid (**7**) [9] (Figure 1).

3.2. Structural Elucidation of Two New Isolated Compounds from *S. caudata*. Compound **1** showed a molecular formula to be $\text{C}_{17}\text{H}_{14}\text{O}_5$ based on the HRESIMS ion at m/z 321.0752 $[\text{M} + \text{Na}]^+$ (calcd. for $\text{C}_{17}\text{H}_{14}\text{O}_5\text{Na}$, 321.0739). The IR spectrum exhibited the presence of hydroxy (3455 cm^{-1}) and carbonyl (1620 cm^{-1}) functionalities. The ^1H NMR spectrum showed signals for two 1,2,4-trisubstituted aromatic rings (δ_{H} 7.94 (d, $J = 8.9\text{ Hz}$, H-6'), 6.45 (dd, $J = 8.9, 2.4\text{ Hz}$, H-5'), 6.35 (d, $J = 2.4\text{ Hz}$, H-3'), 7.43 (d, $J = 8.5\text{ Hz}$, H-6), 6.47 (d, $J = 2.4\text{ Hz}$, H-3), and 6.42 (dd, $J = 8.5, 2.4\text{ Hz}$, H-5)), four olefinic protons (δ_{H} 7.27 (d, $J = 14.5\text{ Hz}$, H- α), 7.68 (dd, $J = 14.5, 11.3\text{ Hz}$, H- β), 7.17 (dd, $J = 15.6, 11.3\text{ Hz}$, H- γ), and 7.35 (d, $J = 15.6\text{ Hz}$, H- δ)), and a distinctive signal of a hydrogen-bonded hydroxy group (δ_{H} 13.68). The ^{13}C NMR data (Table 1) exhibited resonances for a keto-carbonyl (δ_{C} 192.8), twelve aromatic carbons (δ_{C} 103.7–167.6), and four olefinic carbons (δ_{C} 122.1 (C- α), 147.3 (C- β), 125.0 (C- γ), and 139.5 (C- δ)). These were characteristic of those reported for (2*E*,4*E*)-1,5-diaryl-penta-2,4-dien-1-one [10,11]. The HMBC correlations (Figure 2) from OH-2' to C-1' and C-3', from H-3' to C-1' and C-4', from H-5' to C-1', from H-6' to C-2' and C-4', from H-3 to C-1, C-2, and C-4, from H-5 to

C-1, and from H-6 to C-2 and C-4 indicated that four hydroxy groups were located at C-2', C-4', C-2, and C-4. Moreover, the HMBC correlations from H-6', H- α , and H- β to C=O, from H- α to C- γ , from H- β to C- δ , from H- γ to C- α , from H- γ to C- β and C-1, and from H- δ to C- β and C-6 suggested the presence of the $\alpha,\beta,\gamma,\delta$ -unsaturated carbonyl moiety in **1**. The NOESY correlations between H-5' and H-6', H-6' and H- α , H- β and H- δ , H- γ and H-6, and H-6 and H-5 indicated the relative configuration of **1** as shown in Figure 2. Thus, the structure of semedienone (**1**) was concluded as 2*E*,4*E*-1,5-bis(2,4-dihydroxyphenyl)penta-2,4-dien-1-one.

Compound **2** showed the HRESIMS ion at m/z 347.0902 $[\text{M} + \text{Na}]^+$ (calcd. for $\text{C}_{19}\text{H}_{16}\text{O}_5\text{Na}$, 347.0895). Its IR spectrum showed absorption bands for hydroxy (3305 cm^{-1}) and carbonyl (1650 cm^{-1}) groups. The ^1H and ^{13}C NMR spectra of **2** (Table 1) showed signals for two 1,2,4-trisubstituted aromatic rings, which resembled those of **1**. Compound **2** showed the presence of six olefinic protons (δ_{H} 7.26 (d, $J = 14.5\text{ Hz}$, H- α), 7.61 (dd, $J = 14.5, 11.5\text{ Hz}$, H- β), 6.62 (dd, $J = 13.7, 11.5\text{ Hz}$, H- γ), 7.00 (2H, m, H- δ and H- ϵ), and 7.13 (d, $J = 14.6\text{ Hz}$, H- ζ)) in the ^1H NMR spectrum, and six olefinic carbons (δ_{C} 122.8 (C- α), 145.8 (C- β), 129.4 (C- γ), 145.8 (C- δ), 126.1 (C- ϵ), 134.3 (C- ζ)) in the ^{13}C NMR spectrum. These were characteristic of those reported for (2*E*,4*E*,6*E*)-1,7-diarylhepta-2,4,6-trien-1-one [12]. The locations of four hydroxy groups were assigned at C-2', C-4', C-2, and C-4 by the observed HMBC correlations (Figure 1). Moreover, the HMBC correlations from H-6', H- α , and H- β to C=O, from H- α to C- γ , from H- γ to C- β , from H- δ to C- ζ , from H- ϵ to C- ζ and C-1, and from H- ζ to C- δ and C- ϵ suggested the presence of the $\alpha,\beta,\gamma,\delta,\epsilon,\zeta$ -unsaturated carbonyl moiety in **2**. The relative configuration of **2** was deduced based on the NOESY correlations between H-5' and H-6', H-6' and H- α , H- α and H- γ , H- β and H- δ , H- γ and

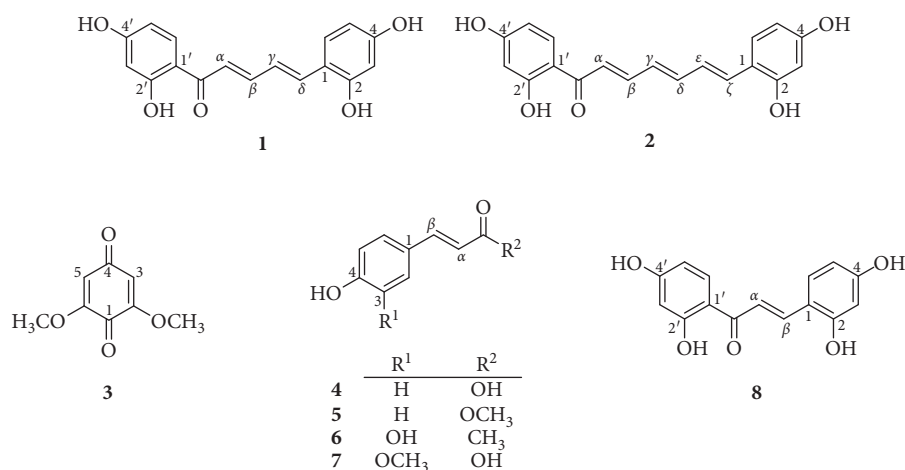


FIGURE 1: Structures of compounds 1-8.

H- ϵ , H- ϵ and H-6, and H-6 and H-5 (Figure 2). Thus, the structure of semetrienone (**2**) was established as 2*E*,4*E*,6*E*-1,7-bis(2,4-dihydroxyphenyl)hepta-2,4,6-trien-1-one.

3.3. Tyrosinase Inhibitory Activity of Isolated Compounds from *S. caudata*. Compounds (**1-7**) were tested for their tyrosinase inhibitory activity [13]. Kojic acid, a purported skin-lightening agent, was used as a positive control. 2,4,2',4'-Tetrahydroxychalcone (**8**), which was synthesized following our previous procedure [14], showed potent activity with an IC₅₀ value of 0.016 μ M (Table 2). Semedienone (**1**) and semetrienone (**2**) exhibited remarkable inhibitory effect with the IC₅₀ values of 0.033 and 0.11 μ M, respectively, more potent than that of kojic acid (IC₅₀, 44.6 μ M). Additionally, compounds **4** and **6** were found to possess tyrosinase inhibitory activity with the IC₅₀ values of 2.35 and 27.0 μ M, respectively.

The presence of α,β -unsaturated hydroxycarbonyl groups in cinnamic acid derivatives were found to enhance activity (**2** \gg **3**). Additionally, the occurrence of a C-3 methoxy group decreased the inhibitory activity (**2** \gg **5**) [15,16]. Diarylalkenoids with 2,4-disubstituted resorcinol subunit on ring B contributed the most to inhibitory activity [17]. Moreover, the length of the conjugated carbon chain in diarylalkenoids led to a change of activity (**8** $>$ **1** $>$ **2**). This result reaffirmed the (*Z*)- β -phenyl- α,β -unsaturated carbonyl scaffold plays an important role for tyrosinase inhibition [18,19]. In previous reports, diarylpentadiene-3-one were not significantly inhibiting tyrosinase activity [20], but some analogues showed moderate antimelanogenesis activity [21]. Some cyclic diarylheptanoids were found to have melanogenesis-inhibitory activity [22]. In this regard, semedienone (**1**) and semetrienone (**2**) could be the potent structural templates for developing new skin-lightening agents.

3.4. Docking Study of the Active Compounds 1, 2, and 8. Tyrosinase has four possible oxidation states (*deoxy*-, *oxy*-, *met*-, and *deact*-form) [23]. *Met*-tyrosinase, having a

hydroxy and the two Cu²⁺ ions in the binding site, is responsible for the oxidation of catechols. In this oxidizing process, *met*-tyrosinase is reduced to *deoxy*-tyrosinase which rapidly binds dioxygen to give *oxy*-tyrosinase form. *Oxy*-tyrosinase, which is the primary form of the enzyme, oxidizes both phenols and catechols to *o*-quinones by the monooxygenase and oxidase mechanisms, respectively. In the active site of *oxy*-tyrosinase, two bound Cu²⁺ ions and the peroxide group play a catalytic oxidation role. Mushroom tyrosinase (EC 1.14.18.1), which was used in the inhibitory assay, plays the same role with respect to *oxy*-tyrosinase form. Thus, in this study, the molecular docking studies of **1**, **2**, and **8**, respectively, with *oxy*-tyrosinase (PDB ID:1WX2) [24] were carried out to explore their interactions and inhibition mechanisms.

In molecular docking study, the imperfect scoring results (false-positive hits), which may be considered as decoys, can be occurred by predicting incorrect ligand geometries or by applying nonbinding molecules. The active and decoy ligands are similar according to some physicochemical properties (molecular weight, number of rotational bonds, total hydrogen bond donors, total hydrogen bond acceptors, topological polar surface area, and the octanol-water partition coefficient), but decoy was presumed to be inactive against a target. According to Choi et al. [25], kojic acid and hypoxanthine showed the tyrosinase inhibitory constant (*K_i*) values of 13 μ M and >1000 μ M, respectively [25]. Thus, in this docking study, kojic acid and hypoxanthine was selected as the active inhibitor and the decoy molecule, respectively, to validate our docking protocol.

The docking studies were performed with Molecular Operating Environment 2016 (MOE 2016.0802) suite [26]. The top-ranked pose with the highest negative binding free energy value (*S* value) was selected for further interaction analysis with BIOVIA Discovery Studio Visualizer 2016 [27].

Compounds **1**, **2**, and **8** showed an H-donor interaction between a hydroxy group and a peroxide bridge PER404, presenting the distances of 1.85, 1.88, and 1.78 Å, respectively, whereas kojic acid showed the interactions with a Cu²⁺ ion, HIS194, and THR203 residues (Figure 3). In the

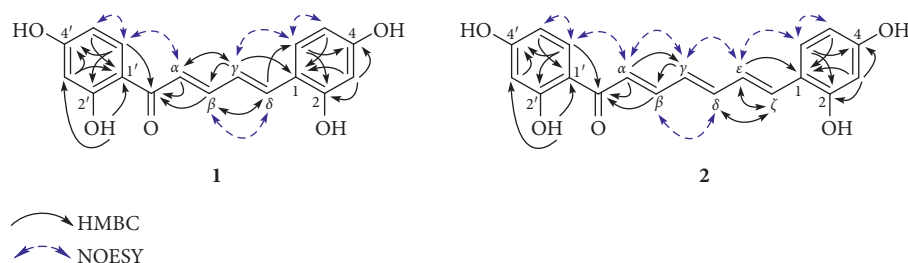


FIGURE 2: Significant HMBC (solid arrows) and selected NOESY correlations (blue dashed arrows) observed for **1** and **2**.

TABLE 2: Tyrosinase inhibitory activities of the isolated compounds **1–8**.

Compound	IC ₅₀ (μM)
1	0.033
2	0.11
3	>100
4	2.35
5	>100
6	27.0
7	>100
8	0.016
Kojic acid ^a	44.6

^aPositive control.

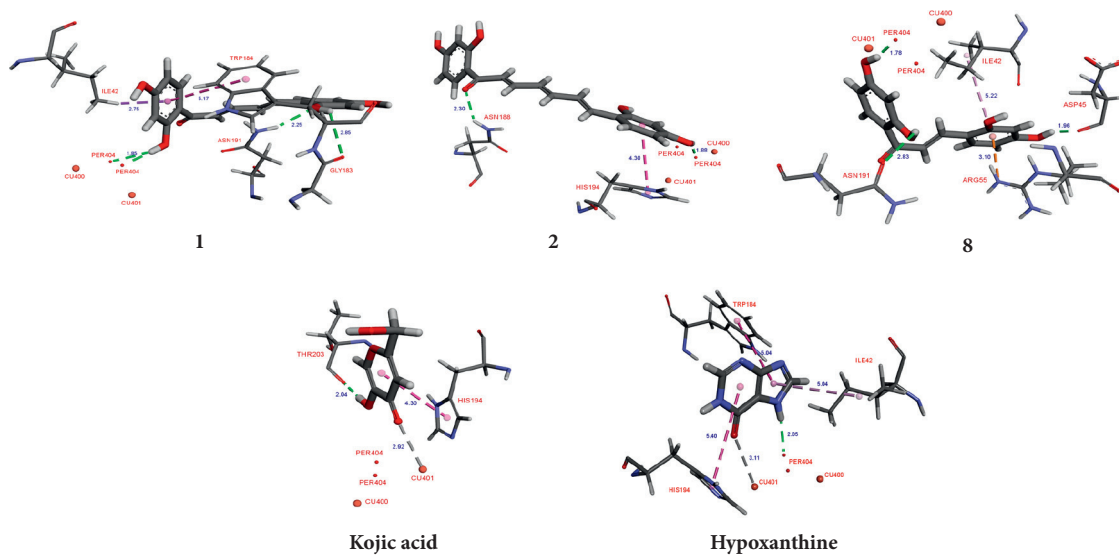


FIGURE 3: 3D docking models of **1**, **2**, **8**, kojic acid, and hypoxanthine with *oxy*-tyrosinase (1WX2).

binding pocket, compounds **1** and **8** showed more interactions with targeting residues than those of **2** (Table 3). These analysis results were consistent with their experimental inhibitory activities (**8** > **1** > **2**). The C-2 hydroxy group of **1** exhibited H-bonding interactions with ASN191 and GLY183 residues. Moreover, the aromatic ring A of **1** formed π - π T-shaped and π - σ interactions with TRP184 and ILE42 residues, respectively. Compound **2** showed an H-acceptor interaction between C=O group and ASN188 residue. In addition, the aromatic ring B of **2** interacted with HIS194 residue via a π - π stacking interaction. Thus, the *S*

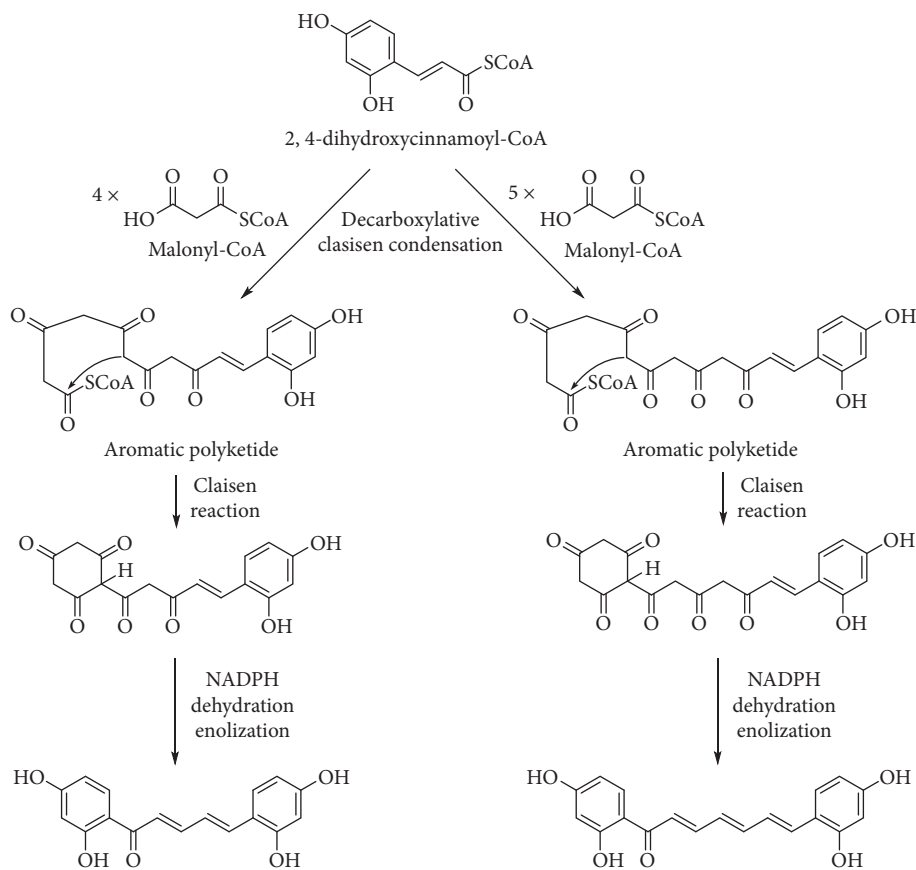
values and these interactions suggested that **1** and **2** showed high binding affinity for *oxy*-tyrosinase than those of kojic acid. Hypoxanthine showed the lower negative *S* value and the longer-distance interactions than that of kojic acid. Apparently, these results could be used to validate the abovementioned docking procedure in this study.

3.5. Proposed Biosynthetic Pathways of **1 and **2**.** We have proposed plausible biogenetic pathways for two new diaryllankanoids (**1** and **2**) (Figure 4) *via* the shikimate and

TABLE 3: Docking results of **1**, **2**, **8**, kojic acid, and hypoxanthine with *oxy*-tyrosinase.

Compound	<i>oxy</i> -tyrosinase (1WX2)			
	S values	Interactions	Targeting residues	Distance (Å)
1	-5.75	H-donor π - σ π - π	PER404	1.85
			ASN191	2.25
			GLY183	2.85
			ILE42	2.75
			TRP184	5.17
2	-6.37	H-donor H-acceptor π - π	PER404	1.88
			ASN188	2.30
			HIS194	4.30
8	-5.54	H-donor π -alkyl π -cation	PER404	1.78
			ASP45	1.96
			ASN191	2.83
			ILE42	5.22
			ARG55	3.10
Kojic acid ^a	-4.50	H-donor Metal-acceptor π - π	THR203	2.04
			CU401	2.92
			HIS194	4.30
			PER404	2.05
Hypoxanthine ^b	-4.34	H-donor Metal-acceptor π - π π -alkyl	PER404	2.05
			CU401	3.11
			HIS194	5.40
			TRP184	5.04
			ILE42	5.04

^aPositive control. ^bDecoy molecule.

FIGURE 4: Plausible biosynthetic pathways for diarylalkanoids **1** and **2**.

acetate pathways [28]. α -Ketoglutarate-dependent hydroxylase is responsible for the C-2 hydroxylation of *p*-coumaroyl-CoA to give 2,4-dihydroxycinnamoyl-CoA [29]. It is condensed with four or five malonyl-CoA moieties to afford the corresponding polyketides, which undergo the intramolecular ring closure *via* Claisen reaction. After that, reduction, dehydration, and enolization must occur to give rise to **1** and **2**.

4. Conclusions

From the CHCl_3 -soluble extract of the stems of *S. caudata*, two new diarylalkanoids were isolated together with five known compounds. Compounds **1** and **2** were found to possess potent tyrosinase inhibitory activity with the IC_{50} values of 0.033 and 0.11 μM , respectively. Binding interaction analyses between the *oxy*-tyrosinase active site and the active compounds (**1** and **2**) have been performed. Plausible biogenetic pathways for formation of two new diarylalkanoids (**1** and **2**) were also proposed.

Data Availability

The data used to support the findings of this study are included within the article.

Conflicts of Interest

The authors declare that there are no conflicts of interest regarding the publication of this paper.

Acknowledgments

This research was funded by Vietnam National University Ho Chi Minh City (VNU-HCM) under grant no. NCM2020-18-01.

Supplementary Materials

^1H and ^{13}C NMR spectra of two new compounds, semedienone (**1**) and semetrieneone (**2**). (*Supplementary Materials*)

References

- [1] J. N. Rodríguez-López, J. Tudela, R. Varón, F. García-Carmona, and F. García-Cánovas, "Analysis of a kinetic model for melanin biosynthesis pathway," *Journal of Biological Chemistry*, vol. 267, no. 6, pp. 3801–3810, 1992.
- [2] H. Decker and F. Tuzcek, "Tyrosinase/catecholoxidase activity of hemocyanins: structural basis and molecular mechanism," *Trends in Biochemical Sciences*, vol. 25, no. 8, pp. 392–397, 2000.
- [3] T. Pillaiyar, M. Manickam, and V. Namasivayam, "Skin whitening agents: medicinal chemistry perspective of tyrosinase inhibitors," *Journal of Enzyme Inhibition and Medicinal Chemistry*, vol. 32, no. 1, pp. 403–425, 2017.
- [4] P. H. Dang, T. T. Nguyen, T. H. Le, H. X. Nguyen, M. T. T. Nguyen, and N. T. Nguyen, "A new bischromanone from the stems of *Semecarpus caudata*," *Natural Product Research*, vol. 32, no. 15, pp. 1745–1750, 2018.
- [5] V. Ibrahim, N. Volkova, S.-H. Pyo, G. Mamo, and R. Hattikaul, "Laccase catalysed modification of lignin subunits and coupling to *p*-aminobenzoic acid," *Journal of Molecular Catalysis B: Enzymatic*, vol. 97, pp. 45–53, 2013.
- [6] J. Sun, X.-M. He, M.-M. Zhao, L. Li, C.-B. Li, and Y. Dong, "Antioxidant and nitrite-scavenging capacities of phenolic compounds from sugarcane (*Saccharum officinarum* L.) tops," *Molecules*, vol. 19, no. 9, pp. 13147–13160, 2014.
- [7] F. Carta, D. Vullo, A. Maresca, A. Scozzafava, and C. T. Supuran, "Mono-/dihydroxybenzoic acid esters and phenol pyridinium derivatives as inhibitors of the mammalian carbonic anhydrase isoforms I, II, VII, IX, XII and XIV," *Bioorganic & Medicinal Chemistry*, vol. 21, no. 6, pp. 1564–1569, 2013.
- [8] A. Baranovsky, B. Schmitt, D. J. Fowler, and B. Schneider, "Synthesis of new biosynthetically important diarylheptanoids and their oxa- and fluoro-analogues by three different strategies," *Synthetic Communications*, vol. 33, no. 6, pp. 1019–1045, 2003.
- [9] H. Xiao and K. Parkin, "Isolation and identification of phase II enzyme-inducing agents from nonpolar extracts of green onion (*Allium* spp.)," *Journal of Agricultural and Food Chemistry*, vol. 54, no. 22, pp. 8417–8424, 2006.
- [10] N. Desideri, R. Fioravanti, L. Proietti Monaco et al., "1,5-Diphenylpenta-2,4-dien-1-ones as potent and selective monoamine oxidase-B inhibitors," *European Journal of Medicinal Chemistry*, vol. 59, pp. 91–100, 2013.
- [11] S. M. Mohd Faudzi, S. W. Leong, F. Abas et al., "Synthesis, biological evaluation and QSAR studies of diarylpentanoic acid analogues as potential nitric oxide inhibitors," *Medicinal Chemistry Communication*, vol. 6, no. 6, pp. 1069–1080, 2015.
- [12] H. Mohamad, N. H. Lajis, F. Abas et al., "Antioxidative constituents of *Etilingera elatior*," *Journal of Natural Products*, vol. 68, no. 2, pp. 285–288, 2005.
- [13] E. T. Arung, I. W. Kusuma, Y. M. Iskandar, S. Yasutake, K. Shimizu, and R. Kondo, "Screening of Indonesian plants for tyrosinase inhibitory activity," *Journal of Wood Science*, vol. 51, no. 5, pp. 520–525, 2005.
- [14] T. H. Bui, N. T. Nguyen, P. H. Dang, H. X. Nguyen, and M. T. T. Nguyen, "Design and synthesis of chalcone derivatives as potential non-purine xanthine oxidase inhibitors," *Springerplus*, vol. 5, no. 1, pp. 1789–1796, 2016.
- [15] T. Takahashi and M. Miyazawa, "Tyrosinase inhibitory activities of cinnamic acid analogues," *Die Pharmazie—An International Journal of Pharmaceutical Sciences*, vol. 65, no. 12, pp. 913–918, 2010.
- [16] Z. Zhang, J. Liu, F. Wu, and L. Zhao, "Inhibitory effects of substituted cinnamic acid esters on mushroom tyrosinase," *Letters in Drug Design & Discovery*, vol. 10, no. 6, pp. 529–534, 2013.
- [17] S. Khatib, O. Nerya, R. Musa, M. Shmuel, S. Tamir, and J. Vaya, "Chalcones as potent tyrosinase inhibitors: the importance of a 2,4-substituted resorcinol moiety," *Bioorganic & Medicinal Chemistry*, vol. 13, no. 2, pp. 433–441, 2005.
- [18] H. R. Kim, H. J. Lee, Y. J. Choi et al., "Benzylidene-linked thiohydantoin derivatives as inhibitors of tyrosinase and melanogenesis: importance of the β -phenyl- α , β -unsaturated carbonyl functionality," *Medicinal Chemistry Communication*, vol. 5, no. 9, pp. 1410–1417, 2014.
- [19] S. J. Kim, J. Yang, S. Lee et al., "The tyrosinase inhibitory effects of isoxazolone derivatives with a (Z)- β -phenyl- α , β -unsaturated carbonyl scaffold," *Bioorganic & Medicinal Chemistry*, vol. 26, no. 14, pp. 3882–3889, 2018.

- [20] K.-H. Lee, F. H. Ab Aziz, A. Syahida et al., "Synthesis and biological evaluation of curcumin-like diarylpentanoid analogues for anti-inflammatory, antioxidant and anti-tyrosinase activities," *European Journal of Medicinal Chemistry*, vol. 44, no. 8, pp. 3195–3200, 2009.
- [21] T. Hosoya, A. Nakata, F. Yamasaki et al., "Curcumin-like diarylpentanoid analogues as melanogenesis inhibitors," *Journal of Natural Medicines*, vol. 66, no. 1, pp. 166–176, 2012.
- [22] T. Akihisa, A. Takeda, H. Akazawa et al., "Melanogenesis-inhibitory and cytotoxic activities of diarylheptanoids from *Acer nikoense* bark and their derivatives," *Chemistry & Biodiversity*, vol. 9, no. 8, pp. 1475–1489, 2012.
- [23] C. A. Ramsden and P. A. Riley, "Tyrosinase: the four oxidation states of the active site and their relevance to enzymatic activation, oxidation and inactivation," *Bioorganic & Medicinal Chemistry*, vol. 22, no. 8, pp. 2388–2395, 2014.
- [24] Y. Matoba, T. Kumagai, A. Yamamoto, H. Yoshitsu, and M. Sugiyama, "Crystallographic evidence that the dinuclear copper center of tyrosinase is flexible during catalysis," *Journal of Biological Chemistry*, vol. 281, no. 13, pp. 8981–8990, 2006.
- [25] J. Choi, Y. M. Lee, and J. G. Jee, "Thiopurine drugs repositioned as tyrosinase inhibitors," *International Journal of Molecular Sciences*, vol. 19, no. 1, p. 77, 2018.
- [26] Chemical Computing Group, "Molecular operating environment (MOE) 2016," Chemical Computing Group, Montreal, QC, Canada, 2016.
- [27] Dassault Systèmes BIOVIA, *BIOVIA Discovery Studio Visualizer*, Dassault Systèmes BIOVIA, San Diego, CA, USA, 2016.
- [28] P. M. Dewick, *Medicinal Natural Products: A Biosynthetic Approach*, John Wiley & Sons, Hoboken, NJ, USA, 3rd edition, 2009.
- [29] S. Martinez and R. P. Hausinger, "Catalytic mechanisms of Fe(II)- and 2-oxoglutarate-dependent oxygenases," *Journal of Biological Chemistry*, vol. 290, no. 34, pp. 20702–20711, 2015.

Research Article

Determining Pharmacological Mechanisms of Chinese Incompatible Herbs Fuzi and Banxia in Chronic Obstructive Pulmonary Disease: A Systems Pharmacology-Based Study

Kaiwen Ni,¹ Xiaolu Cai,¹ Yaling Chen,¹ Linshui Zhou,² Ruilin Chen,² Suqun Zheng,² and Zhen Wang^{1,2}

¹The First Clinical College of Zhejiang Chinese Medical University, Hangzhou, China

²The First Affiliated Hospital of Zhejiang Chinese Medical University, Hangzhou, China

Correspondence should be addressed to Zhen Wang; wangzhen610@sina.cn

Received 18 June 2020; Revised 31 October 2020; Accepted 12 December 2020; Published 31 December 2020

Academic Editor: Akhilesh K. Tamrakar

Copyright © 2020 Kaiwen Ni et al. This is an open access article distributed under the Creative Commons Attribution License, which permits unrestricted use, distribution, and reproduction in any medium, provided the original work is properly cited.

Aconiti Lateralis Radix Praeparata (Fuzi) and *Pinelliae Rhizoma* (Banxia) are among the 18 incompatible medications that are forbidden from use in one formulation. However, there is increasing evidence implying that this prohibition is not entirely correct. According to the theory of Chinese traditional medicine, they can be used for the treatment of chronic obstructive pulmonary disease (COPD). Thus, we analyzed the possible approaches for the treatment of COPD using network pharmacology. The active compounds of Fuzi and Banxia (FB) were collected, and their targets were identified. COPD-related targets were obtained by analyzing the differentially expressed genes between COPD patients and healthy individuals, which were expressed using a Venn diagram of COPD and FB. Protein-protein interaction data and network regarding COPD and drugs used were obtained. Gene ontology and Kyoto Encyclopedia of Genes and Genomes pathway analysis were conducted. The gene-pathway network was constructed to screen the key target genes. In total, 34 active compounds and 47 targets of FB were identified; moreover, 7,153 differentially expressed genes were identified between COPD patients and healthy individuals. The functional annotations of target genes were found to be related to mechanisms such as transcription, cytosol, and protein binding; furthermore, 68 pathways including neuroactive ligand-receptor interaction, Kaposi sarcoma-associated herpesvirus infection, apoptosis, and measles were significantly enriched. FOS, CASP3, VEGFA, ESR1, and PTGS2 were the core genes in the gene-pathway network of FB for the treatment of COPD. Our results indicated that the effect of FB against COPD may involve the regulation of immunological function through several specific biological processes and their corresponding pathways. This study demonstrates the application of network pharmacology in evaluating mechanisms of action and molecular targets of herb-opponents FB.

1. Introduction

As defined by the Global Initiative for Chronic Obstructive Lung Disease (GOLD) Reports 2020, chronic obstructive pulmonary disease (COPD) is characterized by persistent respiratory symptoms and airflow limitation ascribed to airway and/or alveolar abnormalities. Data from the American Lung Association Epidemiology and Statistics Unit show that COPD is projected to be the 3rd by 2020. According to GOLD, smoking cessation is essential in all COPD patients who continue to smoke, whereas bronchodilators, inhaled corticosteroids (ICS), and anti-

inflammatory agents are the primary drugs for COPD patients in stable conditions. However, current treatments are only able to slow the progression of COPD [1].

Recently, traditional Chinese medicine (TCM) has been shown to have potential therapeutic properties against COPD [2]. For instance, Bufe Yishen formula exerted its anti-COPD efficacy by restoring Th17/Treg balance via the modulation of STAT3 and activation of STAT5 [3]. Clinically, chronic and progressive dyspnea are the main characteristic symptoms of COPD, and around a third of patients experience cough and sputum production. According to the theory of TCM, the dyspnea may imply depression of the

chest yang, while sputum production suggests phlegm stagnant. Additionally, the elderly, the primary population of the disease, are often considered to have declination in the kidney yang. These characteristics mentioned belong to one syndrome called yang-deficiency-with-phlegm-stagnant, in TCM.

In TCM, *Aconiti Lateralis Radix Praeparata* (Fuzi, the dried lateral root of *Aconitum carmichaelii* Debx.) improves COPD's yang deficiency by tonifying fire and enhancing yang. *Pinelliae Rhizoma* (Banxia, the dried tuber of *Pinellia ternata* (Thunb.) Breit.) defends against COPD's phlegm stagnant by drying dampness and resolving phlegm. In addition, it is reported that *P. ternata* can be used to reverse various adverse effects of the withdrawal of ICS, such as a rebound in goblet cell number, mucin 5AC (MUC5AC) expression, and interleukin 1 β (IL-1 β) and tumor necrosis factor α (TNF- α) levels, used for the treatment of COPD [4]. Moreover, patients with COPD have higher levels of systemic inflammation markers [5]. Fuzi has a wide range of biological activities, including anti-inflammatory, antitumor, and immunomodulatory effects, as well as effects on energy metabolism [6].

Cotreatment of FB is not to be used in TCM, as indicated in the *Eighteen Incompatible Medicaments Verse* and first noted in the *Rumen Shiqin* [7], owing to high toxicity and side effects of the combination in one apozem. However, increasing evidence shows that they have no significant harmful effects on humans [8]. One clinical study showed that there was no significant toxicity of cotreatment of FB in the heart, liver, kidney, and blood used in patients with malignant tumors. [9] Moreover, as reported in "*Shanghan Zabiing Lun*," a widely used clinical guidebook of TCM, 2000 years ago, FB were used in a formulation called "*Fuzi-jingmi Tang*." [10] As for now, we still do some clinical researches using formulations which contained FB. *Xiaoqinglong-Jiafuzi-Decoction*, including both Fuzi and Banxia, significantly reduced COPD patients' modified Medical Research Council (mMRC) scores, and enhanced their lung function. [11] Another clinical research indicated that *Xiaoqinglong-Jiafuzi-Decoction* sharply increased the negative rate of IgE when compared with conventional Western medicine in the treatment of allergic rhinitis. [12] There was no obvious harmful effectiveness of combination of FB mentioned. Thus, we utilized a network pharmacology method to delineate the mechanisms of action and molecular targets of FB for their possible treatment of COPD.

In TCM, multiple herbs are used in complex herbal formulations for various diseases because of their potentially bioactive components that interact with multiple therapeutic targets. The multicomponent, multitarget, and multipathway of formulations means TCM can provide ideal treatments but also comes with great challenges due to the interactions among them [13]. Network pharmacology is a novel approach that attempts to solve these problems, combining systems network analysis with pharmacology. It can be used to illustrate the synergism among compounds and the potential mechanisms of various components and multitarget drugs at the molecular level through the network levels of compound-compound, compound-target, and

target-disease interactions. Network pharmacology could promote the understanding of the interactions among compounds, genes, proteins, and diseases; moreover, it is suitable for the study of complex TCM formulations [14]. For example, a feasible system pharmacology model based on chemical, pharmacokinetic, and pharmacological data was developed via a network construction approach to clarify the synergistic mechanisms of Huangqi (*Radix Astragali*) and Huanglian (*Rhizoma Coptidis*) [15]. The active ingredients of Fuzheng Huayu formulation were successfully identified, and the mechanisms by which they inhibit hepatic stellate cell viability were determined using network pharmacology and transcriptomics [16]. In this study, for the first time, we explored the action mechanisms and molecular targets of FB for the treatment of COPD using network pharmacology.

2. Materials and Methods

2.1. Active Ingredient Screening. The chemical compositions of FB were identified from the Traditional Chinese Medicine Systems Pharmacology Database and Analysis Platform (TCMSP) [17]. Then, we selected candidate compounds with standard oral bioavailability (OB) \geq 30% and drug-likeness (DL) \geq 0.18 [18].

A total of 34 identified compounds were imported into the DrugBank database [19] to delineate the relevant targets of FB. According to one relevant literature report, 5 representative alkaloids of Fuzi, aconitine (AC), mesaconitine (MA), benzoyleaconine (BAC), benzoylmesaconine (BMA), and benzoylhypaconine (BHA), which were not selected out from the DrugBank were also included in the scope of the study [20]. They are also listed in Table 1.

2.2. Identifying COPD-Related Targets. COPD genes were collected from both Genecards and the Online Mendelian Inheritance in Man (OMIM) databases. There was no threshold applied during this step, so as to collect as many genes as possible.

2.3. Venn Diagram. We have made a Venn diagram using Venny to show the overlapping genes of COPD and FB.

2.4. Network and Protein-Protein Interaction Analysis. Using Cytoscape 3.7.2 software, genes common to the drugs and the disease were connected to visualize the relationship between the compounds used against FB and COPD. Protein-protein interactions (PPI), as per data from STRING, are based on the proteins in common. First, the genes are ranked by calculating the number of times they appear in the network. Then, with the CytoNCA APP, we analyzed degree centrality (DC), closeness centrality (CC), local average connectivity-based method (LAC), betweenness centrality (BC), Eigenvector centrality (EC), and network centrality (NC), all of which indicate a protein's topology potential. It is reported that their definitions and calculation formulas have been used in network pharmacology and system

pharmacology [21]. Meanwhile, we counted the string interactins between nodes to figure out the core genes. To make out the core genes, we used CytoHubba to catch top 5 genes ranked by maximal clique centrality (MCC). [22].

2.5. Bioinformatic Analysis

2.5.1. Gene Ontology (GO) Analysis. GO analysis, based on the biological processes, cellular components, and molecular functions, places genes that are functionally similar into one group [23]. We used R and Bioconductor [24] to visualize the GO analysis. Functional classifications were analyzed within genes (p value cutoff = 0.05, q value cutoff = 0.05).

2.5.2. Kyoto Encyclopedia of Genes and Genomes (KEGG) Database. The KEGG database was used to analyze pathways, in the same manner as GO analysis. Significant changes (p value cutoff = 0.05, q value cutoff = 0.05) were distinguished for further study.

2.6. Visualization of Molecular Docking Analysis of Active Components and Core Genes. The protein expressed by core genes and active components were analyzed to figure out the active ingredients which had both minimum binding energy and polar contact. PYMOL was used to visualize docking effect conformation.

3. Results

3.1. Compound-Target Network Analysis. Twenty-one relevant compounds were obtained from the analysis of Fuzi and 13 from Banxia analysis (Table 1). For Fuzi, the OBs of ignavine, (R)-norcoclaurine, and karanjin are 84.08%, 82.54%, and 69.56%, respectively, which suggests that they may be the most effective active compounds present, while for Banxia, the OBs of (3S, 6S)-3-(benzyl)-6-(4-hydroxybenzyl) piperazine-2, 5-quinone, beta-D-ribofuranoside (xanthine-9), and stigmasterol are 46.89%, 44.72%, and 43.83%, respectively.

All 39 compounds were imported into the DrugBank database to further delineate the targets of FB. After removing 23 compounds with no known corresponding targets, 6 active compounds in Fuzi and 10 in Banxia were identified. From the active compounds, all 47 targets were identified, 13 for Fuzi (Table S1) and 41 for Banxia (Table S2). Genetic symbols of all targets are included for clarity (Table 1). Additionally, we have listed the number of targets corresponding to different components in FB (Table S3) and included the gene symbols of the targets for clarity. Unfortunately, the 5 compounds that were added were filtered without knowing the corresponding target genes.

3.2. Identifying COPD-Related Targets. COPD genes were collected from both Genecards and the OMIM databases, ultimately resulting in a collection of 7,153 related targets.

3.3. Venn Diagram. A Venn diagram (Figure 1(a)) was used to depict the overlapping genes of COPD and FB. The analysis showed that 44 genes are related to both COPD and FB. Another Venn diagram (Figure 1(b)) was used depict the 7 common genes of FB. The 2 drugs may work synergistically through these common genes: ESR1, PTGS1, PRSS1, PGR, NCOA1, NCOA2, and NR3C2.

3.4. Network Analysis. Using Cytoscape 3.7.2 software, the 44 common genes, alongside the network between FB and COPD, were set up and visualized (Figure 2). Between the 16 compounds in both FB and the 44 genes with overlapping relationships with COPD, 147 edges were analyzed. These edges indicate the compound-target interactions.

3.5. PPI Analysis. Based on the same 44 targets, after removal of discrete points, a PPI network was generated (Figure 3), which included 39 nodes and 186 edges, representing 39 interacting proteins and 186 interactions. We counted the appearance of genes in the PPI network and ranked their value roughly (Figure 4).

With the use of the CytoNCA APP, we calculated the median of BC, CC, EC, DC, NC, and LAC as 16.4307, 0.5067, 0.1181, 8, 6.1431, and 3.75, respectively. We selected the targets that demonstrated higher indices for each median, for further analysis. Eventually, 13 targets were obtained: FOS, CASP3, VEGFA, ESR1, PTGS2, RELA, AR, CYCS, HIF1A, PGR, PPARG, NCOA1, and NCOA2. In way of CytoHubba, ranked by MCC, we got top 5 genes as core genes- FOS, CASP3, VEGFA, ESR1, and PTGS2 (Table 2 and Figure 5).

3.6. Molecular Docking Analysis. Molecular docking of the active components and core genes with high mutual attraction is listed in Table 3, while the relating images are shown in Figure 6.

3.6.1. GO. The 13 identified candidate targets were analyzed using Bioconductor by R (threshold; p value cutoff = 0.05, q value cutoff = 0.05). The data of GO analysis are listed in Table S4. Twenty GO terms were analyzed (Figure 7).

3.6.2. KEGG. The critical pathways involved in the FB treatment of COPD were identified by KEGG pathway analysis (Figure 8). The data of KEGG analysis are shown in Table S5. There were 68 enhanced pathways identified (p value cutoff = 0.05, q value cutoff = 0.05), including neuro-active ligand-receptor interaction, human immunodeficiency virus 1 infection, Kaposi sarcoma-associated herpesvirus infection, cholinergic synapse, and hepatitis B. Figure 9 shows the details of four pathways through which the genes were primarily distributed in the p53 signaling pathway, apoptosis pathway, and cholinergic synapse pathway.

The article flow chart to show our job is given in Figure 10.

TABLE 1: Components of Fuzi and Banxia and their parameters.

Id	Name	OB	DL	Source
MOL002421	Ignavine	84.08	0.25	Fuzi
MOL002419	(R)-norcoclaurine	82.54	0.21	Fuzi
MOL002398	karanjin	69.56	0.34	Fuzi
MOL002388	Delphin_qt	57.76	0.28	Fuzi
MOL002395	Deoxyandrographolide	56.3	0.31	Fuzi
MOL002415	6-Demethyl-desoline	51.87	0.66	Fuzi
MOL002397	Karakoline	51.73	0.73	Fuzi
MOL002422	Isotalatizidine	50.82	0.73	Fuzi
MOL002392	Deltoin	46.69	0.37	Fuzi
MOL002401	Neokadsuranic acid B	43.1	0.85	Fuzi
MOL002433	(3R, 8S, 9R, 10R, 13R, 14S, 17R)-3-hydroxy-4, 4, 9, 13, 14-pentamethyl-17-[(E, 2R)-6-methyl-7-[(2R, 3R, 4S, 5S, 6R)-3, 4, 5-trihydroxy-6-[[[(2R, 3R, 4S, 5S, 6R)-3, 4, 5-trihydroxy-6-(hydroxymethyl)oxan-2-yl]oxymethyl]oxan-2-yl]oxyhept-5-en-2-yl]-1, 2, 3, 7, 8, 10, 12, 15, 16, 17-decahydr	41.52	0.22	Fuzi
MOL002211	11, 14-Eicosadienoic acid	39.99	0.2	Fuzi
MOL002406	2, 7-Dideacetyl-2, 7-dibenzoyl-taxayunnanine F	39.43	0.38	Fuzi
MOL002434	Carnosifloside I_qt	38.16	0.8	Fuzi
MOL000359	Sitosterol	36.91	0.75	Fuzi
MOL002393	Demethyl-delavaine A	34.52	0.18	Fuzi
MOL002394	Demethyl-delavaine B	34.52	0.18	Fuzi
MOL002410	Benzoyl-napelline	34.06	0.53	Fuzi
MOL002423	Jesaconitine	33.41	0.19	Fuzi
MOL000538	Hypaconitine	31.39	0.26	Fuzi
MOL002416	Deoxyaconitine	30.96	0.24	Fuzi
MOL002089	Mesaconitine	8.7	0.25	Fuzi
MOL002424	Aconitine	7.87	0.23	Fuzi
MOL002408	Benzoyl-aconine	12.83	0.25	Fuzi
MOL002409	Benzoyl-hypaconine	8.7	0.29	Fuzi
MOL002093	Benzoyl-mesaconine	8.55	0.27	Fuzi
MOL006957	(3S, 6S)-3-(benzyl)-6-(4-hydroxybenzyl) piperazine-2, 5-quinone	46.89	0.27	Banxia
MOL006967	beta-D-ribofuranoside, xanthine-9	44.72	0.21	Banxia
MOL000449	Stigmasterol	43.83	0.76	Banxia
MOL006937	12, 13-Epoxy-9-hydroxynonadeca-7, 10-dienoic acid	42.15	0.24	Banxia
MOL002776	Baicalin	40.12	0.75	Banxia
MOL006936	10, 13-Eicosadienoic	39.99	0.2	Banxia
MOL003578	Cycloartenol	38.69	0.78	Banxia
MOL000358	Beta-sitosterol	36.91	0.75	Banxia
MOL001755	24-Ethylcholest-4-en-3-one	36.08	0.76	Banxia
MOL002670	Cavidine	35.64	0.81	Banxia
MOL002714	Baicalein	33.52	0.21	Banxia
MOL000519	Coniferin	31.11	0.32	Banxia
MOL005030	Gondoic acid	30.7	0.2	Banxia

4. Discussion

Network-based methods are expected to make drug discovery breakthroughs by increasing our understanding of drug actions using multiple layers of information. Moreover, it provides additional support in the development of drug design and determination of the mechanism of action [25]. It is also a useful tool to elucidate the potential mechanisms of action of Chinese herbs on diseases, which may determine whether some theories of TCM are correct or incorrect.

As mentioned above, FB may treat COPD; thus, we evaluated this possibility using network pharmacology. Previously, FB were thought to be incompatible based on the commonsense logic employed in TCM. However, so far, no significant and definite adverse effects have been reported by administering a combination of FB. Many studies have focused on the side effects (hepatorenal toxicity) of FB, and a

few articles focus on the therapeutic effect of them. We think that it is better to discuss the side effects of drugs in the context of sufficient clinical efficacy. Drugs possess therapeutic effects and may also cause complications; for example, tacrolimus (FK506) and other immunosuppressants inhibit the immunity of patients undergoing transplantation, making them vulnerable to infectious diseases (e.g., BK virus infection) or hypertension mentioned in the drug specification. However, owing to their therapeutic effect, their risks are tolerated. Therefore, it is necessary to study and overcome the possible side effects of FB; however, proving the drugs' therapeutic effect seems to have more clinical value.

In this study, we evaluated some valuable compounds, such as baicalein in Banxia and ignavine and karanjin in Fuzi. Ignavine is a novel allosteric modulator of the μ opioid receptor and has an analgesic effect in vivo [26]. Karanjin decreases reactive oxygen species (ROS) levels

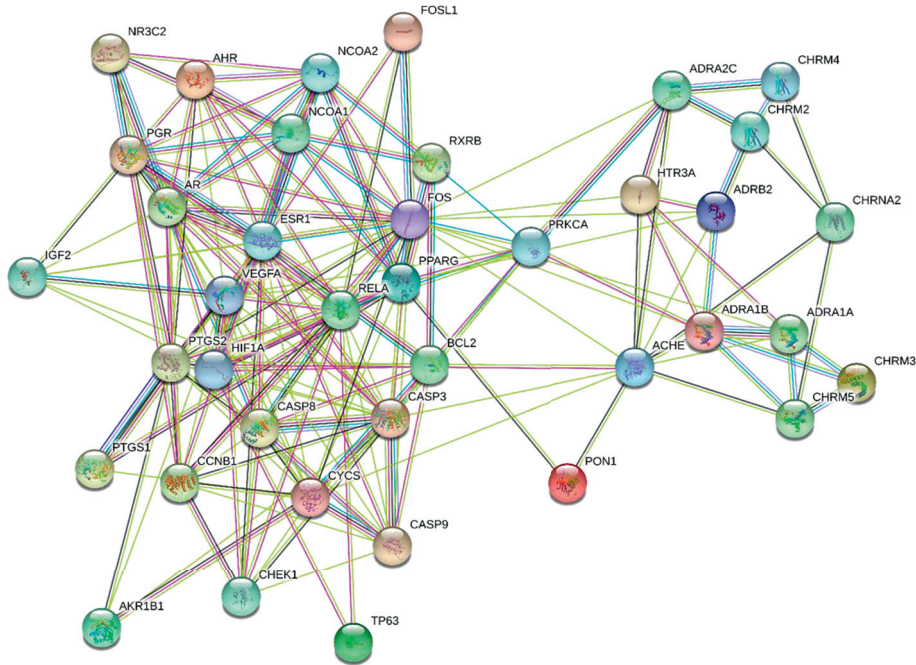


FIGURE 3: PPI network for COPD and FB.

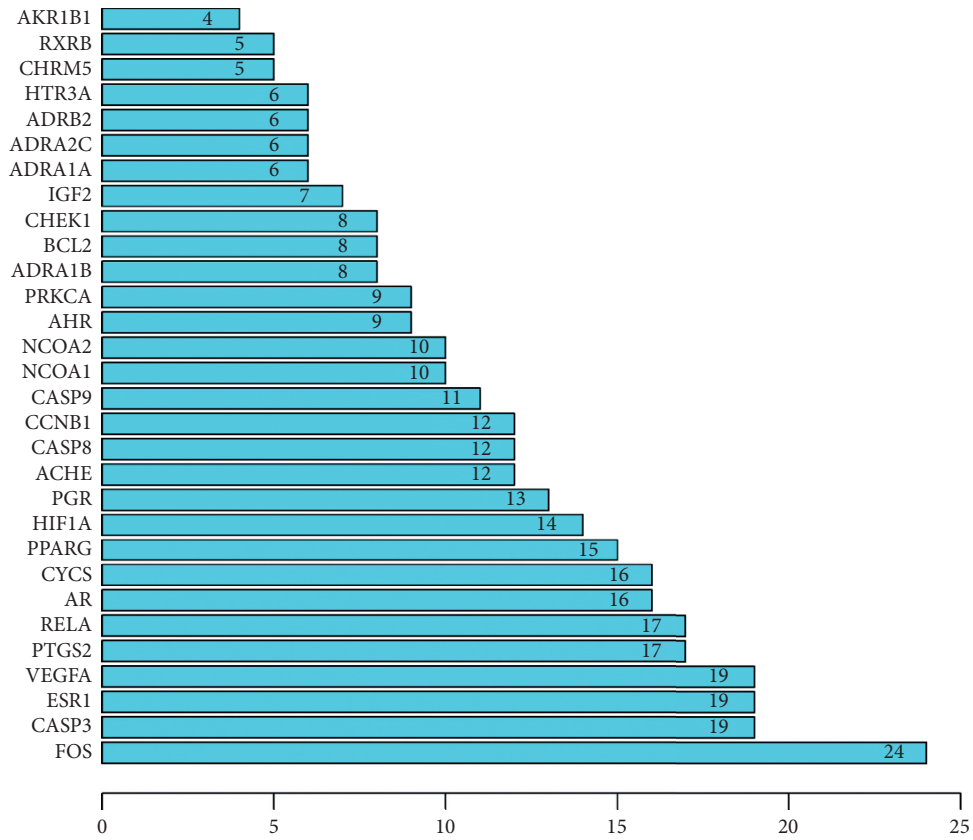


FIGURE 4: Bar plot of PPI for COPD and FB. The number showed the appearance times of the genes in PPI. Larger number means more important.

TABLE 2: Targets identified above each median.

	Degree	Eigenvector	LAC	Betweenness	Closeness	Network
FOS	24	0.30	8.58	379.38	0.73	19.12
CASP3	19	0.28	9.68	75.48	0.63	15.54
VEGFA	19	0.28	9.68	56.57	0.61	16.07
ESR1	19	0.28	9.79	52.61	0.60	16.30
PTGS2	17	0.26	9.18	65.09	0.61	13.13
RELA	17	0.25	8.47	70.93	0.59	13.15
AR	16	0.25	9.25	38.73	0.58	13.01
CYCS	16	0.24	8.25	62.59	0.60	12.18
HIF1A	14	0.22	7.29	45.81	0.57	9.76
PGR	13	0.20	7.69	26.13	0.55	10.18
PPARG	15	0.19	5.47	108.42	0.58	8.28
NCOA1	10	0.14	5.40	22.35	0.53	7.01
NCOA2	10	0.14	5.40	22.35	0.53	7.01

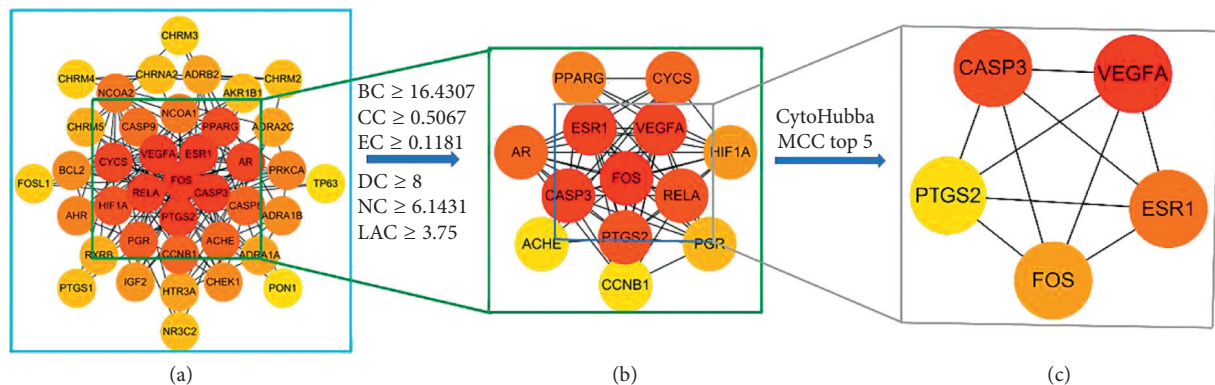


FIGURE 5: (a). Identification of targets of FB against COPD. From red to yellow indicates higher DC scores to low DC scores. (b) Targets identified above the medians. From red to yellow indicates higher DC scores to lower DC scores. (c). Core genes of FB and COPD.

TABLE 3: Molecular docking of core genes and active components.

Core gene	Active component	Binding energy
Caspase-3	Stigmasterol	-5.35
ESR1	Stigmasterol	-5.41
FOS	Cavidine	-5.38
PTGS2	Stigmasterol	-4.01
VEGFA	Cavidine	-4.07

was explored and identified common targets that scored higher than the medians in the analyzed parameters. The top 13 targets identified were FOS, CASP3, VEGFA, ESR1, PTGS2, RELA, AR, CYCS, HIF1A, PGR, PPARG, NCOA1, and NCOA2.

Oxidative stress can destroy biomacromolecules in tissues, leading to cell dysfunction or cell death [31]. This study shows that the correlated target genes or pathways are highly associated with oxidative stress, which is a major contributor to the pathogenesis of COPD. For example, Recuperating Lung Decoction could inhibit the MAPK/AP-1 signaling pathway to downregulate oxidative stress, resulting in the improvement of antioxidation of COPD. [32] Indeed, apoptosis was the second most indicated pathway in KEGG analysis. Whether in p53 signaling way, Kaposi sarcoma-associated herpesvirus infection pathway, or human

immunodeficiency virus 1 infection pathway, the genes were primarily involved in apoptosis pathway (Figure 10). CSE induced endothelial apoptosis in COPD through the ERK pathway [33]. In turn, oxidative stress can promote the development of lung inflammation and form a chronic state of mucus secretion. The Fos-related antigen-1 (Fra-1) transcription factor is thought to play a key role in promoting chronic cigarette smoke- (CS-) induced lung macrophagic inflammation in vivo and experiments have shown that the absence of Fra-1 in mice bone marrow can reduce the expression of inflammatory factors and the aggregation of macrophages in the lung [34]. Additionally, Fos-related antigen-2 (Fra-2) expression has also been described in COPD for the upregulation of monocyte-derived macrophages upon CS stimulation [35]. Activating transcription factor 3 (ATF3) may be involved in transcriptional promotion of CS-induced MUC5AC expression, which is a key pathologic feature of COPD in airway epithelial cells. Moreover, the knockout of ATF3 can significantly reduce the production of mucus and reduce the chronic mucus hypersecretion of airways [36].

Protease-antiprotease imbalance is the third main pathogenic mechanism of COPD. CS leads to the infiltration of many neutrophils and macrophages in the lung, releasing excessive neutrophil elastase and matrix metalloproteinase

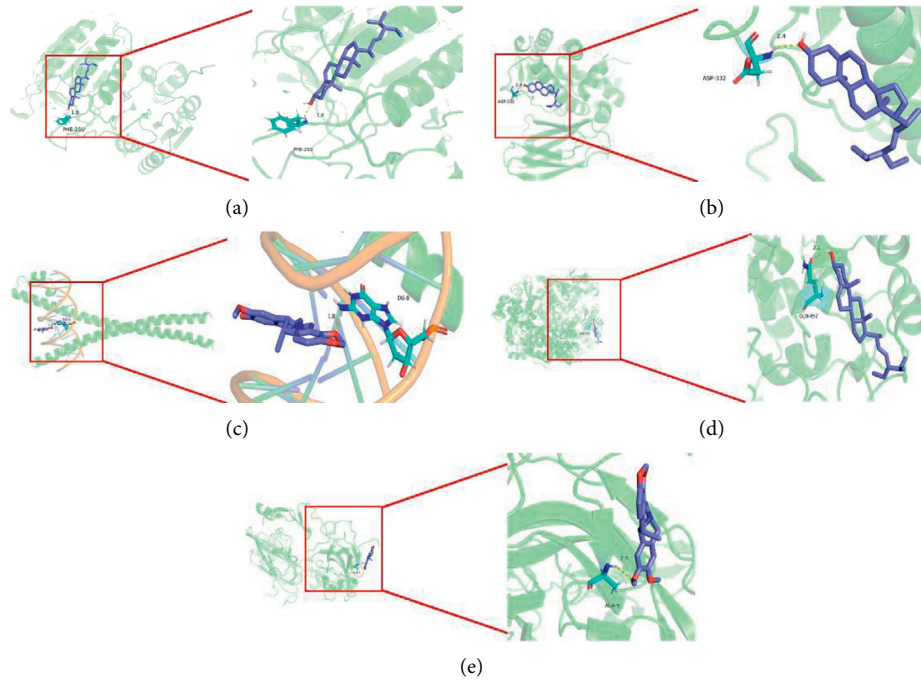


FIGURE 6: Molecular docking charts of core genes and active components. (a) CASP3 and Stigmasterol. (b) ESR1 and Stigmasterol. (c) FOS and Cavidine. (d) PTGS2 and Stigmasterol. (e) VEGFA and Cavidine.

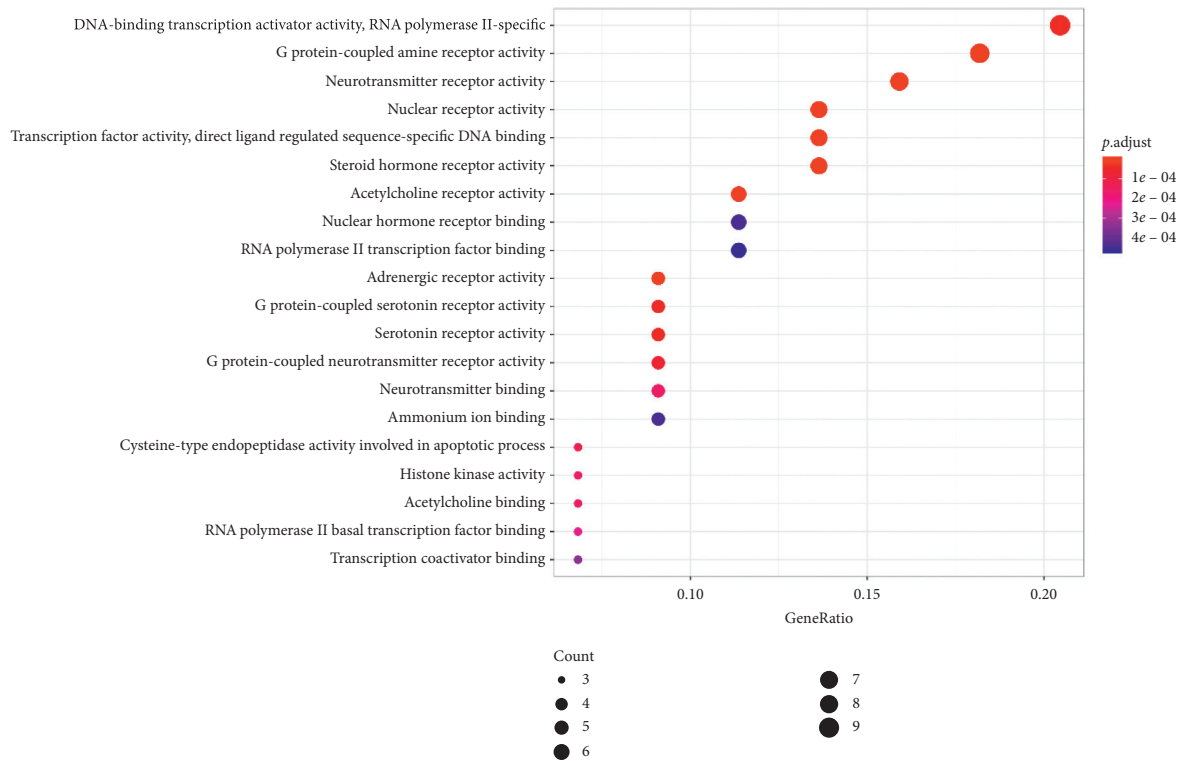


FIGURE 7: Gene ontology terms of candidate targets of FB against COPD. They were identified by the threshold of p value cutoff ≤ 0.05 . The size of the spot represents the number of genes, and the color represents the adjusted p value.

(MMP). Through the protease antiprotein imbalance mechanism, the expression of placenta growth factor (PGF) is increased and drives caspase-3- and caspase-9-dependent

apoptosis in bronchial epithelial cells [37]. Pulmonary emphysema, a significant characteristic of COPD, is considered to result from the epithelial cell death caused by

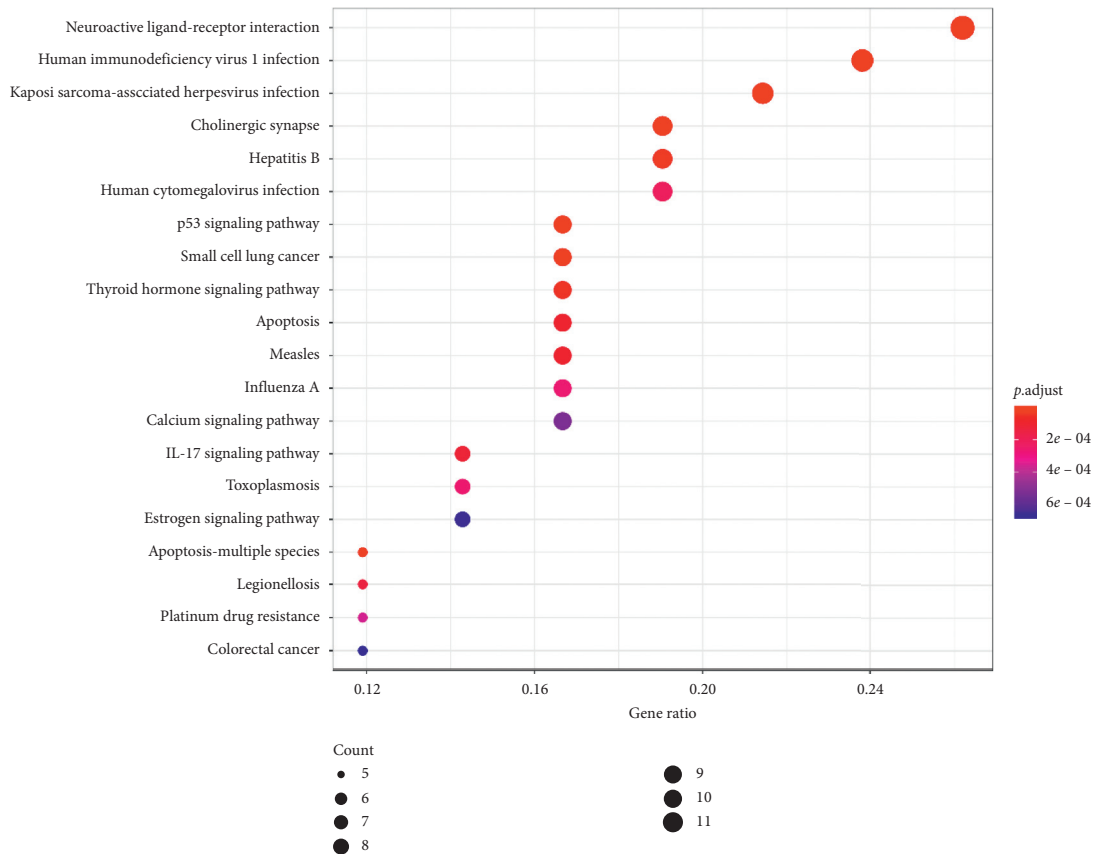


FIGURE 8: KEGG pathway identification of FB candidate targets against COPD. They were identified by the threshold of value cutoff ≤ 0.05 . The size of the spot represents the number of genes, and the color represents the adjusted value.

smoking [38]. It shows that the normal pulling force of alveoli to small airways has been reduced, making the alveoli easily collapsible with obviously reduced elasticity. The failure of the small airway is an important but easily overlooked mechanism of COPD because it occurs in the very early stages of the disease, and continues throughout the process [39]. Small airway disease is composed of small airway inflammation, fibrotic tissue, and lumen mucus plug. The the abovementioned mechanisms jointly promote the most characteristic symptom of COPD: continuous airflow restriction. ICS are very effective in the treatment of COPD. However, ICS resistance is becoming a major barrier to the effective treatment of COPD [40]. There has been evidence indicating that the loss of Hsp90 could contribute to steroid resistance in COPD [41]. Meanwhile, one clinical study has illustrated that smokers with COPD possessed significantly increased expression levels of p53 when compared to smokers without COPD and normal subjects, and at the same time, increased cleaved caspase-3 may also promote apoptosis [42]. All these biological processes were analyzed in the present study. As shown in Figure 8, the caspase-3, caspase-9, and p53 signaling pathways form the core of the network between FB and COPD. Moreover, the highlighted parts in the major pathways are mainly related to apoptosis.

As is demonstrated in the present study, FB are multicomponent, multitarget, and multipathway drugs. A total of 68 pathways were enhanced in this drug, including

those related to IL-17 signaling, P53 signaling, cholinergic synapse, and apoptosis. IL-17A regulates airway inflammation, oxidative stress, and the reduction of steroid sensitivity [43], as well as attenuating IFN- λ expression [44] in COPD. Cellular senescence and apoptosis of alveolar epithelial cells in lung tissues are important characteristics of COPD pathogenesis. p53 is a tumor suppressor, which can induce cellular senescence of type II alveolar epithelial cells (AECII) [45]. p53 expression in the cytoplasm also increased with CSE treatment. In addition, the interaction of p53 with Parkin (a core mitophagy-regulating protein) was highly increased during CSE-induced cellular senescence [46]. The cholinergic anti-inflammatory pathway was involved in regulating inflammation; moreover, COPD mouse showed high levels of AChE and nicotinic acetylcholine receptor $\alpha 7$ subunit ($\alpha 7nAChR$) [47]. The nonneuronal cholinergic system was overexpressed in neutrophils of COPD patients, such as the increase of muscarinic receptors (M2, M4, and M5) expression [48]. Additionally, in this study, several other viral pathways were enhanced. Studies which use polymerase chain reaction have demonstrated the presence of viruses in 80–85% of asthma exacerbations in children and 60–80% of exacerbations in adults, after viral clearance, and symptom resolution follows, but lasting inflammatory markers and oxidative

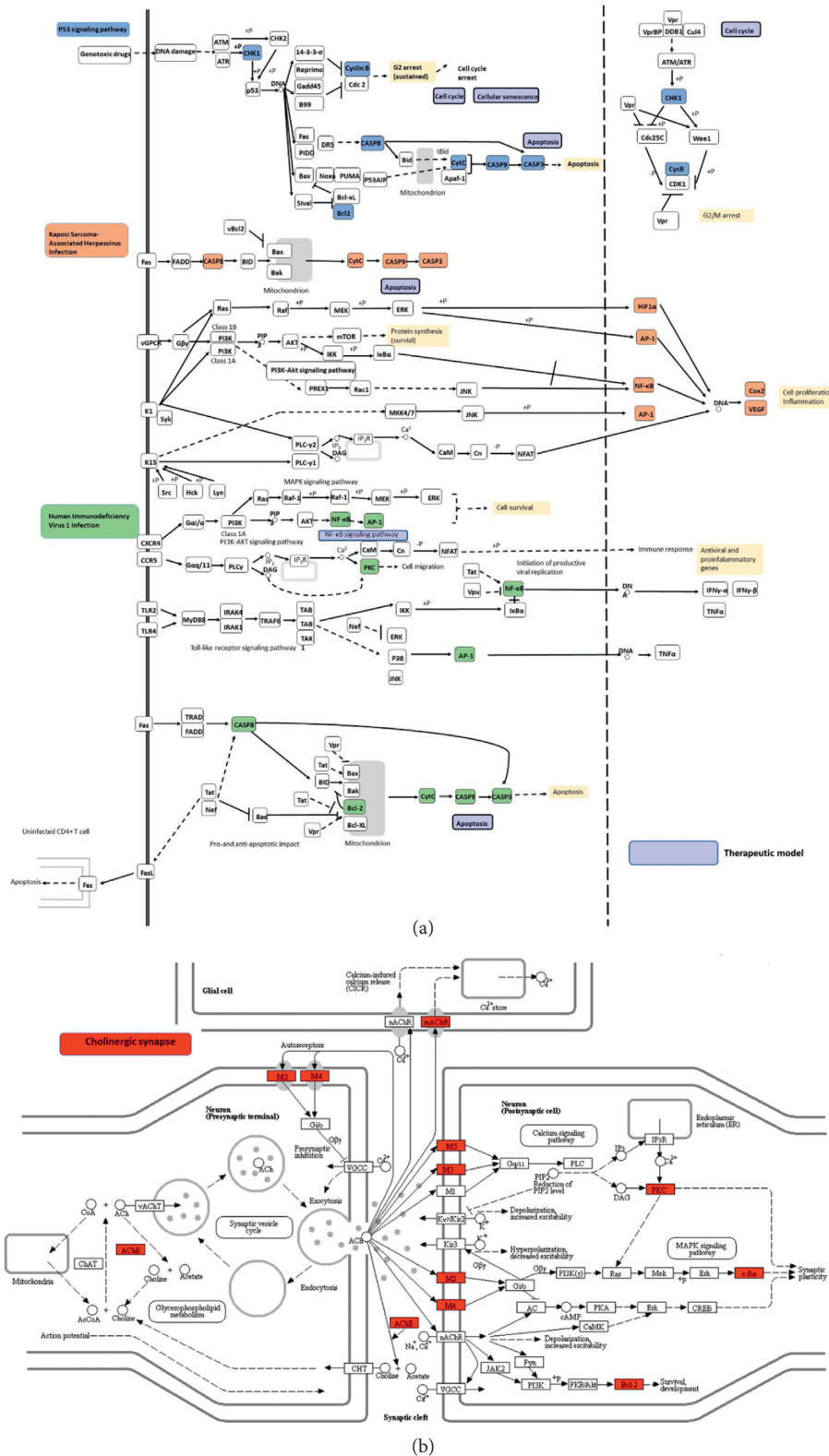


FIGURE 9: (a) KEGG pathway details identified by FB against COPD. Three pathways (shown in different colors) consisted the compressed KEGG pathway. The solid and dashed arrows mean direct and indirect activations, and the T arrows indicate the inhibition effects. (b) Cholinergic synapse details identified by FB against COPD.

stress remain [49], which suggests a perpetual autoimmune response. FB may regulate the immunological function through some specific infections' pathways, such

as Kaposi sarcoma-associated herpesvirus infection, human immunodeficiency virus 1 infection, human cytomegalovirus infection, hepatitis C, influenza A, and

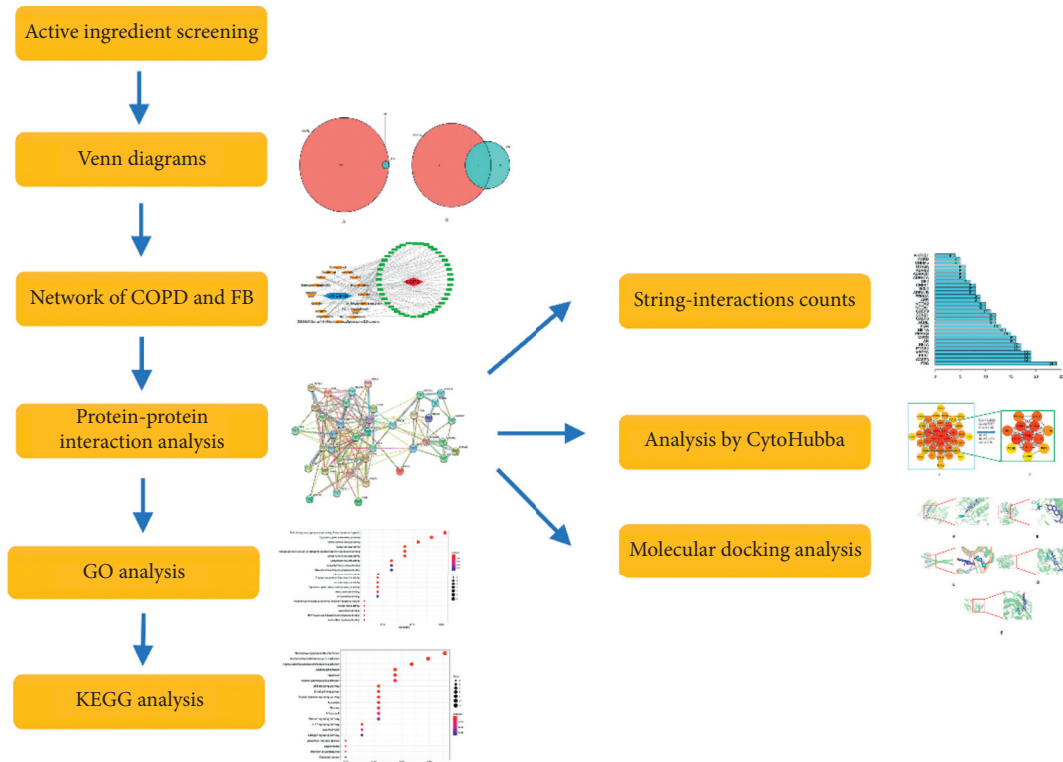


FIGURE 10: Article flow chart.

Epstein–Barr virus infections. COPD is an independent risk factor for non-small-cell lung cancer (NSCLC) and significantly associated with lung cancer mortality [50]. Fuzi reduced the proportion of Treg cells, decreased serum levels of cytokines and transforming growth factor (TGF)- β , and downregulated the expression of programmed death ligand-1 in mice, which suggests that Fuzi has immunomodulation properties to improve radiotherapy against lung cancer [51]. In this study, the pathways mentioned above were enhanced as well.

In the network we set up, FOS may be the core target gene. In addition, CASP3 and VEGFA may be key target genes. The overexpression of FOS and CASP3 suggests excessive apoptosis [52]. Additionally, activated c-Fos can influence colon cancer invasion [53]; c-Fos in T24 cells can induce significant cell morphology changes, reduce viability, and increase cell death [54]. In osteosarcoma (OS), only tumors expressing both epidermal growth factor receptor (EGFR) and c-Fos respond to anti-EGFR therapy [55]. CASP3 plays a central role in executing cell apoptosis; carcinogenesis studies have found that CASP3 polymorphisms and smoking interactions were related to a higher risk of lung cancer [56], whereas lower expression of CASP3 is linked to a higher risk of NSCLC [57, 58]. Although no difference in the expression of ESR1 was observed between patients and healthy individuals, the increased expression of enzymes involved in the local synthesis of active estrogens were observed [59]. Vascular endothelial-derived growth factor (VEGF) may play a key role in ongoing vascular

remodeling processes, a key characteristic sign of COPD, in the distal lung compartments [60].

The mechanisms of action and molecular targets of FB against COPD were explored using a network pharmacology in this study. FB regulates some biological processes, such as gene expression, apoptotic processes, neuroactive ligand-receptor interaction and p53 class mediators, and cholinergic synapse, and the enhanced pathways include the IL-17 signaling and thyroid hormone signaling pathway. FB may regulate immunological function through some specific viral pathways, such as Kaposi sarcoma-associated herpesvirus infection, human immunodeficiency virus 1 infection, human cytomegalovirus infection, hepatitis C and influenza A, and Epstein–Barr virus infection, which are associated with COPD. As judged by DC, the top 3 key genes are FOS, CASP3, and ESR1 in the PPI of FB for the treatment of COPD. Network pharmacology seems to be a suitable approach for the study of complex TCM incompatible drugs; however, it may filter compounds that may be associated with unknown target genes or lower OB and DL, such as BAC, BHA, and BMA identified in this study. Moreover, various formulas with effective compositions may be produced using the decocting process, instead of the original preparation methods; the compounds so obtained may have different molecular structures because they are obtained by boiling. As TCM research is difficult, although not an ideal approach, network pharmacology does offer a new and reliable approach to analyze TCMs and associate them with diseases. It can be used to

verify whether a theory of TCM is valid through modern experimental methods in order to conveniently and accurately explain how drugs function.

Data Availability

The data used to support the findings of this study are included within the supplementary material files.

Conflicts of Interest

The authors declare that the research was conducted in the absence of any commercial or financial relationships that could be construed as potential conflicts of interest.

Authors' Contributions

KN conducted the main analysis and drafted this manuscript. KN and XC designed the research. YC, LZ, and ZW joined in the discussion and offered interesting ideas. RC and SZ assisted in the preparation of the research. ZW reviewed the text and guided the structure of the manuscript. All authors took part in the research and wrote, read, and approved the manuscript.

Acknowledgments

The authors would like to thank Editage (<http://www.editage.com>) for English language editing and biowolf (<http://www.biowolf.cn/>) for guidance on Internet pharmacology methods and R language. This work was supported by the National Key R&D Program of China (2018YFC2002500).

Supplementary Materials

Supplementary Table 1. Gene targets of Fuzi. Supplementary Table 2. Gene targets of Banxia. Supplementary Table 3. Number of targets corresponding to different components. Supplementary Table 4. The data of GO enrichment analysis. Supplementary Table 5. The data of KEGG enrichment analysis. (*Supplementary Materials*)

References

- [1] L. Tanner and A. B. Single, "Animal models reflecting chronic obstructive pulmonary disease and related respiratory disorders: translating pre-clinical data into clinical relevance," *Journal of Innate Immunity*, vol. 12, no. 3, pp. 203–225, 2019.
- [2] Y.-N. Liao, W.-L. Hu, H.-J. Chen, and Y.-C. Hung, "The use of Chinese herbal medicine in the treatment of chronic obstructive pulmonary disease (COPD)," *The American Journal of Chinese Medicine*, vol. 45, no. 2, pp. 225–238, 2017.
- [3] P. Zhao, J. Li, Y. Tian et al., "Restoring Th17/Treg balance via modulation of STAT3 and STAT5 activation contributes to the amelioration of chronic obstructive pulmonary disease by Bufeishen formula," *Journal of Ethnopharmacology*, vol. 217, pp. 152–162, 2018.
- [4] W. Du, J. Su, D. Ye, Y. Wang, Q. Huang, and X. Gong, "Pinellia ternata attenuates mucus secretion and airway inflammation after inhaled corticosteroid withdrawal in COPD rats," *The American Journal of Chinese Medicine*, vol. 44, no. 5, pp. 1027–1041, 2016.
- [5] S. T. Gulen, U. Eryilmaz, M. Yilmaz, and F. Karadag, "Left ventricular dysfunction in relation with systemic inflammation in chronic obstructive pulmonary disease patients," *The Korean Journal of Internal Medicine*, vol. 34, no. 3, pp. 569–578, 2019.
- [6] G. Zhou, L. Tang, X. Zhou, T. Wang, Z. Kou, and Z. Wang, "A review on phytochemistry and pharmacological activities of the processed lateral root of aconitum carmichaelii Debeaux," *Journal of Ethnopharmacology*, vol. 160, pp. 173–193, 2015.
- [7] N. Li, L. L. Li, C. X. Li, Y. H. Chen, and X. L. Li, "Analysis of the historical evolution of "eighteen incompatible medications" and "nineteen medicaments of mutual restraint" of TCM and its clinical application," *China Pharmacy*, vol. 30, pp. 513–517, 2019, in Chinese.
- [8] J. Wu, Z. Cheng, L. Zhu et al., "Coadministration of Pinellia ternata can significantly reduce Aconitum carmichaelii to inhibit CYP3A activity in rats," *Evidence-based Complementary and Alternative Medicine*, eCAM, vol. 2014, Article ID 734867, 10 pages, 2014.
- [9] X. W. Mo, W. X. He, X. H. Liu, J. Zhang, and H. Deng, "Study on the safety of compatibility of aconite and Pinellia ternata in the treatment of malignant tumors," *Psychologist*, vol. 24, no. 27, pp. 127–129, 2018, in Chinese.
- [10] T. Yu, S. Xiao, F. Cao, and L. M. Liu, "Study on the compatibility of aconite and pinellia ternate in "shanghan zabing Lun"" *Journal of Basic Chinese Medicine*, vol. 23, no. 11, pp. 626–627, 2017, in Chinese.
- [11] J. Y. Li, "To observe the curative effect of Xiaoqinglong-Jiafuzi-decoction on chronic obstructive pulmonary disease," *Medical Diet and Health*, vol. 18, no. 12, p. 11, 2020, in Chinese.
- [12] D. F. Chen, Z. L. Zhang, H. B. Xiao, and L. H. Xiao, "Analysis of clinical effect of "Five-step method of differentiating yang deficiency" combined with "Xiaoqinglong decoction plus aconite" in the treatment of allergic rhinitis," *China Practical Medical*, vol. 12, no. 14, pp. 128–129, 2017, in Chinese.
- [13] H. Liu, L. Zeng, K. Yang, and G. Zhang, "A network pharmacology approach to explore the pharmacological mechanism of Xiaoyao powder on anovulatory infertility," *Evidence-Based Complementary and Alternative Medicine*, vol. 2016, Article ID 2960372, 13 pages, 2016.
- [14] Y. Chen, J. Wei, Y. Zhang et al., "Anti-endometriosis mechanism of jiawei foshou san based on network pharmacology," *Frontiers in Pharmacology*, vol. 9, p. 811, 2018.
- [15] S. J. Yue, J. Liu, W. W. Feng et al., "System pharmacology-based dissection of the synergistic mechanism of Huangqi and huanglian for diabetes mellitus," *Frontiers in Pharmacology*, vol. 8, p. 694, 2017.
- [16] X. Xing, S. Chen, L. Li et al., "The active components of Fuzheng Huayu formula and their potential mechanism of action in inhibiting the hepatic stellate cells viability—a network pharmacology and transcriptomics approach," *Frontiers in Pharmacology*, vol. 9, p. 525, 2018.
- [17] J. Ru, P. Li, J. Wang et al., "TCMSP: a database of systems pharmacology for drug discovery from herbal medicines," *Journal of Cheminformatics*, vol. 6, p. 13, 2014.
- [18] J. Li, P. Zhao, Y. Li, Y. Tian, and Y. Wang, "Systems pharmacology-based dissection of mechanisms of Chinese medicinal formula Bufeishen as an effective treatment for chronic obstructive pulmonary disease," *Scientific Reports*, vol. 5, Article ID 15290, 2015.

- [19] V. Law, C. Knox, Y. Djoumbou et al., "DrugBank 4.0: shedding new light on drug metabolism," *Nucleic Acids Research*, vol. 42, no. D1, pp. D1091–D1097, 2014.
- [20] L. L. Miao, Q. M. Zhou, C. Peng, C. W. Meng, X. Y. Wang, and L. Xiong, "Aconitum carmichaelii discrimination of the geographical origin of the lateral roots of using the fingerprint, multicomponent quantification, and chemometric methods," *Molecules (Basel, Switzerland)*, vol. 24, no. 22, 4124 pages, 2019.
- [21] Y. Tang, M. Li, J. Wang, Y. Pan, and F.-X. Wu, "CytoNCA: a cytoscape plugin for centrality analysis and evaluation of protein interaction networks," *Biosystems*, vol. 127, pp. 67–72, 2015.
- [22] C.-H. Chin, S.-H. Chen, H.-H. Wu, C.-W. Ho, M.-T. Ko, and C.-Y. Lin, "CytoHubba: identifying hub objects and sub-networks from complex interactome," *BMC Systems Biology*, vol. 8, no. Suppl 4, p. S11, 2014.
- [23] D. W. Huang, B. T. Sherman, and R. A. Lempicki, "Systematic and integrative analysis of large gene lists using DAVID bioinformatics resources," *Nature Protocols*, vol. 4, no. 1, pp. 44–57, 2009.
- [24] L. Gatto, L. M. Breckels, T. Naake, and S. Gibb, "Visualization of proteomics data using R and bioconductor," *Proteomics*, vol. 15, no. 8, pp. 1375–1389, 2015.
- [25] B. Boezio, K. Audouze, P. Ducrot, and O. Taboureau, "Network-based approaches in pharmacology," *Molecular Informatics*, vol. 36, no. 10, 2017.
- [26] K. Ohbuchi, C. Miyagi, Y. Suzuki et al., "Ignavine: a novel allosteric modulator of the μ opioid receptor," *Scientific Reports*, vol. 6, Article ID 31748, 2016.
- [27] R. Roy, D. Pal, S. Sur, S. Mandal, P. Saha, and C. K. Panda, "Pongapin and Karanjin, furanoflavanoids of Pongamia pinnata, induce G2/M arrest and apoptosis in cervical cancer cells by differential reactive oxygen species modulation, DNA damage, and nuclear factor kappa-light-chain-enhancer of activated B cell signaling," *Phytotherapy Research*, vol. 33, no. 4, pp. 1084–1094, 2019.
- [28] M. Bose, M. Chakraborty, S. Bhattacharya, D. Mukherjee, S. Mandal, and R. Mishra, "Prevention of arthritis markers in experimental animal and inflammation signalling in macrophage by karanjin isolated from Pongamia pinnata Seed extract," *Phytotherapy Research*, vol. 28, no. 8, pp. 1188–1195, 2014.
- [29] L. Ye, S. Gao, Q. Feng et al., "Development and validation of a highly sensitive UPLC-MS/MS method for simultaneous determination of aconitine, mesaconitine, hypaconitine, and five of their metabolites in rat blood and its application to a pharmacokinetics study of aconitine, mesaconitine, and hypaconitine," *Xenobiotica*, vol. 42, no. 6, pp. 518–525, 2012.
- [30] S. Saadat and J. Boskabadi, M. H. Boskabady, Contribution of potassium channels, beta2-adrenergic and histamine H1 receptors in the relaxant effect of baicalein on rat tracheal smooth muscle," *Iranian Journal of Basic Medical Sciences*, vol. 22, no. 11, pp. 1347–1352, 2019.
- [31] C. H. Wiegman, C. Michaeloudes, G. Haji et al., "Oxidative stress-induced mitochondrial dysfunction drives inflammation and airway smooth muscle remodeling in patients with chronic obstructive pulmonary disease," *Journal of Allergy and Clinical Immunology*, vol. 136, no. 3, pp. 769–780, 2015.
- [32] C. L. Li, Q. S. Y. Y et al., "Recuperating lung decoction attenuates the oxidative stress state of chronic obstructive pulmonary disease by inhibiting the MAPK/AP-1 signal pathway and regulating γ GCS," *Evidence-Based Complementary and Alternative Medicine*, vol. 2017, Article ID 9264914, 12 pages, 2017.
- [33] D. Zong, J. Li, S. Cai et al., "Notch1 regulates endothelial apoptosis via the ERK pathway in chronic obstructive pulmonary disease," *American Journal of Physiology-Cell Physiology*, vol. 315, no. 3, pp. C330–C340, 2018.
- [34] M. Vaz, S. Rajasekaran, H. R. Potteti, and S. P. Reddy, "Myeloid-specific Fos-related antigen-1 regulates cigarette smoke-induced lung inflammation, not emphysema, in mice," *American Journal of Respiratory Cell and Molecular Biology*, vol. 53, no. 1, pp. 125–134, 2015.
- [35] A. Birnhuber, V. Biasin, D. Schnoegl, L. M. Marsh, and G. Kwapiszewska, "Transcription factor Fra-2 and its emerging role in matrix deposition, proliferation and inflammation in chronic lung diseases," *Cellular Signalling*, vol. 64, Article ID 109408, 2019.
- [36] Y.-P. Wu, Y.-F. Wu, C. Zhang et al., "Activating transcription factor 3 Is essential for cigarette smoke-induced mucin expression via interaction with activator protein-1," *The American Journal of Pathology*, vol. 187, no. 2, pp. 280–291, 2017.
- [37] H.-H. Hou, H.-C. Wang, S.-L. Cheng, Y.-F. Chen, K.-Z. Lu, and C.-J. Yu, "MMP-12 activates protease-activated receptor-1, upregulates placenta growth factor, and leads to pulmonary emphysema," *American Journal of Physiology-Lung Cellular and Molecular Physiology*, vol. 315, no. 3, pp. L432–L442, 2018.
- [38] K. Mizumura, S. Maruoka, T. Shimizu, and Y. Gon, "Autophagy, selective autophagy, and necroptosis in COPD," *International Journal of Chronic Obstructive Pulmonary Disease*, vol. 13, pp. 3165–3172, 2018.
- [39] M. S. Eapen, P. M. Hansbro, K. McAlinden et al., "Abnormal M1/M2 macrophage phenotype profiles in the small airway wall and lumen in smokers and chronic obstructive pulmonary disease (COPD)," *Scientific Reports*, vol. 7, no. 1, p. 13392, 2017.
- [40] J. Knobloch, D. Jungck, J. Kronsbein, E. Stoelben, K. Ito, and A. Koch, "LABAs and p38MAPK inhibitors reverse the corticosteroid-insensitivity of IL-8 in airway smooth muscle cells of COPD," *Journal of Clinical Medicine*, vol. 8, no. 12, 2058 pages, 2019.
- [41] G. Hodge, E. Roscioli, H. Jersmann et al., "Steroid resistance in COPD is associated with impaired molecular chaperone Hsp90 expression by pro-inflammatory lymphocytes," *Respiratory Research*, vol. 17, no. 1, p. 135, 2016.
- [42] M. M. Gouda, S. B. Shaikh, D. Chengappa, I. Kandhal, A. Shetty, and Y. Bhandary, "Changes in the expression level of IL-17A and p53-fibrinolytic system in smokers with or without COPD," *Molecular Biology Reports*, vol. 45, no. 6, pp. 2835–2841, 2018.
- [43] G. Anzalone, G. D. Albano, A. M. Montalbano et al., "IL-17A-associated IKK-alpha signalling induced TSLP production in epithelial cells of COPD patients," *Experimental & Molecular Medicine*, vol. 50, no. 10, p. 131, 2018.
- [44] M. Niwa, T. Fujisawa, K. Mori et al., "IL-17A attenuates IFN- λ expression by inducing suppressor of cytokine signaling expression in airway epithelium," *The Journal of Immunology*, vol. 201, no. 8, pp. 2392–2402, 2018.
- [45] C. Gu, Y. Li, J. Liu et al., "LncRNA-mediated SIRT1/FoxO3a and SIRT1/p53 signaling pathways regulate type II alveolar epithelial cell senescence in patients with chronic obstructive pulmonary disease," *Molecular Medicine Reports*, vol. 15, no. 5, pp. 3129–3134, 2017.

- [46] T. Ahmad, I. K. Sundar, C. A. Lerner et al., "Impaired mitophagy leads to cigarette smoke stress-induced cellular senescence: implications for chronic obstructive pulmonary disease," *The FASEB Journal*, vol. 29, no. 7, pp. 2912–2929, 2015.
- [47] X.-F. Zhang, S.-Y. Xiang, W.-Y. Geng et al., "Electro-acupuncture regulates the cholinergic anti-inflammatory pathway in a rat model of chronic obstructive pulmonary disease," *Journal of Integrative Medicine*, vol. 16, no. 6, pp. 418–426, 2018.
- [48] J. Milara, A. Cervera, A. De Diego et al., "Non-neuronal cholinergic system contributes to corticosteroid resistance in chronic obstructive pulmonary disease patients," *Respiratory Research*, vol. 17, no. 1, p. 145, 2016.
- [49] R. Hewitt, H. Farne, A. Ritchie, E. Luke, S. L. Johnston, and P. Mallia, "The role of viral infections in exacerbations of chronic obstructive pulmonary disease and asthma," *Therapeutic Advances in Respiratory Disease*, vol. 10, no. 2, pp. 158–174, 2016.
- [50] E. Ytterstad, P. Moe, and A. Hjalmsen, "COPD in primary lung cancer patients: prevalence and mortality," *International Journal of Chronic Obstructive Pulmonary Disease*, vol. 11, pp. 625–636, 2016.
- [51] Q. Zhang, X. Chen, Y. Luo, H. Ren, and T. Qiao, "Fuze enhances anti-tumor efficacy of radiotherapy on lung cancer," *Journal of Cancer*, vol. 8, no. 19, pp. 3945–3951, 2017.
- [52] L. Wen, L. Liu, L. Tong et al., "NDRG4 prevents cerebral ischemia/reperfusion injury by inhibiting neuronal apoptosis," *Genes & Diseases*, vol. 6, no. 4, pp. 448–454, 2019.
- [53] Y. Ding, K. Hao, Z. Li et al., "c-Fos separation from Lamin A/C by GDF15 promotes colon cancer invasion and metastasis in inflammatory microenvironment," *Journal of Cellular Physiology*, vol. 235, no. 5, pp. 4407–4421, 2020.
- [54] T. Zhang, J. He, S. Zhang et al., "Brazilin induces T24 cell death through c-Fos and GADD45 β independently regulated genes and pathways," *IUBMB Life*, vol. 70, no. 11, pp. 1101–1110, 2018.
- [55] M. Linder, E. Glitzner, S. Srivatsa et al., "EGFR is required for FOS-dependent bone tumour development via RSK2/CREB signalling," *EMBO Molecular Medicine*, vol. 10, no. 11, 2018.
- [56] J. Lin, Y. Zhang, H. Wang et al., "Genetic polymorphisms in the apoptosis-associated gene CASP3 and the risk of lung cancer in Chinese population," *PLoS One*, vol. 11, no. 10, Article ID e0164358, 2016.
- [57] R. Cui, T. Kim, M. Fassan et al., "MicroRNA-224 is implicated in lung cancer pathogenesis through targeting caspase-3 and caspase-7," *Oncotarget*, vol. 6, no. 26, pp. 21802–21815, 2015.
- [58] J. Javid, R. Mir, and A. Saxena, "Involvement of CASP3 promoter polymorphism (–1337 C > G) in the development and progression of non-small cell lung cancer," *Tumor Biology*, vol. 37, no. 7, pp. 9255–9262, 2016.
- [59] G. F. J. Konings, N. L. Reynaert, B. Delvoux et al., "Increased levels of enzymes involved in local estradiol synthesis in chronic obstructive pulmonary disease," *Molecular and Cellular Endocrinology*, vol. 443, pp. 23–31, 2017.
- [60] G. Westergren-Thorsson, M. Bagher, A. Andersson-Sjöland et al., "VEGF synthesis is induced by prostacyclin and TGF- β in distal lung fibroblasts from COPD patients and control subjects: implications for pulmonary vascular remodelling," *Respirology*, vol. 23, no. 1, pp. 68–75, 2018.

Research Article

To Explore the Mechanism and Equivalent Molecular Group of Fuxin Mixture in Treating Heart Failure Based on Network Pharmacology

Yi-ding Yu ¹, Yi-ping Xiu,¹ Yang-fan Li,¹ and Yi-tao Xue ²

¹Shandong University of Traditional Chinese Medicine, Jinan 250014, China

²Affiliated Hospital of Shandong University of Traditional Chinese Medicine, Jinan 250014, China

Correspondence should be addressed to Yi-ding Yu; 1078607526@qq.com and Yi-tao Xue; xytsdzdyfy@126.com

Received 3 September 2020; Revised 25 October 2020; Accepted 11 November 2020; Published 21 November 2020

Academic Editor: Siba shanak

Copyright © 2020 Yi-ding Yu et al. This is an open access article distributed under the Creative Commons Attribution License, which permits unrestricted use, distribution, and reproduction in any medium, provided the original work is properly cited.

Fuxin mixture (FXHJ) is a prescription for the treatment of heart failure. It has been shown to be effective in clinical trials, but its active ingredients and mechanism of action are not completely clear, which limits its clinical application and international promotion. In this study, we used network pharmacology to find, conclude, and summarize the mechanism of FXHJ in the treatment of heart failure. From FXHJ, we found 39 active ingredients and 47 action targets. Next, we constructed the action network and was conducted enrichment analysis. The results showed that FXHJ mainly treated heart failure by regulating the MAPK signaling pathway, PI3K/Akt signaling pathway, cAMP signaling pathway, TNF signaling pathway, toll-like receptor signaling pathway, VEGF signaling pathway, NF- κ B signaling pathway, and the apoptotic signaling molecule BCL2. Through the research method of network pharmacology, this study summarized the preliminary experiments of the research group and revealed the probable mechanism of FXHJ in the treatment of heart failure to a certain extent, which provided some ideas for the development of new drugs.

1. Introduction

Heart failure (HF) is a closed result of most cardiovascular diseases, which may be caused by damage to ventricular filling from various structural or functional disorders of the heart [1]. In observational data from Europe, the 1-year all-cause mortality rate for HF was greater than 20 percent [2]. In search of a cheap, safe, and effective drug, we turned to traditional Chinese medicine (TCM).

FXHJ is a prescription for the treatment of heart failure obtained by Dr. Xue through the combination of clinical experience and literature data. It is composed of *Aconiti Lateralis Radix Praeparata* (FZ), *Angelicae Sinensis Radix* (DG), *Phellodendri Chinensis Cortex* (HB), *Lepidii Semen Descurainiae Semen* (TLZ), *Epimedium Herba* (YYH), and *Alisma Orientale* (ZX). Preliminary clinical trials of the research group have shown that FXHJ can significantly improve cardiac function, delay left ventricular remodeling,

extend the 6WMT distance, improve exercise tolerance, reduce plasma BNP level, and improve patients' quality of life [3].

Due to the multicomponent and multitarget characteristics of Traditional Chinese medicine, it is difficult for us to clearly understand its mechanism of action. Therefore, we turn our attention to network pharmacology. Network pharmacology is an emerging discipline based on the integration of systems biology, molecular biology, pharmacology, and a variety of network computing platforms in the context of the era of big data [4]. Because it is compatible with the systematic and holistic treatment concept of TCM, it breaks the shackles of traditional medicine research focusing on single ingredient, single target, and single disease, so it is widely used in the study of TCM efficacy and its mechanism of action [5]. In particular, its multipart network modularization analysis and machine learning approach to explore meridian classification provide novel insights into the relationship between traditional

medicine and modern medicine [6, 7]. In addition, when exploring the relationship between drugs and diseases, it is also customary to report that drugs with known efficacy can reverse predict the pathogenesis of diseases [8]—at the same time, combining computer network analysis algorithm to simulate and predict the mechanism of action of drugs. It can better display the advantages and characteristics of the systematicness of traditional Chinese medicine [9].

The mechanism of multicomponent and multitarget action of TCM has hindered the establishment of an evidence-based model of TCM and the study of toxic and side effects. Therefore, the concept of “equivalent molecular group” is suggested in this study. The various components in FXHJ can be roughly classified into three categories in the treatment of heart failure. The first had no association with the treatment of heart failure. The second had a positive effect on the treatment of heart failure, which we called active compounds. The third had a negative effect on the treatment of heart failure. Although the three components acted differently, on the whole, their final results were affirmative. After eliminating the inactive components, we take the sum of the components of positive and negative effects and turn them into the equivalent molecular group. In short, an equivalent molecular group is a collection of disease-related components, whether they play a positive or negative role in a disease.

In this study, we used the method of network pharmacology to explore the equivalent molecular group of FXHJ through the previous experimental results and elucidated the material basis and potential mechanism of action of FXHJ in the treatment of heart failure so as to provide some ideas for the development of new drugs.

2. Methods

2.1. Data Collection and Processing. Chinese medicine systematic pharmacology database (TCMSP) (<http://tcmssp.com/tcmssp.php>) is an open and comprehensive database of Chinese medicine ingredients and action targets. In clinical treatment, TCM is often used by oral administration. Oral bioavailability (OB) and drug-likeness (DL), two ADME-related models, are the main variables affecting the absorption of drugs from the gastrointestinal tract. Therefore, we screened bioactive components under the conditions of $OB \geq 30\%$ and $DL \geq 0.18$. Next, we find the target from the list of compounds. At the same time, we used the PubChem database (<https://pubchem.ncbi.nlm.nih.gov/>) to standardize the names of active ingredients. In order to make the results concise and convenient, we utilized the Uniprot database (<https://www.uniprot.org/>) to convert the protein name of the target into the gene name. Then, we take the union of all the consequences and delete the duplicates. In order to get the disease target of heart failure, we used “heart failure” as the keyword to retrieve the target of heart failure in the Genecards database (<https://www.genecards.org/>). After the intersection of the target of FXHJ and the target of heart failure, we obtained the exact target of FXHJ in the treatment of heart failure.

2.2. Network Construction. We constructed the network diagram of “herb-compound-target” of FXHJ and the equivalent molecular group by Cytoscape 3.6.1. In the network diagram, “node” refers to the compound or target, and “edge” refers to the relationship between the compound and the target. Based on the analysis of the network diagram of the equivalent molecule group, we select the compound whose degree is greater than the average as the main component of the equivalent molecule group.

2.3. Enrichment Analysis. Direct targets were recorded into David 6.8 database (<https://david.ncicrf.gov/summary.jsp>) to obtain KEGG signaling pathway data. We analyzed the results with P value less than 0.05 to obtain the results. According to the enrichment results and the preceding experimental results, we obtained the functional pathway of FXHJ in the treatment of heart failure. After that, we screened the effective targets and components in reverse according to the action pathway and obtained the equivalent molecular group.

2.4. Molecular Docking. AutoDock Vina_1.1.2 software was used to conduct molecular docking between major components and key targets of potential pathways so as to ensure their interaction activity. AutoDock Vina USES semiflexible molecular docking. That is, the pharmacophore is flexible while the protein remains rigid during the docking. The docking results are evaluated by semiempirical free energy function.

2.5. Specific Steps

- (1) In the PubChem website (<https://pubchem.ncbi.nlm.nih.gov/>), download the 3d structure of the active ingredient file (“SDF” format). Open Babel is used to hydrogenate atoms in molecular structure. Select the MMFF94 field to add the charge and minimize energy. Finally, AutoDock Tools are utilized to convert the compound into a PDBQT format file.
- (2) Download the crystal structure of the key targets molecule from the PDB website (<http://www.rcsb.org/>).
- (3) AutoDock Tools were used to separate the target protein and its ligand, add hydrogen atom, calculate the electric charge, and export it to the PDBQT format file. AutoDock Tools were used to identify the size and center of the docking box. The center of the docking box was defined as the center of the protein crystal structure of the original ligand, and the size of the docking box included the key residues in the active site of the original ligand.
- (4) At last, Vina was utilized to connect the active ingredients with the target protein in turn, and Affinity was extracted. PyMol was utilized to analyze and plot the results.

3. Result

3.1. FXHJ Data Collection. From the TCMSP database, we can get that DG has 2 blood active components and 67 predicted targets. FZ has 21 blood active components and 32 predicted targets. HB has 27 blood active components and 93 predicted targets. TLZ has 12 blood active components and 123 predicted targets. YYH has 23 blood active components and 140 predicted targets. ZX has 10 blood active components and 9 predicted targets. After adding up and deleting the duplicates of 6 Chinese herbs, we obtained 64 and 157 targets of blood components. We searched the Genecards database and obtained 10,961 targets for heart failure. Next, we took the intersection of TCM action targets and heart failure targets and obtained 144 targets. Meanwhile, we constructed the action network of FXHJ as shown in Figure 1.

3.2. Enrichment Analysis of Data. The enrichment analysis showed that the key target of FXHJ in the treatment of heart failure was concentrated in 113 pathways, among which 104 were with P value less than 0.05. The top 20 bits of the enrichment results are shown in Figure 2. In addition to the pathways and targets previously demonstrated by the team, the results showed that the toll-like receptor signaling pathway, VEGF signaling pathway, and NF-kappa B signaling pathway might be potential pathways for the treatment of heart failure.

3.3. Construction of Equivalent Molecular Clusters. According to the enrichment analysis results, 5 Chinese herbs, 39 compounds, and 47 action targets were reverse-screened. We constructed the action network diagram of the equivalent molecular group, as shown in Figure 3. From the analysis of the network diagram, we can find that the main components of the equivalent molecular group are 17 compounds. We ranked these compounds by degree value from large to small as quercetin, Kaempferol, Luteolin, p-sitosterol, 2, 7-dihydrohomoerysotrine, Isocorypalmine, Protopine, Stigmasterol, 8-(3-methylbut-2-enyl)-2-phenylchromen-4-one, Cavidine, Anhydroicaritin, Rutaecarpine, Phellopterin, Liquiritigenin, berberine, palmatine, and isorhamnetin.

3.4. Molecular Docking Results. AutoDock Vina evaluates the binding ability of small molecules to proteins, mainly by affinity. Affinity less than 0 indicates that the ligand can spontaneously bind to the receptor, and the smaller the value is, the higher the binding energy is, and the easier the active component is to bind to the receptor.

We select five key targets from toll-like receptor signaling pathway, VEGF signaling pathway, and NF-kappa B signaling pathway according to the intersection of the pathway and degree value, namely VEGFA (1VPF), TNF (2AZ5), PIK3CG (2CHZ), PTGS2 (5KIR), and MAPK1 (5NHV). The docking results are shown in Table 1.

We visualized the combination of ligand and receptor with the highest Affinity, as shown in Figure 4. From the figure, we can see that the compound enters the target protein target active site and its binding pattern.

4. Discussion

In the treatment of heart failure, how to slow or even reverse ventricular remodeling has grown up to be a hot topic in recent years. Transforming growth factor beta, angiotensin II, aldosterone and endothelin, and myocardial damage or stress produce cytokines and chemokines can induce the formation of muscle fibroblasts [10, 11]. In the early stage, we have studied the relevant pathways, including the MAPK signaling pathway, the PI3K/Akt signaling pathway, the cAMP signaling pathway, the TNF signaling pathway, and the apoptotic conduction molecule BCL2.

There are three subclasses in the MAPK signaling pathway, namely ERK, JNK, and p38MAPK. Cipolletta et al. demonstrated that the inhibition of p-ERK volume could delay cardiac hypertrophy and improve cardiac volume [12]. Our previous experiments showed that FXHJ could significantly reduce the ERK level of rat cardiac tissue compared with the model group ($P < 0.01$) [13].

The active form of PI3K can activate AKT, thereby promoting cell proliferation and inhibiting the apoptotic pathway. Overexpression of PI3K can cause cardiac hypertrophy. The GSK3 β cytokine downstream of PI3K/Akt, which can be inactivated by phosphorylation, is a key negative regulator of cardiac hypertrophy [14]. Our previous experiments have shown that FXHJ can reduce the expression of PI3K and AKT, improve the expression of GSK3, and thus inhibit ventricular remodeling [15].

cAMP ACTS as excitation-coupled phosphorylation of cardiomyocyte proteins, including l-type calcium channels, sarcoplasmic reticulum ATPase 2 regulatory protein phosphor, clonidine receptor 2, phosphatase 1 inhibitors, and various contractile proteins [16]. Lin B et al. demonstrated that activation of the cAMP signaling pathway could stabilize cardiac function in rats with heart failure [17]. We studied the β 1-AR-cAMP-PKA pathway in previous experiments and found that compared with the model group, both the FXHJ group and the captopril group could reduce the plasma cAMP level, increase the cAMP reserve of cardiomyocytes, improve cardiac function, and delay ventricular remodeling [18].

Tumor necrosis factor α (TNF- α) and the apoptotic signaling molecule BCL2 play important roles in the progression of heart failure. Liu W et al.'s serum examination of patients with chronic heart failure found that, compared with the healthy control group, the serum TNF in patients with heart failure was significantly increased, while bcl-2 was significantly decreased [19]. Studies have shown that increased TNF- α levels exacerbate heart failure. The optimal use of diuretics, ACE inhibitors, beta-blockers, and standard treatment with digoxin for heart failure can significantly reduce circulating TNF levels [20]. Siltanen A's experiments showed that BCL2 gene transplantation in rats with chronic heart failure could effectively improve cardiac function,

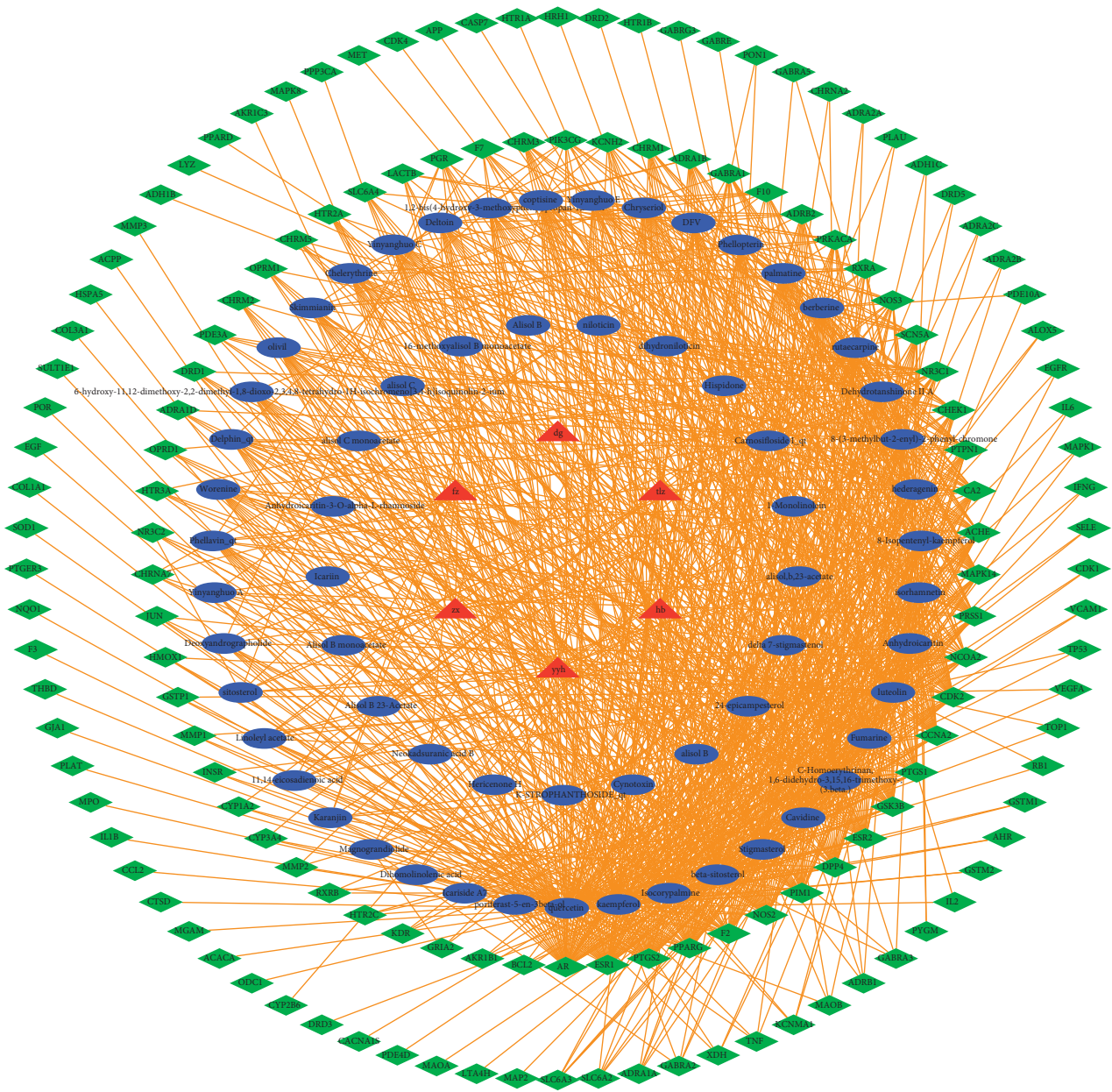


FIGURE 1: Function network diagram of FXHJ. The red triangle represents the Chinese herbs, the blue oval represents the compound, and the green diamond represents the target.

enhance paracrine angiogenic signals, and promote cell proliferation and survival in failing myocardium [21]. Our previous animal experiments showed that FXHJ could effectively reduce the level of TNF- α in rats with heart failure, improve the expression of the BCL2 gene, and thus inhibit a variety of myocardial cell apoptosis pathways [22, 23].

In addition, through the research method of network pharmacology, we analyzed and found that the mechanism of action of FXHJ in the treatment of heart failure may also be related to the toll-like receptor signaling pathway, VEGF signaling pathway, and NF-kappa B signaling pathway. Studies have shown that 8 weeks after knocking out NF-kappa B subunit P50/NF-B1 in mice with myocardial infarction, the degree of ventricular expansion is mild, and

ventricular systolic function is preserved. Therefore, the absence of the NF-kappa B subunit P50 can improve the prognosis of heart failure caused by myocardial infarction. At the same time, inhibition of the NF-kappa B signaling pathway can inhibit ventricular remodeling to a certain extent, which may be related to the reduction of preinflammatory response and the regulation of extracellular matrix [24]. Inhibiting the activation of NF-kappa B65 can prevent myocardial fibrosis and protect cardiac function by reducing the inflammatory response [25]. Vascular endothelial growth factor (VEGF) plays an important role in mediating normal cardiac function by maintaining vascular homeostasis. VEGF maintains vascular homeostasis mainly through the following mechanisms: Improve the sensitivity

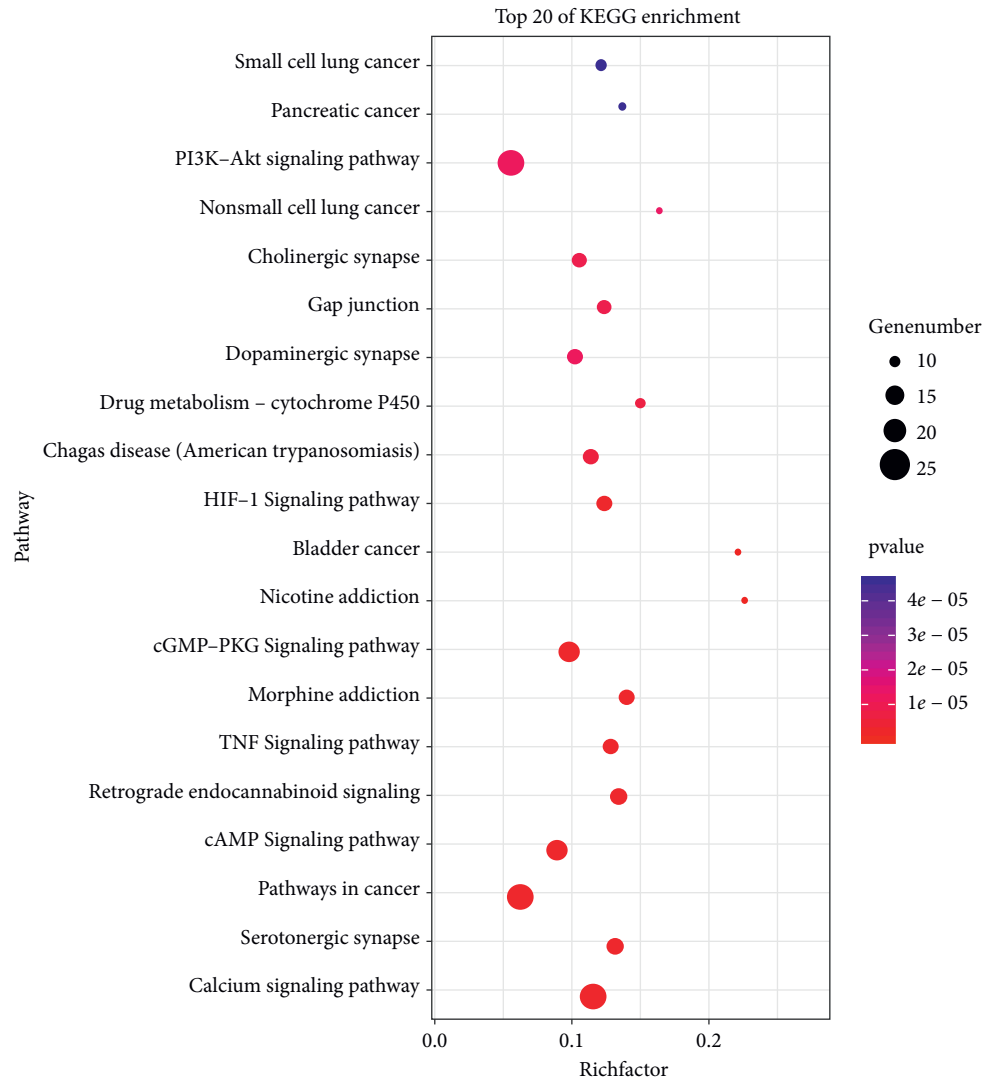


FIGURE 2: The top 20 of enrichment results. Among them, pi3k-akt signaling pathway, TNF signaling pathway, cAMP signaling pathway, and the BCL2 targets in multiple cancer pathways have been confirmed by previous experiments.

of blood vessels to nerve response, improve the permeability of blood vessels, promote the generation and stability of new blood vessels, and recruit stem cells and promote their homing [26]. The research of Meng-Ying He showed that when the VEGF signaling pathway was inhibited, it would lead to the imbalance of vascular homeostasis, which would lead to the generation of heart failure [27]. Toll-like receptor signaling pathway mediates the occurrence of various myocardial injuries, such as myocardial remodeling and myocardial ischemia reperfusion injury [28]. Animal studies have shown that the symptoms of myocardial ischemia in mice with toll-like receptor knockout are reduced. At the same time, toll-like receptor inhibitors could reduce myocardial ischemia in myocardial ischemia model mice [29, 30].

The analysis of the equivalent molecular group shows that there is no ZX in it. This is because the active components of ZX are mainly Alisol A 24-acetate and Alisol B, which have similar structures to aldosterone and its

antagonists. They compete for aldosterone receptors to inhibit reabsorption in different parts of the tubules, inhibiting water reabsorption and increasing urine output [31]. This belongs to the category of diuretics, which is different from the screening scope of this study.

Some of the components in the equivalent molecular group have been studied experimentally, which can provide some reference for the further selection of the components. Moon DO et al. demonstrated that β -sitosterol promotes apoptosis by regulating the ERK and PI3Kakt signaling pathways [32], which is not conducive to the treatment of heart failure. Animal experiments on Kaempferol have shown that Kaempferol can treat heart failure by inhibiting the MAPK signaling pathway, NF-kappa B signaling pathway, and PI3Kakt signaling pathway, activating the VEGF signaling pathway and upregulating the expression of GSK3 β [33–37]. Min Z's experiment proved that quercetin could significantly reduce the phosphorylation of ERK and inhibit myocardial cell fibrosis [38]. Meanwhile, quercetin

TABLE 1: The figures in the table represent the affinity of molecular docking (kcal/mol). The red figure indicates that the compound has the highest affinity to the target.

Compound	VEGFA	TNF	PIK3CG	PTGS2	MAPK1
Protopine	-7.8	-9.2	-9.4	-5.4	-9.5
Cavidine	-7.4	-8.4	-8.6	-5.1	-9.3
Rutaecarpine	-7.8	-9.8	-9.2	-8.9	-9.1
8-(3-Methylbut-2-enyl)-2-phenylchromen-4-one	-7.5	-8.7	-9.6	-10.7	-9
Luteolin	-7.2	-7.8	-8.8	-9.7	-8.6
Quercetin	-7.2	-7.2	-7.7	-9.7	-8.6
Isorhamnetin	-7.2	-7.3	-7.8	-9.7	-8.5
Berberine	-7.2	-8.6	-8.5	-6	-8.5
Liquiritigenin	-7.3	-7.6	-8.8	-9.3	-8.4
Kaempferol	-6.9	-6.9	-7.5	-9.8	-8.3
Stigmasterol	-6.9	-8.3	-8.3	-7.9	-8.2
Phellopterin	-6.5	-7.4	-8	-8.3	-8.1
Palmitine	-6.2	-8	-7.5	-5.2	-7.8
Isocorypalmine	-7	-7.8	-7.7	-4.9	-7.7
Anhydrocaritin	-7.7	-8	-8.6	6.6	-7.5
2-7-Dihydrohomoerysotrine	-6	-7.4	-7.1	-2.8	-6.3

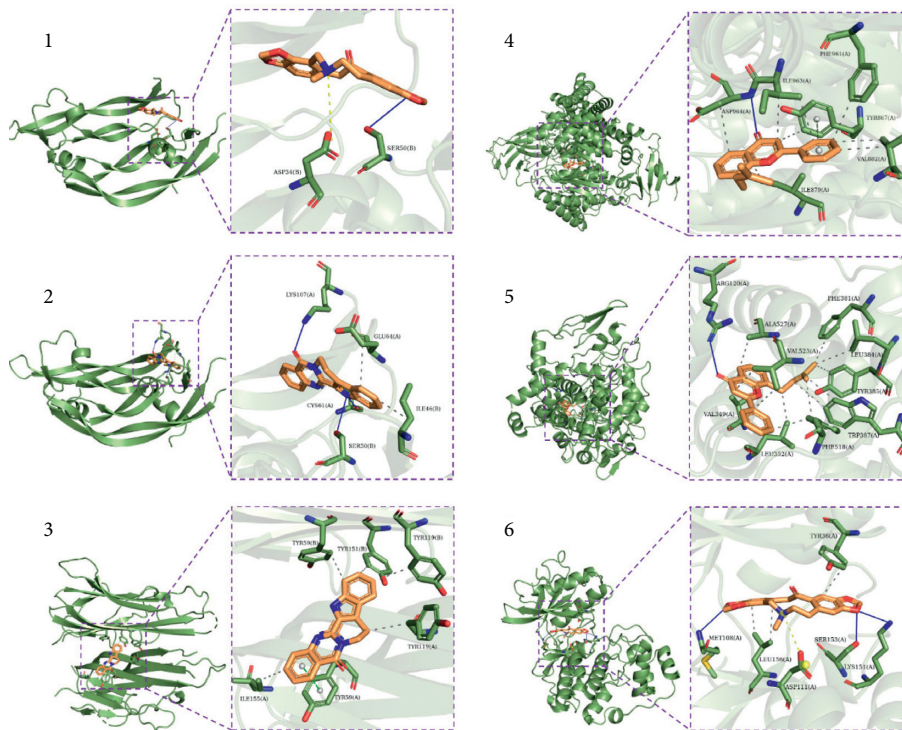


FIGURE 4: Number 1 is the combination of protopine and VEGFA. Number 2 is the combination of Rutaecarpine and VEGFA. Number 3 is the combination of Rutaecarpine and TNF. Number 4 is the combination of 8-(3-Methylbut-2-enyl)-2-phenylchromen-4-one and PIK3CG. Number 5 is the combination of 8-(3-Methylbut-2-enyl)-2-phenylchromen-4-one and PTGS2. Number 6 is the combination of protopine and MAPK1. Among them, the solid blue line represents a hydrogen bond, the dotted yellow line represents a salt bridge, the dotted gray line represents hydrophobic interaction, and the dotted green line represents pi-stacking between benzene rings.

cancer [50–52]. Studies have shown that tumor growth is associated with increased levels of inflammatory cytokines and a significant decrease in ventricular systolic function [53]. We know that heart failure has the same risk factors as cancer. Patients with heart failure have a higher rate of cancer than healthy control populations [54]. We also know that modern anticancer therapies are often associated with cardiotoxicity, which exacerbates or accelerates acute or

chronic heart failure [55]. It may be that a combination of traditional Chinese medicine can reduce the risk of cancer in patients with heart failure [56], but more experiments and studies are needed to confirm this view.

However, there were a few shortcomings in this study. Due to limited funds, this study did not obtain the blood composition of FXHJ by mass spectrometry but selected database screening, which may cause certain errors.

Secondly, although animal experiments and clinical trials have shown that FXHJ has a beneficial therapeutic effect, there is still a lack of experimental research on some components. Further research is needed to determine whether these components will cause side effects.

In summary, this study revealed the mechanism of FXHJ in the treatment of heart failure through the research method of network pharmacology and summarized the previous experimental results of the research group. It wishes to point out the direction for new drug development and further research. At the same time, the concept of the equivalent molecular group provides innovative ideas for the transformation and research of the modernization of TCM.

Data Availability

The data used to support the findings of this study are available from the corresponding author upon request.

Disclosure

The authors report no conflicts of interest in this work.

Conflicts of Interest

The authors declare that they have no conflicts of interest.

Authors' Contributions

YDY drafted the manuscript, contributed to data analysis, and revised the final manuscript. YPX and YFL examined the data collection and processing process. YTX provided advice during the study and manuscript preparation. All authors read and approved the final manuscript.

Acknowledgments

The authors sincerely thank the National Natural Science Foundation of China (Grants no. 81774247) for its support.

References

- [1] S. A. Hunt, W. T. Abraham, M. H. Chin et al., "ACC/AHA 2005 guideline update for the diagnosis and management of chronic heart failure in the adult-summary article," *Journal of the American College of Cardiology*, vol. 46, no. 6, pp. 1116–1143, 2005.
- [2] A. P. Maggioni, U. Dahlström, G. Filippatos et al., "EURObservationalResearch programme: regional differences and 1-year follow-up results of the heart failure pilot survey (ESC-HF pilot)," *European Journal of Heart Failure*, vol. 15, no. 7, pp. 808–817, 2013.
- [3] X. Yitao, "Effect of Fuxin mixture on the expression of beta₁-AR mRNA in lymphocytes of patients with chronic congestive heart failure and clinical observation," *China Journal of Traditional Chinese Medicine*, vol. 33, no. 3, pp. 533–536, 2015.
- [4] A. L. Hopkins, "Network pharmacology: the next paradigm in drug discovery," *Nature Chemical Biology*, vol. 4, no. 11, pp. 682–690, 2008.
- [5] J. Fang, C. Liu, Q. Wang, P. Lin, and F. Cheng, "In silico polypharmacology of natural products," *Brief Bioinformatics*, vol. 19, no. 6, pp. 1153–1171, 2018.
- [6] M. Jafari, Y. Wang, A. Amiryousefi, and J. Tang, "Unsupervised learning and multipartite network models: a promising approach for understanding traditional medicine," *Frontiers in Pharmacology*, vol. 11, p. 1319, 2020 PMID: 32982738; PMCID: PMC7479204.
- [7] Y. Wang, M. Jafari, Y. Tang, and J. Tang, "Predicting Meridian in Chinese traditional medicine using machine learning approaches," *PLOS Computational Biology*, vol. 15, no. 11, e1007249 pages, 2019, PMID: 31765369; PMCID: PMC6876772, Article ID e1007249.
- [8] M. Kibble, N. Saarinen, J. Tang, K. Wennerberg, S. Mäkelä, and T. Aittokallio, "Network pharmacology applications to map the unexplored target space and therapeutic potential of natural products," *Natural Product Reports*, vol. 32, no. 8, pp. 1249–1266, 2015.
- [9] H. Yuan, Q. Ma, H. Cui et al., "How can synergism of traditional medicines benefit from network pharmacology?" *Molecules*, vol. 22, no. 7, p. 1135, 2017.
- [10] Y. Sun, "Myocardial repair/remodelling following infarction: roles of local factors," *Cardiovascular Research*, vol. 81, no. 3, pp. 482–490, 2009.
- [11] M. Delaunay, H. Osman, S. Kaiser, and D. Diviani, "The role of cyclic AMP signaling in cardiac fibrosis," *Cells*, vol. 9, no. 1, p. 69, 2019.
- [12] E. Cipolletta, M. R. Rusciano, A. S. Maione et al., "Targeting the CaMKII/ERK interaction in the heart prevents cardiac hypertrophy," *Plos One*, vol. 10, no. 6, e0130477 pages, Article ID e0130477, 2015.
- [13] Yi-tao Santulli, "Effects of fuxin mixture on the signal pathway of raf-mek-erk in rats with heart failure," *Chinese Journal of Traditional Chinese Medicine*, vol. 33, no. 4, pp. 791–794, 2015.
- [14] X. Yitao, "Relationship between heart failure and PI3K-Akt-GSK3 β pathway and progress in traditional Chinese medicine," *Chinese Medicine Emergency*, vol. 25, no. 6, pp. 1066–1069, 2015.
- [15] Yi-tao Xue, "Effects of fuxin decoction on the pathway of pi3k-akt-gsk3 β in heart failure rats," *Shanghai Journal of Traditional Chinese Medicine*, vol. 49, no. 8, pp. 74–78, 2015.
- [16] C. C. Sucharov, S. J. Nakano, D. Slavov et al., "A PDE3A promoter polymorphism regulates cAMP-induced transcriptional activity in failing human myocardium," *Journal of the American College of Cardiology*, vol. 73, no. 10, pp. 1173–1184, 2019.
- [17] B. Lin, D. G. Feng, and J. Xu, "microRNA-665 silencing improves cardiac function in rats with heart failure through activation of the cAMP signaling pathway," *Journal of Cellular Physiology*, vol. 234, no. 8, pp. 13169–13181, 2019.
- [18] Y.-t. Xu, "Effects of fuxin mixture on the β_1 -ar-camp-pka pathway in rats with heart failure," *Chinese Journal of Integrated Traditional and Western Medicine*, vol. 37, no. 4, pp. 453–457, 2017.
- [19] W. Liu, L. Ru, C. Su, S. Qi, and X. Qi, "Serum levels of inflammatory cytokines and expression of BCL2 and BAX mRNA in peripheral blood mononuclear cells and in patients with chronic heart failure," *Medical Science Monitor*, vol. 25, pp. 2633–2639, 2019.
- [20] B. Bozkurt, D. L. Mann, and A. Deswal, "Biomarkers of inflammation in heart failure," *Heart Failure Reviews*, vol. 15, no. 4, pp. 331–341, 2010.
- [21] A. Siltanen, K. Kitabayashi, T. Pätälä et al., "Bcl-2 improves myoblast sheet therapy in rat chronic heart failure," *Tissue Engineering Part A*, vol. 17, no. 1-2, pp. 115–125, 2011.

- [22] X. Yitao et al., "Effects of Fuxin decoction on myocardial cytokines TNF- α and BNP in rats with heart failure," *Journal of Integrated Traditional Chinese and Western Medicine Cardio-Cerebrovascular Disease*, vol. 11, no. 7, pp. 833-834, 2013.
- [23] X. Yitao, "Effects of fuxin decoction on expression of bcl-2, a signal transduction molecule, in cardiac myocytes of rats with heart failure," *China Journal of Traditional Chinese Medicine*, vol. 31, no. 12, pp. 2717-2720, 2013.
- [24] J.-L. Jin and J.-R. Wei, "Research progress on the relationship between Notch signaling and NF-kappa B signaling pathway and ventricular remodeling after myocardial infarction," *Chinese Journal of Circulation*, vol. 30, no. 07, pp. 718-720, 2015.
- [25] J. E. Toblli, G. Cao, C. Rivas, J. F. Giani, and F. P. Dominici, "Intravenous iron sucrose reverses anemia-induced cardiac remodeling, prevents myocardial fibrosis, and improves cardiac function by attenuating oxidative/nitrosative stress and inflammation," *International Journal of Cardiology*, vol. 212, pp. 84-91, 2016.
- [26] Z. Taimeh, J. Loughran, E. J. Birks, and R. Bolli, "Vascular endothelial growth factor in heart failure," *Nature Reviews Cardiology*, vol. 10, no. 9, pp. 519-530, 2013.
- [27] M.-Y. Bolli, Z.-W. Yin, Y.-R. Zhao, H.-P. Li, W. Zheng, and J.-G. Jiang, "Mir-320a mediates adriamycin cardiac injury by targeting VEGF signaling pathway," *Chinese Journal of Molecular Cardiology*, vol. 18, no. 05, pp. 2594-2599, 2008.
- [28] E. M. Y. Moresco, D. LaVine, and B. Beutler, "Toll-like receptors," *Current Biology*, vol. 21, no. 13, pp. R488-R493, 2011.
- [29] C.-F. Liang, J. T. Liu, Y. Wang, A. Xu, and P. M. Vanhoutte, "Toll-like receptor 4 mutation protects obese mice against endothelial dysfunction by decreasing NADPH oxidase isoforms 1 and 4," *Arteriosclerosis, Thrombosis, and Vascular Biology*, vol. 33, no. 4, pp. 777-784, 2013.
- [30] Yu-J. Xu and W. Huang, "Research progress of toll-like receptor 2, 4 and myocardial ischemia-reperfusion injury," *Advances in Cardiology*, vol. 34, no. 2, p. 240, 2013.
- [31] Yu-hui Zhao, "Research progress on the chemical constituents and diuretic mechanism of fuling, fuling skin, polyporin and alisma," *Chinese Journal of Pharmacology and Toxicology*, vol. 28, no. 04, pp. 594-599, 2014.
- [32] D.-O. Moon, K.-J. Lee, Y. H. Choi, and G.-Y. Kim, "Beta β -Sitosterol-induced-apoptosis is mediated by the activation of ERK and the downregulation of Akt in MCA-102 murine fibrosarcoma cells," *International Immunopharmacology*, vol. 7, no. 8, pp. 1044-1053, 2007.
- [33] F. Zhang and C. Ma, "Kaempferol suppresses human gastric cancer SNU-216 cell proliferation, promotes cell autophagy, but has no influence on cell apoptosis," *Brazilian Journal of Medical and Biological Research*, vol. 52, no. 2, Article ID e7843, 2019.
- [34] Z. Zhuang, G. Ye, and B. Huang, "Kaempferol alleviates the interleukin-1 β -induced inflammation in rat osteoarthritis chondrocytes via suppression of NF- κ B," *Medical Science Monitor*, vol. 23, pp. 3925-3931, 2017.
- [35] H.-Y. Wang, J.-G. Zhao, Z.-G. Wei, and Y.-Q. Zhang, "The renal protection of flavonoid-rich ethanolic extract from silkworm green cocoon involves in inhibiting TNF- α -p38 MAP kinase signalling pathway in type 2 diabetic mice," *Biomedicine & Pharmacotherapy*, vol. 118, p. 109379, 2019.
- [36] L. Zhang, Z. Guo, Y. Wang, J. Geng, and S. Han, "The protective effect of kaempferol on heart via the regulation of Nrf2, NF- κ B, and PI3K/Akt/GSK-3 β signaling pathways in isoproterenol-induced heart failure in diabetic rats," *Drug Development Research*, vol. 80, no. 3, pp. 294-309, 2019.
- [37] H. K. Chin, C. T. Horng, Y. S. Liu et al., "Kaempferol inhibits angiogenic ability by targeting VEGF receptor-2 and down-regulating the PI3K/AKT, MEK and ERK pathways in VEGF-stimulated human umbilical vein endothelial cells," *Oncology Reports*, vol. 39, pp. 2351-2357, 2018.
- [38] Z. Lu, L. Yangchun, W. Yuquan, and Z. Changying, "Quercetin inhibition of myocardial fibrosis through regulating MAPK signaling pathway via ROS," *Pakistan Journal of Pharmaceutical Sciences*, vol. 32, no. 3, pp. 1355-1359, 2019.
- [39] A. Tripathi, M. Kumar, P. Kaur, B. Kumar, and S. S. K. Sagi, "Efficacy of Quercetin as a potent sensitizer of β 2-AR in combating the impairment of fluid clearance in lungs of rats under hypoxia," *Respiratory Physiology & Neurobiology*, vol. 273, Article ID 103334, 2020.
- [40] S.-C. Cheng, W.-C. Huang, J.-H. S. Pang, Y.-H. Wu, and C.-Y. Cheng, "Quercetin inhibits the production of IL-1 β -induced inflammatory cytokines and chemokines in ARPE-19 cells via the MAPK and NF- κ B signaling pathways," *International Journal of Molecular Sciences*, vol. 20, no. 12, p. 2957, 2019.
- [41] R. Gupta, R. K. Shukla, A. Pandey et al., "Involvement of PKA/DARPP-32/PP1 α and β -arrestin/akt/GSK-3 β signaling in cadmium-induced DA-D2 receptor-mediated motor dysfunctions: protective role of quercetin," *Scientific Reports*, vol. 8, no. 1, p. 2528, 2018.
- [42] W. Hu, T. Xu, P. Wu et al., "Luteolin improves cardiac dysfunction in heart failure rats by regulating sarcoplasmic reticulum Ca²⁺-ATPase 2a," *Scientific Reports*, vol. 7, no. 1, p. 41017, 2017.
- [43] G. Wang, W. Li, X. Lu, P. Bao, and X. Zhao, "Luteolin ameliorates cardiac failure in type I diabetic cardiomyopathy," *Journal of Diabetes and Its Complications*, vol. 26, no. 4, pp. 259-265, 2012.
- [44] C. Li, Q. Wang, S. Shen, X. Wei, and G. Li, "HIF-1 α /VEGF signaling-mediated epithelial-mesenchymal transition and angiogenesis is critically involved in anti-metastasis effect of Luteolin in melanoma cells," *Phytotherapy Research*, vol. 33, no. 3, pp. 798-807, 2019.
- [45] M. Zang, L. Hu, B. Zhang et al., "Luteolin suppresses angiogenesis and vasculogenic mimicry formation through inhibiting Notch1-VEGF signaling in gastric cancer," *Biochemical and Biophysical Research Communications*, vol. 490, no. 3, pp. 913-919, 2017.
- [46] M.-H. Bao, W. Dai, Y.-J. Li, and C.-P. Hu, "Rutaecarpine prevents hypoxia-reoxygenation-induced myocardial cell apoptosis via inhibition of NADPH oxidases," *Canadian Journal of Physiology and Pharmacology*, vol. 89, no. 3, pp. 177-186, 2011.
- [47] Y. Ying, K. Chen, X. Dong et al., "Berberine inhibits cardiac remodeling of heart failure after myocardial infarction by reducing myocardial cell apoptosis in rats," *Experimental and Therapeutic Medicine*, vol. 16, pp. 2499-2505, 2018.
- [48] K. Chen, G. Li, F. Geng et al., "Berberine reduces ischemia/reperfusion-induced myocardial apoptosis via activating AMPK and PI3K-Akt signaling in diabetic rats," *Apoptosis*, vol. 19, no. 6, pp. 946-957, 2014.
- [49] L. Gao, R. Yao, Y. Liu et al., "Isorhamnetin protects against cardiac hypertrophy through blocking PI3K-AKT pathway," *Molecular and Cellular Biochemistry*, vol. 429, no. 1-2, pp. 167-177, 2017.
- [50] G. Kroemer and J. Pouyssegur, "Tumor cell metabolism: cancer's Achilles' heel," *Cancer Cell*, vol. 13, no. 6, pp. 472-482, 2008.

- [51] R. R. Ramjiawan, A. W. Griffioen, and D. G. Duda, "Anti-angiogenesis for cancer revisited: is there a role for combinations with immunotherapy?" *Angiogenesis*, vol. 20, no. 2, pp. 185–204, 2017.
- [52] F. Balkwill and A. Mantovani, "Inflammation and cancer: back to Virchow?" *The Lancet*, vol. 357, no. 9255, pp. 539–545, 2001.
- [53] M. Buoncervello, S. Maccari, B. Ascione et al., "Inflammatory cytokines associated with cancer growth induce mitochondria and cytoskeleton alterations in cardiomyocytes," *Journal of Cellular Physiology*, vol. 234, no. 11, pp. 20453–20468, 2019.
- [54] A. M. Richards, "Can heart failure cause cancer?" *Nature Reviews Cardiology*, vol. 16, no. 1, pp. 7–8, 2019.
- [55] A. Lena, A. J. S. Coats, and M. S. Anker, "Metabolic disorders in heart failure and cancer," *ESC Heart Failure*, vol. 5, no. 6, pp. 1092–1098, 2018.
- [56] M. S. Anker, S. von Haehling, U. Landmesser, A. J. S. Coats, and S. D. Anker, "Cancer and heart failure-more than meets the eye: common risk factors and co-morbidities," *European Journal of Heart Failure*, vol. 20, no. 10, pp. 1382–1384, 2018.

Research Article

Study on Medication Rules of Traditional Chinese Medicine against Antineoplastic Drug-Induced Cardiotoxicity Based on Network Pharmacology and Data Mining

Wenchao Dan ^{1,2}, Jinlei Liu ^{1,2}, Xinyuan Guo ³, Boran Zhang ², Yi Qu ^{1,2}, and Qingyong He ¹

¹Department of Cardiology, China Academy of Chinese Medical Sciences Guanganmen Hospital, No. 5, North Line Pavilion, Xicheng District, Beijing 100053, China

²Graduate School of Beijing University of Chinese Medicine, Beijing 100029, China

³Department of Radiation Therapy, Cancer Hospital Chinese Academy of Medical Sciences, No. 17, South Panjiayuan, Chaoyang District, Beijing 100021, China

Correspondence should be addressed to Qingyong He; heqingyong@163.com

Received 20 May 2020; Revised 16 August 2020; Accepted 21 October 2020; Published 18 November 2020

Academic Editor: Akhilesh K. Tamrakar

Copyright © 2020 Wenchao Dan et al. This is an open access article distributed under the Creative Commons Attribution License, which permits unrestricted use, distribution, and reproduction in any medium, provided the original work is properly cited.

Background and Aim. Antineoplastic drug-induced cardiotoxicity (ADIC) becomes the second leading cause of death for tumor survivors after tumor recurrence and metastasis, and there may be great room for development in the future of traditional Chinese medicine (TCM). However, the theory of anticardiotoxicity of TCM has not yet formed a system. This study aimed to explore the material basis and the rule of TCM against ADIC based on network pharmacology and data mining. **Methods.** The targets of antineoplastic drugs with cardiotoxicity were obtained from the National Center for Biotechnology Information (NCBI) database, China national knowledge infrastructure (CNKI) database, and Swiss Target Prediction platform. Then, the cardiotoxicity-related targets were derived from the Gene Cards, Disgenet, OMIM, and DrugBank databases, as well as the drug of current clinical guidelines. The targets both in these two sets were regarded as potential targets to alleviate ADIC. Then, candidate compounds and herbs were matched via Traditional Chinese Medicine Systems Pharmacology (TCMSP) platform. Cytoscape3.7.1 was used to set up the target-compound-herb network. Molecular docking between core targets and compounds was performed with Auto-dockVina1.1.2. The rules of herbs were summarized by analyzing their property, flavor, and channel tropism. **Results.** Twenty-one potential targets, 332 candidate compounds, and 400 kinds of herbs were obtained. Five core targets including potassium voltage-gated channel subfamily H member 2 (KCNH2), cyclin-dependent kinase 1 (CDK1), matrix metalloproteinase 2 (MMP2), mitogen-activated protein kinase1 (MAPK1), and tumor protein p53 (TP53) and 29 core compounds (beta-sitosterol, quercetin, kaempferol, etc.) were collected. Five core herbs (Yanhusuo, Gouteng, Huangbai, Lianqiao, and Gancao) were identified. Also, the TCM against ADIC were mainly bitter and acrid in taste, warm in property, and distributed to the liver and lung meridians. **Conclusion.** TCM against ADIC has great potential. Our study provides a new method and ideas for clinical applications of integrated Chinese and western medicine in treating ADIC.

1. Background

Since the 1970s, there have been reports of cardiotoxic reactions caused by anthracyclines [1]. With the continuous enrichment of cancer treatment methods, the survival time of cancer patients has been greatly improved, and there are more and more reports of cardiac toxicity. According to statistics, about 51% of cancer patients die from recurrent

disease, and about 33% of them die from heart disease, which is related to the increased incidence of coronary artery disease and valve heart disease [2]. At present, there are many research studies related to cardiotoxicity in tumor treatment drugs. For example, tyrosine kinase (TK) is a ubiquitous phosphorylase that controls many signaling pathways, such as VEGF and EGFR. Inhibition of this pathway by antibodies has become a new method of clinical

treatment, which is accompanied by damage to heart function after inhibition of signal transduction. For example, sunitinib can inhibit more than 50 different kinases to play an antitumor effect, but at the same time, inhibiting AMPK affects the oxidative stress response and increases the chance of heart failure [3]. ERBB receptor antibody is a commonly used drug in the clinical treatment of breast cancer. At the same time of treatment, it inhibits the signal transduction of neuromodulin 1 (NRG-1), affects the metabolism of cardiomyocytes, and leads to the development of cardiac toxicity [4]. Cardiotoxic reactions caused by anthracycline antibiotics are more common. During doxorubicin chemotherapy, reactive oxygen species (ROS) production, DNA damage, and mitochondrial dysfunction can be caused, resulting in increased left ventricular wall pressure and decreased left ventricular ejection fraction (LVEF), arrhythmia and highly symptomatic congestive heart failure, and other adverse consequences [5]. Radiation therapy is widely used in cancer treatment, and it also causes heart-related side effects during treatment. Its combination with anthracycline drugs also increases the risk of disease, which causes atherosclerosis, valve insufficiency, and other diseases [6].

At present, although the detection of certain biological markers can predict the impairment of cardiac function, such as troponin levels are associated with diastolic dysfunction caused by anthracyclines [7], the mechanism of most cardiac toxic drugs is still unclear. Only by using certain β -blockers, ACEI inhibitors, angiotensin receptor blockers, and other drugs for symptomatic treatment, the side effects of radiotherapy and chemotherapy can be alleviated [8]. The period of cardiotoxicity also has a great impact on tumor treatment. Early toxicity affects the progress of tumor treatment, and the tumor growth cannot be controlled in time, which leads to the deterioration of the condition; the late onset of toxicity often leads to the destruction of cardiac function, affecting the quality of life of patients. Moreover, the complexity of clinical symptoms increases the difficulty of distinguishing cardiac toxicity and cardiac dysfunction [9]. Therefore, an in-depth study of the mechanism of tumor cardiotoxicity can choose a more appropriate treatment approach for tumor patients and improve the quality of life of tumor patients.

TCM shows remarkable curative effects in clinical treatment of many diseases, and Chinese herbal medicine is a treasure trove of natural compounds, which have the advantages of wide source, multiple effective compounds, stable compound structure, and guaranteed safety. Reports have demonstrated that Xinmailong injection is effective for the treatment of cardiotoxicity caused by sequential chemotherapy of trastuzumab and anthracyclines in breast cancer, which could effectively improve the clinical symptoms of patients, attenuate myocardial injury, reduce blood viscosity, and inhibit expressions of serum IL-6 and TNF- α [10]. It was confirmed that Danshen injection has particular preventive effects on cardiotoxicity caused by chemotherapy of pyrruxine or epirubicin, and the effect includes protecting the myocardium, relieving myocardial damage, and improving cardiac function [11]. However, there is less research

on the Chinese herbs medicine against cardiac toxicity caused by antineoplastic drugs. A meta-analysis study showed that Wenxin grenules can prevent and reduce tachycardia caused by anthracyclines, but its efficacy in improving overall efficiency and preventing and reducing atrial premature beats, ventricular premature beats, atrial fibrillation, and SOD levels is not clear; meanwhile, Baoxinkang can protect myocardial SOD activity [12]. Therefore, it is of great value to further explore Chinese herbs medicine against cardiac toxicity caused by antineoplastic drugs and to develop related preparations. However, TCM and compound medicines have the characteristics of multi-compound, multitarget, and multimechanism system regulation. If a single drug, single target, and single research idea are used for research, it is difficult to systematically reflect the intervention mechanism of TCM; as an emerging research discipline, Chinese medicine started late in this field, and no research has systematically summarized the rules of TCM against cardiac toxicity caused by antineoplastic drugs.

Network pharmacology is a combination of system pharmacology, multidirectional pharmacology, bioinformatics, data mining, and other multidisciplinary. By constructing a network to analyze the relationship between the various compounds and the key nodes in the network, it could show the material basis and mechanism of action of Chinese medicine or compound [13, 14]. Therefore, it is currently widely used in the research of the mechanism of action and new drug development of Chinese medicine and compound.

In this study, we used the method of network pharmacology, used the relevant targets of cardiac toxicity caused by antineoplastic drugs as entry points, and matched the relevant ligands and TCM. As a result, we systematically predicted and analyzed the complex relationship between the target, compound and TCM, meanwhile initially discussed the material basis and general rules, which could provide ideas and theoretical basis for the follow-up selection of TCM, theoretical discussion, new drug development, and clinical integration of traditional Chinese and Western medicine. The flow chart of this study is shown in Figure 1.

2. Materials and Methods

2.1. The Collection of Potential Targets for Herbs against Antineoplastic Drug-Induced Cardiotoxicity. The ADIC is mainly manifested as arrhythmia, heart failure, and ischemic heart disease [15]. To obtain relevant targets, cardiotoxicity-related words, such as “arrhythmia,” “heart failure,” and “myocardial ischemia,” were used as keywords to query the following electronic databases: Genecards database [16] (<https://www.genecards.org/>), OMIM database [17] (<https://omim.org/>), DrugBank database [18], and Disgenet database [19] (<http://www.disgenet.org>). Results were merged, and duplicates were removed to obtain target group I. The sdf format files of antineoplastic drugs, including anthracyclines (doxorubicin (DOX), epirubicin, pirarubicin, aclarubicin, idarubicin, amrubicin, and daunorubicin), taxanes

pharmacokinetic parameters (ADME) and the Lipinski rules [26], candidate compounds were screened. The specific screening criteria were oral availability (OB) $\geq 30\%$, drug likeness [27] (DL) ≥ 0.18 , drug half-life > 4 h, topological polar surface area [28] < 140 angstroms, rotatable bonds number [29] ≤ 10 ; and molecular weight ≤ 500 Da. Considering that the parameters provided by the TCMSP platform is predicted by the computer, part of the data may be inconsistent with the actual situation, and the deleted compounds were checked one by one to supplement the relevant active compounds after the initial screening. The revised compounds were regarded as candidate compounds. Along with these compounds, the potential targets were imported into Cytoscape3.7.2 software [30] to construct a target-compound network and calculate the topology parameter (degree) of the nodes in the network. Core targets, compounds, and herbs were defined based on the degree.

2.3. Herb Matching and Target-Compound-Herb Network Construction.

We collected herbs containing candidate compounds and constructed the compound-herb network. The "target-compound" network and the compound-herb network were combined through the merge function module in the Cytoscape3.7.2 to establish the target-compound-herb network. Furthermore, we identified key nodes based on the degree of each node in the network and evaluated the strength of efficacy of the Chinese medicines and compounds in treating ADIC.

2.4. Characteristics of the Candidate Herbs.

A frequency analysis was performed to summarize the rules of candidate herbs against ADIC. Characteristics under investigation included property, flavor, and channel tropism. Considering the heterogeneity of the information on characteristics from different sources, the priority order of standards we adopted in this study was *Chinese Pharmacopoeia* (2015) [31], *Chinese Pharmacy* ("Thirteenth Five-Year Plan" textbook) [32], and *Chinese Dictionary of Clinical Medicine* [33]. Herbs lacking of relevant information were deleted.

2.5. Molecular Docking of the Target-Compound.

To assess the credibility of the connection between the target and the compound and identify new candidate herbs for ADIC treatment, molecular docking of the core compounds with core targets was carried out. Five targets with the highest degree in the "target-compound-herb" network were treated as receptors, and core compounds, as well as anti-ADIC drugs (atenolol, captopril, dexrazoxane, enalapril, irbesartan, metoprolol, and telmisartan) recommended by the guideline, were treated as ligands.

The crystal structure of the 5 proteins was downloaded from the Protein Data Bank (<http://www.rcsb.org/pdb>) and saved in a PDB format. The three-dimensional (3D) conformer structure of candidate compounds was downloaded from the PubChem database (<https://pubchem.ncbi.nlm.nih.gov/>) and saved in a SDF format that was subsequently converted to a PDB format with Open babel 2.4.1.

Ligands and receptors were prepared via AutoDock Tools (v.1.5.6) and PyMOL (v.2.3). The work of preparing receptors included deleting the original ligands and water molecules from the crystal structure of receptors, adding nonpolar hydrogens, and calculating Gasteiger partial charges. The flow of handling ligands contained applying energy minimization and assigning atomic charges and atom. All the prepared receptors and ligands were saved in a pdbqt format.

Then, the affinity indicating binding strength between the ligand and the target protein was evaluated with Autodock Vina (v.1.1.2). Affinity < -4.25 kcal/mol means that ligands and receptors have possibility of combination, affinity < -5.00 kcal/mol indicates good binding strength, and affinity < -7.00 kcal/mol suggests satisfactory binding strength [34]. Pymol 2.3 and LigPlot 2.2 were used to visualize and analyze the docked conformations, and from the binding conformations of the docking results of each compound, the docking results with lower binding energy and better conformation were selected for presentation.

3. Results

3.1. Target Acquisition and Screening.

A total of 84 anti-neoplastic drug-induced cardiotoxicity targets were obtained through Swisstarget Prediction and the literature, and 2,059 cardiotoxicity-related targets were obtained through the disease databases. A total of 40 targets were obtained from the intersection of the aforementioned two datasets. Additional 4 targets (ACE, AGTR1, AGTR2, and IFNAR1) of the anti-ADIC drugs (ACEI, ARB, and beta-blockers) recommended by clinical guidelines were also counted. Among these 44 targets, 21 were successfully matched to compounds that met the ADME and Lipinski screening criteria and were defined as potential targets for herbs against ADIC, as shown in Table 1.

3.2. Candidate Compound Acquisition and Target-Compound Network Construction.

The potential targets were mapped by 13,729 small-molecule compounds in the TCMSP database, among which 332 candidate compounds met the ADME and Lipinski criteria. The target-compound network constructed by the potential targets and candidate compounds is shown in Figure 2. The network consisted of 353 nodes and 337 edges. The red nodes in the figure represent target points, the blue nodes represent compounds, the edges represent relations between two adjacent nodes, and the degrees represent the number of connected edges of nodes. The larger the degrees are, the greater regulatory roles the nodes play in the entire network. Figure 2 shows that KCNH2, CDK1, MMP2, MAPK1, and TP53 were the core targets, and their corresponding degrees were 239, 16, 15, 14, and 12, respectively. Single targets with multiple compounds dominated the network but not vice versa.

3.3. Herb Acquisition and Target-Compound-Herb Network Construction.

A total of 446 herbs were matched to the 332 compounds through the TCMSP database, 46 of which were

TABLE 1: Information of potential targets.

ID	Gene symbol	Uniprot ID	Protein name
1	ACE	P12821	Angiotensin-converting enzyme
2	AGTR1	P30556	Type-1 angiotensin II receptor
3	CA1	P00915	Carbonic anhydrase I
4	CD274	Q9NZQ7	Programmed cell death 1 ligand 1
5	CDK1	P06493	Cell division control protein 2 homolog
6	EGF	P01133	Proepidermal growth factor
7	EGFR	P00533	Epidermal growth factor receptor
8	ERBB2	P04626	Receptor tyrosine-protein kinase erbB-2
9	F3	P13726	Tissue factor
10	HDAC6	Q9UBN7	Histone deacetylase 6
11	IGFBP3	P17936	Insulin-like growth factor-binding protein 3
12	INSR	P06213	Insulin receptor
13	KCNH2	Q12809	Potassium voltage-gated channel subfamily H member 2
14	MAPK1	P28482	Mitogen-activated protein kinase 1
15	MAPK3	P27361	Mitogen-activated protein kinase 3
16	MMP2	P08253	72 kDa type IV collagenase
17	NTRK1	P04629	High affinity nerve growth factor receptor
18	PARP1	P09874	Poly [ADP-ribose] polymerase 1
19	PDE5A	Q76074	CGMP-specific 3',5'-cyclic phosphodiesterase
20	SLC2A1	P11166	Solute carrier family 2, facilitated glucose transporter member 1
21	TP53	P04637	Cellular tumor antigen p53

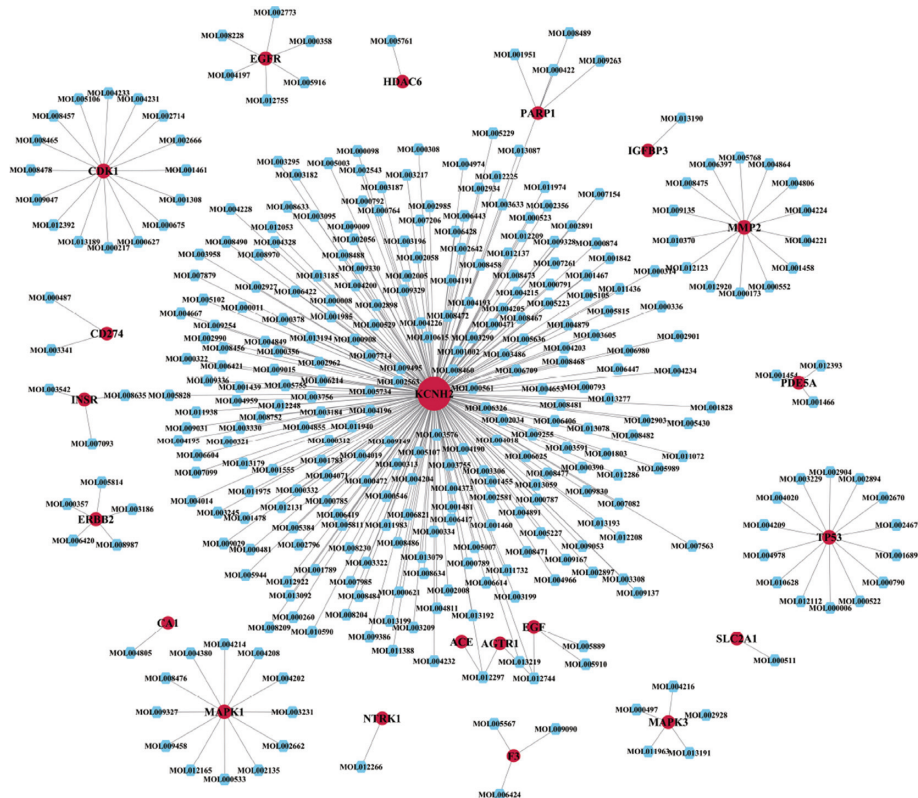


FIGURE 2: Target-compound network.

not included in the *Chinese Pharmacopoeia* (2015), *Chinese Pharmacy* (“*Thirteenth Five-Year Plan*” textbook), and *Chinese Dictionary of Clinical Medicine*, so we finally collected 400 herbs. Based on this, we constructed a compound-herb network. The network contained 732 nodes and 1,925 edges. Among them, the top 8 herb nodes with the highest

degree were Yanhusuo, Gouteng, Huangbo, Gancao, Lianqiao, Guanhuangbo, Leigongteng, and Duzhong, and they contained 42, 27, 22, 21, 20, 18, 18, and 17 candidate compounds, respectively. The targets of herbs were collected through the bridging of candidate compounds. The results showed that Yanhusuo, Gouteng, Lianqiao, Huangqin,

Huangbo, Guanhuangbo, Xiakucao, and Nvzhenzi contained the most targets (9, 9, 9, 8, 8, 8, and 8, respectively). Therefore, we speculate that the abovementioned herbs have stronger regulatory effect on alleviating ADIC in the 400 herbs. The number of candidate compounds and targets of the herbs is shown in Figure 3. The median of the compound degree was 4, and compounds with a degree greater than 8 were considered as potential core compounds. The top 5 compounds were beta-sitosterol, quercetin, daucosterol, kaempferol, and oleic acid. The remaining compounds are shown in Table 2.

In order to present the relation among potential targets, compounds, and herbs more concisely, our study reconstructed the target-compound-herb network by selecting herbs with degree ≥ 5 and their related compounds and targets, as shown in Figure 4. In the figure, the red nodes represented targets, the blue nodes represented compounds, and the green nodes represented herbs. The size of each node was positively correlated with the degree.

3.4. Properties, Tastes, and Meridian Tropism of Herbs. By analyzing the information of properties, tastes, and meridian tropism of the 400 herbs intervening ADIC, our results showed that herbs with bitter taste had the highest frequency, followed by acrid and sweet taste, and the proportion of the three tastes was 80.51%; most herbs were warm. In terms of the meridian tropism, herbs belonging to liver meridian tropism accounted for the most proportion among the 400 herbs, which was 21.36%, herbs belonging to lung meridian tropism accounted for 17.48%, and herbs belonging to both liver and lung meridian tropism accounted for 38.83%. The results are shown in Table 3 and Figure 5.

3.5. Molecular Docking. Twenty-nine core potential compounds were molecularly docked with 5 core targets including KCNH2 (PDBID: 6SYG), CDK1 (PDBID: 4Y72), TP53 (PDBID: 3Q05), MMP2 (PDBID: 1RTG), and MAPK1 (PDBID: 6SLG). A total of 145 pairs of receptor-ligand combinations were obtained, among which 79 combinations had affinity < -7 kcal/mol, accounting for 54.48%. Twenty-five combinations were in the target-compound network, with the strongest binding in MMP2-coptisine (-10.2 kcal/mol) and the weakest in KCNH2-arachidonic acid (-4.4 kcal/mol). The average value of the 25 combinations was -6.684 kcal/mol, suggesting that the binding between the potential core targets and the compounds was strong.

The remaining 120 combinations were outside the target-compound network. The top 3 combinations with the highest affinity were CDK1-coptisine (-11.3 kcal/mol), CDK1-emodin (-10.7 kcal/mol), and MAPK1-diosgenin (-10.6 kcal/mol). There were 6 combinations with affinity < -10.2 kcal/mol. The docking strength of these 6 combinations exceeded that of the 25 combinations in the target-compound network. The docking results indicated that the number of potential compound-target combinations may be far greater than that of the compound-target combinations included in the TCMSP database, which shows that there are still a large number of connections

between active TCM compounds and cardiotoxicity targets waiting to be further studied and excavated. The docking results can provide data support for future experimental screening of related TCM and compounds. The results are shown in Figure 6.

Comprehensively considering the molecular docking affinity value and the degree value in the target-compound-herb network, the results of docking with affinity < -10 kcal/mol in the network and those with the top 4 affinity outside the network were shown in the 3D and 2D format. It can be seen from the figure that each compound ligand is embedded in the active pocket of the receptor target and interacts with multiple residues of the target through hydrophobic interaction and hydrogen bond. The diagrams are shown in Figures 7(a)~7(h).

4. Discussion

A number of reports have shown the potential of natural herbs in decreasing the cardiotoxic effects of chemotherapeutic agents on healthy cells, without negatively affecting their antineoplastic activity [35]. Subsequent improvement in heart function and quality of life may make chemotherapy more sustainable and reduce treatment-related mortality. Besides, most of TCM has anticancer effects with few side effects. Some physicians, thus, turned to use TCM as an alternative or complementary treatment to prevent and treat ADIC [36]. However, systematic studies of TCM intervention on ADIC are still insufficient. It is of great clinical significance to study the intervention mechanism of TCM against ADIC and to develop related pharmaceutical preparations on this basis.

4.1. Targets. In this study, 5 core targets (KCNH2, CDK1, MMP2, MAPK1, and TP53) were identified from the target-compound-herb network. Dysfunction of KCNH2 activation will lead to the decrease of hERG current and a prolongation of the action potentials recorded in cardiomyocytes [37]. Dysfunction of KCNH2 expression is related to QT prolongation syndrome [38]. Inhibition of the KCNH2 potassium channel can lead to cardiotoxicity [39].

The overexpression of four regulatory factors of cell cycle including CDK1 was shown to efficiently induce cell division in postmitotic mouse, rat, and human cardiomyocytes, lead to a significant improvement in cardiac function after acute or subacute myocardial infarction, and improve heart function as indicated by significant improvement in the ejection fraction, stroke volume, and cardiac output.

MMP-2 can hydrolyze sarcomeric proteins in the heart, remodel the extracellular matrix, and lead to cardiotoxicity. Anthracycline drugs such as DOX can enhance the activity of MMP-2 in cardiomyocytes and may cause heart failure, so inhibition of MMP-2 activity can interfere with the cardiotoxicity of anticancer drugs [40].

DOX-induced mitochondrial reactive oxygen species (ROS) release was demonstrated to activate ERK-mediated heat shock factor 2 (HSF2) nuclear translocation and AT1R upregulation, which caused DOX-damaged heart failure

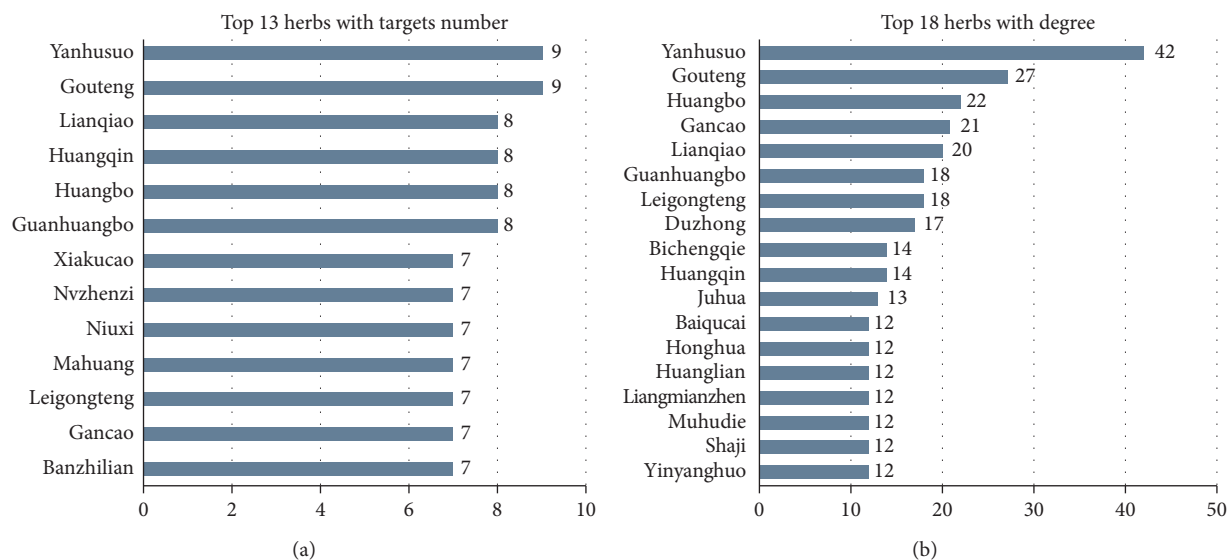


FIGURE 3: Distribution of candidate compounds and target sites in herbs.

TABLE 2: Information of candidate core compounds (degree > 8).

MolID	MolName	CAS	Degree	OB	DL
MOL000358	Beta-sitosterol	83-46-5	225	36.91391	0.75123
MOL000098	Quercetin	117-39-5	174	46.43335	0.27525
MOL000357	Sitogluside	474-58-8	170	20.63194	0.6241
MOL000422	Kaempferol	520-18-3	122	41.88225	0.24066
MOL000675	Oleic acid	112-80-1	109	33.12836	0.14243
MOL000006	Luteolin	491-70-3	83	36.16263	0.24552
MOL000008	Apigenin	520-36-5	75	23.06216	0.21306
MOL000511	Ursolic acid	77-52-1	72	16.7749	0.75457
MOL000908	Beta-elemene	515-13-9	45	25.63362	0.060519
MOL000356	Lupeol	545-47-1	36	12.12076	0.77716
MOL000561	Astragalin	480-10-4	35	14.02685	0.73616
MOL002773	Beta-carotene	7235-40-7	28	37.18433	0.58358
MOL000472	Emodin	518-82-1	28	24.39832	0.23916
MOL000874	Paeonol	552-41-0	26	28.78724	0.039185
MOL001689	Acacetin	480-44-4	20	34.97357	0.24082
MOL002008	Myricetin	529-44-2	20	13.74833	0.31057
MOL004328	Naringenin	67604-48-2	20	59.2939	0.21128
MOL001308	Elaidic acid	112-79-8	17	33.12836	0.14262
MOL001002	Ellagic acid	476-66-4	17	43.06456	0.43417
MOL000546	Eiosgenin	512-04-9	14	80.87792	0.80979
MOL001439	Arachidonic acid	506-32-1	13	45.57325	0.20409
MOL000481	Genistein	446-72-0	13	17.93288	0.21384
MOL002714	Baicalein	491-67-8	12	33.51892	0.20888
MOL000390	Daidzein	486-66-8	11	19.44106	0.18694
MOL001789	Isoliquiritigenin	961-29-5	11	85.3218	0.14805
MOL001842	Pinoresinol	487-36-5	11	4.250519	0.5159
MOL001458	Coptisine	3486-66-6	10	30.67185	0.85647
MOL000173	Wogonin	632-85-9	10	30.68457	0.22942
MOL002891	Magnoflorine	2141/9/5	9	0.479985	0.54735

[41]. It is suggested that the activation of the ERK2 pathway of the mitogen-activated protein kinase (MAPK) family can protect cardiomyocytes from DOX-induced cardiotoxicity [42].

The wild-type p53 protein, which is encoded by the TP53 gene, plays an important role as a tumor suppressor in

regulation of cell cycle arrest, DNA repair, and apoptosis. The association between p53 overexpression, mutations, and drug resistance has been reported in bladder, breast, ovarian, and other types of cancer. Mutation of p53 protein was indicated to decrease sensitivity to anthracycline treatments in human bladder TCC cells [43]. Reactivation of mutant

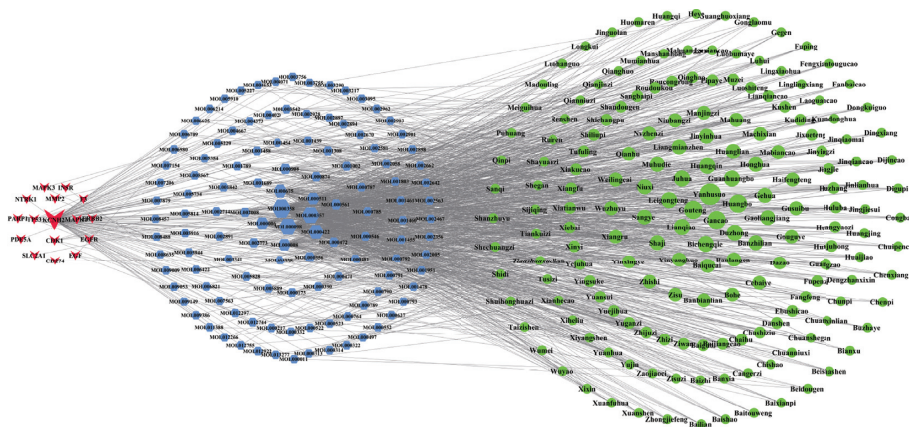


FIGURE 4: Target-compound-herb network (degree of herb ≥ 5).

TABLE 3: Properties and tastes of herbs.

Taste	Frequency	Proportion (%)	Nature	Frequency	Proportion (%)
Bitter	222	35.58	Warm	107	33.23
Acrid	165	26.44	Cold	97	30.12
Sweet	150	24.04	Slight cold	48	14.91
Astringent	31	4.97	Cool	36	11.18
Sour	29	4.65	Slight warm	24	7.45
Salty	16	2.56	Hot	10	3.11
Light	11	1.76			

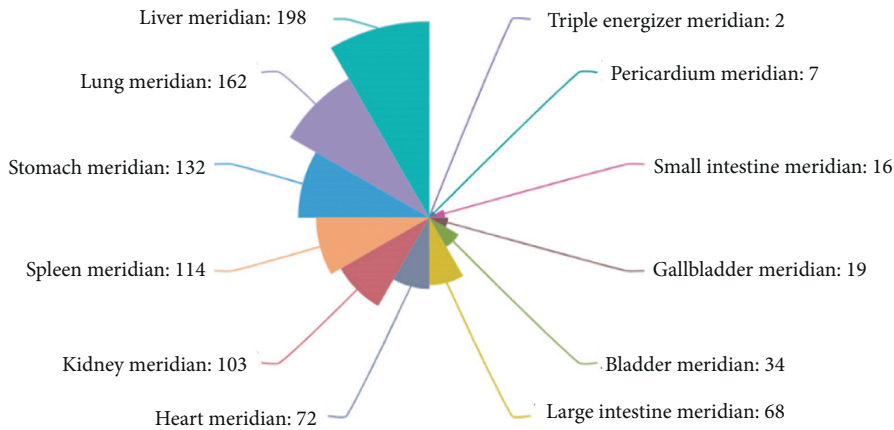


FIGURE 5: Meridian tropism of herbs.

p53 in those tumor cells may restore p53 tumor-suppressor function and sensitize mt-p53 cells to chemotherapy treatments [44]. Therefore, this study speculates that regulation of TP53 can enhance the sensitivity of tumor to anthracycline and other chemotherapy drugs, so as to reduce the dosage of these drugs and decrease their cardiotoxicity accordingly.

4.2. Compound. The core compounds obtained in this study included beta-sitosterol, quercetin, kaempferol, and oleic acid. Studies have shown that one of the core mechanisms of cardiotoxicity caused by anthracyclines is that ROS and reactive nitrogen species (RNS) will accumulate along with

the metabolism of anthracyclines. A large amount of ROS and RNS may activate cytotoxic signals [45] in cardiomyocytes, leading to cardiac dysfunction through DNA damage, mitochondrial dysfunction, decreased antioxidant enzymes, and intracellular calcium homeostasis [46].

The intake of beta-sitosterol can enhance the storage of nonenzymatic antioxidants such as glutathione I, vitamin C, and vitamin E [47]. Glutathione, the main antioxidative stress buffer in the cell, is widely used in cancer treatment. It mainly exists in the form of reduced glutathione (GSH) and oxidized glutathione (GSSG) in the human body. Experiments have shown that beta-sitosterol has a protective effect on the reduction of antioxidants containing GSH in colon

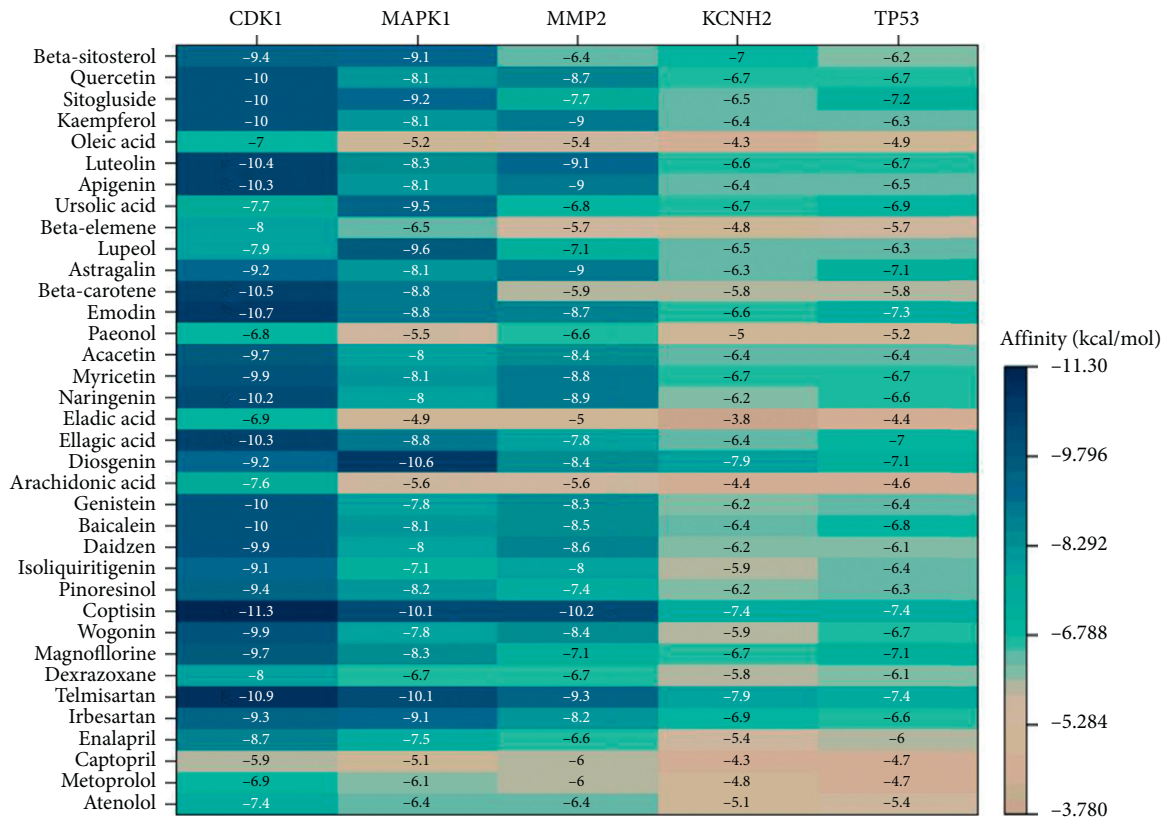


FIGURE 6: Results of molecular docking.

and liver tissues induced by 1, 2-dimethyl hydrazine [48]. Therefore, it is speculated that beta-sitosterol may mitigate ADIC by increasing the content of nonenzymatic antioxidants to compensate for the absence of antioxidant enzymes caused by anthracyclines.

Research showed that quercetin had significant anticancer activities against MCF-7, SKBR-3, and MDA-MB-231 human breast cancer cells and CT26 mouse colon cancer cells. It could also reduce the cardiotoxicity caused by DOX in the Balb/c mice model [49].

Some studies demonstrated that kaempferol protected against DOX-induced cardiotoxicity by regulating the 14-3-3 γ , MAPK, and ADMA/DDAHII/eNOS/NO pathway, inhibiting the activation of p53-mediated, mitochondrion-dependent apoptotic signaling, and improving mitochondrial function [50]. It has been reported that kaempferol dose dependently restored hemodynamic, left ventricular functions, decreased cardiac injury marker enzymes in serum, increased antioxidant levels, and reduced lipid peroxidation, TNF- α level, and apoptosis, so to alleviate cardiotoxicity [51].

Oleic acid has been found to have an excellent antioxidant effect. It was shown that oleic acid had a protective effect on myocardial mitochondrial injury induced by adrenaline in several aspects, such as inhibiting the elevated levels of lipid peroxidation and mitochondrial DNA damage, maintaining membrane intactness and the level of glutathione and keeping mitochondrial enzyme and membrane potential stable in rat experiments [52].

In conclusion, the potential core targets and compounds screened in this study were related to cardiotoxicity, which may play an important protective role in exploring the effects of TCM on ADIC.

4.3. Molecular Docking. The results of molecular docking showed that, in the target-compound network, the combination of MMP2-coptisine performed best, with affinity of -10.2 kcal/mol. There is considerable accumulating evidence suggesting a role of MMP-2, MMP-3, MMP-9 in promoting tumor cell invasion and infiltration [53,54]. The activation of the PI3K/Akt pathway associated with matrix metalloproteinases (MMPs) is essential for the growth and survival of cancer cells. Coptisine is a natural isoquinoline alkaloid. Studies have confirmed that coptisine has an improvement effect on cardiovascular disease in vitro and in vivo. It has strong antioxidant activity, helps maintain cell membrane integrity, improves mitochondrial respiratory dysfunction, and reduces cardiomyocyte apoptosis [55]. At the same time, it can protect cardiomyocytes from hypoxia or reoxidation-induced damage by inhibiting autophagy [56]. Simultaneously, coptisine can intervene in cancer through multiple ways. For instance, coptisine was found to induce apoptosis by strengthening the expression of the 67kD laminin receptor/cGMP pathway in various human hepatoma cells [57]. It can also affect a variety of apoptosis-related targets, including Apaf-a, ROS, Bcl-2-XL, Bax, cytochrome c, Bid, AIF, XIAP, caspase-3, and caspase-9 to

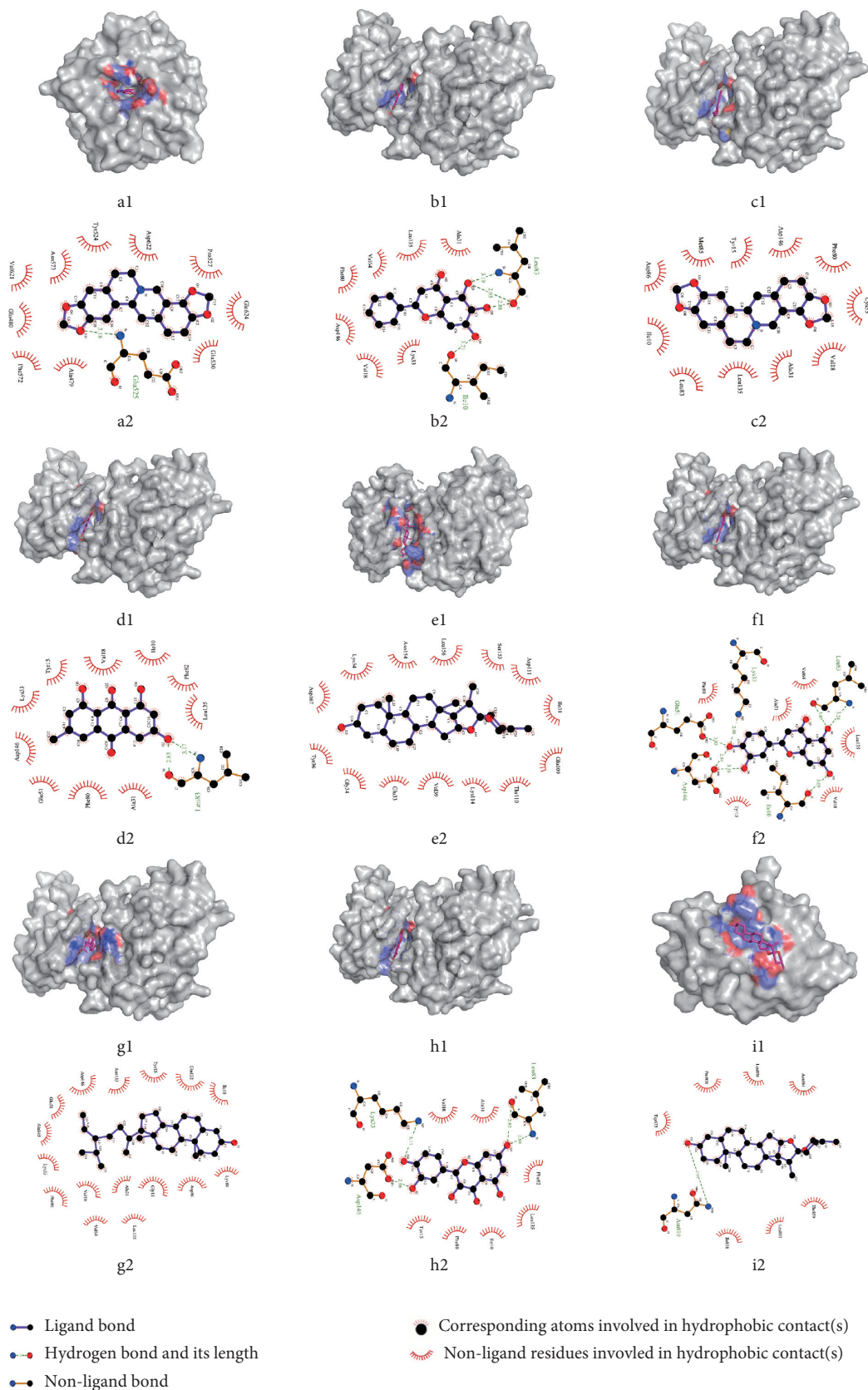


FIGURE 7: Molecular docking of compounds with core targets. (a) MMP2-coptisine; (b) CDK1-baicalein; (c) CDK1-coptisine; (d) CDK1- emodin; (e) MAPK1-diosgenin; (f) CDK1-luteolin; (g) CDK1- β -sitosterol; (h) CDK1- quercetin; (i) KCNH2-diosgenin.

inhibit the activity, adhesion, and migration of HCT-116 cells [58]. The abovementioned studies proved the reliability of this target-compound combination relationship in the network. We speculate that if coptisine is developed as a clinical drug, it may reduce the dose of cardiotoxic anti-tumor drugs, and at the same time, it may alleviate the oxidative stress response in cardiomyocytes caused by anti-tumor drugs, thereby improving myocardial function.

In addition to the target-compound network, the molecular docking results also showed that the six combinations of CDK1-coptisine, CDK1-emodin, MAPK1-diosgenin, CDK1-luteolin, CDK1-Apigenin, and CDK1-ellagicacid had good binding activity. Among them, emodin has been widely used in clinics because of its various pharmacological properties such as anticancer, antibacterial, antiviral, and liver protection properties [59]. Luteolin has been used clinically as a natural flavonoid. Clinical trials have shown that preparations containing luteolin have good anti-inflammatory effects [60], and in the treatment of glioma, combined with olaparib (PARP inhibition agent) or ionizing radiation treatment has certain clinical value [61]. Therefore, it can be regarded as one of the candidate drugs dealing with ADIC in future experimental or clinical researches.

4.4. Herbs. In order to better cooperate with tumor drug treatment, the selected herb can not only protect the heart but also has a certain antitumor effect. The core herbs obtained in this study included Yanhusuo, Gouteng, Huangbai, Lianqiao, and Gancao. Yanhusuo has the most therapeutic potential. Modern pharmacological research showed that corydalis had many functions such as antiarrhythmia, antimyocardial infarction, coronary artery expansion, antitumor, and antithrombosis functions [62], and the extract from corydalis had a protective effect on myocardial ischemia-reperfusion injury, which was closely associated with the inhibition of myocardial apoptosis through modulation of the Bcl-2 family [63]. Tetrahydropalmatine (THP), an effective compound of corydalis, with the analgesic effects on bone cancer pain may underlie the inhibition of microglial cell activation and the increase in proinflammatory cytokine. Meanwhile, THP can reverse the ventricular tachycardia induced by drugs in rabbits and exert an antiarrhythmia effect [64].

Alkaloid extracted from Gouteng may intervene in tachycardia and arrhythmia through blocking the calcium channel and opening the potassium channel [65]. Iso-rhynchophylline, extracted from Gouteng, has the potential of inhibiting cardiac hypertrophy through Nrf2 nuclear translocation and the MAPK pathway [66].

Huangbai has showcased a wide range of pharmacological effects, including anticancer, anti-inflammatory, and antimicrobial effects. The compound ((21S, 23R) epoxy-24-hydroxy-21 β , 25-diethoxy) tirucalla-7-en-3-one has a relatively strong effect as adriamycin against four tumors. Polysaccharides from an aqueous extract of phellodendri act on cell-mediated stimulation and humoral immunity instead of tumor cell inhibition to exert tumoricidal activity [67]. Meanwhile, Huangbai has an antiarrhythmic effect [68].

The main components of Lianqiao suspense are phillyrin, forsythiaside, chlorogenic acid, and so on. Phillyrin can improve heart function by regulating the myocardial contractility index and reduce myocardial fibrosis after myocardial infarction, which showed an effect similar to that of enalapril [69]. Forsythiaside can effectively prevent hydrogen peroxide-induced mitochondrial membrane potential depolarization. Cytochrome C, caspase-9, and caspase-3 are markers of mitochondrial-dependent apoptotic pathways that induce cell death, which is an oxidative stress reaction. Forsythiaside can effectively prevent this reaction induced by hydrogen peroxide [70]. Chlorogenic acid (CGA) attenuates TNF- α -induced cardiomyocyte apoptosis by inhibiting JNK [71]. Li et al. found that CGA could inhibit isotype-induced cardiac hypertrophy through blocking the NF- κ B signaling pathway [72]. CGA can significantly reverse the decline in cardiac mitochondrial membrane potential induced by TNF- α . Therefore, it is suggested that inhibiting TNF- α may help maintain the stability of mitochondrial membrane potential and prevent adriamycin-induced cardiotoxicity in isolated rat hearts [73].

Gancao has protective effects on the heart, and the hydrolysates of its main components glycyrrhizin is glycyrrhetic acid, which has the effect of intervening the permeability transition (MPT) of rat heart mitochondria [74]. The extract of Gancao can maintain the integrity of the cell membrane, improve lipid homeostasis, and stabilize actin. Gancao extract can reduce ROS levels and repair antioxidant status, thus helping to repair DNA damage and mitochondrial function. The SIRT-1-mediated pathway and its downstream activator PPARs are important for the maintenance of cell function. Glycyrrhiza extract could restore nuclear SIRT-1 and PPAR- γ levels in H9C2 cardiomyocytes reduced by DOX interference [75]. It is concluded that Gancao extract can antagonize the cardiotoxicity induced by DOX and maintain the normal function of cardiac myocytes.

The herbs mentioned above may have the potential of mitigating ADIC; meanwhile, some of them have extra beneficial effects on cancer patients. This will provide an alternative scheme for related trials on treating ADIC with TCM. At the same time, the information of herbal taste and meridian tropism can lay a certain foundation for the theoretical discussion and research of TCM on ADIC in the future. Herbs with multiple targets might be of great importance due to their potential broad-spectrum effects against ADIC. A combination of herbs containing various compounds corresponding to multiple targets might be an alternative strategy. The obtained core herbs and compounds can provide reference for the prescription exploration in integrating traditional Chinese and Western medicine to treat ADIC.

5. Strengths and Limitations

The advantage of this study lies in the use of network pharmacology, data mining, and molecular docking methods to obtain herbs and compounds that can potentially resist ADIC from a large number of TCM, which can save economic cost and time in the future study. Meantime, many rare diseases still lack effective means, and the efficacy of some common diseases is not ideal. Chinese medicine may have

certain advantages, but screening out the ideal herb is very time consuming and costly, such as artemisinin. The method used in this research can provide a reference for similar research to narrow the selection scope. The deficiency of this study is that we focus on the relation among targets, compounds, and herbs, but the efficacy of herbs between the targets and the compounds and the compound content of each herb have not been fully discussed. There is a wide variety of antitumor drugs, and new drugs are emerging one after another. The drugs selected in this study came from the existing literature. However, some new drugs with potential cardiotoxicity are not included because of insufficient clinical evidence and no relevant reports have been seen so far. Thus, we will continue to follow-up related progress in the future.

6. Conclusions

This study constructed a target-compound-herb network using ADIC-related targets from multiple databases and compounds and herbs matched from the TCMSP platform. Core targets (KCNH2, CDK1, and MMP2), compounds (beta-sitosterol, quercetin, and kaempferol), and herbs (Yanhusuo, Gouteng, Huangbai, Lianqiao, and Gancao) that may be helpful in treating ADIC were identified from the network. The binding activity between the core targets and the core compounds were strong, verifying the reliability of their connection beyond the network. Most of the candidate herbs were bitter, acrid, and warm, belonging to liver and lung meridians. These conclusions provide new ideas for the screening of herbs that can intervene ADIC in an advanced, evidence-based, and systematic way, and also provide reference for the prescription combining TCM and Western medicine.

Abbreviations

TCM:	Traditional Chinese medicine
TCMSP:	Traditional Chinese Medicine Systems Pharmacology
DL:	Drug likeness
OB:	Oral availability
HL:	Drug half-life
TPSA:	Topological polar surface area
RBN:	Rotatable bonds number
MW:	Molecular weight
PDB:	Protein Data Bank
3D:	Three dimensional
KCNH2:	Potassium voltage-gated channel subfamily H member 2
CDK1:	Cyclin-dependent kinase 1
MMP2:	Matrix metalloproteinase 2
MAPK1:	Mitogen-activated protein kinase1
MAPK:	Mitogen-activated protein kinase
TP53:	Tumor protein p53
TK:	Tyrosine kinase
VEGF:	Vascular endothelial growth factor
EGFR:	Epidermal growth factor receptor
AMPK:	Adenosine 5'-monophosphate- (AMP-) activated protein kinase

ERBB2:	Human epidermal growth factor receptor (HER-2)
NRG-1:	Neuromodulin 1
ROS:	Reactive oxygen species
LVEF:	Left ventricular ejection fraction
ACEI:	Angiotensin-converting enzyme inhibitor
SOD:	Superoxide dismutase
ARB:	Angiotensin receptor blocker
hERG:	Human Ether-a-go-go Related Gene
EF:	Ejection fraction
ERK1/2:	Extracellular regulatory protein kinase1/2
AT1 R:	Angiotensin receptor1
DOX:	Doxorubicin
TCC cells:	Transitional cell carcinoma
mt-p53:	Mutation of p53
RNS:	Reactive nitrogen species
GSH:	Glutathione
GSSG:	Oxidized glutathione
DMH:	1: 2-dimethyl hydrazine
TNF- α :	Tumor necrosis factor- α
ADMA:	Asymmetric dimethylarginine
DDAH II:	Dimethylarginine dimethylamine hydrolase II
eNOS:	Endothelial nitric oxide synthase
NO:	Nitric oxide
MCF-7:	Human breast cancer cells MCF-7
SKBR-3:	Human breast cancer cells SKBR-3
MDA-MB-231:	Human breast cancer cells MDA-MB-231
CT26:	Mouse colon cancer cells CT26
FoxO1:	Forkhead box O1
NFATc3:	Nuclear factor of activated T-cells, cytoplasmic, calcineurindependent 3
PI3K/Akt:	Phosphatidylinositol 3 kinase / protein kinase B
MMPs:	Matrix metalloproteinases
cGMP:	Cyclic guanosine monophosphate
Apaf-a:	Apoptotic protease activating factor-a
Bax:	BCL2-associated X
BID:	BH3-interacting domain death agonist
AIF:	Apoptosis inducing factor
XIAP:	x-linked inhibitor of apoptosis protein
HCT-116:	Human colon cancer Cell HCT-116
PARP:	Poly ADP-ribose Polymerase
IR:	Ionizing radiation
Bcl-2:	b-cell lymphoma-2
THP:	Tetrahydropalmatine
VT:	Ventricular tachycardia
Nrf2:	Nuclear factor E2-related factor 2
CGA:	Chlorogenic acid.

Data Availability

The datasets used and/or analyzed during the current study are available from the corresponding author on reasonable request.

Conflicts of Interest

All authors declare that there are no conflicts of interest.

Authors' Contributions

DWC and LJL contributed equally to this paper, and they designed the study. Experimental work and data collection were conducted by DWC and LJL. GXY and ZBR analyzed and interpreted the data. DWC and LJL drafted the manuscript. HQY and GXY provided critical comments and revised the manuscript. ZBR and QY helped perform the analysis with constructive discussions. All authors read and approved the final version of the manuscript.

Acknowledgments

The authors gratefully acknowledge the contribution of Jianliang Li and Jianbo Guo (Beijing University of Chinese Medicine) in the study design and guidance. This study was supported by the project Beijing Science and Technology Rising Star (Z181100006218035). The present study was supported by the National Natural Science Foundation of China (81202803) and the National Administration of TCM Project Fund (G2T-FJS-2019-203). The funders had no role in study design, data collection and analysis, decision to publish, or preparation of the manuscript.

References

- [1] D. D. Von Hoff, "Risk factors for doxorubicin-induced congestive heart failure," *Annals of Internal Medicine*, vol. 91, no. 5, pp. 710–717, 1979.
- [2] H. A. Preti, "Points to remember: practical pearls in oncocardiology," *Methodist DeBakey Cardiovascular Journal*, vol. 11, no. 4, p. 254, 2015.
- [3] B. Sherry-Ann, R. C. Jordan, and H. Joerg, "Precision cardio-oncology: a systems-based perspective on cardiotoxicity of tyrosine kinase inhibitors and immune checkpoint inhibitors," *Journal of Cardiovascular Translational Research*, vol. 13, no. 3, pp. 402–416, 2020.
- [4] G. D'Uva, A. Aharonov, M. Lauriola et al., "ERBB2 triggers mammalian heart regeneration by promoting cardiomyocyte dedifferentiation and proliferation," *Nature Cell Biology*, vol. 17, no. 5, pp. 627–638, 2015.
- [5] E. A. Pinheiro, T. Magdy, and P. W. Burridge, "Human in vitro models for assessing the genomic basis of chemotherapy-induced cardiovascular toxicity," *Journal of Cardiovascular Translational Research*, vol. 13, no. 3, pp. 377–389, 2020.
- [6] S. Schultz-Hector and T. Klaus-Rüdiger, "Radiation-induced cardiovascular diseases: is the epidemiologic evidence compatible with the radiobiologic data?" *International Journal of Radiation Oncology, Biology, Physics*, vol. 67, no. 1, pp. 10–18, 2007.
- [7] C. Cardinale, B. Giulia, M. Beggiato, A. Colombo, and C. M. Carlo, "Strategies to prevent and treat cardiovascular risk in cancer patients," *Seminars in Oncology*, vol. 40, no. 2, pp. 186–198, 2013.
- [8] S. Seicean, A. Seicean, J. C. Plana, G. T. Budd, and M. H. Thomas, "Effect of statin therapy on the risk for incident heart failure in patients with breast cancer receiving anthracycline chemotherapy: an observational clinical cohort study," *Journal of the American College of Cardiology*, vol. 60, no. 23, pp. 2384–2390, 2012.
- [9] M. W. Bloom, C. E. Hamo, D. Cardinale et al., "Cancer therapy-related cardiac dysfunction and heart failure: Part 1: definitions, pathophysiology, risk factors, and imaging," *Circulation Heart Failure*, vol. 9, no. 1, Article ID e2661, 2016.
- [10] Y. Tiezhu, X. Zhihong, M. Jing-tao, and Z. Ning, "Protection effect of Xinmailong injection in treating breast cancer patients with myocardial damage caused by sequential chemotherapy of protection effect of Xinmailong injection in treating breast cancer patients with myocardial damage caused by sequential chemotherapy of trastuzumab and anthracyclines," *Chinese Journal of Experimental Traditional Medical Formulae*, vol. 22, no. 6, pp. 154–158, 2016.
- [11] Z. Xianjin, S. Lianxun, and C. Liuzhong, "Research on effects of danshen injection in preventing cardiotoxicity induced by chemotherapy of pyrroxine or epirubicin," *Evaluation and Analysis of Drug-Use in Hospitals of China*, vol. 18, no. 4, pp. 511–513, 2018.
- [12] Z. Qin, Y. Xinyu, Z. Xiaoyu, and S. Hongcai, "Efficacy of traditional Chinese medicine for arrhythmia caused by anthracycline drugs: a systematic review," *Chinese Journal of Evidence-Based Medicine*, vol. 18, no. 6, pp. 604–609, 2018.
- [13] W. Zhang, Y. Huai, Z. Miao, A. Qian, and Y. Wang, "Systems pharmacology for investigation of the mechanisms of action of traditional Chinese medicine in drug discovery," *Frontiers in Pharmacology*, vol. 10, p. 743, 2019.
- [14] R. Zhang, X. Zhu, H. Bai, and K. Ning, "Network pharmacology databases for traditional Chinese medicine: review and assessment," *Frontiers in Pharmacology*, vol. 10, p. 123, 2019.
- [15] K. Athanasios, A. Ntalianis, E. Repasos, E. Kastritis, M.-A. Dimopoulos, and I. Paraskevaids, "Cardio-oncology: a focus on cardiotoxicity," *European Cardiology*, vol. 13, no. 1, pp. 64–69, 2018.
- [16] S. Marilyn, D. Irina, A. Justin et al., "GeneCards Version 3: the human gene integrator," *Database The Journal of Biological Databases and Curation*, vol. 2010, p. 20, 2010.
- [17] J. S. Amberger, C. A. Bocchini, S. François, A. F. Scott, and H. Ada, "OMIM.org: online mendelian inheritance in man (OMIM®), an online catalog of human genes and genetic disorders," *Nucleic Acids Research*, vol. 43, no. D1, pp. D789–D798, 2015.
- [18] D. S. Wishart, Y. D. Feunang, A. C. Guo et al., "DrugBank 5.0: a major update to the DrugBank database for 2018," *Nucleic Acids Research*, vol. 46, no. D1, pp. D1074–D1082, 2017.
- [19] J. Piñero, J. M. Ramírez-Anguita, J. Saüch-Pitarch et al., "The DisGeNET knowledge platform for disease genomics: 2019 update," *Nucleic Acids Research*, vol. 48, no. D1, pp. D845–D855, 2020.
- [20] A. Daina, O. Michielin, and V. Zoete, "SwissTargetPrediction: updated data and new features for efficient prediction of protein targets of small molecules," *Nucleic Acids Research*, vol. 47, no. W1, pp. W357–W364, 2019.
- [21] S. H. Armenian, C. Lacchetti, and A. Barac, "Prevention and monitoring of cardiac dysfunction in survivors of adult cancers: American society of clinical oncology clinical practice guideline," *Journal of Clinical Oncology*, vol. 35, no. 8, pp. 893–911, 2017.
- [22] S. A. Virani, S. Dent, C. Brezden-Masley et al., "Canadian cardiovascular society guidelines for evaluation and management of cardiovascular complications of cancer therapy," *Canadian Journal of Cardiology*, vol. 32, no. 7, pp. 831–841, 2016.
- [23] J. L. Zamorano, P. Lancellotti, D. Aboyans et al., "2016 ESC Position Paper on cancer treatments and cardiovascular toxicity developed under the auspices of the ESC committee

- for practice guidelines," *European Heart Journal*, vol. 37, no. 36, pp. 2768–2801, 2016.
- [24] A. Rolf, B. Amos, C. H. Wu et al., "UniProt: the universal protein knowledgebase," *Nucleic Acids Research*, vol. 32, no. suppl_1, 2004.
- [25] J. Ru, P. Li, J. Wang et al., "TCMSP: a database of systems pharmacology for drug discovery from herbal medicines," *Journal of Cheminformatics*, vol. 6, no. 1, pp. 1–6, 2014.
- [26] C. A. Lipinski, F. Lombardo, B. W. Dominy, and P. J. Feeney, "Experimental and computational approaches to estimate solubility and permeability in drug discovery and development settings," *Advanced Drug Delivery Reviews*, vol. 23, no. 1–3, pp. 3–25, 2012.
- [27] W. Tao, X. Xu, X. Wang et al., "Network pharmacology-based prediction of the active ingredients and potential targets of Chinese herbal Radix Curcumae formula for application to cardiovascular disease," *Journal of Ethnopharmacology*, vol. 145, no. 1, pp. 1–10, 2013.
- [28] P. Ertl, B. Rohde, and P. Selzer, "Fast calculation of molecular polar surface area as a sum of fragment-based contributions and its application to the prediction of drug transport properties," *Journal of Medicinal Chemistry*, vol. 43, no. 20, pp. 3714–3717, 2000.
- [29] D. F. Veber, S. R. Johnson, H.-Y. Cheng, B. R. Smith, K. W. Ward, and K. D. Kopple, "Molecular properties that influence the oral bioavailability of drug candidates," *Journal of Medicinal Chemistry*, vol. 45, no. 12, pp. 2615–2623, 2002.
- [30] D. Otasek, J. H. Morris, J. Bouças, A. R. Pico, and B. Demchak, "Cytoscape Automation: empowering workflow-based network analysis," *Genome Biology*, vol. 20, no. 1, p. 185, 2019.
- [31] NP Committee, *Chinese Pharmacopoeia*, China Medical Science and Technology Press, Beijing, China, 2015.
- [32] Z. Gansheng, *Chinese Pharmacy*, China Press of Traditional Chinese Medicine, Beijing, China, 2016.
- [33] P. Cheng, *Chinese Dictionary of Clinical Medicine*, China Medical Science and Technology Press, Beijing, China, 2018.
- [34] H. Kun-Yi, G. Samik, and K. Hiroaki, "Combining machine learning systems and multiple docking simulation packages to improve docking prediction reliability for network pharmacology," *PLoS One*, vol. 8, no. 12, Article ID e83922, 2013.
- [35] O. Shunsuke and T. Hiroshi, "Herbal medicines for the treatment of cancer chemotherapy-induced side effects," *Frontiers in Pharmacology*, vol. 6, p. 14, 2015.
- [36] Y. Xinyu, N. Liu, X. Li et al., "A review on the effect of traditional Chinese medicine against anthracycline-induced cardiac toxicity," *Frontiers in Pharmacology*, vol. 9, p. 444, 2018.
- [37] R. Caballero, R. G. Utrilla, I. Amorós et al., "Tbx20 controls the expression of the KCNH2 gene and of hERG channels," *Proceedings of the National Academy of Sciences*, vol. 114, no. 3, pp. E416–E425, 2017.
- [38] M. Santoni, G. Occhipinti, E. Romagnoli et al., "Different cardiotoxicity of palbociclib and ribociclib in breast cancer: gene expression and pharmacological data analyses, biological basis, and therapeutic implications," *BioDrugs: Clinical Immunotherapeutics, Biopharmaceuticals and Gene Therapy*, vol. 33, no. 6, pp. 613–620, 2019.
- [39] M. A. Tamer, A. Yen-Sin, E. Radzinsky et al., "Regulation of cell cycle to stimulate adult cardiomyocyte proliferation and cardiac regeneration," *Cell*, vol. 173, no. 1, pp. 104–116, 2018.
- [40] C. Brandon, A. Roczkowsky, C. J. Woo et al., "MMP inhibitors attenuate doxorubicin cardiotoxicity by preventing intracellular and extracellular matrix remodeling," *Cardiovascular Research*, 2020.
- [41] C.-Y. Hang, J. Y. Chen, C. H. Kuo et al., "Mitochondrial ROS-induced ERK1/2 activation and HSF2-mediated AT R upregulation are required for doxorubicin-induced cardiotoxicity," *Journal of Cellular Physiology*, vol. 233, no. 1, pp. 463–475, 2018.
- [42] L. Yang, C. Luo, C. Chen, X. Wang, W. Shi, and J. Liu, "All-trans retinoic acid protects against doxorubicin-induced cardiotoxicity by activating the ERK2 signalling pathway," *British Journal of Pharmacology*, vol. 173, no. 2, pp. 357–371, 2016.
- [43] S. Pandey, J. Bourn, and M. Cekanova, "Mutations of p53 decrease sensitivity to the anthracycline treatments in bladder cancer cells," *Oncotarget*, vol. 9, no. 47, pp. 28514–28531, 2018.
- [44] A. N Bullock and A. R. Fersht, "Rescuing the function of mutant p53," *Nature Reviews Cancer*, vol. 1, no. 1, pp. 68–76, 2001.
- [45] G. Takemura and H. Fujiwara, "Doxorubicin-induced cardiomyopathy," *Progress in Cardiovascular Diseases*, vol. 49, no. 5, pp. 330–352, 2007.
- [46] D. Cappetta, A. De Angelis, L. Sapio et al., "Oxidative stress and cellular response to doxorubicin: a common factor in the complex milieu of anthracycline cardiotoxicity," *Oxidative Medicine and Cellular Longevity*, vol. 2017, Article ID 1521020, 13 pages, 2017.
- [47] M. S. Bin Sayeed and S. S. Ameen, "Beta-sitosterol: a promising but orphan nutraceutical to fight against cancer," *Nutrition and Cancer*, vol. 67, no. 8, pp. 1216–1222, 2015.
- [48] A. A. Basker, A. N. S. Khalid, G. M. Paulraj, A. M. Alsaif, M. A. Muamar, and S. Ignacimuthu, "β-sitosterol prevents lipid peroxidation and improves antioxidant status and histology in rats with 1,2-dimethylhydrazine-induced colon cancer," *Journal of Medicinal Food*, vol. 15, no. 4, pp. 335–343, 2012.
- [49] C.-E. Chen, C.-M. Hsieh, S.-C. Huang, C.-Y. Su, M.-T. Sheu, and H.-O. Ho, "Lecithin-stabilized polymeric micelles (L_{sb}PMs) for delivering quercetin: pharmacokinetic studies and therapeutic effects of quercetin alone and in combination with doxorubicin," *Scientific Reports*, vol. 8, no. 1, p. 17640, 2018.
- [50] W. Wu, B. Yang, Y. Qiao, Z. Qing, H. He, and M. He, "Kaempferol protects mitochondria and alleviates damages against endotheliotoxicity induced by doxorubicin," *Bio-medicine & Pharmacotherapy*, vol. 126, p. 110040, 2020.
- [51] K. Suchal, S. Malik, N. Gamad et al., "Kampeferol protects against oxidative stress and apoptotic damage in experimental model of isoproterenol-induced cardiac toxicity in rats," *Phytomedicine: International Journal of Phytotherapy and Phytopharmacology*, vol. 23, no. 12, pp. 1401–1408, 2016.
- [52] J. Samanta, A. Mondal, S. Saha, S. Chakraborty, and A. Sengupta, "Oleic acid protects from arsenic-induced cardiac hypertrophy via AMPK/FoxO/NFATc3 pathway," *Cardiovascular Toxicology*, vol. 20, no. 3, pp. 261–280, 2020.
- [53] P. Pittayapruek, J. Meephansan, O. Prapapan, M. Komine, and M. Ohtsuki, "Role of matrix metalloproteinases in photoaging and photocarcinogenesis," *International Journal of Molecular Sciences*, vol. 17, no. 6, 2016.
- [54] Q. Chen, M. Jin, F. Yang, J. Zhu, Q. Xiao, and L. Zhang, "Matrix metalloproteinases: inflammatory regulators of cell behaviors in vascular formation and remodeling," *Mediators of Inflammation*, vol. 2013, Article ID 928315, 14 pages, 2013.
- [55] Y. Wang, Q. Wang, L. Zhang et al., "Coptisine protects cardiomyocyte against hypoxia/reoxygenation-induced damage via inhibition of autophagy," *Biochemical and*

- Biophysical Research Communications*, vol. 490, no. 2, pp. 231–238, 2017.
- [56] L.-L. Gong, L.-H. Fang, S.-B. Wang et al., “Coptisine exert cardioprotective effect through anti-oxidative and inhibition of RhoA/Rho kinase pathway on isoproterenol-induced myocardial infarction in rats,” *Atherosclerosis*, vol. 222, no. 1, pp. 50–58, 2012.
- [57] L. Zhou, F. Yang, G. Li et al., “Coptisine induces apoptosis in human hepatoma cells through activating 67-kDa laminin receptor/cGMP signaling,” *Frontiers in Pharmacology*, vol. 9, p. 517, 2018.
- [58] W. Zhang, P. Cheng, W. Hu et al., “Inhibition of microRNA-384-5p alleviates osteoarthritis through its effects on inhibiting apoptosis of cartilage cells via the NF- κ B signaling pathway by targeting SOX9,” *Cancer Gene Therapy*, vol. 25, no. 11–12, pp. 326–338, 2018.
- [59] X. Dong, J. Fu, X. Yin et al., “Emodin: a review of its pharmacology, toxicity and pharmacokinetics,” *Phytotherapy Research*, vol. 30, no. 8, pp. 1207–1218, 2016.
- [60] N. Aziz, M.-Y. Kim, and J. Y. Cho, “Anti-inflammatory effects of luteolin: a review of in vitro, in vivo, and in silico studies,” *Journal of Ethnopharmacology*, vol. 225, pp. 342–358, 2018.
- [61] C. Yi, G. Li, D. N. Ivanov et al., “Luteolin inhibits Musashi1 binding to RNA and disrupts cancer phenotypes in glioblastoma cells,” *RNA Biology*, vol. 15, no. 11, pp. 1420–1432, 2018.
- [62] B. Tian, M. Tian, and S.-M. Huang, “Advances in phytochemical and modern pharmacological research of *Rhizoma corydalis*,” *Pharmaceutical Biology*, vol. 58, no. 1, pp. 265–275, 2020.
- [63] B. Tian, M. Tian, and S.-M. Huang, “Advances in phytochemical and modern pharmacological research of *Rhizoma corydalis*,” *Pharmaceutical Biology*, vol. 58, no. 1, pp. 265–275, 2020.
- [64] H. Ling, L. Wu, and L. Li, “Corydalis yanhusuo rhizoma extract reduces infarct size and improves heart function during myocardial ischemia/reperfusion by inhibiting apoptosis in rats,” *Phytotherapy Research: PTR*, vol. 20, no. 6, pp. 448–453, 2006.
- [65] J. S. Shi, J. X. Yu, X. P. Chen, and R. X. Xu, “Pharmacological actions of gouteng alkaloids, rhynchophylline and isorhynchophylline,” *ACTA Pharmacologica Sinica*, vol. 24, no. 2, pp. 97–101, 2003.
- [66] Y. Zhang, Y. Cui, S. Deng et al., “Isorhynchophylline enhances Nrf₂ and inhibits MAPK pathway in cardiac hypertrophy,” *Naunyn-Schmiedeberg’s Archives of Pharmacology*, vol. 393, no. 2, pp. 203–212, 2020.
- [67] Y. Sun, G. B. Lenon, and A. W. H. Yang, “Phellodendri cortex: a phytochemical, pharmacological, and pharmacokinetic review,” *Evidence-Based Complementary and Alternative Medicine*, vol. 2019, Article ID 7621929, 45 pages, 2019.
- [68] C. Yang, L. Wenqing, P. Guangchun, J. Yuanying, and C. Yongbing, “Advances in studies on pharmacological actions of proberberine,” *Drugs & Clinic*, vol. 28, no. 6, pp. 1012–1017, 2013.
- [69] L. Wang, W. Zhang, Z. Lu et al., “Functional gene module-based identification of phillyrin as an anticardiac fibrosis agent,” *Frontiers in Pharmacology*, vol. 11, p. 1077, 2020.
- [70] C. Huang, Y. Lin, H. Su, and D. Ye, “Forsythiaside protects against hydrogen peroxide-induced oxidative stress and apoptosis in PC12 cell,” *Neurochemical Research*, vol. 40, no. 1, pp. 27–35, 2015.
- [71] L. Tian, C. P. Su, Q. Wang et al., “Chlorogenic acid: a potent molecule that protects cardiomyocytes from TNF- α -induced injury via inhibiting NF- κ B and JNK signals,” *Journal of Cellular and Molecular Medicine*, vol. 23, no. 7, pp. 4666–4678, 2019.
- [72] Y. Li, D. Shen, X. Tang et al., “Chlorogenic acid prevents isoproterenol-induced hypertrophy in neonatal rat myocytes,” *Toxicology Letters*, vol. 226, no. 3, pp. 257–263, 2014.
- [73] D. Montaigne, X. Marechal, R. Baccouch et al., “Stabilization of mitochondrial membrane potential prevents doxorubicin-induced cardiotoxicity in isolated rat heart,” *Toxicology and Applied Pharmacology*, vol. 244, no. 3, pp. 300–307, 2010.
- [74] V. Battaglia, A. M. Brunati, C. Fiore et al., “Glycyrrhetic acid as inhibitor or amplifier of permeability transition in rat heart mitochondria,” *Biochimica et Biophysica Acta (BBA)-Bio-membranes*, vol. 1778, no. 1, pp. 313–323, 2008.
- [75] S. Upadhyay, A. K. Mantha, and M. Dhiman, “Glycyrrhiza glabra (Licorice) root extract attenuates doxorubicin-induced cardiotoxicity via alleviating oxidative stress and stabilising the cardiac health in H9c2 cardiomyocytes,” *Journal of Ethnopharmacology*, vol. 258, Article ID 112690, 2020.